

博士論文

Development of an *in vitro* human model for inhalation
toxicology based on a whole cigarette smoke exposure system
and a three-dimensional bronchial tissue culture
(全たばこ煙曝露システムと三次元培養気管支組織を用いた
in vitro ヒト吸入毒性評価モデルの開発)

石川 晋吉

Contents

Contents	i
Abbreviations	ix
Chapter 1. General introduction	1
1.1 Research background.....	2
1.1.1 Inhalation toxicities of aerosols in a regulatory context.....	2
1.1.2 Generation of CS and its aerosol properties.....	3
1.1.3 Harmful chemicals in CS and smoking-related lung disease.....	5
1.1.4 <i>In vivo</i> toxicity testing for CS.....	7
1.1.5 Traditional <i>in vitro</i> toxicity testing for CS	8
1.1.6 Development of a 3D culture model for <i>in vitro</i> inhalation toxicity testing	10
1.1.7 Development of a whole CS exposure system for <i>in vitro</i> inhalation toxicity testing	12
1.1.8 Whole CS exposure of 3D culture model of human bronchial epithelium	14
1.2 Thesis outline	16
1.2.1 General objectives.....	16
1.2.2 Study approaches	17
1.3 References	19
Chapter 2. Whole CS exposure for the Ames test.....	27
2.1 Introduction	28
2.1.1 Objectives	28

2.1.2 Study approaches	29
2.2 Materials and methods	32
2.2.1 Test cigarettes	32
2.2.2 Generation of whole CS or the GVP fraction and exposure of bacterial cells	32
2.2.3 Bacterial strains and culture conditions	33
2.2.4 Ames reverse mutation assay	33
2.2.5 Analyses of the masses of TPM and solanesol in the CS produced by the test cigarettes	34
2.2.6 Collection of solanesol deposited on the culture surface	34
2.2.7 HPLC conditions for analyzing solanesol	35
2.2.8 Statistical analysis	35
2.3 Results	36
2.3.1 Mutagenicity of whole CS generated under the ISO standard regime	36
2.3.2 Mutagenicity of whole CS generated under the ISO intensive regime	37
2.3.3 Mutagenicity of the GVP fraction of whole CS generated under the ISO intensive regime.....	40
2.3.4 Amounts of TPM and solanesol in the mainstream CS	41
2.3.5 Estimating the level of TPM exposure for the cultured cells	41
2.3.6 Analysis of the specific mutagenic activity of the CS produced by each test cigarette.....	43
2.4 Discussion	46
2.5 Conclusions	48
2.6 References	49

Chapter 3. Development of a 3D bronchial tissue model	53
3.1 Introduction	54
3.1.1 Objectives	54
3.1.2 Study approaches	54
3.2 Materials and methods	57
3.2.1 Construction of a 3D culture model of human bronchial tissue	57
3.2.2 TGF- β stimulation and collagen gel contraction	58
3.2.3 Histological analysis of the tissues	58
3.2.4 Measurement of matrix metalloproteinases by gelatin zymography	59
3.2.5 Measurement of tissue inhibitor of metalloproteinases by a multiplex assay	60
3.2.6 PCR array analysis for ECM-related genes	60
3.2.7 Statistical analysis	60
3.3 Results	61
3.3.1 Mucociliary differentiation of the 3D bronchial tissue model	61
3.3.2 Collagen gel contraction following TGF- β 1 stimulation	62
3.3.3 Histological changes induced by TGF- β 1 stimulation	64
3.3.4 Effect of TGF- β 1 on expression of MMPs	66
3.3.5 Effect of TGF- β 1 on expression of TIMPs	68
3.3.6 Effect of TGF- β 1 on ECM-related genes	69
3.3.7 Effect of TGF- β 1 on the ECM protein expression pattern	70
3.3.8 Effect of TGF- β 1 on a fibroblast mono-culture	72
3.4 Discussion	74
3.5 Conclusions	78

3.6 References	79
Chapter 4. Establishment of whole CS exposure conditions reproducing actual human airway tissue doses.....	85
4.1 Introduction	86
4.1.1 Objectives	86
4.1.2 Study approaches	86
4.2 Materials and methods	91
4.2.1 <i>In vitro</i> dosimetry test	91
4.2.2 Human retention study for the <i>in vivo</i> dosimetry test	93
4.2.3 HPLC conditions	96
4.2.4 Statistical analysis	96
4.3 Results	97
4.3.1 <i>In vitro</i> dosimetry test with the Cultex RFS module.....	97
4.3.2 Human retention study for the <i>in vivo</i> dosimetry test	99
4.3.3 Comparison of <i>in vitro</i> and <i>in vivo</i> dosimetry.....	101
4.4 Discussion	103
4.5 Conclusions	106
4.6 References	107
Chapter 5. Repeated whole CS exposure of the 3D bronchial tissue model.....	111
5.1 Introduction	112
5.1.1 Objectives	112
5.1.2 Study approaches	112
5.2 Materials and methods	113
5.2.1 Whole CS exposure of the 3D bronchial tissue model	113

5.2.2 Interleukin-13 stimulation	115
5.2.3 Cytochrome P450 and lactate dehydrogenase cytotoxicity assay	115
5.2.4 Histological analysis of the tissues	116
5.2.5 RNA extraction, reverse transcription, and quantitative PCR.....	116
5.2.6 Analysis of secreted cytokines	117
5.2.7 Statistical analysis	117
5.3 Results	117
5.3.1 Effects of a single exposure to whole CS.....	117
5.3.2 Tissue histology following repeated exposure to whole CS	118
5.3.3 Gene expression of differentiation markers and growth factors following repeated exposure to whole CS	121
5.3.4 Gene expression of NFκB-signaling components following repeated exposure to whole CS.....	122
5.3.5 Cytokine secretion into the basolateral medium during repeated exposure to whole CS	124
5.4 Discussion	127
5.5 Conclusions	131
5.6 References	132
Chapter 6. Omics analysis of the 3D bronchial tissue model following repeated whole CS exposure.....	135
6.1 Introduction	136
6.1.1 Objectives	136
6.1.2 Study approaches	136
6.2 Materials and methods	137

6.2.1 Whole CS exposure of the 3D bronchial tissue model	137
6.2.2 Analysis of secreted cytokines	138
6.2.3 Histological analysis of the tissues	139
6.2.4 Adenylate kinase cytotoxicity assay.....	139
6.2.5 Global metabolome analysis	139
6.2.6 Targeted metabolomic analysis	140
6.2.7 Microarray analysis	141
6.2.8 Microarray data processing	141
6.2.9 Ingenuity pathway analysis	142
6.2.10 PCR array analysis	143
6.2.11 ASL proteomics analysis	143
6.2.12 Measurement of MMP by gelatin zymography	143
6.3 Results	144
6.3.1 Cytokine secretion and tissue damage following repeated whole CS exposure	144
6.3.2 Dose-dependent perturbation of metabolites by repeated whole CS exposure and its effect on central carbon metabolism	146
6.3.3 Microarray analysis of central carbon metabolism perturbation	149
6.3.4 Global gene expression and pathway analysis from microarray data ...	150
6.3.5 Multi-omics-based estimation of epidermal growth factor receptor-related network perturbation	153
6.3.6 Proteomic analysis of apical secretions of mucins and MMPs in CS-exposed 3D bronchial tissue cultures	156
6.4 Discussion	158

6.5 Conclusions	161
6.6 References	162
Chapter 7. General conclusions and perspectives	165
7.1 Achievements of the research	166
7.2 Limitations of the research	169
7.2.1 Composition of 3D cell culture.....	170
7.2.2 Whole CS exposure dose.....	171
7.2.3 Whole CS exposure duration	172
7.3 Future perspectives	172
7.4 References	174
Supplementary information	177
List of Figures	181
List of Tables	185
Publications and conference presentations	187
Acknowledgements	191

Abbreviations

3D, three dimensional

3-PG, 3-phosphoglycerate

6-PG, 6-phosphogluconate

AAT, alpha-1 antitrypsin

ADME, absorption, distribution, metabolism, and excretion

AhR, aryl hydrocarbon receptor

ALI, air–liquid interface

ALK, activin receptor-like kinase

ASL, airway surface liquid

CC1, 1-mg of tar commercial cigarette

COPD, chronic obstructive pulmonary disease

CS, cigarette smoke

CYP, cytochrome P450

DAB, diaminobenzidine

DEG, differentially expressed gene

DNPH, 2,4-dinitrophenylhydrazine

E4P, erythrose 4-phosphate

ECM, extracellular matrix

EDTA, ethylenediaminetetraacetic acid

EGFR, epidermal growth factor receptor

EMT, epithelial–mesenchymal transition

EMTU, epithelial–mesenchymal trophic unit

EU, European Union

F6P, fructose 6-phosphate

FBP, fructose 1,6-bisphosphate

FBS, fetal bovine serum

FDR, false discovery rate

G6P, glucose 6-phosphate

G-CSF, granulocyte-colony stimulating factor

GM-CSF, granulocyte macrophage-colony stimulating factor

GSH, reduced glutathione

GSSG, oxidized glutathione

GVP, gas/vapor phase

HBEC, human bronchial epithelial cell

HC, heated cigarette

HPLC, high performance liquid chromatography

IL, interleukin

IPA, ingenuity pathway analysis

ISO, the International Organization for Standardization

LDH, lactate dehydrogenase

M-CSF, macrophage-colony stimulating factor

MEM, minimum essential medium

MMP, matrix metalloproteinase

MN, micronucleus

NA, not analyzed

NF κ B, nuclear factor-kappa B

Nrf2, nuclear factor erythroid 2-related factor 2

NRU, neutral red uptake

PBPK, physiologically based pharmacokinetics

PBS, phosphate-buffered saline

PEP, phosphoenolpyruvate

PM, particulate matter

PP, particulate phase

PPP, pentose phosphate pathway

R5P, ribose 5-phosphate

Ru5P, ribulose 5-phosphate

SCGB, secretoglobin

SD, standard deviation

Abbreviations

SMA, smooth muscle actin

TCA, tricarboxylic acid

TG, test guideline

TGF, transforming growth factor

TIMP, tissue inhibitor of metalloproteinase

TPM, total particulate matter

US, United States

VEGF, vascular endothelial growth factor

Chapter 1.

General introduction

1.1 Research background

1.1.1 Inhalation toxicities of aerosols in a regulatory context

An aerosol means a suspension of fine solid or liquid particles in gas. Aerosols, such as diesel exhaust and particulate matter (PM) in the ambient air (e.g., PM with a diameter less than 2.5 μm is known as PM_{2.5}), are closely related to environmental deterioration and affect the quality of human life ¹⁻⁵. The inhalation toxicities of these aerosols are of global concern. Apart from air pollution, assessment of the inhalation toxicities of various chemicals and nanomaterials is necessary in the context of decision-making by regulatory authorities worldwide ⁶. For example, the European Union (EU) Registration, Evaluation, Authorization and Restriction of Chemicals implemented by the European Chemical Agency demands extensive safety testing, including inhalation toxicity testing of existing and new chemicals, before importation, use, or manufacture ⁷⁻⁹. In the case of nanomaterials, several legislation in the EU regulatory framework covers them explicitly or implicitly ¹⁰. Thus, risk assessment of inhalation exposure to nanomaterials is covered by existing legislation ^{11, 12}. Because nanomaterials are useful technology and relevant in many industries (e.g., chemicals, consumer products, and pharmaceuticals), their use is rapidly growing ^{13, 14}. Within this background, there is an urgent need for information on the inhalation toxicities of various chemicals and nanomaterials.

In vivo animal testing is the gold standard for assessment of inhalation toxicity ¹⁵. For example, the Organization for Economic Co-operation and Development test guidelines (TGs) provide standard protocols for acute (TG 403), sub-acute (TG 412; 28-day or 14-day study), and sub-chronic (TG 413; 90-day study) inhalation toxicity tests for identification and characterization of the hazards of various aerosols ¹⁶⁻¹⁸. However, animal testing is expensive and time-consuming. Moreover, the use of animals in experiments should be decreased according to accepted ethical standards for the regulation of animal experimentation described by the 3Rs (Replacement, Reduction, and Refinement) ¹⁹. Thus, the *in vitro* tests need to be developed as alternatives to animal experimentation for inhalation toxicity assessments ^{20, 21}.

This thesis describes the development of *in vitro* tests for evaluation of the toxicological effects of cigarette smoke (CS). Because CS is an aerosol, *in vitro* tests developed for evaluation of the inhalation toxicity of CS can also be utilized as alternatives to animal experimentation for assessments of inhalation exposure to other chemicals and nanomaterials.

1.1.2 Generation of CS and its aerosol properties

CS is a complex aerosol that reportedly contains thousands of chemicals²². The chemicals in whole mainstream CS are distributed in the particulate phase (PP) and gas/vapor phase (GVP) (Figure 1.1). The PP reportedly contains a high concentration of particles (up to 3×10^9 particles/cm³) with a count median diameter of 0.22 μm ^{23, 24}. The PP accounts for approximately 4.4% of the whole CS mass and is composed of water, nicotine, and tar, which contains various chemicals (Figure 1.2). The main components in whole CS are gaseous N₂ and O₂, which originate from inhaled air (Figure 1.2). The vapor phase accounts for approximately 5.5% of the whole CS mass and contains water and various other chemicals (Figure 1.2).

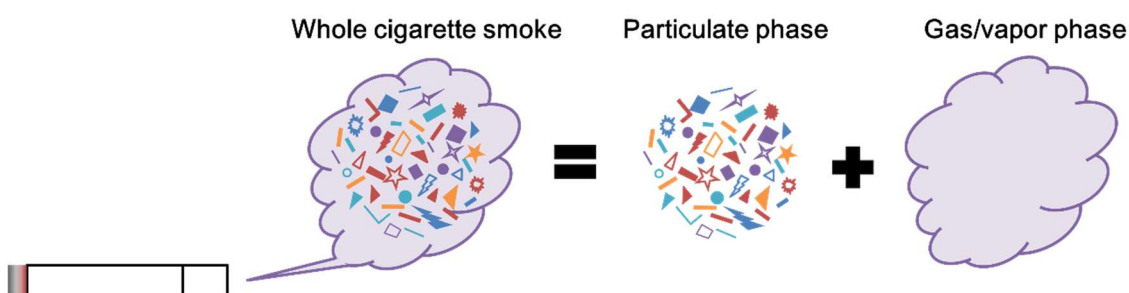


Figure 1.1 Phase composition of whole mainstream cigarette smoke.

Whole mainstream cigarette smoke is composed of particulate and gas/vapor phases.

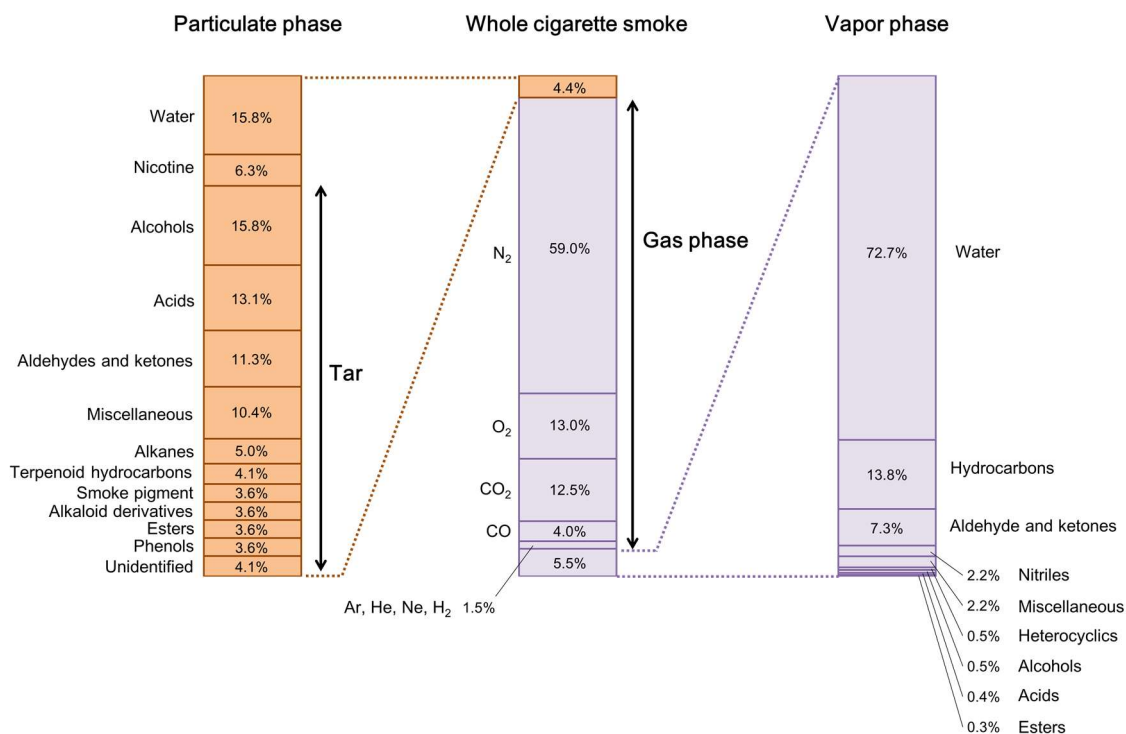


Figure 1.2 Approximate composition of whole mainstream cigarette smoke.

The values are expressed as percent weights (%). The data are reproduced from the literature ²⁵.

The chemicals in whole mainstream CS are generated within two zones in a burning cigarette: a combustion zone with sufficient oxygen supply and a pyrolysis zone without it. The majority of CS chemicals are generated in the pyrolysis zone through various mechanisms ^{26, 27}. The key elements of these processes (e.g., temperature, heating rate, oxygen level, and gas flow rate) are affected by the puffing behavior of the smoker (e.g. puff volume, puff duration, and puff interval). Consequently, the chemical composition of CS is dependent on smoking behavior ^{28, 29}. Therefore, several standard protocols for smoke generation have been developed for use with smoking machines to generate CS for chemical analyses and biological tests (Figure 1.3) ³⁰. Typical protocols are the International Organization for Standardization (ISO) standard smoking regime (35-mL puff volume, 60-s puff interval, 2-s puff duration, and no blocking of ventilation holes) and ISO intensive smoking regime (55-mL puff volume, 30-s puff interval, 2-s puff duration, and 100% blocking of ventilation holes) ³¹⁻³³. It is recommended by the World

Health Organization that governmental health authorities in each country should provide their data on tar, nicotine, and carbon monoxide content per cigarette under both the ISO standard and intensive smoking regimens³⁴. Therefore, biological tests for CS are also frequently performed with CS generated by both smoking regimes.

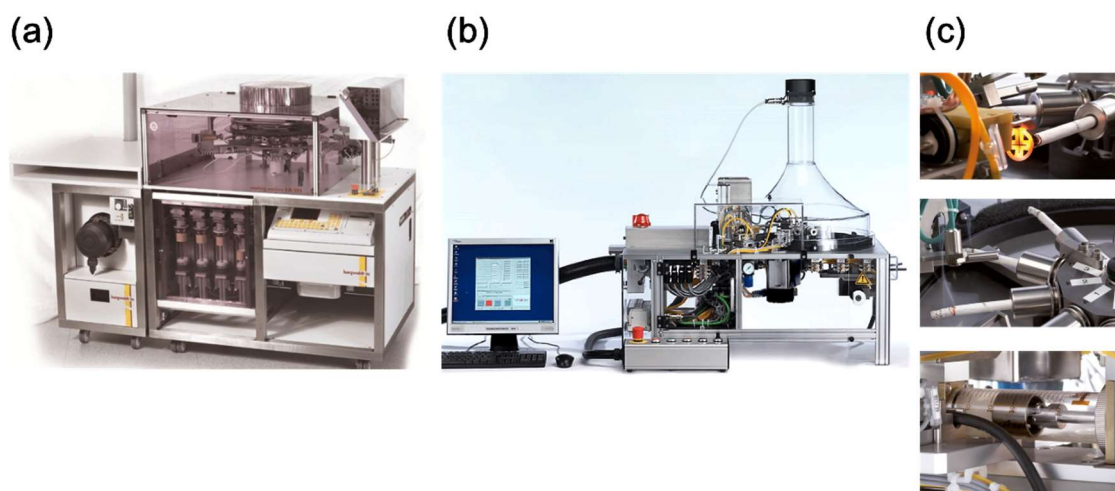


Figure 1.3 Smoking machines used for generation of whole mainstream cigarette smoke.

(a) The rotary Borgwaldt RM20S smoking machine (Borgwaldt KC GmbH, Hamburg, Germany). (b) The Vitrocell VC10 smoking robot (Vitrocell Systems GmbH, Waldkirch, Germany). (c) Enlarged views of the VC10 smoking robot. Cigarettes can be ignited by a computer-controlled lighter, and smoked by a computer-controlled smoking syringe with an appropriate smoking profile. These images are reproduced from the literature³⁰.

1.1.3 Harmful chemicals in CS and smoking-related lung disease

Several chemicals in CS reportedly have adverse health effects and are classed as harmful or potentially harmful constituents by the United States (US) Food and Drug Administration^{35, 36}. PP chemicals such as polycyclic aromatic hydrocarbons and tobacco-specific nitrosamines are reportedly related to the formation of various cancers including lung cancer³⁷⁻³⁹. GVP chemicals such as carbonyls are reportedly correlated with chronic obstructive pulmonary disease (COPD)⁴⁰. Based on epidemiological studies, smoking has been identified as a risk factor for these lung diseases^{41, 42}.

The main symptoms of COPD are shortness of breath, chronic coughing, sputum production, and wheezing (Figure 1.4). These symptoms are caused by two major phenotypic changes in the lungs: chronic bronchitis, which obstructs the airways; and emphysema, which destroys alveoli (Figure 1.4)^{43, 44}. Although obstruction of bronchi is caused by airway remodeling, this change includes various types of structural changes in bronchial tissue, such as goblet cell hyperplasia, squamous metaplasia, and subepithelial fibrosis (Figure 1.4). Phenotypically, lung cancer shows uncontrollable cell growth in the lung tissues and formation of malignant lung tumors^{43, 44}. Although epidemiological findings show that smoking is a risk factor, there are various other environmental factors, such as diet and genetic background, behind the development of COPD⁴⁵.

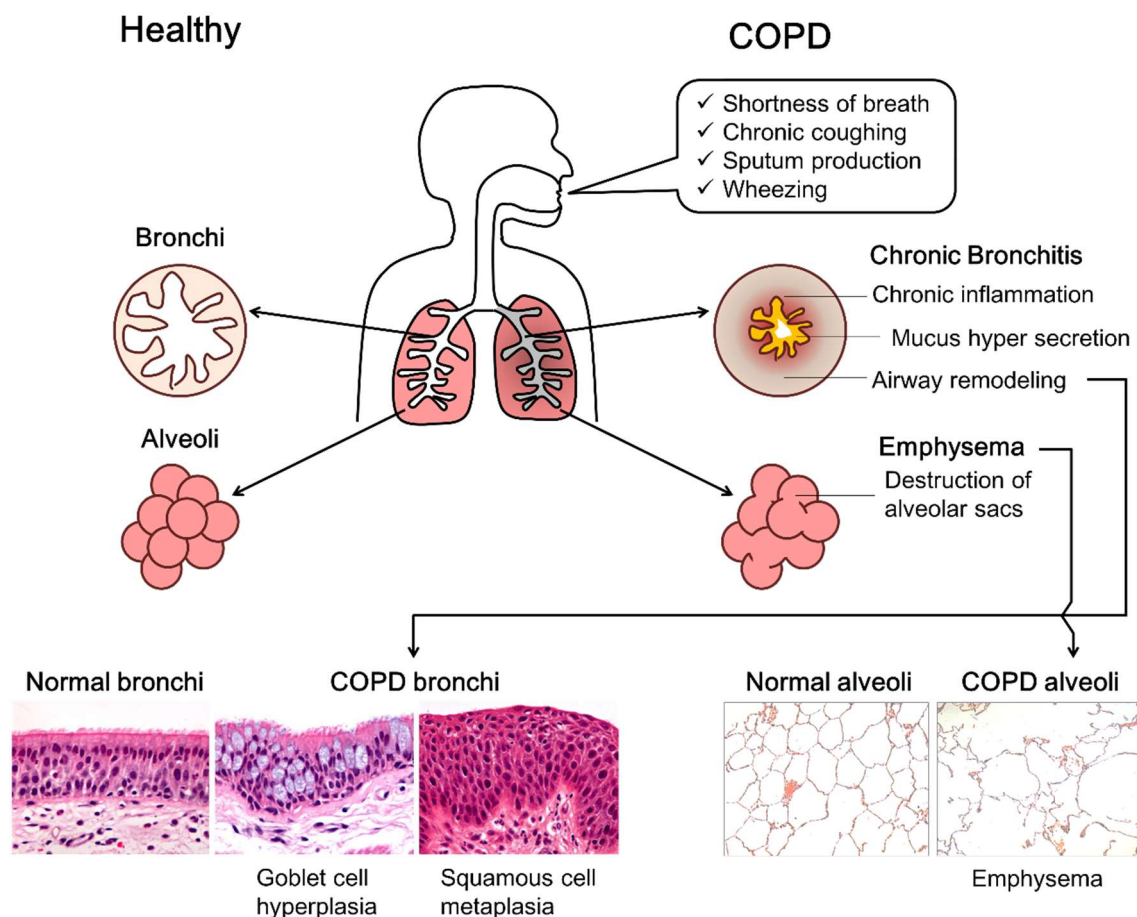


Figure 1.4 Symptoms and phenotypic changes observed in COPD patients.

The histological images are reproduced from the literature^{46, 47}. COPD, chronic obstructive pulmonary disease.

1.1.4 *In vivo* toxicity testing for CS

To complement epidemiological findings, various *in vivo* inhalation experiments have been performed to experimentally detect disease relevant changes in the lungs caused by CS exposure⁴⁸⁻⁵⁰. For *in vivo* inhalation experiments, CS generated by a smoking machine is directed into an exposure chamber that contains animals. Generally, rodents are used for *in vivo* inhalation testing in a nose-only exposure chamber or whole-body exposure chamber (Figure 1.5)^{30, 51, 52}. The advantage of *in vivo* testing is its availability for lifetime chronic exposure and the accessibility of various endpoints related to organ/organism responses. For example, measurements of breathing parameters and histological analysis of the lungs can reveal if COPD-like disease symptoms and phenotypes are induced in animals by CS exposure⁵³. Several *in vivo* inhalation experiments have revealed that CS exposure can induce phenotypic changes related to COPD (e.g., emphysema and airway remodeling) in rodents (Figure 1.5)⁵⁴⁻⁵⁶. Although *in vivo* testing enables detection of chronic effects arising from lifetime exposure of organisms to CS, there are interspecies differences between animals and humans, such as in their respiratory geometries and metabolic capacities^{57, 58}. These interspecies differences are sometimes problematic when interpreting *in vivo* results to determine human outcomes. This is apparent in drug development, where unexpected toxicological effects that were not detected in animal testing have been observed in clinical tests^{59, 60}. To overcome the issues associated with interspecies differences and decrease the use of animals in experiments, the development of an *in vitro* test system that is more relevant to humans is highly anticipated.

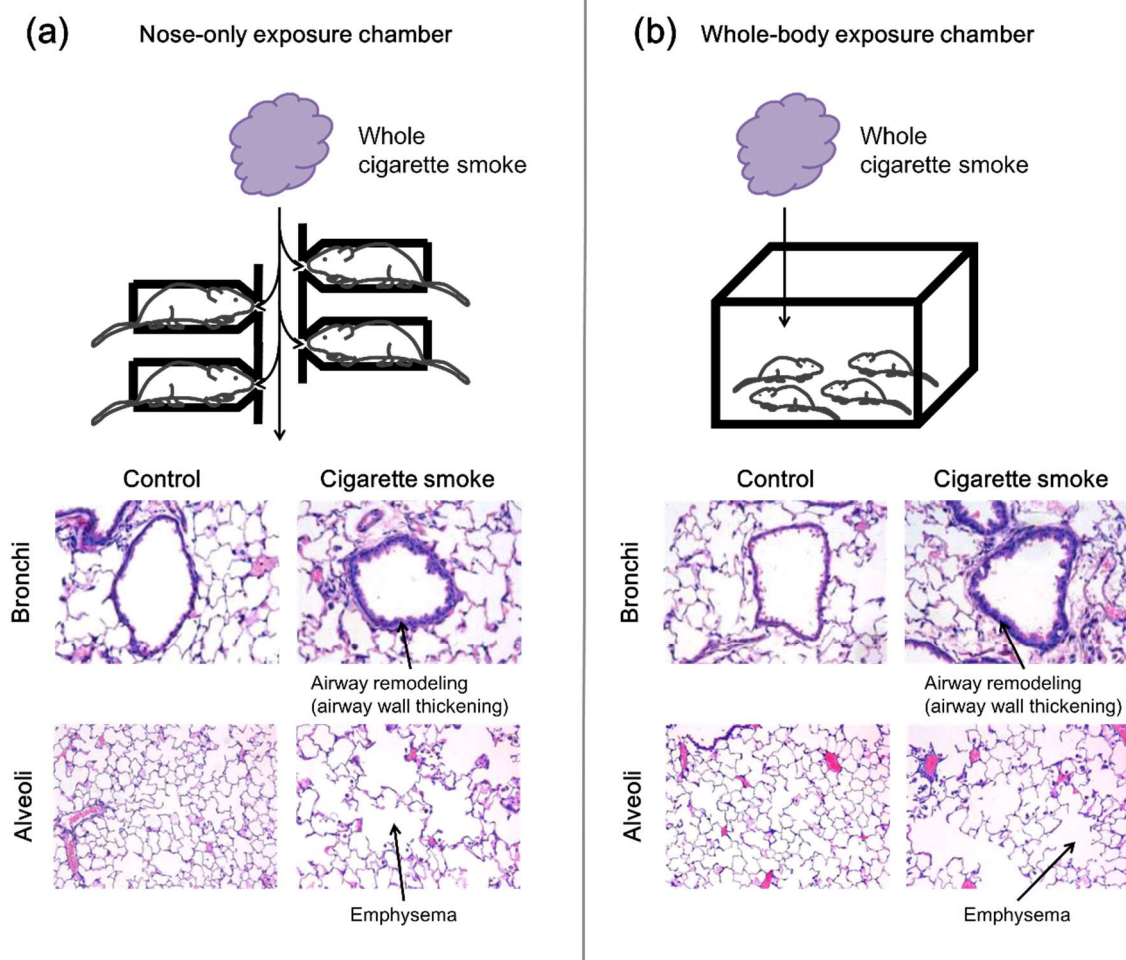


Figure 1.5 An aerosol exposure system for *in vivo* inhalation experiments with rodents.

(a) A nose-only exposure chamber. (b) A whole-body exposure chamber. The histological section images are reproduced from the literature⁶¹ and show induction of chronic obstructive pulmonary disease-like histological changes in mice exposed to whole cigarette smoke for 10 weeks, following lipopolysaccharides challenges.

1.1.5 Traditional *in vitro* toxicity testing for CS

In addition to *in vivo* tests, there are several established standard *in vitro* toxicological tests for evaluating the toxicological effects of CS. For *in vitro* tests, an aerosol extract of CS is used for exposure. Whole mainstream CS generated by a smoking machine can be passed through a glass filter to capture PP chemicals (Figure 1.6). The PP chemicals

trapped on the glass filter are referred to as total particulate matter (TPM). The captured TPM is extracted with an appropriate solvent, such as dimethyl sulfoxide, for the *in vitro* tests. GVP chemicals that pass through the glass filter can be bubbled into an appropriate solution, such as phosphate-buffered saline (PBS), in an impinger (Figure 1.6). The GVP solution can also be used for *in vitro* tests.

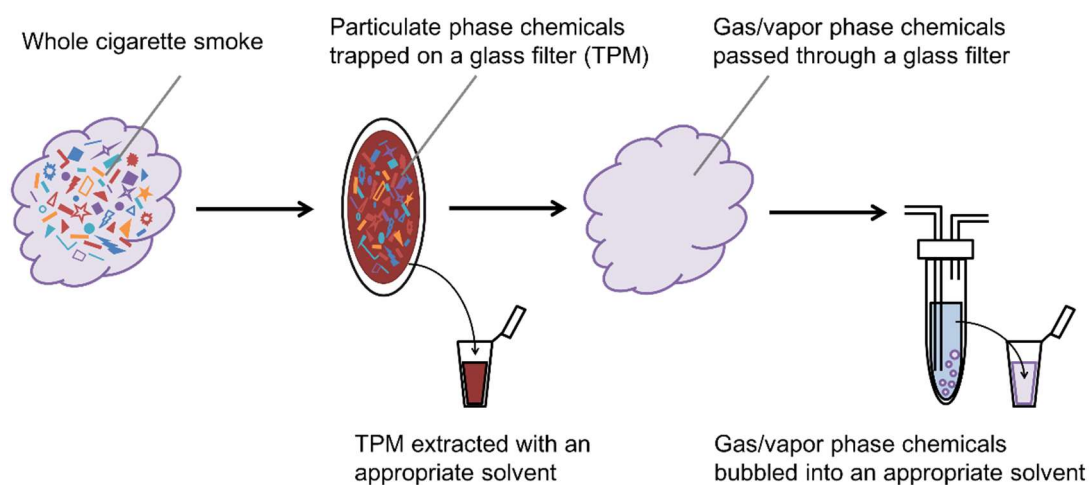


Figure 1.6 Schematic view of the preparation of a cigarette smoke extract.

Whole cigarette smoke captured on a glass filter is extracted with an appropriate solvent to prepare a total particulate matter (TPM) extract. Gas/vapor phase chemicals that pass through the filter are bubbled into an appropriate solvent to prepare a solution of these chemicals.

These CS extracts are added to a culture medium for exposure of animal or bacterial cells and their toxicological effects are analyzed (Figure 1.7). Various studies have indicated that CS extracts are cytotoxic and genotoxic⁶²⁻⁶⁵. Although these *in vitro* tests are undoubtedly useful, they have several limitations. For example, the Ames bacterial mutagenicity assay is the gold standard for identifying the genotoxicity of a chemical. However, Ames positive chemicals are not necessarily genotoxic *in vivo* and their genotoxicity should be examined further in rodents⁶⁶. Thus, an *in vitro* toxicological assay that could be used for detection of adverse effects on both the molecular/cellular

level and tissue/organ level, which usually requires an *in vivo* test, will be useful for evaluating the toxicological effects of CS.

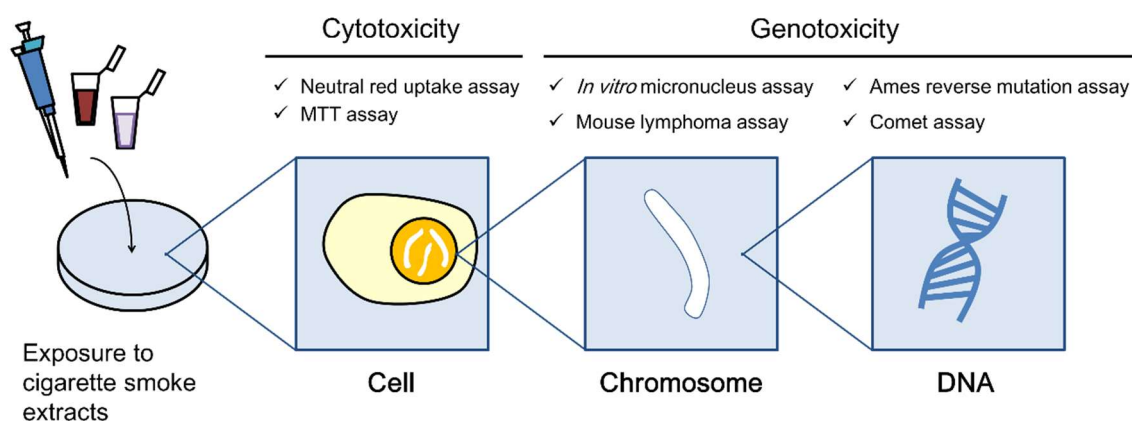


Figure 1.7 Standard *in vitro* test methods used with cigarette smoke extracts.

These assays can detect cytotoxicity towards cells and genotoxicity towards genetic material.

1.1.6 Development of a 3D culture model for *in vitro* inhalation toxicity testing

Apart from standard *in vitro* toxicological assay, various experiments have been performed to develop more advanced *in vitro* toxicological assays. The advancement of modern *in vitro* technology has enabled the use of human cells for toxicity testing. The use of human cell cultures in toxicological tests avoids issues with inter-species differences, which are of concern in animal testing. Moreover, the use of three-dimensional (3D) culture technology is gaining popularity in *in vitro* experiments^{67, 68}. Various human tissues have been developed as 3D culture models using human cells, and these models are distinct from traditional cell culture models because they allow for reproduction of physiological cell–cell contact, cell–extracellular matrix (ECM) contact, co-culturing of multiple types of cells, and cell differentiation observed in actual human tissue⁶⁹⁻⁷¹. Thus, it is expected that 3D culture models could be used as *in vitro* test systems for detection of toxicological effects on the human tissue/organ level, which is

not possible with traditional *in vitro* toxicological assays⁷²⁻⁷⁴. The application of several 3D culture models in toxicological testing is already in practice. Skin corrosion, skin irritation, and eye irritation tests with 3D models have been validated and adopted as OECD TGs^{75, 76}.

In the field of respiratory toxicology, several *in vitro* models of the human respiratory system have been developed²¹. The human respiratory tree branches dichotomously and has a complex structure (Figure 1.8a). Among the various *in vitro* lung models, the 3D culture model composed of primary human bronchial epithelial cells (HBECs) is most commonly used. HBECs isolated from human tissue are expanded in a culture flask and then seeded onto a porous membrane of a cell culture insert for an air–liquid interface (ALI) culture (Figure 1.8b). This culture method enables HBEC growth under human physiologically relevant conditions (i.e., supply of the medium from the bottom of the porous membrane, and the cells facing the air) and differentiation of pseudostratified bronchial epithelial tissue containing goblet cells and ciliated cells (Figure 1.8c)⁷⁷⁻⁷⁹. This 3D culture model of the human bronchial epithelium has some xenobiotic metabolic and mucus-producing capacity in actual human tissue⁸⁰⁻⁸⁴. Although there is no validated method, it is expected this model could be used as an alternative to animal experimentation in inhalation toxicity testing⁸⁵⁻⁸⁷.

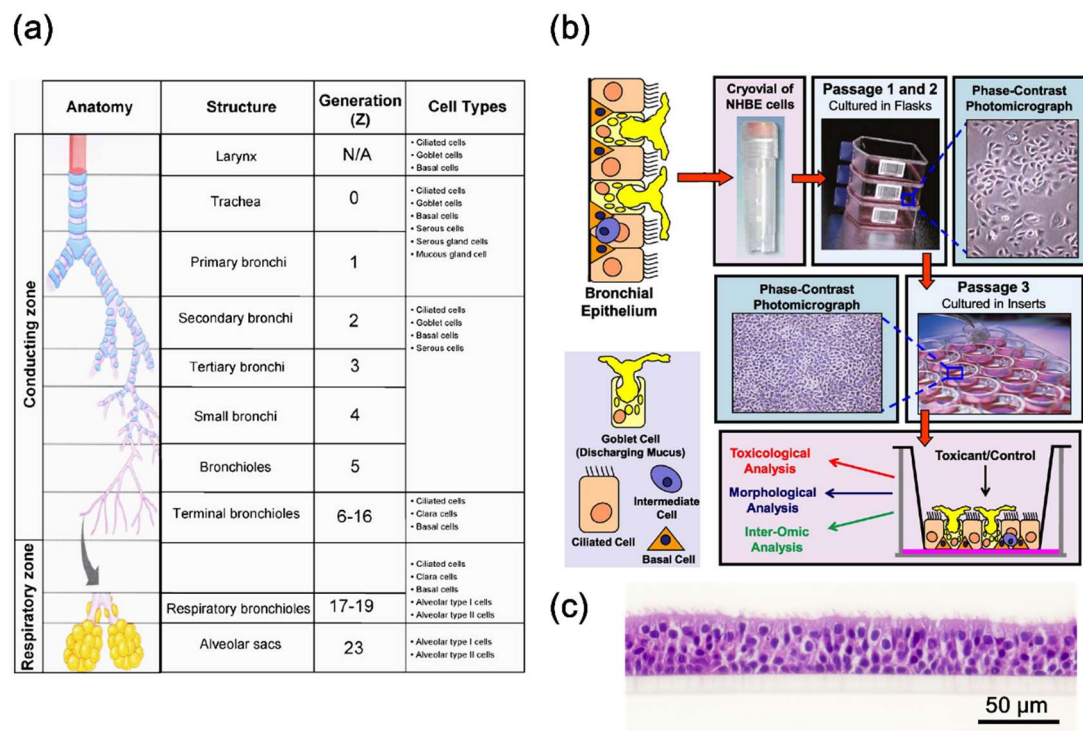


Figure 1.8 Illustration of the human respiratory system and the 3D culture model of human bronchial epithelium.

(a) The human respiratory system can be divided into several structures and branching patterns, and each structure contains different types of cells. (b) The workflow to generate a 3D culture model of human bronchial epithelium. Tracheobronchial epithelial cells can be isolated and seeded onto a culture insert. After an air–liquid interface culture, the cells can be differentiated into bronchial epithelium containing basal cells, ciliated cells, and goblet cells. (c) Histological section of a 3D culture model of human bronchial epithelium. The data, diagrams, and images in (a) and (b) were reproduced from the literature ⁷⁹.

1.1.7 Development of a whole CS exposure system for *in vitro* inhalation toxicity testing

In addition to cellular technology, *in vitro* aerosol exposure technology has also been advancing ⁸⁸. As mentioned previously, CS extracts are generally used for *in vitro* exposure experiments (Figure 1.7). However, there are several concerns about the use of CS extracts, including re-evaporation of trapped chemicals from extracts, chemical

reaction during the extraction process, loss of information about aerosol properties such as the particle diameter, and the inability to extract water insoluble GVP chemicals. To overcome these concerns, a system that enables direct exposure of cells to whole mainstream CS has been developed³⁰. This system is called a whole CS exposure system and its main components are a smoking machine and exposure module. The whole CS exposure systems from Cultex Technology GmbH (Hannover, Germany) and Vitrocell Systems GmbH are widely used in tobacco research^{89, 90} (Figure 1.9a and b). There are several types of exposure modules, but all are used following the same basic protocol. First, ALI-cultured cells are placed in the exposure module, and then whole CS generated by a smoking machine is introduced (Figure 1.9c). Because the cells are exposed to fresh whole CS, this exposure method is expected to minimize changes in chemical composition and aerosol properties that could occur with extraction of CS. Aerosol properties such as particle size are reported to be important parameters in the toxicological profiles of aerosols⁹¹. Therefore, the use of a whole CS exposure system with standard *in vitro* tests (Figure 1.7) provides more reliable CS toxicity data than the use of CS extracts. Moreover, this exposure scenario is consistent with actual CS exposure in the human respiratory system. It is anticipated that the use of a whole CS exposure system with a 3D culture model of human bronchial epithelium will reproduce the actual *in vivo* exposure conditions and tissue composition.

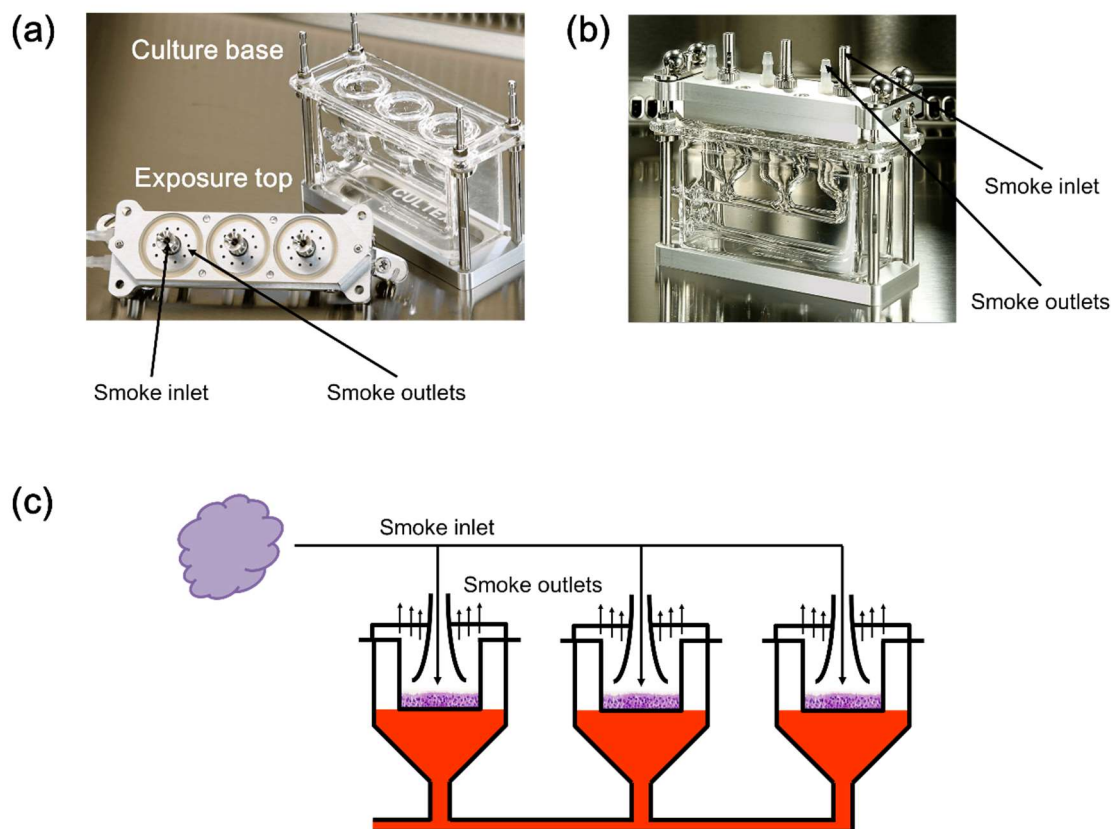


Figure 1.9 Whole cigarette smoke exposure modules from Cultex Technology GmbH and Vitrocell Systems GmbH.

(a) Glass culture base and a stainless steel exposure top. The exposure top has a central trumpet-shaped smoke inlet and smoke outlets arranged in a circle. (b) The culture base and exposure top are connected for exposure. (c) Schematic view of the set-up for whole cigarette smoke exposure. Three air–liquid interface culture cells are exposed to whole cigarette smoke introduced through the smoke inlet at a constant flow rate. The images in (a) and (b) are reproduced from the literature ^{30, 90}.

1.1.8 Whole CS exposure of 3D culture model of human bronchial epithelium

Several experiments were performed to develop alternatives to testing CS via animal inhalation using 3D culture models of human bronchial epithelium and whole CS exposure systems ⁹²⁻⁹⁸. Table 1.1 summarizes the study design and output. These experiments used the commercially available 3D culture models, MucilAir (Epithelix Sàrl, Geneva, Switzerland) and EpiAirway (MatTek, Ashland, MA, USA) composed of ALI-

cultured HBECs. MucilAir cultured with human fibroblasts (MucilAir-HF) was used in two experiments^{93, 94}. The results indicated that the expressions of genes related to oxidative stress responses and secretion of inflammation-related cytokines were perturbed after whole CS exposure⁹²⁻⁹⁸. The bronchial epithelium of COPD patients exhibits phenotypic changes such as goblet cell hyperplasia and squamous cell metaplasia (Figure 1.4). Therefore, the histology of a 3D bronchial epithelial model was analyzed in several experiments after whole CS exposure; however, no squamous cell metaplasia was reported (Table 1.1). In cases of goblet cell hyperplasia, only one experiment reported that local goblet cell numbers were slightly increased after CS exposure (Table 1.1). Other reports indicated that goblet cell numbers either decreased or remained the same after whole CS exposure (Table 1.1).

Table 1.1 Studies of whole CS exposure using 3D culture models of human bronchial epithelium

	3D culture model		Exposure conditions			Histological analysis	
	Name	Fibroblasts	Concentration	Duration	Repetition	Goblet cell	Squamous cell
Mathis et al. (2013)	EpiAirway	without	15%	7–28 min	1 day	-	-
Talikka et al. (2014)	MucilAir-HF	with	16.7%	24–28 min	1 day	Slight increase	-
Iskandar et al. (2015)	MucilAir-HF	with	8, 15%	28 min	1 day	-	-
Haswell et al. (2017)	MucilAir	without	3.3%	60 min	1 day	No change	-
Iskandar et al. (2017)	MucilAir	without	8, 15%	28 min	1 day	Decrease	-
Haswell et al. (2018)	MucilAir	without	3.3%	60 min	1 day	No change	-
Iskandar et al. (2018)	MucilAir	without	7, 13%	28 min	1 day	No change	-

Summary of data from previous publications⁹²⁻⁹⁸.

Phenotypic changes in the bronchial epithelium are important endpoints because they can cause airway obstruction in COPD patients (Figure 1.4). Therefore, reproducing these phenotypic changes in 3D bronchial epithelial models by whole CS exposure is important for developing human models for inhalation toxicology of CS as alternatives to animal testing. Reproducing these phenotypic changes may require co-culturing HBECs with fibroblasts, as several previous studies have indicated that this promotes goblet and

squamous cell differentiation of HBECs⁹⁹⁻¹⁰². Co-culturing MucilAir with fibroblasts (MucilAir-HF) slightly increased the goblet cell numbers after whole CS exposure (Table 1.1). Therefore, relevance of the human tissue composition (i.e., co-culturing with other cell types) should be increased to reproduce the phenotypic changes by whole CS exposure.

In addition to tissue composition, the relevance of studying humans under whole CS exposure conditions should be increased. *In vivo* experiments showed that two weeks of CS exposure induced squamous cell metaplasia in rodents¹⁰³. Therefore, repeated whole CS exposure in 3D bronchial epithelial models may be required to induce phenotypic changes. However, in the reports summarized in Table 1.1, exposure was performed in one day (i.e., no repeated exposure) and histological analysis was performed within 72 hours after exposure. In these experiments, the amount of smoke delivered to the tissues was controlled by the CS concentration and exposure duration. However, these reports did not indicate whether the amount of CS delivered to the 3D bronchial epithelial models was equivalent to the amount of CS delivered to the actual human bronchial epithelia of smokers. To reproduce the phenotypic changes observed *in vivo*, actual bronchial epithelial doses should be reproduced by whole CS exposure.

1.2 Thesis outline

1.2.1 General objectives

CS is closely related to human life and its toxicological effects are of great concern. Because CS is a dynamic aerosol with a complex nature, its toxicological effects are also complex and related to various airway diseases. Therefore, *in vivo* inhalation studies have been conducted to understand its toxicological effects on organ/organism level. However, extrapolation of animal toxicity to humans is not simple because of interspecies differences. Moreover, the use of animals in experiments should be decreased according to the 3Rs principle. Therefore, as alternatives to *in vivo* inhalation studies, the development of *in vitro* test methods that can detect CS toxicity in human lungs is highly anticipated. Although *in vitro* tests have also been used to investigate toxicological effects

of CS, the traditional *in vitro* test methods are designed to detect specific molecular/cellular-level toxicity of CS, and it is difficult to detect complex CS toxicities in actual human airway tissue. The objective of this study was to develop an *in vitro* human model to study CS inhalation toxicology and detect the phenotypic changes observed in COPD patients to overcome the limitations of traditional *in vivo* and *in vitro* studies.

1.2.2 Study approaches

Various innovative technologies described in this chapter were used to improve the human relevance of traditional *in vitro* tests for CS from the viewpoints of the CS exposure method and *in vitro* assays (Figure 1.10). In the experiment described in Chapter 2, a whole CS exposure system was applied to a standard *in vitro* toxicological assay, the Ames reverse mutation assay, which is usually performed with CS extracts (Figure 1.10). Then, the whole CS exposure system was used to develop an advanced toxicological assay with 3D culture technology, as described in Chapters 3–6 (Figure 1.10). In Chapter 3, an original 3D culture model of human bronchial tissue, which consisted of a mucociliary differentiated epithelial and collagen-embedded fibroblast layers, was developed (Figure 1.11). Before applying this model to the whole CS exposure system, characterization of the newly developed whole CS exposure module (RFS module developed by Cultex Technology GmbH) was performed as described in Chapter 4 (Figure 1.11). The characterization was performed from the viewpoint of whether this exposure module can reproduce a whole CS exposure dose relevant to the actual human tissue dose. Then, whole CS exposure of the 3D bronchial tissue model was performed. The exposure was performed for two weeks at a dose similar to an actual smoker, and then the differentiation status (phenotypic changes) and inflammatory response of the tissue were analyzed as described in Chapter 5 (Figure 1.11). In the last experiment detailed in Chapter 6, the condition of the 3D bronchial tissue model after repeated whole CS exposure was comprehensively investigated by multiomics technologies (Figure 1.11). The omics technologies were used to clarify the mechanisms underlying CS-induced

changes in the 3D bronchial tissue model. A general summary and future perspectives are presented in Chapter 7.

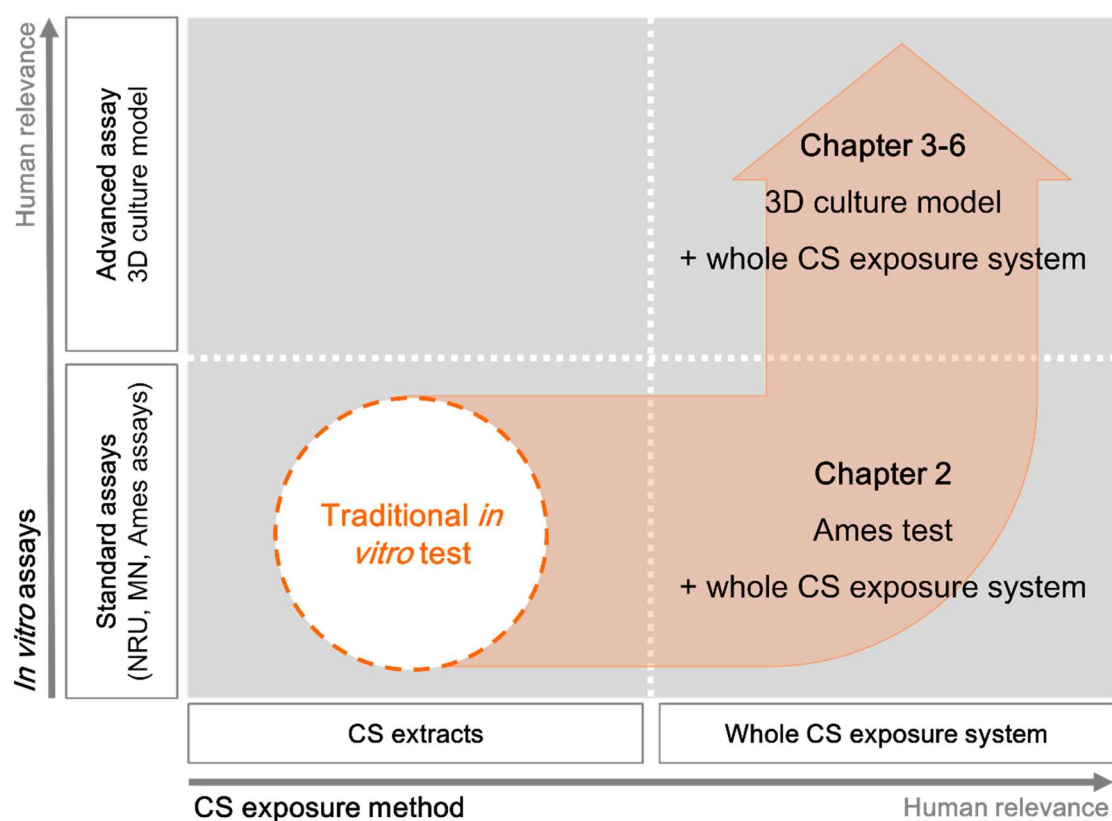


Figure 1.10 Conceptual framework of the thesis.

CS, cigarette smoke; MN, micronucleus; NRU, neutral red uptake.

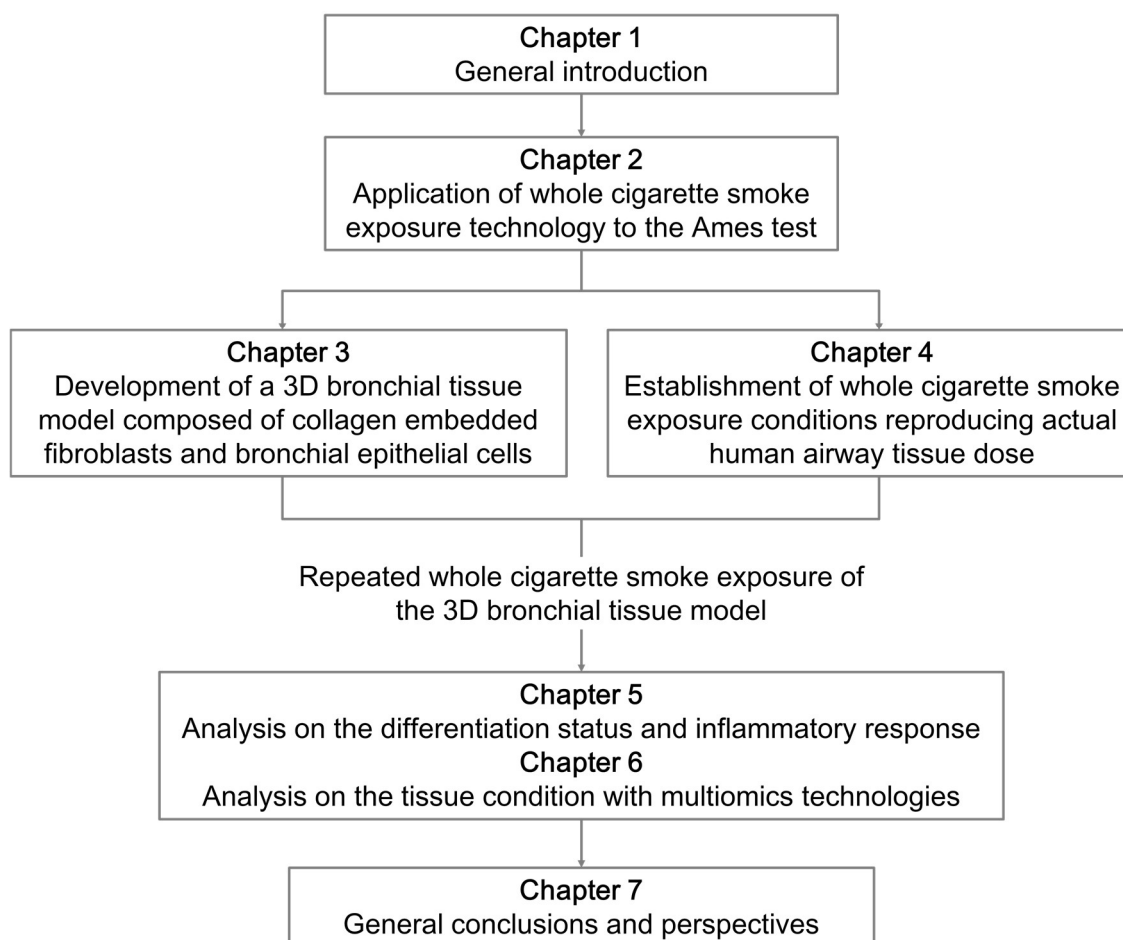


Figure 1.11 Workflow for Chapters 1–7.

1.3 References

1. Gauderman, W.J. *et al.* Association between air pollution and lung function growth in southern California children: results from a second cohort. *Am J Respir Crit Care Med* **166**, 76-84 (2002).
2. Gauderman, W.J. *et al.* Association between air pollution and lung function growth in southern California children. *Am J Respir Crit Care Med* **162**, 1383-1390 (2000).
3. Pope, C.A., 3rd *et al.* Lung cancer, cardiopulmonary mortality, and long-term exposure to fine particulate air pollution. *Jama* **287**, 1132-1141 (2002).
4. Riedl, M. & Diaz-Sanchez, D. Biology of diesel exhaust effects on respiratory function. *J Allergy Clin Immunol* **115**, 221-228; quiz 229 (2005).
5. Sydbom, A. *et al.* Health effects of diesel exhaust emissions. *Eur Respir J* **17**, 733-746 (2001).

6. Clippinger, A.J. *et al.* Alternative approaches for acute inhalation toxicity testing to address global regulatory and non-regulatory data requirements: An international workshop report. *Toxicol In Vitro* **48**, 53-70 (2018).
7. European Commission Regulation (EC) No 1907/2006 of the European Parliament and of the Council of 18 December 2006 concerning the Registration, Evaluation, Authorisation and Restriction of Chemicals (REACH), establishing a European Chemicals Agency, amending Directive 1999/45/EC and repealing Council Regulation (EEC) No 793/93 and Commission Regulation (EC) No 1488/94 as well as Council Directive 76/769/EEC and Commission Directives 91/155/EEC, 93/67/EEC, 93/105/EC and 2000/21/EC (2006).
8. Rovida, C. & Hartung, T. Re-evaluation of animal numbers and costs for in vivo tests to accomplish REACH legislation requirements for chemicals - a report by the transatlantic think tank for toxicology (t(4)). *Altex* **26**, 187-208 (2009).
9. Grindon, C. The new EU REACH regulation has finally been adopted: is this the end of the campaign trail... or just the beginning? *Altern Lab Anim* **35**, 239-242 (2007).
10. European Commission Second Regulatory Review on Nanomaterials. (2012).
11. Rauscher, H., Rasmussen, K. & Sokull - Klüttgen, B. Regulatory Aspects of Nanomaterials in the EU. *Chemie Ingenieur Technik* **89**, 224-231 (2017).
12. Schwirn, K., Tietjen, L. & Beer, I. Why are nanomaterials different and how can they be appropriately regulated under REACH? *Environmental Sciences Europe* **26**, 4 (2014).
13. Inshakova, E. & Inshakov, O. in MATEC web of conferences, Vol. 129 02013 (EDP Sciences, 2017).
14. Piccinno, F., Gottschalk, F., Seeger, S. & Nowack, B. Industrial production quantities and uses of ten engineered nanomaterials in Europe and the world. *Journal of Nanoparticle Research* **14**, 1109 (2012).
15. Arts, J.H. *et al.* Inhalation toxicity studies: OECD guidelines in relation to REACH and scientific developments. *Exp Toxicol Pathol* **60**, 125-133 (2008).
16. Organisation for Economic Co-operation and Development Test No. 412: Subacute Inhalation Toxicity: 28-Day Study. (1981).
17. Organisation for Economic Co-operation and Development Test No. 403: Acute Inhalation Toxicity. (1981).
18. Organisation for Economic Co-operation and Development Test No. 413: Subchronic Inhalation Toxicity: 90-day Study. (1981).
19. Russell, W.M.S. & Burch, R.L. *The principles of humane experimental technique*, Vol. 238. (Methuen London, 1959).
20. BeruBe, K.A. Alternatives for lung research: stuck between a rat and a hard place. *Altern Lab Anim* **39**, 121-130 (2011).

21. BeruBe, K. *et al.* In vitro models of inhalation toxicity and disease. The report of a FRAME workshop. *Altern Lab Anim* **37**, 89-141 (2009).
22. Rodgman, A. & Perfetti, T.A. *The chemical components of tobacco and tobacco smoke*. (CRC press, 2016).
23. Chen, B., Namenyi, J., Yeh, H., Mauderly, J. & Cuddihy, R. Physical characterization of cigarette smoke aerosol generated from a Walton smoke machine. *Aerosol Science and Technology* **12**, 364-375 (1990).
24. Davies, C. Cigarette smoke: generation and properties of the aerosol. *Journal of aerosol science* **19**, 463-469 (1988).
25. Perfetti, T.A. & Rodgman, A. The complexity of tobacco and tobacco smoke. *Beiträge zur Tabakforschung International/Contributions to Tobacco Research* **24**, 215-232 (2011).
26. Baker, R.R. & Bishop, L.J. The pyrolysis of tobacco ingredients. *Journal of analytical and applied pyrolysis* **71**, 223-311 (2004).
27. Baker, R.R., Massey, E.D. & Smith, G. An overview of the effects of tobacco ingredients on smoke chemistry and toxicity. *Food Chem Toxicol* **42 Suppl**, S53-83 (2004).
28. Marian, C. *et al.* Reconciling human smoking behavior and machine smoking patterns: implications for understanding smoking behavior and the impact on laboratory studies. *Cancer Epidemiol Biomarkers Prev* **18**, 3305-3320 (2009).
29. Matsumoto, M. *et al.* Smoking topography and biomarkers of exposure among Japanese smokers: associations with cigarette emissions obtained using machine smoking protocols. *Environ Health Prev Med* **18**, 95-103 (2013).
30. Klus, H., Boenke-Nimphius, B. & Müller, L. Cigarette mainstream smoke: The evolution of methods and devices for generation, exposure and collection. *Beiträge Zur Tabakforschung International/contributions to Tobacco Research* **27**, 137-274 (2016).
31. Health Canada T115: Determination of 'Tar', Nicotine and Carbon Monoxide in Mainstream Tobacco Smoke. (1999).
32. International Organization for Standardization ISO 20778: Routine Analytical Cigarette Smoking Machine — Definitions and Standard Conditions with an Intense Smoking Regime. (2018).
33. International Organization for Standardization ISO 3308: Routine Analytical Cigarette Smoking Machine — Definitions and Standard Conditions. (2012).
34. World Health Organization Guiding Principles for the Development of Tobacco Product Research and Testing Capacity and Proposed Protocols for the Initiation of Tobacco Product Testing. (2005).
35. Oldham, M.J., DeSoi, D.J., Rimmer, L.T., Wagner, K.A. & Morton, M.J. Insights from analysis for harmful and potentially harmful constituents (HPHCs) in tobacco products. *Regul Toxicol Pharmacol* **70**, 138-148 (2014).

36. The US Food and Drug Administration Harmful and Potentially Harmful Constituents in Tobacco Products and Tobacco Smoke: Established List. (2012).
37. Hoffmann, D. & Hoffmann, I. The changing cigarette, 1950-1995. *J Toxicol Environ Health* **50**, 307-364 (1997).
38. International Agency for Research on Cancer Smokeless Tobacco and Some Tobacco-specific N-Nitrosamines. *IARC Monographs on the Evaluation of Carcinogenic Risks to Humans* **89** (2007).
39. International Agency for Research on Cancer Some Non-heterocyclic Polycyclic Aromatic Hydrocarbons and Some Related Exposures. *IARC Monographs on the Evaluation of Carcinogenic Risks to Humans* **92** (2010).
40. Yao, H. & Rahman, I. Current concepts on oxidative/carbonyl stress, inflammation and epigenetics in pathogenesis of chronic obstructive pulmonary disease. *Toxicol Appl Pharmacol* **254**, 72-85 (2011).
41. National Center for Chronic Disease, P., Health Promotion Office on, S. & Health Reports of the Surgeon General, in *The Health Consequences of Smoking-50 Years of Progress: A Report of the Surgeon General* (Centers for Disease Control and Prevention (US), Atlanta (GA); 2014).
42. Fukuchi, Y. *et al.* COPD in Japan: the Nippon COPD Epidemiology study. *Respirology* **9**, 458-465 (2004).
43. Durham, A.L. & Adcock, I.M. The relationship between COPD and lung cancer. *Lung Cancer* **90**, 121-127 (2015).
44. Houghton, A.M. Mechanistic links between COPD and lung cancer. *Nat Rev Cancer* **13**, 233-245 (2013).
45. Eisner, M.D. *et al.* An official American Thoracic Society public policy statement: Novel risk factors and the global burden of chronic obstructive pulmonary disease. *Am J Respir Crit Care Med* **182**, 693-718 (2010).
46. Higham, A., Quinn, A.M., Cancado, J.E.D. & Singh, D. The pathology of small airways disease in COPD: historical aspects and future directions. *Respir Res* **20**, 49 (2019).
47. Randell, S.H. Airway epithelial stem cells and the pathophysiology of chronic obstructive pulmonary disease. *Proc Am Thorac Soc* **3**, 718-725 (2006).
48. Coggins, C.R. A review of chronic inhalation studies with mainstream cigarette smoke in rats and mice. *Toxicol Pathol* **26**, 307-314; discussion 315 (1998).
49. Coggins, C.R. A review of chronic inhalation studies with mainstream cigarette smoke, in hamsters, dogs, and nonhuman primates. *Toxicol Pathol* **29**, 550-557 (2001).
50. Coggins, C.R. A minireview of chronic animal inhalation studies with mainstream cigarette smoke. *Inhal Toxicol* **14**, 991-1002 (2002).
51. Phalen, R.F., Mannix, R.C. & Drew, R.T. Inhalation exposure methodology. *Environ Health Perspect* **56**, 23-34 (1984).

52. Wong, B.A. Inhalation exposure systems: design, methods and operation. *Toxicol Pathol* **35**, 3-14 (2007).
53. Lo Sasso, G. *et al.* The Apoe(-/-) mouse model: a suitable model to study cardiovascular and respiratory diseases in the context of cigarette smoke exposure and harm reduction. *J Transl Med* **14**, 146 (2016).
54. Martorana, P.A., Beume, R., Lucattelli, M., Wollin, L. & Lungarella, G. Roflumilast fully prevents emphysema in mice chronically exposed to cigarette smoke. *Am J Respir Crit Care Med* **172**, 848-853 (2005).
55. Shapiro, S.D. *et al.* Neutrophil elastase contributes to cigarette smoke-induced emphysema in mice. *Am J Pathol* **163**, 2329-2335 (2003).
56. Shen, L.L. *et al.* Inhalation of glycopyrronium inhibits cigarette smoke-induced acute lung inflammation in a murine model of COPD. *Int Immunopharmacol* **18**, 358-364 (2014).
57. Reczynska, K. *et al.* Animal models of smoke inhalation injury and related acute and chronic lung diseases. *Adv Drug Deliv Rev* **123**, 107-134 (2018).
58. Martignoni, M., Groothuis, G.M. & de Kanter, R. Species differences between mouse, rat, dog, monkey and human CYP-mediated drug metabolism, inhibition and induction. *Expert Opin Drug Metab Toxicol* **2**, 875-894 (2006).
59. Olson, H. *et al.* Concordance of the toxicity of pharmaceuticals in humans and in animals. *Regul Toxicol Pharmacol* **32**, 56-67 (2000).
60. Voisin, E.M., Ruthsatz, M., Collins, J.M. & Hoyle, P.C. Extrapolation of animal toxicity to humans: interspecies comparisons in drug development. *Regul Toxicol Pharmacol* **12**, 107-116 (1990).
61. Shu, J. *et al.* Comparison and evaluation of two different methods to establish the cigarette smoke exposure mouse model of COPD. *Sci Rep* **7**, 15454 (2017).
62. Bombick, D.W., Putnam, K. & Doolittle, D.J. Comparative cytotoxicity studies of smoke condensates from different types of cigarettes and tobaccos. *Toxicol In Vitro* **12**, 241-249 (1998).
63. Johnson, M.D., Schilz, J., Djordjevic, M.V., Rice, J.R. & Shields, P.G. Evaluation of in vitro assays for assessing the toxicity of cigarette smoke and smokeless tobacco. *Cancer Epidemiol Biomarkers Prev* **18**, 3263-3304 (2009).
64. Bombick, D.W. *et al.* Evaluation of the genotoxic and cytotoxic potential of mainstream whole smoke and smoke condensate from a cigarette containing a novel carbon filter. *Fundam Appl Toxicol* **39**, 11-17 (1997).
65. Andreoli, C., Gigante, D. & Nunziata, A. A review of in vitro methods to assess the biological activity of tobacco smoke with the aim of reducing the toxicity of smoke. *Toxicol In Vitro* **17**, 587-594 (2003).

66. Nohmi, T. Past, present and future directions of gpt delta rodent gene mutation assays. *Food Safety* **4**, 1-13 (2016).
67. van Duinen, V., Trietsch, S.J., Joore, J., Vulto, P. & Hankemeier, T. Microfluidic 3D cell culture: from tools to tissue models. *Curr Opin Biotechnol* **35**, 118-126 (2015).
68. Simian, M. & Bissell, M.J. Organoids: A historical perspective of thinking in three dimensions. *J Cell Biol* **216**, 31-40 (2017).
69. Tibbitt, M.W. & Anseth, K.S. Hydrogels as extracellular matrix mimics for 3D cell culture. *Biotechnol Bioeng* **103**, 655-663 (2009).
70. Rossi, G., Manfrin, A. & Lutolf, M.P. Progress and potential in organoid research. *Nat Rev Genet* **19**, 671-687 (2018).
71. Gambara, G., Gaebler, M., Keilholz, U., Regenbrecht, C.R.A. & Silvestri, A. From Chemotherapy to Combined Targeted Therapeutics: In Vitro and in Vivo Models to Decipher Intra-tumor Heterogeneity. *Front Pharmacol* **9**, 77 (2018).
72. Sun, T., Jackson, S., Haycock, J.W. & MacNeil, S. Culture of skin cells in 3D rather than 2D improves their ability to survive exposure to cytotoxic agents. *J Biotechnol* **122**, 372-381 (2006).
73. Schaaf, S. *et al.* Human engineered heart tissue as a versatile tool in basic research and preclinical toxicology. *PLoS One* **6**, e26397 (2011).
74. Mazzoleni, G., Di Lorenzo, D. & Steimberg, N. Modelling tissues in 3D: the next future of pharmaco-toxicology and food research? *Genes Nutr* **4**, 13-22 (2009).
75. Lee, M., Hwang, J.H. & Lim, K.M. Alternatives to In Vivo Draize Rabbit Eye and Skin Irritation Tests with a Focus on 3D Reconstructed Human Cornea-Like Epithelium and Epidermis Models. *Toxicol Res* **33**, 191-203 (2017).
76. Eskes, C. *et al.* Regulatory assessment of in vitro skin corrosion and irritation data within the European framework: Workshop recommendations. *Regul Toxicol Pharmacol* **62**, 393-403 (2012).
77. Fulcher, M.L., Gabriel, S., Burns, K.A., Yankaskas, J.R. & Randell, S.H. Well-differentiated human airway epithelial cell cultures. *Methods Mol Med* **107**, 183-206 (2005).
78. Carsin, A. *et al.* Bronchial epithelium in children: a key player in asthma. *Eur Respir Rev* **25**, 158-169 (2016).
79. Berube, K., Prytherch, Z., Job, C. & Hughes, T. Human primary bronchial lung cell constructs: the new respiratory models. *Toxicology* **278**, 311-318 (2010).
80. Baxter, A. *et al.* Targeted omics analyses, and metabolic enzyme activity assays demonstrate maintenance of key mucociliary characteristics in long term cultures of reconstituted human airway epithelia. *Toxicol In Vitro* **29**, 864-875 (2015).
81. Hill, D.B. & Button, B. Establishment of respiratory air-liquid interface cultures and their use in studying mucin production, secretion, and function. *Methods Mol Biol* **842**, 245-258 (2012).

82. Kesimer, M. *et al.* Tracheobronchial air-liquid interface cell culture: a model for innate mucosal defense of the upper airways? *Am J Physiol Lung Cell Mol Physiol* **296**, L92-L100 (2009).
83. Tarran, R., Grubb, B.R., Gatzky, J.T., Davis, C.W. & Boucher, R.C. The relative roles of passive surface forces and active ion transport in the modulation of airway surface liquid volume and composition. *J Gen Physiol* **118**, 223-236 (2001).
84. Boei, J. *et al.* Xenobiotic metabolism in differentiated human bronchial epithelial cells. *Arch Toxicol* **91**, 2093-2105 (2017).
85. Clippinger, A.J. *et al.* Pathway-based predictive approaches for non-animal assessment of acute inhalation toxicity. *Toxicol In Vitro* **52**, 131-145 (2018).
86. Lacroix, G. *et al.* Air-liquid interface in vitro models for respiratory toxicology research: Consensus workshop and recommendations. *Applied in vitro toxicology* **4**, 91-106 (2018).
87. Upadhyay, S. & Palmberg, L. Air-Liquid Interface: Relevant In Vitro Models for Investigating Air Pollutant-Induced Pulmonary Toxicity. *Toxicol Sci* **164**, 21-30 (2018).
88. Bakand, S. & Hayes, A. Troubleshooting methods for toxicity testing of airborne chemicals in vitro. *J Pharmacol Toxicol Methods* **61**, 76-85 (2010).
89. Li, X. In vitro toxicity testing of cigarette smoke based on the air-liquid interface exposure: A review. *Toxicol In Vitro* **36**, 105-113 (2016).
90. Thorne, D. & Adamson, J. A review of in vitro cigarette smoke exposure systems. *Exp Toxicol Pathol* **65**, 1183-1193 (2013).
91. Gliga, A.R., Skoglund, S., Wallinder, I.O., Fadeel, B. & Karlsson, H.L. Size-dependent cytotoxicity of silver nanoparticles in human lung cells: the role of cellular uptake, agglomeration and Ag release. *Part Fibre Toxicol* **11**, 11 (2014).
92. Mathis, C. *et al.* Human bronchial epithelial cells exposed in vitro to cigarette smoke at the air-liquid interface resemble bronchial epithelium from human smokers. *Am J Physiol Lung Cell Mol Physiol* **304**, L489-503 (2013).
93. Talikka, M. *et al.* The response of human nasal and bronchial organotypic tissue cultures to repeated whole cigarette smoke exposure. *Int J Toxicol* **33**, 506-517 (2014).
94. Iskandar, A.R. *et al.* Impact Assessment of Cigarette Smoke Exposure on Organotypic Bronchial Epithelial Tissue Cultures: A Comparison of Mono-Culture and Coculture Model Containing Fibroblasts. *Toxicol Sci* **147**, 207-221 (2015).
95. Haswell, L.E. *et al.* Reduced biological effect of e-cigarette aerosol compared to cigarette smoke evaluated in vitro using normalized nicotine dose and RNA-seq-based toxicogenomics. *Sci Rep* **7**, 888 (2017).
96. Iskandar, A.R. *et al.* A systems toxicology approach for comparative assessment: Biological impact of an aerosol from a candidate modified-risk tobacco product and cigarette smoke on human organotypic bronchial epithelial cultures. *Toxicol In Vitro* **39**, 29-51 (2017).

97. Haswell, L.E. *et al.* In vitro RNA-seq-based toxicogenomics assessment shows reduced biological effect of tobacco heating products when compared to cigarette smoke. *Sci Rep* **8**, 1145 (2018).
98. Iskandar, A.R. *et al.* Comparative biological impacts of an aerosol from carbon-heated tobacco and smoke from cigarettes on human respiratory epithelial cultures: A systems toxicology assessment. *Food Chem Toxicol* **115**, 109-126 (2018).
99. Araya, J. *et al.* Squamous metaplasia amplifies pathologic epithelial-mesenchymal interactions in COPD patients. *J Clin Invest* **117**, 3551-3562 (2007).
100. Kobayashi, K. *et al.* Effect of fibroblasts on tracheal epithelial regeneration in vitro. *Tissue Eng* **12**, 2619-2628 (2006).
101. Nomoto, Y. *et al.* Effect of fibroblasts on epithelial regeneration on the surface of a bioengineered trachea. *Ann Otol Rhinol Laryngol* **117**, 59-64 (2008).
102. Vermeer, P.D., Panko, L., Karp, P., Lee, J.H. & Zabner, J. Differentiation of human airway epithelia is dependent on erbB2. *Am J Physiol Lung Cell Mol Physiol* **291**, L175-180 (2006).
103. Tsuji, H. *et al.* Comparison of mouse strains and exposure conditions in acute cigarette smoke inhalation studies. *Inhal Toxicol* **23**, 602-615 (2011).

Chapter 2.

Whole CS exposure for the Ames test

2.1 Introduction

2.1.1 Objectives

Various *in vitro* tests have been developed for initial screening of pharmaceuticals and chemicals¹⁻³. These tests have also been used to evaluate the toxicological effects of CS extracts (Figure 1.7)⁴⁻⁶. Previously, the whole CS exposure system has been applied to neutral red uptake and *in vitro* micronucleus assays to detect cytotoxicity and genotoxicity, respectively^{7,8}. In addition to these assays, the Ames reverse mutation assay has been widely used to detect the mutagenic potential of CS for more than 40 years⁹ (Figure 2.1). These three tests are the standard *in vitro* tests to investigate the biological effects of CS^{4,5}. The objective of this chapter was to apply whole CS exposure technology to the Ames test.

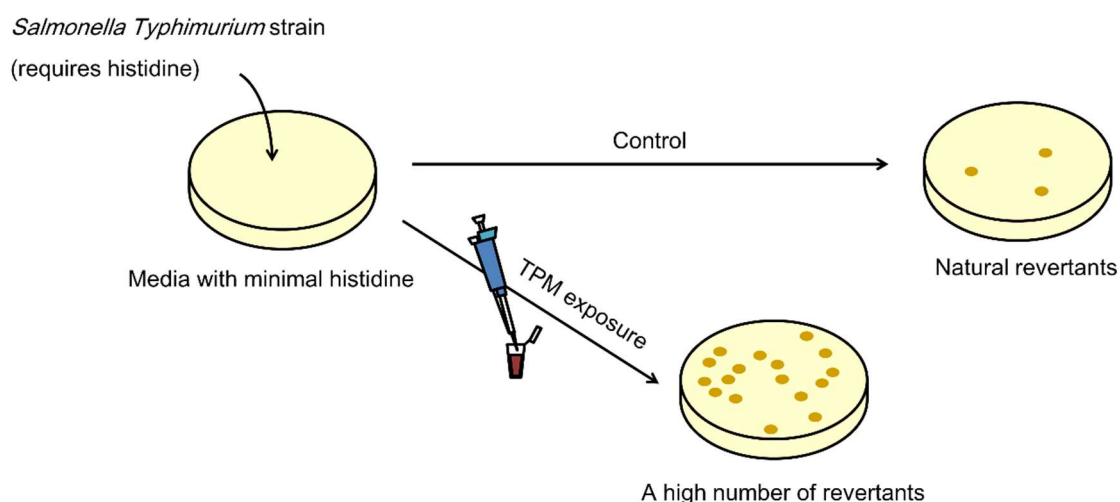


Figure 2.1 A schematic view of the Ames reverse mutation assay.

When *Salmonella typhimurium* is exposed to mutagenic chemicals such as total particulate matter (TPM) from cigarette smoke, the bacteria can be grown even under minimal histidine conditions because of mutation. The mutagenicity is distinguished by the number of colonies growing on the plate, which indicates the number of revertants.

2.1.2 Study approaches

In this chapter, Ames tests were performed using a Vitrocell whole CS exposure system for the Ames test ¹⁰. There are three functional steps with this system: generation of CS with a smoking machine, dilution of CS with air in a tunnel, and exposure of cells to the CS in a specially designed module (Figure 2.2). The whole CS exposure with the Ames test procedure was performed with three different test cigarettes that generated similar levels of TPM under the ISO standard regime and with four different test cigarettes that generated similar levels of TPM generation the ISO intensive regime. The CS generated from each test cigarette was diluted to four different dilutions with air to control the exposure dose. Petri dishes, containing air–agar interface cultured *Salmonella typhimurium* TA98 or TA100 cells, were placed in the exposure module and exposed to diluted whole CS in a constant flow of air (Figure 2.3). Then, the numbers of revertants induced in the TA98 and TA100 cells by whole CS from the different test cigarettes were compared. The TA98 and TA100 cells were used as standard Ames test strains to detect frameshift mutations and base-pair substitutions, respectively ¹¹. Exposure of the cells was performed under metabolically activated conditions with addition of a S9 mixture, and under unactivated conditions. Several chemical constituents in CS, such as benzo[a]pyrene, require metabolic activation before reaction with DNA as an essential step in exertion of their mutagenic effects ¹². The experimental conditions are summarized in Table 2.1.

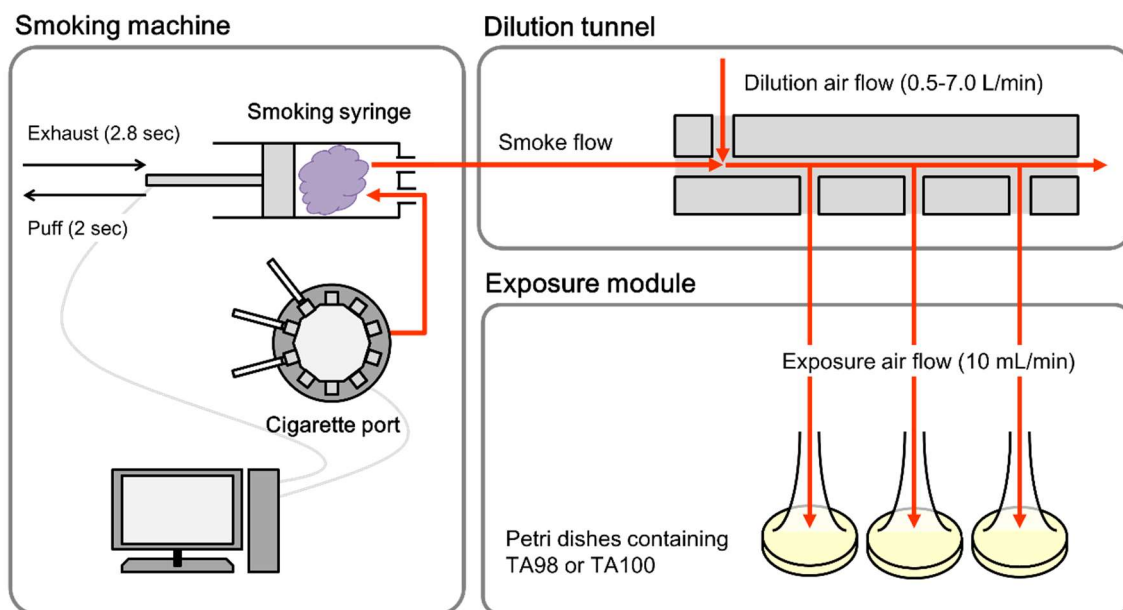


Figure 2.2 Illustration of the Vitrocell whole cigarette smoke exposure system for the Ames test. Test cigarettes are inserted into the cigarette holder on a cigarette port and smoked by a computer-controlled syringe. The puff volume taken by the syringe is 35 mL in the ISO standard regime and 55 mL in the ISO intensive regime. Then, the generated cigarette smoke is introduced into a dilution tunnel with a 2.8-s puff exhaust time. Next, the cigarette smoke is mixed with air in the dilution tunnel and introduced into the exposure module with a constant air flow of 10 mL/min.

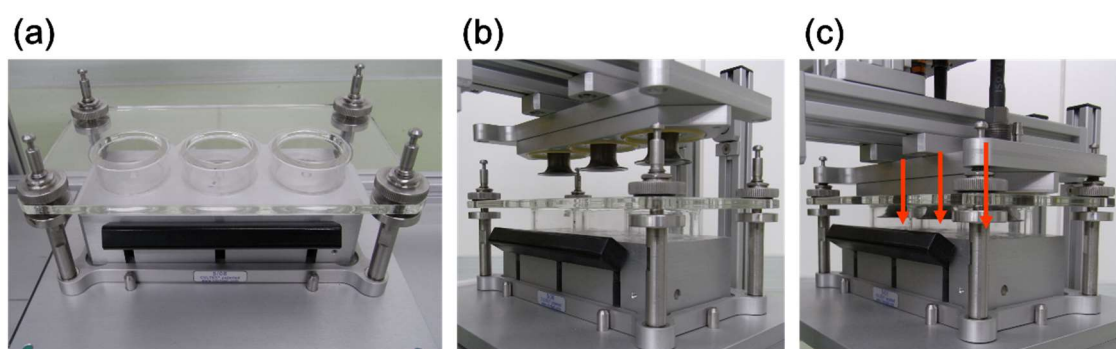


Figure 2.3 Vitrocell whole cigarette smoke exposure module for the Ames test.

(a) Three dishes with *Salmonella typhimurium* on minimal histidine media in the module. (b) The trumpet-shaped nozzles are on the top of the module. (c) Whole cigarette smoke is delivered through these nozzles to the air-agar interface cultured bacterial cells.

Table 2.1 Experimental conditions for the whole cigarette smoke exposure Ames test

Smoking regimen	Bacterial strain	Metabolic activation	Results
ISO standard	TA98	+	Figure 2.5a
		-	Figure 2.5b
	TA100	+	Figure 2.5c
		-	Figure 2.5d
ISO intensive	TA98	+	Figure 2.6a
		-	Figure 2.6b
	TA100	+	Figure 2.6c
		-	Figure 2.6d, Figure 2.7*

*The effect of the gas/vapor phase fraction of whole cigarette smoke was also analyzed in this condition.

For further comparison, the specific mutagenic activity of each cigarette was calculated from the slope of the linear dose–response curve for that cigarette⁵. The slope indicates the mutagenic potential of the CS per exposure dose. Solanesol was used as a PP marker because it is abundant in the PP fraction of CS and is not volatile^{13, 14}, and the mass of solanesol delivered to the cells for each dilution was analyzed. Then, the mass of TPM that was deposited on the cells was estimated. The *in vitro* dosimetry data (i.e., CS exposure dose of the cells) were plotted in dose–response curves to describe the relationship between the number of revertants induced and the masses of TPM deposited, when the cells were exposed to CS produced by the different cigarettes.

The experiments described in this chapter demonstrate how the Ames test can be applied to the whole CS exposure system. Because the Ames tests were performed with two smoking regimes, two bacterial strains, and two metabolic activation conditions (Table 2.1), the results can be used to clarify how experimental conditions affect the mutagenicity of whole CS. Moreover, *in vitro* dosimetry data can be used for analysis of the mutagenic potential of whole CS.

2.2 Materials and methods

2.2.1 Test cigarettes

Four products were used in this experiment: heated cigarettes (HCs) produced by Japan Tobacco Inc. (Tokyo, Japan) (Figure 2.4), conventional 1-mg of tar commercial cigarettes (CC1s), 1R5F reference cigarettes (University of Kentucky, Lexington, KY, USA), and 3R4F reference cigarettes (University of Kentucky). In the HC, a carbon heat source heats the tobacco leaves to generate mainstream smoke. Each product was conditioned at 22 ± 2 °C and a relative humidity of $60 \pm 5\%$ for 48 h before use.

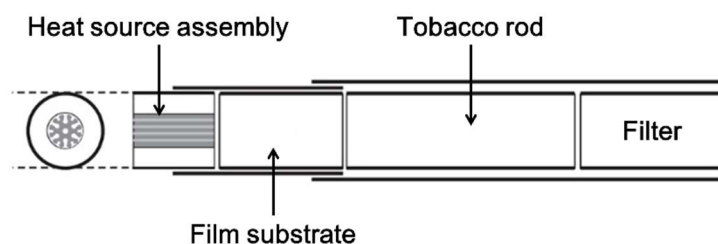


Figure 2.4 Illustration of the heated cigarette used in this experiment.

The heated cigarette has four parts: a heat source assembly comprising a carbon heat source covered with a glass mat, a film substrate containing tobacco leaves, a tobacco rod also containing tobacco leaves, and a filter.

2.2.2 Generation of whole CS or the GVP fraction and exposure of bacterial cells

A VC10 smoking robot (Vitrocell Systems GmbH) was used to generate whole CS or its GVP fraction, and exposure of bacteria on petri dishes was performed using a Vitrocell Ames module (Vitrocell Systems GmbH) (Figure 2.2 and 2.3). Each cigarette was smoked according to the ISO standard smoking regime (35-mL puff volume, 60-s puff interval, 2-s puff duration, and no blocking of ventilation holes) or the ISO intensive smoking regime (55-mL puff volume, 30-s puff interval, 2-s puff duration, and 100% blocking of ventilation holes). Each cigarette, except the HC, was smoked until a point 3 mm from

the tipping paper was reached. The HC was smoked until the heat source assembly was completely exhausted. A piece of 44-mm Cambridge filter pad (Borgwaldt KC GmbH, Hamburg, Germany) was inserted between the cigarette port and the smoking machine syringe, to remove the PP fraction of the whole CS and to obtain a GVP fraction for bacterial cells exposure. The whole CS or GVP fraction generated by the smoking machine was released into a dilution tunnel with a 2.8-s puff exhaust time, and diluted with clean air. A series of air flow rates of 3.5, 2.5, 1.5, and 0.5 L/min or 7.0, 6.0, 5.0, and 4.0 L/min were used for dilution in each experiment. The diluted whole CS or GVP fraction was directed into the exposure module using a vacuum pump with a flow rate of 10 mL/min. The exposure module held three culture dishes, each containing bacterial cells. Bacterial cells exposed to clean air were prepared as an air-exposed control.

2.2.3 Bacterial strains and culture conditions

The *S. typhimurium* strains TA98 and TA100, from the National Institute of Health Sciences (Tokyo, Japan), were used in the Ames tests. Single colonies of each strain were isolated, and the characteristics of the strains were checked following the procedure described by Maron and Ames ¹⁵. Suitable colonies were then kept in a freezer. Before use, a frozen bacterial suspension was incubated at 37 °C overnight with shaking at 50 rpm. Bacteria in the late logarithmic growth phase were used in the experiments. The bacterial densities were measured using a U-3100 spectrophotometer (Hitachi, Tokyo, Japan) set to a wavelength of 650 nm. After the incubation period, the bacterial density was approximately 2.7×10^9 bacteria/mL for the TA98 cells and approximately 1.7×10^9 bacteria/mL for the TA100 cells.

2.2.4 Ames reverse mutation assay

Approximately 4.0×10^7 TA98 cells or 2.5×10^7 TA100 cells were seeded using the spread culture method on 3 mL of selective agar (Tesmedia AN; Oriental Yeast Co., Ltd.,

Tokyo, Japan) in a 35-mm Petri dish. A 120- μ L aliquot of a bacterial solution containing 15 μ L of bacterial suspension, 30 μ L of a 1.2% sodium hydroxide solution containing 0.5 mM histidine and 0.5 mM biotin, and either 75 μ L of 0.1 M PBS or 75 μ L of 20% S9 mixture (Oriental Yeast Co., Ltd.) were poured directly onto the surface of the selective agar. The bacterial solution was distributed homogeneously over the entire agar surface by rotating the dish. Triplicate dishes containing bacterial cells were exposed to the whole CS. Then, the dishes were turned upside down and incubated at 37 °C for 48–72 h. Three experiments, each using triplicate dishes, were performed for each test, and the mean and standard deviation of the number of revertants were calculated.

2.2.5 Analyses of the masses of TPM and solanesol in the CS produced by the test cigarettes

CS from a test cigarette was passed through a 44-mm Cambridge filter pad inserted between the cigarette port and the syringe in the smoking machine, and the mass of TPM collected was measured. The trapped TPM was then extracted with 10 mL of methanol, and the solanesol concentration in the extract was determined. The extract was passed through a DISMIC-13HP filter (pore size 0.2 μ m; Advantec, Tokyo, Japan) and diluted with methanol to an appropriate concentration for analysis by high performance liquid chromatography (HPLC).

2.2.6 Collection of solanesol deposited on the culture surface

Solanesol deposited on a culture dish was collected using a 35-mm Petri dish (150318; Nunc, Copenhagen, Denmark) containing 3 mL of methanol rather than agar. Triplicate dishes were exposed to each CS, and then the methanol in each dish was collected and analyzed by HPLC. When the mass of collected solanesol was low, each 3-mL methanol sample was transferred to a test tube and evaporated for 2.5 h at 37 °C in a vacuum evaporator (EZ-2 plus; Genevac, Ipswich, UK). The residue was dissolved in 200 μ L of

methanol and analyzed by HPLC. Three experiments were performed—each using triplicate dishes—for each test CS, and the mean and standard deviation of the results were calculated.

2.2.7 HPLC conditions for analyzing solanesol

The mass of solanesol in each sample was determined by HPLC using an ultraviolet detector. The method was based on the Cooperation Centre for Scientific Research Relative to Tobacco method No. 52¹⁶. An Agilent 1100 series instrument (Agilent Technologies, Santa Clara, CA, USA), fitted with an Xbridge Shield RP18 column (250 mm × 4.6 mm inside diameter, 5-μm particle size; Waters Corporation, Milford, MA, USA), was used for the analyses. The injection volume was 100 μL, and the flow rate of isocratic mobile phase (5% methanol in acetonitrile) was 1.0 mL/min.

2.2.8 Statistical analysis

Comparison of the number of revertants induced by exposure to each whole CS or GVP fraction was carried out as follows. When the number of revertants induced was two or more times the number of revertants in the air-exposed control, the number of revertants was compared with the number of revertants observed in the air-exposed control using Dunnett's test. The results were considered to be significant if $p < 0.05$. Logarithmic transformation was performed before Dunnett's test to normalize the distribution. Comparison of the specific mutagenic activity indicated by the slope of the dose–response curve was performed with Tukey's test. The results were considered to be significant if $p < 0.05$. All statistical analyses were performed with Ekuseru Toukei software (Social Survey Research Information Co., Ltd., Tokyo, Japan).

2.3 Results

2.3.1 Mutagenicity of whole CS generated under the ISO standard regime

Whole CS was generated with the ISO standard smoking regime from the HCs, CC1s, and 1R5F cigarettes, and diluted with clean air at an appropriate flow rate for detection of dose-dependent changes. These three test cigarettes generate similar levels of TPM under the ISO standard smoking regime. When the dilution flow rate increases, the concentration of whole CS introduced into the exposure module will decrease. TA98 and TA100 cells were used with and without metabolic activation and the numbers of revertants induced were determined (Figure 2.5). When TA98 cells with metabolic activation were exposed to whole CS from all test cigarettes, the number of revertants increased dose-dependently (Figure 2.5a). When TA100 cells with metabolic activation were exposed to whole CS from CC1s or 1R5F cigarettes, the number of revertants also increased dose-dependently (Figure 2.5c). However, no significant increase in the number of revertants was observed when the cells were exposed to whole CS from the HCs (Figure 2.5c).

Without metabolic activation, no significant increase in the numbers of revertants was observed in any of the tests at any of the dilution flow rates (Figure 2.5b and d).

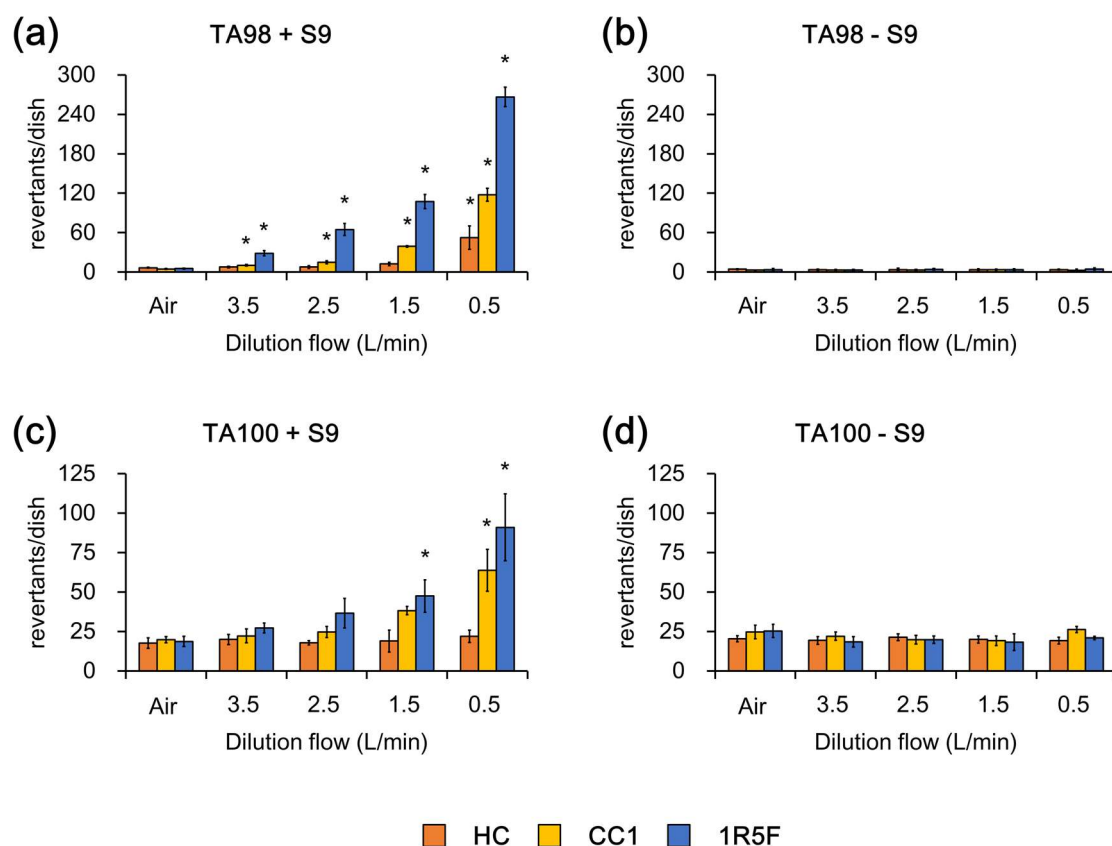


Figure 2.5 Mean number of revertants induced by whole cigarette smoke exposure produced by three different cigarettes with the ISO standard smoking regime.

Whole cigarette smoke generated with the ISO standard regime was used for exposure of (a) TA98 cells with metabolic activation, (b) TA98 cells without metabolic activation, (c) TA100 cells with metabolic activation, and (d) TA100 cells without metabolic activation. Six cigarettes were smoked in each experiment. The means and standard deviations are shown ($n = 3$). * The number of revertants is two or more times higher than, and significantly different ($p < 0.05$, Dunnett's test with log-transformed data) from the number of revertants observed in the air-exposed control. CC1, 1-mg of tar commercial cigarette; HC, heated cigarette.

2.3.2 Mutagenicity of whole CS generated under the ISO intensive regime

The mutagenicities of whole CS from the HCs, CC1s, and 1R5F and 3R4F cigarettes generated under the ISO intensive smoking regime were compared (Figure 2.6). These

four test cigarettes generate similar levels of TPM under the ISO intensive smoking regime. With metabolic activation, the numbers of revertants increased dose-dependently when TA98 cells were exposed to whole CS from all test cigarettes (Figure 2.6a). When TA100 cells with metabolic activation were exposed to whole CS from CC1s, 1R5F cigarettes, or 3R4F cigarettes, the numbers of revertants also increased dose-dependently (Figure 2.6c). When TA100 cells with metabolic activation were exposed to HC smoke, the number of revertants did not increase at any of the dilution rates (Figure 2.6c).

The number of revertants induced in the TA98 cells without metabolic activation did not increase when the cells were exposed to CS from any of the test cigarettes (Figure 2.6b). By contrast, the number of revertants increased dose-dependently when TA100 cells were exposed to whole CS from 1R5F and 3R4F cigarettes without metabolic activation, and a significant increase in the number of revertants was found when the dilution flow rate was 0.5 L/min (Figure 2.6d).

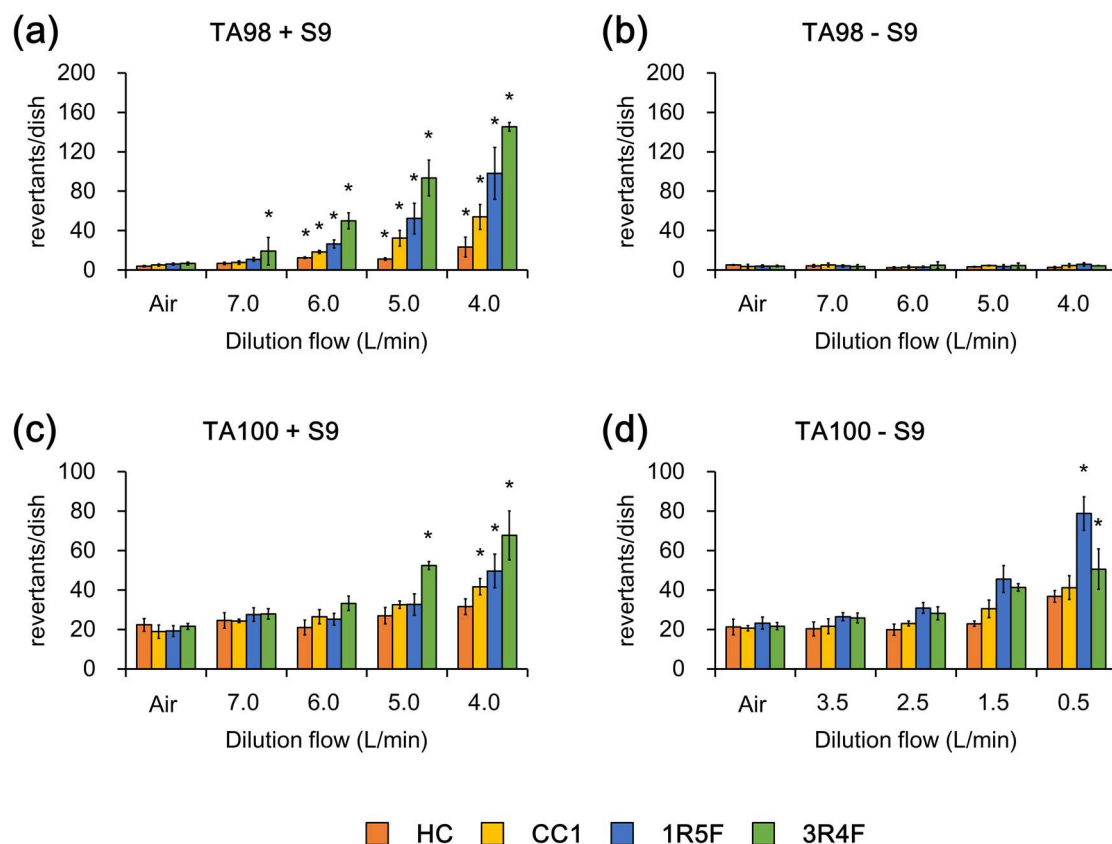


Figure 2.6 Mean number of revertants induced by exposure to whole cigarette smoke produced by four different cigarettes with the ISO intensive smoking regime.

Whole cigarette smoke generated with the ISO intensive regime was used for exposure of (a) TA98 cells with metabolic activation, (b) TA98 cells without metabolic activation, (c) TA100 cells with metabolic activation, and (d) TA100 cells without metabolic activation. The number of cigarettes smoked was (a) three, (b) three, (c) three, and (d) four. The means and standard deviations are shown ($n = 3$). * The number of revertants is two or more times higher than, and significantly different ($p < 0.05$, Dunnett's test with log-transformed data) from the number of revertants observed in the air-exposed control. CC1, 1-mg of tar commercial cigarette; HC, heated cigarette.

2.3.3 Mutagenicity of the GVP fraction of whole CS generated under the ISO intensive regime

Without metabolic activation, only the TA100 cells reacted to whole CS (Figure 2.6d). According to previous reports, the GVP fraction could have mutagenic activity under these conditions^{17, 18}. Thus, exposure of TA100 cells to the GVP fraction from each test cigarette was performed without metabolic activation. The number of revertants dose-dependently increased on exposure to the GVP fractions from the 1R5F and 3R4F cigarettes, and a significant increase was observed for 1R5F GVP fraction at a dilution flow rate of 0.5 L/min (Figure 2.7).

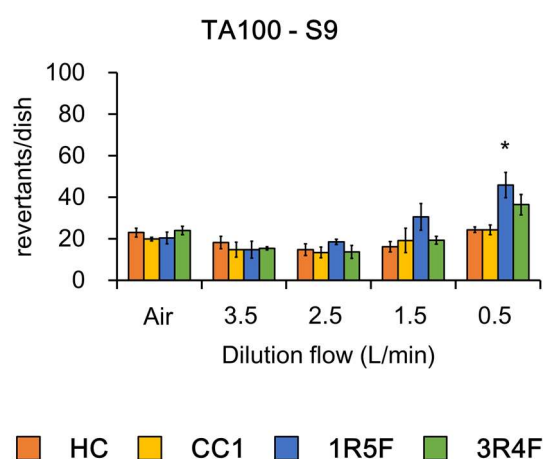


Figure 2.7 Mean number of revertants induced by exposure to the GVP fractions produced by four different cigarettes with the ISO intensive smoking regime.

TA100 cells without metabolic activation were exposed to GVP fractions produced by four cigarettes. The means and standard deviations are shown ($n = 3$). * The number of revertants is two or more times higher than, and significantly different ($p < 0.05$, Dunnett's test with log-transformed data) from the number of revertants observed in the air-exposed control. CC1, 1-mg of tar commercial cigarette; HC, heated cigarette.

2.3.4 Amounts of TPM and solanesol in the mainstream CS

The masses of TPM and solanesol in the whole CS produced by the test cigarettes under both the ISO standard and intensive regimes were analyzed (Table 2.2). The solanesol mass fraction (%) was lower in the TPM from the HC smoke than that in the TPM from the CS produced by the other cigarettes under both the ISO standard and intensive regimes (Table 2.2).

Table 2.2 Yields of TPM and solanesol from whole smoke produced by the tested cigarettes

	ISO standard			ISO intensive		
	TPM (mg/cig.)	solanesol (µg/cig.)	% solanesol	TPM (mg/cig.)	solanesol (µg/cig.)	% solanesol
	mean ± SD	mean ± SD	by TPM weight	mean ± SD	mean ± SD	by TPM weight
HC	1.32 ± 0.07	7.08 ± 1.42	0.53	35.48 ± 1.31	151.22 ± 0.89	0.43
CC1	1.50 ± 0.05	40.94 ± 0.85	2.74	20.43 ± 0.27	382.65 ± 22.50	1.87
1R5F	2.68 ± 0.34	62.80 ± 6.74	2.35	23.15 ± 0.78	478.62 ± 17.07	2.07
3R4F	10.92 ± 0.35	268.51 ± 8.50	2.46	38.20 ± 1.26	642.91 ± 15.77	1.68

Mean and standard deviation (SD) of three independent experiments. CC1, 1-mg of tar commercial cigarette; HC, heated cigarette; TPM, total particulate matter.

2.3.5 Estimating the level of TPM exposure for the cultured cells

The quantity of the CS PP fraction to which cells were exposed was estimated through measurement of the solanesol mass that was deposited on the culture dish at each dilution flow rate. The results obtained under the ISO standard and intensive regimes are shown in Table 2.3 and 2.4, respectively. The TPM mass that was deposited on each culture dish was calculated, as a TPM equivalent, from the %solanesol by TPM mass in Table 2.2. When the dilution flow rate was decreased, the masses of deposited solanesol and TPM equivalents were increased (Tables 2.3 and 2.4).

Table 2.3 Summary of dosimetry for smoke exposure on the cell surface under the ISO standard smoking regime

Dilution (L/min)		3.5	2.5	1.5	0.5
		mean \pm SD	mean \pm SD	mean \pm SD	mean \pm SD
HC	Solanesol (ng/cig.)	4.2 \pm 0.2	7.3 \pm 2.6	12.9 \pm 2.9	31.5 \pm 5.4
	TPM equivalent (μ g/cig.)	0.8 \pm 0.0	1.4 \pm 0.5	2.4 \pm 0.6	5.9 \pm 1.0
CC1	Solanesol (ng/cig.)	19.5 \pm 2.4	28.3 \pm 2.4	52.4 \pm 3.8	153.6 \pm 12.1
	TPM equivalent (μ g/cig.)	0.8 \pm 0.1	1.2 \pm 0.1	2.1 \pm 0.2	6.3 \pm 0.5
1R5F	Solanesol (ng/cig.)	32.3 \pm 5.5	52.4 \pm 3.6	83.7 \pm 11.1	229.7 \pm 13.0
	TPM equivalent (μ g/cig.)	1.4 \pm 0.2	2.2 \pm 0.2	3.6 \pm 0.5	9.8 \pm 0.6

Mean and standard deviation (SD) of three independent experiments. CC1, 1-mg of tar commercial cigarette; HC, heated cigarette; TPM, total particulate matter.

Table 2.4 Summary of dosimetry for smoke exposure on the cell surface under the ISO intensive smoking regime

Dilution (L/min)		7.0	6.0	5.0	4.0
		mean \pm SD	mean \pm SD	mean \pm SD	mean \pm SD
HC	Solanesol (ng/cig.)	17.1 \pm 4.2	24.2 \pm 0.3	37.4 \pm 5.9	75.7 \pm 8.0
	TPM equivalent (μ g/cig.)	4.0 \pm 1.0	5.7 \pm 0.1	8.8 \pm 1.4	17.8 \pm 1.9
CC1	Solanesol (ng/cig.)	28.9 \pm 2.8	52.7 \pm 4.7	96.7 \pm 9.9	156.6 \pm 8.8
	TPM equivalent (μ g/cig.)	1.5 \pm 0.2	2.8 \pm 0.2	5.2 \pm 0.5	8.4 \pm 0.5
1R5F	Solanesol (ng/cig.)	31.1 \pm 1.6	66.1 \pm 12.8	88.4 \pm 21.5	158.6 \pm 14.5
	TPM equivalent (μ g/cig.)	1.5 \pm 0.1	3.4 \pm 0.7	4.3 \pm 1.0	8.2 \pm 0.8
3R4F	Solanesol (ng/cig.)	38.9 \pm 6.8	98.4 \pm 5.4	143.3 \pm 25.1	302.8 \pm 36.2
	TPM equivalent (μ g/cig.)	2.3 \pm 0.4	4.8 \pm 0.3	8.5 \pm 1.5	14.9 \pm 1.8

Mean and standard deviation (SD) of three independent experiments. CC1, 1-mg of tar commercial cigarette; HC, heated cigarette; TPM, total particulate matter.

2.3.6 Analysis of the specific mutagenic activity of the CS produced by each test cigarette

Dose–response curves (Figure 2.8) were plotted to describe the relationship between the numbers of revertants induced in TA98 and TA100 cells with metabolic activation (Figures 2.5a, 2.5c, 2.6a, and 2.6c) and the mass of TPM equivalents that would have been deposited on the cultured cells (Tables 2.3 and 2.4). The slope of the linear regression line for the CS produced by each of the test cigarettes was calculated and defined as the specific mutagenic activity for that cigarette (Table 2.5). The specific mutagenic activities of the test cigarettes were compared statistically (Figure 2.9). The specific mutagenic activity of the HCs was significantly smaller than that of other test cigarettes under all exposure conditions with metabolic activation (Figure 2.9). There were significant differences between the CC1s and 1R5F cigarettes in TA98 cells with metabolic activation (Figure 2.9a and c), but no other significant differences were observed among CC1s, 1R5F cigarettes, and 3R4F cigarettes (Figure 2.9).

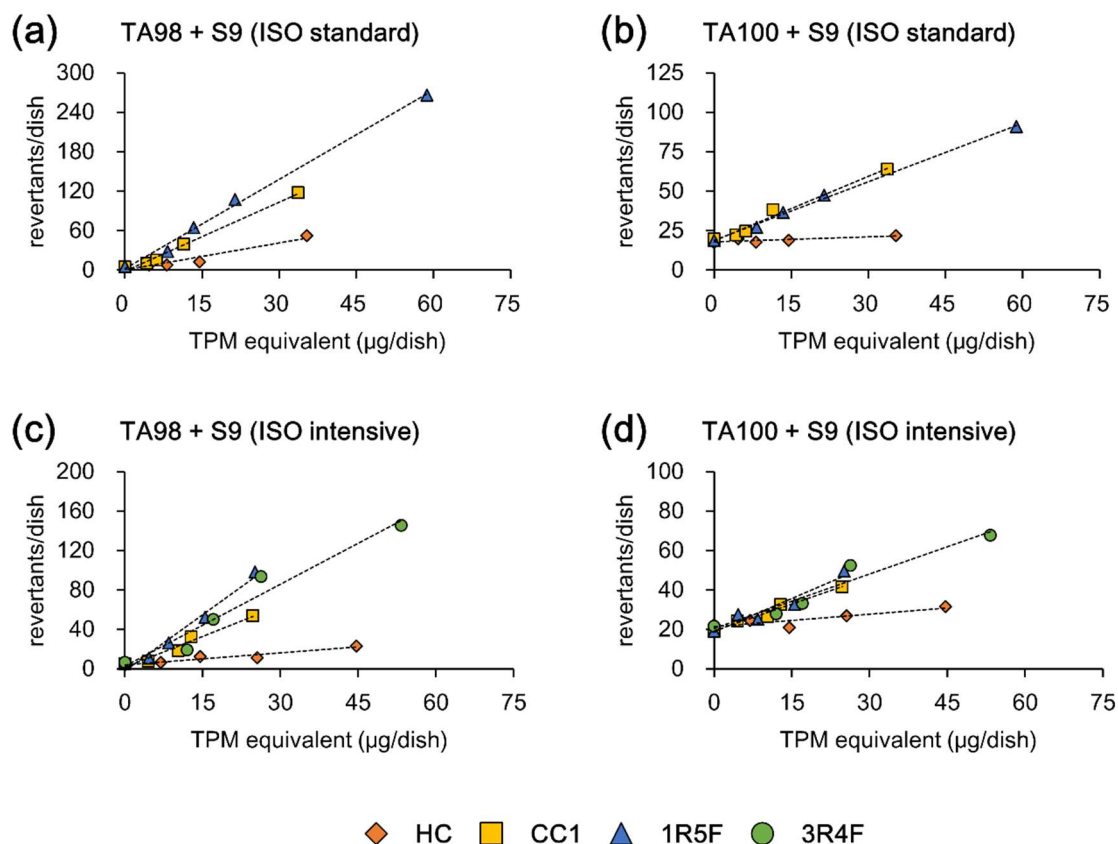


Figure 2.8 Relationship between the numbers of revertants induced by whole cigarette smoke and the TPM equivalents that were delivered to the cells.

Whole cigarette smoke generated with the ISO standard regime was used for exposure of (a) TA98 cells with metabolic activation and (b) TA100 cells with metabolic activation. Whole cigarette smoke generated with the ISO intensive regime was used for exposure of (c) TA98 cells with metabolic activation and (d) TA100 cells with metabolic activation. The means and standard deviations are shown ($n = 3$). CC1, 1-mg of tar commercial cigarette; HC, heated cigarette; TPM, total particulate matter.

Table 2.5 Linear regression analysis of dose-dependent curves generated using the Ames and dosimetry data.

Smoking regimen	Bacterial condition	Cigarette	Predictive equation				R^2
ISO standard	TA98 + S9	HC	y	=	1.37	x + 0.29	0.917
		CC1	y	=	3.50	x - 1.64	0.991
		1R5F	y	=	4.53	x + 2.37	0.995
	TA100 + S9	HC	y	=	0.11	x + 17.87	0.714
		CC1	y	=	1.36	x + 18.58	0.979
		1R5F	y	=	1.24	x + 18.99	0.997
ISO intensive	TA98 + S9	HC	y	=	0.41	x + 4.15	0.916
		CC1	y	=	2.10	x + 1.54	0.962
		1R5F	y	=	3.79	x - 1.85	0.975
		3R4F	y	=	2.77	x + 2.78	0.950
	TA100 + S9	HC	y	=	0.21	x + 21.46	0.767
		CC1	y	=	0.91	x + 19.22	0.972
		1R5F	y	=	1.13	x + 18.74	0.922
		3R4F	y	=	0.92	x + 20.52	0.940

Means of three independent experiments. CC1, 1-mg of tar commercial cigarette; HC, heated cigarette.

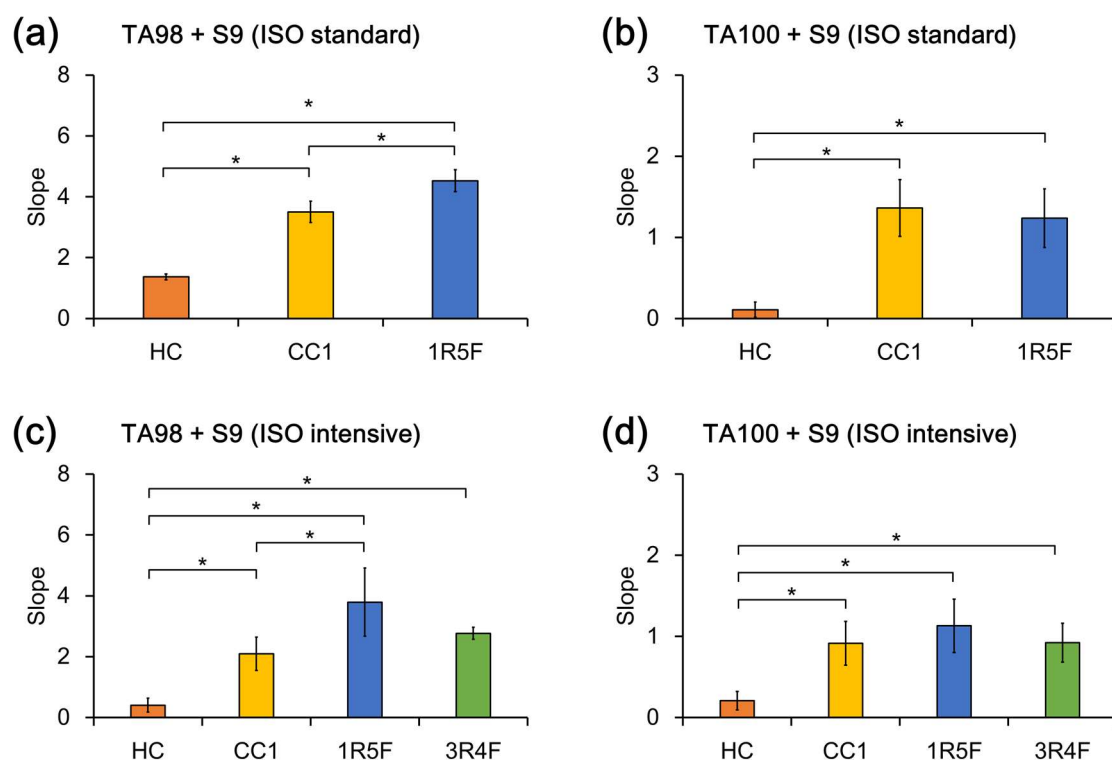


Figure 2.9 Specific mutagenic activity of each test cigarette.

The specific mutagenic activity was calculated as the slope of the dose–response curve (Figure 2.6). The slope obtained by exposure to whole cigarette smoke generated with the ISO standard regime in (a) TA98 cells with metabolic activation and (b) TA100 cells with metabolic activation. The slope obtained by exposure to whole cigarette smoke generated with the ISO intensive regime in (c) TA98 cells with metabolic activation and (d) TA100 cells with metabolic activation. The means and standard deviations are shown ($n = 3$). * Significant difference between the cigarettes ($p < 0.05$, Tukey’s test). CC1, 1-mg of tar commercial cigarette; HC, heated cigarette.

2.4 Discussion

The mutagenic potentials of whole CS produced by different cigarettes were compared using the Ames test and a whole CS exposure system. As previously found^{17,18}, exposure to CS increased the numbers of revertants dose-dependently in TA98 and TA100 cells with metabolic activation, except for TA100 cells exposed to HC smoke (Figures 2.5a,

2.5c, 2.6a, and 2.6c). Under these conditions, the number of revertants induced was in the following order: 3R4F > 1R5F > CC1 > HC. This order aligned with the mass of TPM equivalents delivered to the cells in each exposure condition (Tables 2.3 and 2.4). Thus, in these conditions, the number of revertants induced by exposure to whole CS from each test cigarette was highly dependent on the TPM exposure dose.

Without metabolic activation, TA98 cells did not show increase in the number of revertants by exposure to whole CS generated from any of the test cigarettes under either the ISO standard or intensive regimes (Figures 2.5b and 2.6b). These findings are similar to the results obtained in a previous study, in which TA98 cells did not increase the number of colonies with exposure to a CS extract^{19, 20}. Without metabolic activation, TA100 cells increased the number of revertants when the cells were exposed to whole CS under the ISO intensive regime (Figure 2.6d). Under this condition, more revertants were induced by 1R5F than 3R4F CS. This is discrepant with the mass of TPM equivalents delivered because the cells were exposed to approximately two times the TPM equivalents from 3R4F than from 1R5F (Table 2.4). Therefore, the TA100 results without metabolic activation suggest chemicals in the GVP fraction contribute to the mutagenic activity. Indeed the number of revertants induced by exposure to the GVP fraction of 1R5F CS was more than the number of revertants induced by exposure to the GVP fraction of 3R4F CS (Figure 2.7). A previous study found that nitrogen oxides in the GVP fraction of whole CS had direct mutagenic activity in a gas-exposure Ames test¹⁷. Therefore, analysis of the quantity of nitrogen oxide delivered to cells will be necessary for further understanding of the GVP chemicals that contribute to the mutagenic activity observed in TA100 without metabolic activation.

In whole CS exposure experiments, specific techniques would need to be applied for measurement of the smoke doses to which cells are exposed because CS is a complex aerosol. In some studies using whole CS exposure systems, the doses of whole CS directed into exposure modules have been calculated from smoke dilution ratios^{7, 8, 21}. The masses of CS particles that are deposited on the cell culture surfaces were measured by quartz crystal microbalances in several previous studies^{22, 23}. These dosimetry data are required to plot dose–response curves^{24, 25}. In this experiment, solanesol was selected as

a marker of the PP, and the masses of TPM deposited on the cells under the test conditions were estimated from the masses of solanesol found on the culture surfaces. The results are presented in Tables 2.3 and 2.4 as TPM equivalents.

In each dose–response curve, the number of revertants in TA98 and TA100 with metabolic activation was plotted against the TPM equivalents deposited on the cell culture surface (Figure 2.8) because PP chemicals reportedly contribute to mutagenic activity under these conditions^{17, 18}. The numbers of revertants induced in TA98 and TA100 cells with metabolic activation correlated with the masses of TPM equivalent to which the cells were exposed, consistent with the Ames test results in previous studies using CS extracts^{26, 27}. From the linear regression line for the dose–response curve, the specific mutagenic activity of the whole mainstream CS generated from each cigarette was determined (Figure 2.9). The calculated specific activity of the HC smoke was lower than that of the CS produced by the other test cigarettes under both the ISO standard and intensive regimes (Figure 2.9). This is aligned with previous studies, which indicated that CS from HCs contains smaller quantities of several harmful chemicals than that from conventional cigarettes and has lower toxicological effects in *in vitro* and *in vivo* experiments²⁸⁻³¹. By comparison, the differences in specific activities among the other cigarettes (CC1, 1R5F, and 3R4F) were rather small (Figure 2.9). This indicates that even though the mass of TPM generated from these cigarettes differed, there were no distinct differences in the mutagenicities of conventional cigarettes per TPM mass, especially on TA100 cells with metabolic activation.

2.5 Conclusions

In conclusion, the mutagenicities of CS samples produced by different cigarettes were determined using a whole CS exposure system and the Ames test. Whole CS exposure enabled comparison of the number of revertants induced by whole CS from the different test cigarettes. Moreover, dosimetry data were used to calculate mutagenic potentials from the slope of the dose–response curve for each test CS. Under the ISO standard and

intensive regimes in TA98 and TA100 cells with metabolic activation, the specific activity of whole CS from the HC was lower than those for CS samples from all of the other test cigarettes. These results are aligned with the results obtained from *in vivo* experiments. Overall, the results indicate that differences among the mutagenicities of fresh CS samples produced by different cigarettes can be identified using a whole CS exposure system and the Ames test.

2.6 References

1. Goh, J.-Y., Weaver, R.J., Dixon, L., Platt, N.J. & Roberts, R.A. Development and use of in vitro alternatives to animal testing by the pharmaceutical industry 1980–2013. *Toxicology Research* **4**, 1297-1307 (2015).
2. Kirkland, D., Reeve, L., Gatehouse, D. & Vanparys, P. A core in vitro genotoxicity battery comprising the Ames test plus the in vitro micronucleus test is sufficient to detect rodent carcinogens and in vivo genotoxins. *Mutat Res* **721**, 27-73 (2011).
3. Vanparys, P. *et al.* Application of in vitro cell transformation assays in regulatory toxicology for pharmaceuticals, chemicals, food products and cosmetics. *Mutat Res* **744**, 111-116 (2012).
4. Dempsey, R., Coggins, C.R. & Roemer, E. Toxicological assessment of cigarette ingredients. *Regul Toxicol Pharmacol* **61**, 119-128 (2011).
5. Scott, K. *et al.* The resolving power of in vitro genotoxicity assays for cigarette smoke particulate matter. *Toxicol In Vitro* **27**, 1312-1319 (2013).
6. Bombick, D.W. *et al.* Evaluation of the genotoxic and cytotoxic potential of mainstream whole smoke and smoke condensate from a cigarette containing a novel carbon filter. *Fundam Appl Toxicol* **39**, 11-17 (1997).
7. Nara, H., Fukano, Y., Nishino, T. & Aufderheide, M. Detection of the cytotoxicity of water-insoluble fraction of cigarette smoke by direct exposure to cultured cells at an air-liquid interface. *Exp Toxicol Pathol* **65**, 683-688 (2013).
8. Okuwa, K. *et al.* In vitro micronucleus assay for cigarette smoke using a whole smoke exposure system: a comparison of smoking regimens. *Exp Toxicol Pathol* **62**, 433-440 (2010).
9. Kier, L.D., Yamasaki, E. & Ames, B.N. Detection of mutagenic activity in cigarette smoke condensates. *Proc Natl Acad Sci U S A* **71**, 4159-4163 (1974).
10. Thorne, D. & Adamson, J. A review of in vitro cigarette smoke exposure systems. *Exp Toxicol Pathol* **65**, 1183-1193 (2013).

11. Chin, J.B., Sheinin, D.M. & Rauth, A.M. Screening for the mutagenicity of nitro-group containing hypoxic cell radiosensitizers using Salmonella typhimurium strains TA 100 and TA98. *Mutat Res* **58**, 1-10 (1978).
12. Denissenko, M.F., Pao, A., Tang, M. & Pfeifer, G.P. Preferential formation of benzo[a]pyrene adducts at lung cancer mutational hotspots in P53. *Science* **274**, 430-432 (1996).
13. Jenkins, R.A., Tomkins, B. & Guerin, M.R. *The chemistry of environmental tobacco smoke: composition and measurement*. (CRC Press, 2000).
14. Tang, H. *et al.* Solanesol: a tracer for environmental tobacco smoke particles. *Environmental Science & Technology* **24**, 848-852 (1990).
15. Maron, D.M. & Ames, B.N. Revised methods for the Salmonella mutagenicity test. *Mutat Res* **113**, 173-215 (1983).
16. CORESTA recommended method N° 52 Environmental Tobacco Smoke - Estimation of its Contribution to Respirable Suspended Particles - Method based on Solanesol Determination. (2002).
17. Aufderheide, M. & Gressmann, H. A modified Ames assay reveals the mutagenicity of native cigarette mainstream smoke and its gas vapour phase. *Exp Toxicol Pathol* **58**, 383-392 (2007).
18. Aufderheide, M. & Gressmann, H. Mutagenicity of native cigarette mainstream smoke and its gas/vapour phase by use of different tester strains and cigarettes in a modified Ames assay. *Mutat Res* **656**, 82-87 (2008).
19. Lofroth, G. & Lazaridis, G. Environmental tobacco smoke: comparative characterization by mutagenicity assays of sidestream and mainstream cigarette smoke. *Environ Mutagen* **8**, 693-704 (1986).
20. Williams, K. & Lewtas, J. Metabolic activation of organic extracts from diesel, coke oven, roofing tar, and cigarette smoke emissions in the Ames assay. *Environ Mutagen* **7**, 489-500 (1985).
21. Weber, S., Hebestreit, M., Wilms, T., Conroy, L.L. & Rodrigo, G. Comet assay and air-liquid interface exposure system: a new combination to evaluate genotoxic effects of cigarette whole smoke in human lung cell lines. *Toxicol In Vitro* **27**, 1987-1991 (2013).
22. Adamson, J., Hughes, S., Azzopardi, D., McAughey, J. & Gaca, M.D. Real-time assessment of cigarette smoke particle deposition in vitro. *Chem Cent J* **6**, 98 (2012).
23. Adamson, J., Thorne, D., Dalrymple, A., Dillon, D. & Meredith, C. Assessment of cigarette smoke particle deposition within the Vitrocell(R) exposure module using quartz crystal microbalances. *Chem Cent J* **7**, 50 (2013).
24. Kilford, J. *et al.* A method for assessment of the genotoxicity of mainstream cigarette-smoke by use of the bacterial reverse-mutation assay and an aerosol-based exposure system. *Mutat Res Genet Toxicol Environ Mutagen* **769**, 20-28 (2014).

25. Li, X. *et al.* Evaluation method for the cytotoxicity of cigarette smoke by in vitro whole smoke exposure. *Exp Toxicol Pathol* **66**, 27-33 (2014).
26. Foy, J.W. *et al.* A comparison of in vitro toxicities of cigarette smoke condensate from Eclipse cigarettes and four commercially available ultra low-"tar" cigarettes. *Food Chem Toxicol* **42**, 237-243 (2004).
27. Roemer, E., Tewes, F.J., Meisgen, T.J., Veltel, D.J. & Carmines, E.L. Evaluation of the potential effects of ingredients added to cigarettes. Part 3: in vitro genotoxicity and cytotoxicity. *Food Chem Toxicol* **40**, 105-111 (2002).
28. Fujimoto, H. *et al.* Biological responses in rats exposed to mainstream smoke from a heated cigarette compared to a conventional reference cigarette. *Inhal Toxicol* **27**, 224-236 (2015).
29. Fukushima, T. & Tsujimoto, T. Chemical and biological characterisation of mainstream smoke generated from commercial cigarettes available on the Japanese market. *CORESTA Congress, SSPTPOST 05* (2012).
30. Sakaguchi, C., Kakehi, A., Minami, N., Kikuchi, A. & Futamura, Y. Exposure evaluation of adult male Japanese smokers switched to a heated cigarette in a controlled clinical setting. *Regul Toxicol Pharmacol* **69**, 338-347 (2014).
31. Tsuji, H. *et al.* Comparison of dermal tumor promotion activity of cigarette smoke condensate from prototype (heated) cigarette and reference (combusted) cigarette in SENCAR mice. *Food Chem Toxicol* **72**, 187-194 (2014).

Chapter 3.

Development of a 3D bronchial tissue model

3.1 Introduction

3.1.1 Objectives

In the previous chapter, a whole CS exposure system was applied to the Ames test, which is a standard *in vitro* genotoxicity test to detect frame shift mutations and base-pair substitutions, with *Salmonella* DNA. Standard *in vitro* tests (e.g., Ames, neutral red uptake, and *in vitro* micronucleus assays) can detect the toxicological effects of compounds on the molecular/cellular level. However, the *in vivo* toxicological effects of CS on the human respiratory system are observed as a complex disease phenotype. Therefore, in addition to standard toxicity tests, an *in vitro* test system with improved human relevance, which can detect tissue/organ level responses, is necessary to investigate the toxicological effects of CS. The objective of this chapter was to develop a 3D culture model of human bronchial tissue for use with the whole CS exposure system to investigate the toxicological effects of CS on human bronchial tissue *in vitro*.

3.1.2 Study approaches

With recent advancements in *in vitro* cell culture technology, various 3D culture models of human tissue have been developed. These models have been applied to toxicity testing of pharmaceuticals and chemicals. The 3D culture model of human bronchial epithelium is one such model. Early experiments performed by Whitcutt et al.¹ revealed that when HBECs were cultured on a permeable membrane under ALI conditions (i.e., supply of the medium from the bottom membrane of the cell culture insert and the cell surface in contact with the air), the cells developed a pseudostratified 3D layer of bronchial epithelium with mucociliary differentiation (Figure 3.1a). Various previous experiments have revealed that this model has xenobiotic metabolism and mucus secretion capacities similar to actual human bronchial tissue²⁻⁶. Therefore, this model has the potential to detect tissue/organ level toxicological responses following CS exposure.

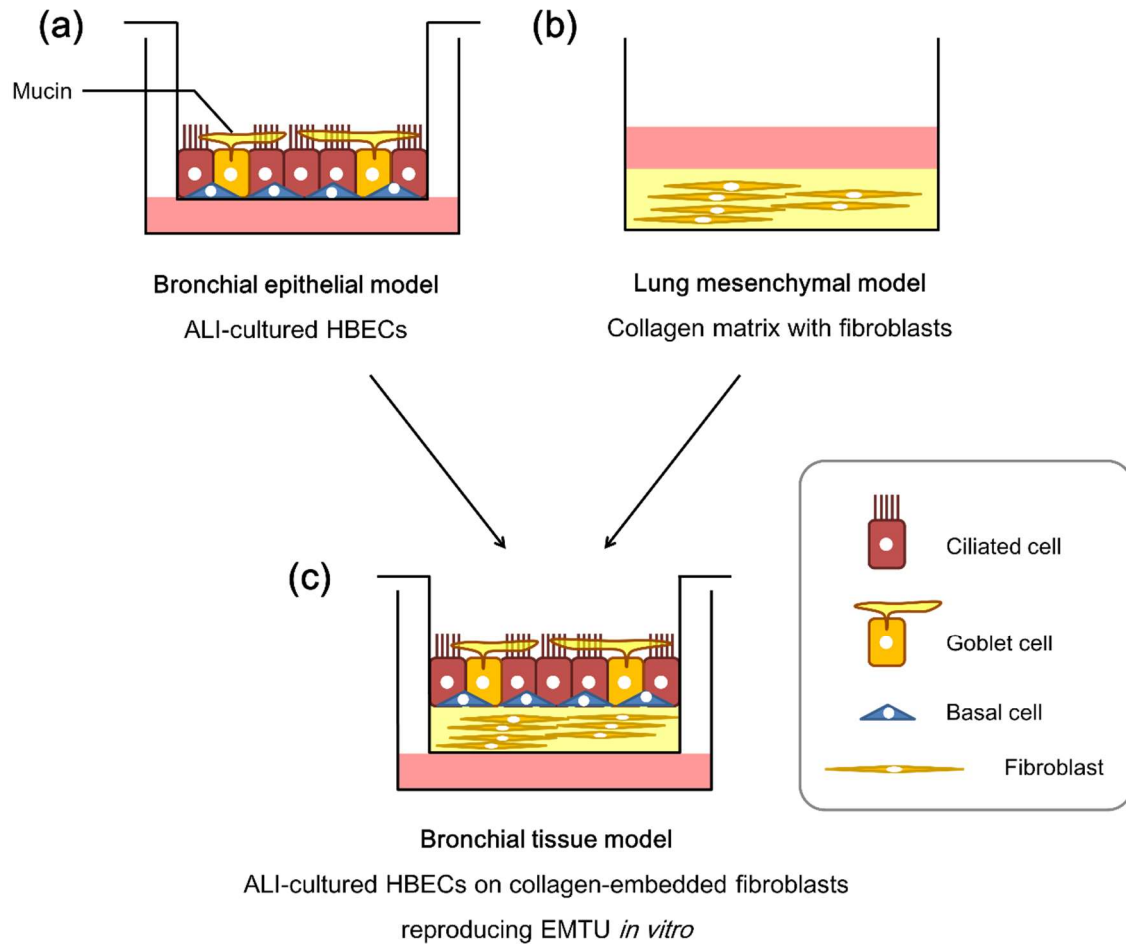


Figure 3.1 Illustration of human 3D lung models.

(a) A bronchial epithelial model constructed by an air-liquid interface (ALI) culture of human bronchial epithelial cells (HBECs). (b) A lung mesenchymal model composed of collagen-embedded lung fibroblasts. (c) A bronchial tissue model composed of collagen-embedded fibroblasts and ALI-cultured bronchial epithelial cells. EMTU is the epithelial–mesenchymal trophic unit.

In parallel with the development of the 3D culture model of human bronchial epithelium, a 3D mesenchymal model of the human lungs composed of human lung fibroblasts in a thick collagen matrix has been developed (Figure 3.1b). Under appropriate stimulation, fibroblasts in a collagen matrix differentiate into myofibroblasts and show a contractile phenotype⁷⁻⁹. It is considered that this process recapitulates airway remodeling such as subepithelial fibrosis, which includes mesenchymal alterations (e.g.,

increase of smooth-muscle cells, accumulation of myofibroblasts, and increased deposition of ECM proteins)^{10, 11}. Because airway remodeling is a critical process in the pathogenesis of inflammatory lung diseases such as asthma and COPD¹², the 3D collagen matrix model has been used to investigate the mechanisms behind disease development.

Bronchial epithelium acts as a barrier to inhaled airborne chemicals, including CS¹³. Exposure to airborne chemicals induces damage-repair or inflammatory responses in bronchial epithelium and continual exposure disrupts these responses¹⁴⁻¹⁶. Several previous reports have shown the importance of the epithelial–mesenchymal trophic unit (EMTU) in this damage-repair response^{17, 18}. EMTU is comprised of bronchial epithelial and mesenchymal cells and ECM, and their local interactions are essential in the responses to various stimuli (Figure 3.2). For example, the importance of EMTU in the response to CS and the development of COPD have been reported previously^{19, 20}.

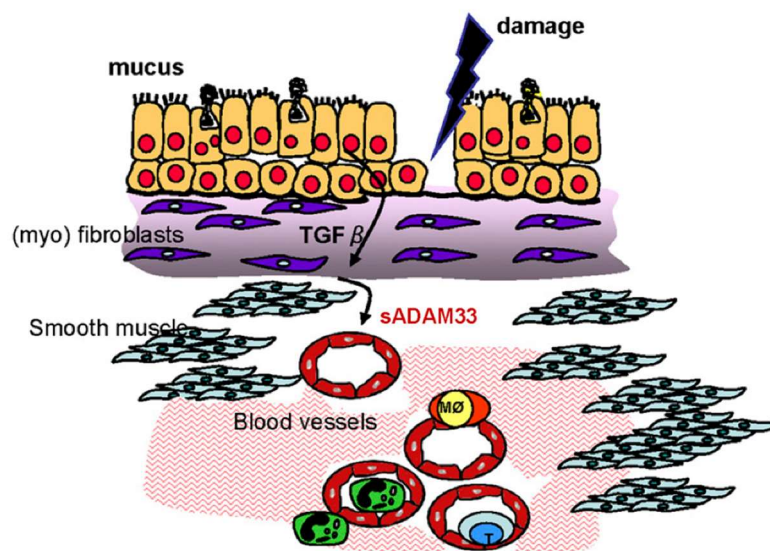


Figure 3.2 Model showing the importance of the epithelial–mesenchymal trophic unit following exposure-induced damage.

Increase in (myo)fibroblasts, smooth muscle cells, and microvascular leakage can be induced through communication between the epithelial layer and mesenchymal layer. The diagram is reproduced from the literature²¹.

Within this background, a 3D culture model of human bronchial tissue composed of both an epithelial layer and mesenchymal layer would be useful to reproduce disease-relevant phenotypical changes induced by whole CS exposure. Therefore, in this chapter, a 3D bronchial tissue model was developed by preparing a collagen matrix containing fibroblasts as the mesenchymal layer, applying HBECs to the matrix, and culturing the cells under ALI conditions (Figure 3.1c). Before applying this model to whole CS exposure experiments, the potential of this *in vitro* EMTU model to represent the disease phenotype was investigated following an appropriate stimulation. Transforming growth factor (TGF)- β 1 is key player in the fibrosis observed in various lung diseases, including COPD¹⁹. Therefore, the 3D bronchial tissue model was stimulated with TGF- β 1 and analyzed to see if fibrotic changes were induced in this model.

3.2 Materials and methods

3.2.1 Construction of a 3D culture model of human bronchial tissue

Human fetal lung fibroblasts (IMR-90) were obtained from the American Type Culture Collection (Manassas, VA, USA) and grown in minimum essential medium (MEM) (Life Technologies, Carlsbad, CA, USA) with 10% fetal bovine serum (FBS; MP Biomedicals, Santa Ana, CA, USA). Normal HBECs (Lonza, Basel, Switzerland) were grown in Airway Epithelial Cell Growth Medium with SupplementPack (PromoCell, Heidelberg, Germany).

CellMatrix Type I-A (Nitta Gelatin, Osaka, Japan), 10 \times MEM, and reconstitution buffer (Nitta Gelatin) were mixed in a 8:1:1 volume ratio and applied to a cell culture insert (\varnothing 10.5 mm, 1.0- μ m pore size; Becton Dickinson, Franklin Lakes, NJ, USA) in 100- μ L aliquots to prepare a base layer. The base layer was gelled by placing the insert in an incubator at 37 °C under a 5% CO₂ atmosphere for more than 1 h. IMR-90 cells (approximately 2.5×10^6 cells/mL in FBS), CellMatrix Type I-A, CellMatrix Type I-P (Nitta Gelatin), 10 \times MEM, and reconstitution buffer were mixed in a 1:4:4:1:1 volume ratio and poured onto the base layer in 250- μ L aliquots to prepare a collagen-embedded

fibroblast layer. The fibroblast layer was gelled by placing the insert in an incubator at 37 °C under a 5% CO₂ atmosphere for more than 1 h.

After 2 days of cultivation with MEM containing 10% FBS, HBECs suspended in Airway Epithelial Cell Growth Medium (approximately 3.0×10^5 cells/mL) were seeded onto the collagen layer to prepare the co-culture model, and cultured under submerged conditions until reaching a semi-confluent state. PneumaCult-ALI medium (Stemcell Technologies, Vancouver, BC, Canada) was supplemented with heparin (Stemcell Technologies) and hydrocortisone (Stemcell Technologies) in accordance with the manufacturer's instructions. GM6001 (30 nM; Sigma-Aldrich, St. Louis, MO, USA) and 1% FBS were also added to prepare the ALI culture medium. The apical and basolateral media were removed, and 600 µL of the ALI culture medium was added to the bottom well.

3.2.2 TGF-β stimulation and collagen gel contraction

Stimulation of TGF-β signaling with TGF-β1 (R&D Systems, Minneapolis, MN, USA) and inhibition of TGF-β signaling with a TGF-β receptor type I blocker (SB525334; FUJIFILM Wako Pure Chemical Corporation, Osaka, Japan) were performed from the first day of ALI culturing. The ALI culture was maintained for 21 days. Images of each collagen gel were obtained, and gel contraction was analyzed with ImageJ software (National Institutes of Health, Bethesda, MD, USA). Data are expressed as percentages relative to the initial gel area.

3.2.3 Histological analysis of the tissues

After fixation in 4% paraformaldehyde at 4 °C on ALI culture day 21, bronchial tissue samples were embedded in paraffin and 5-µm sections were prepared using a microtome. Sections were deparaffinized and subjected to hematoxylin and eosin staining or immunostaining. Immunostaining was performed with Polink-2 Plus (GBI Labs, Bothell, WA, USA) using the antibodies listed in Table 3.1. Before staining, the tissues were

subjected to heat-induced antigen retrieval with citrate buffer or ethylenediaminetetraacetic acid at approximately 90 °C for 30 min (Table 3.1). Image analysis of immunostained sections was conducted with ImageJ software. Three sections were prepared for each experimental condition, and the area of the epithelial layer and mesenchymal collagen layer was measured. The Colour Deconvolution plugin²² was used for diaminobenzidine (DAB) and hematoxylin stain separation, and the DAB-positive areas in the epithelial and mesenchymal layers were measured. The results are expressed as the percentage of DAB-positive area in each layer.

Table 3.1 Antibodies used for immunohistochemical staining.

Antibody	Cat. #	Dilution	Heat-induced antigen retrieval
Acetylated α -tubulin	ab24610	1:250	10-mM sodium citrate buffer (pH 6.0)
Mucin 5AC	ab3649	1:250	10-mM sodium citrate buffer (pH 6.0)
Cytokeratin 5	ab52635	1:100	10-mM sodium citrate buffer (pH 6.0)
E-cadherin	ab40772	1:250	10-mM sodium citrate buffer (pH 6.0)
Vimentin	ab92547	1:250	1-mM EDTA (pH 8.0)
α -smooth muscle actin	ab5694	1:1000	10-mM sodium citrate buffer (pH 6.0)
Fibronectin	ab2413	1:250	10-mM sodium citrate buffer (pH 6.0)
Tenascin-C	ab108930	1:250	1-mM EDTA (pH 8.0)

EDTA, ethylenediaminetetraacetic acid.

3.2.4 Measurement of matrix metalloproteinases by gelatin zymography

The activities of matrix metalloproteinases (MMPs) in the culture medium were determined using gelatin zymography. Culture medium collected on ALI culture day 21 was subjected to sodium dodecyl sulfate-polyacrylamide gel electrophoresis in 7.5% acrylamide gel containing 0.9 mg/mL gelatin. After electrophoresis, the gels were washed twice (30 min and 45 min) in wash buffer (0.5% Triton X-100, 2.5 mM Tris-HCl, 150 mM NaCl), incubated for 19 h in incubation buffer (2.5 mM Tris-HCl, 20 mM NaCl, 10

mM CaCl₂), and stained with 0.1% Coomassie blue. Images were obtained with ImageQuant LAS 4000 (GE Healthcare, Little Chalfont, UK), and signal densities were quantified using ImageQuant TL (GE Healthcare). Data are expressed as the fold change relative to the band density in the control.

3.2.5 Measurement of tissue inhibitor of metalloproteinases by a multiplex assay

The concentrations of tissue inhibitor of metalloproteinases (TIMPs) secreted into the culture medium were analyzed with a Bio-Plex Pro Human TIMP Panel (Bio-Rad, Hercules, CA, USA), using the Bio-Plex system (Bio-Rad) in accordance with the manufacturer's instructions. Culture medium collected on ALI culture day 21 was diluted at 1:10,000 for TIMP-1 analysis or 1:100 for TIMP-2 analysis. The concentrations of TIMP-3 and TIMP-4 were lower than the detection limits even when the culture medium was analyzed without dilution.

3.2.6 PCR array analysis for ECM-related genes

Total RNA was isolated from tissues using RNeasy (Qiagen, Hilden, Germany), and the RNA quality was analyzed with an Agilent 2100 Bioanalyzer (Agilent Technologies, Santa Clara, CA, USA). The RNA integrity number of the samples was ≥ 7.6 . Complementary DNA was synthesized with a High-Capacity complementary DNA Reverse Transcription Kit (Applied Biosystems, Waltham, MA, USA). The gene expression profile was analyzed with the Human Extracellular Matrix and Adhesion Molecules RT 2 Profiler PCR Array (PAHS-013, SABiosciences, Frederick, MD, USA) on an ABI 7900 PCR system (Applied Biosystems).

3.2.7 Statistical analysis

With the exception of the PCR array results, data are presented as the means and standard deviations of triplicate inserts. Dunnett's or student's *t*-test was used and the results were

considered to be significant at $p < 0.05$. All statistical analyses, except for those of the PCR array data, were performed using Ekuseru Toukei software (Social Survey Research Information Co., Ltd.). The PCR array data were analyzed using RT 2 Profiler PCR Array Data Analysis version 3.5 (SABiosciences).

3.3 Results

3.3.1 Mucociliary differentiation of the 3D bronchial tissue model

Culture conditions for the 3D bronchial tissue model were established through several preliminary studies (summarized in Supplementary information). After 21 days of ALI culture, the differentiation status of the 3D bronchial tissue model was evaluated by histological analysis. A histological section of the bronchial tissue model showed similar morphology to actual human bronchial tissue (Figure 3.3a and b). To confirm the mucociliary differentiation, the tissues were stained using anti-acetylated α -tubulin antibody (a marker for ciliated cells), anti-mucin 5AC antibody (a marker for goblet cells), and anti-cytokeratin 5 antibody (a marker for basal cells). These markers were used to confirm mucociliary differentiation of the bronchial epithelium *in vitro*^{23, 24}. The results indicated that the 3D bronchial tissue had cilia on the apical surface of epithelial layer, goblet cells in the epithelial layer, and basal cells on the basal side of the epithelium (Figure 3.3c). These expression patterns are consistent with actual human tissue (Figure 3.3a).

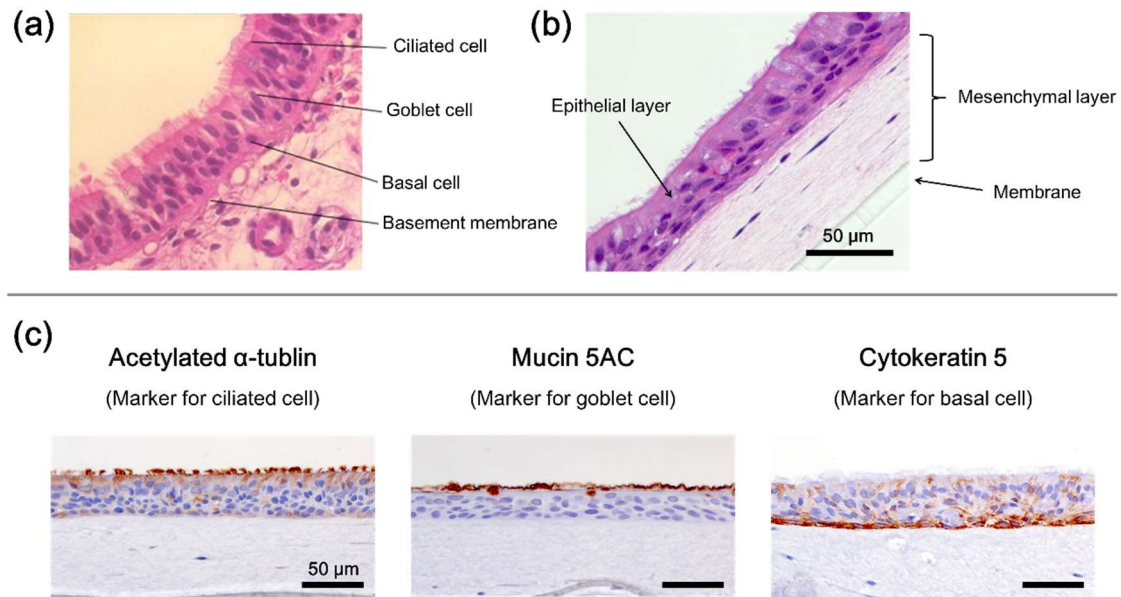


Figure 3.3 Histological analysis of the differentiation status of the bronchial tissue model.

(a) An image of actual human bronchial tissue reproduced from the literature ²⁵. (b) Hematoxylin and eosin staining of the bronchial tissue model developed in this study. The model is composed of the epithelial layer and mesenchymal layer of the porous membrane of the cell culture insert. (c) Immunohistochemical analysis of differentiation markers. The results confirmed the presence of acetylated α -tubulin-positive ciliated cells, mucin 5AC-positive goblet cells, and cytokeratin 5-positive basal cells.

3.3.2 Collagen gel contraction following TGF- β 1 stimulation

Because the 3D bronchial tissue model has a similar morphology to actual *in vivo* tissue, the responses of the tissue model to TGF- β 1 stimulation were analyzed. The 3D bronchial tissue model was stimulated with TGF- β 1 for 21 days under ALI culture conditions. Collagen gel contraction is a typical phenomenon observed in the collagen matrix model of fibroblasts, and this was also observed in the untreated control 3D bronchial tissue model on ALI culture days 7, 14, and 21 (Figure 3.4a–c). This contraction was significantly enhanced by stimulation with TGF- β 1 (Figure 3.4c). On ALI culture day 21, detachment of the collagen gel from the sidewall of the cell culture insert was detected following stimulation with 4 or 10 ng/mL TGF- β 1 (Figure 3.4b, arrowheads). When TGF- β signaling was blocked by 5 μ M SB525334 (TGF- β receptor type I blocker), gel contraction was not observed (Figure 3.4b and c).

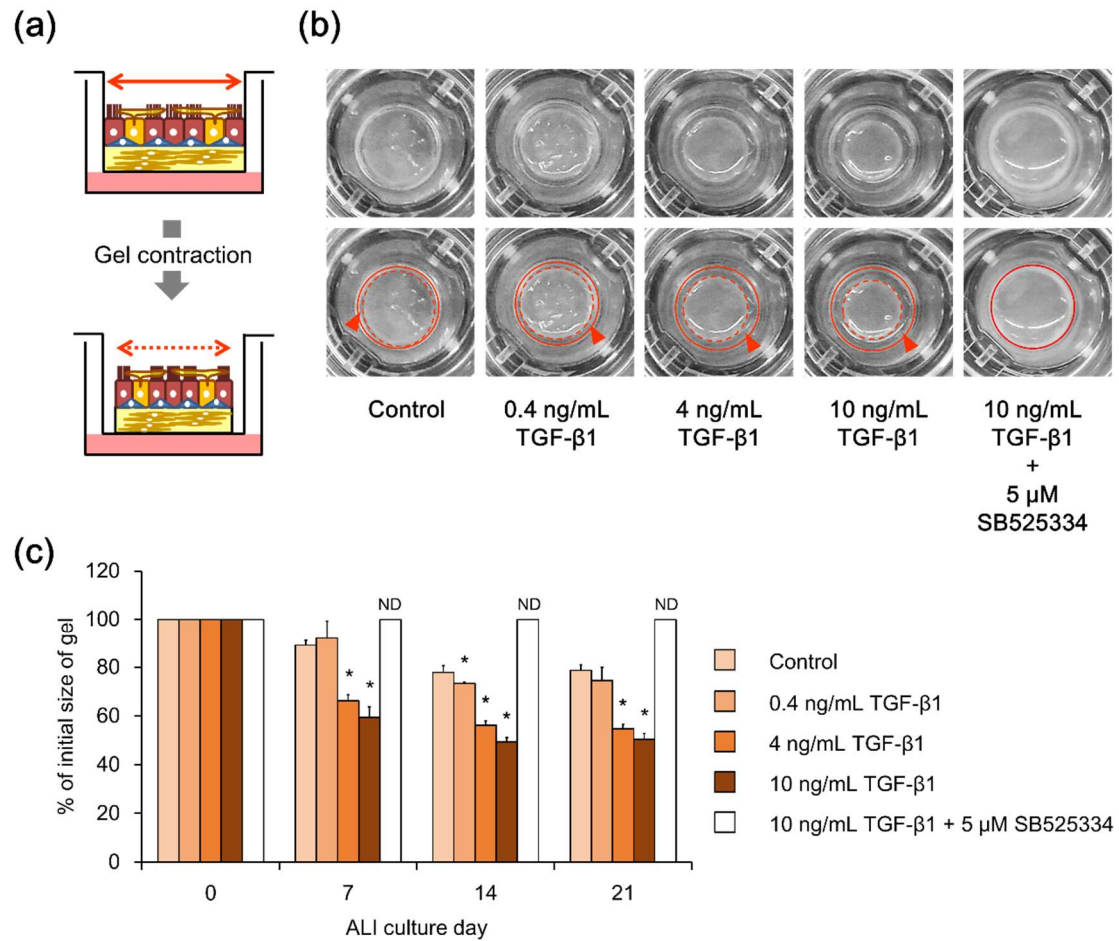


Figure 3.4 Quantitative analysis of collagen gel contraction in the bronchial tissue model stimulated with TGF-β1.

(a) Illustration of collagen gel contraction. The bronchial tissue model shrunk because of collagen gel contraction, and a gap appeared between the wall of the cell culture insert and the collagen gel. (b) Images of the bronchial tissue model on air-liquid interface (ALI) culture day 21. The edge of cell culture insert (red line) and the edge of the collagen gel matrix (red dotted line) are shown in the second row of images. Arrowheads indicate gaps between the wall of the cell culture insert and the collagen gel. (c) Quantification of collagen gel contraction. The level of the contraction is expressed as the percentage of the final gel area relative to the initial gel area. Analyses were performed on ALI culture days 0, 7, 14, and 21. The results indicate means and standard deviations of three tissue samples. * $p < 0.05$ in Dunnett's test against the control at each time point. ND, not detected; TGF, transforming growth factor.

3.3.3 Histological changes induced by TGF- β 1 stimulation

To understand the mechanism behind the gel contraction induced by TGF- β 1, histological analysis was performed on tissues collected on ALI culture day 21. The tissues were stained using anti-E-cadherin antibody (an epithelial cell marker), anti-vimentin antibody (a mesenchymal cell marker), and anti- α -SMA antibody (a myofibroblast marker). These markers are frequently used to investigate the effect of TGF- β on epithelial cells (induction of the epithelial-mesenchymal transition [EMT]) and mesenchymal cells (myofibroblast differentiation) in *in vitro* experiments^{26, 27}. In the epithelial layer, decreased thickness and E-cadherin expression were observed following TGF- β stimulation (Figure 3.5). In line with the decrease in E-cadherin expression, an increase in vimentin expression was confirmed in the basal cells in the epithelium (Fig 3.5, arrowheads). In the mesenchymal layer, increases in vimentin-expressing fibroblasts and α -smooth muscle actin (SMA)-expressing myofibroblasts were confirmed (Figure 3.5). All these changes were blocked by 5 μ M SB525334.

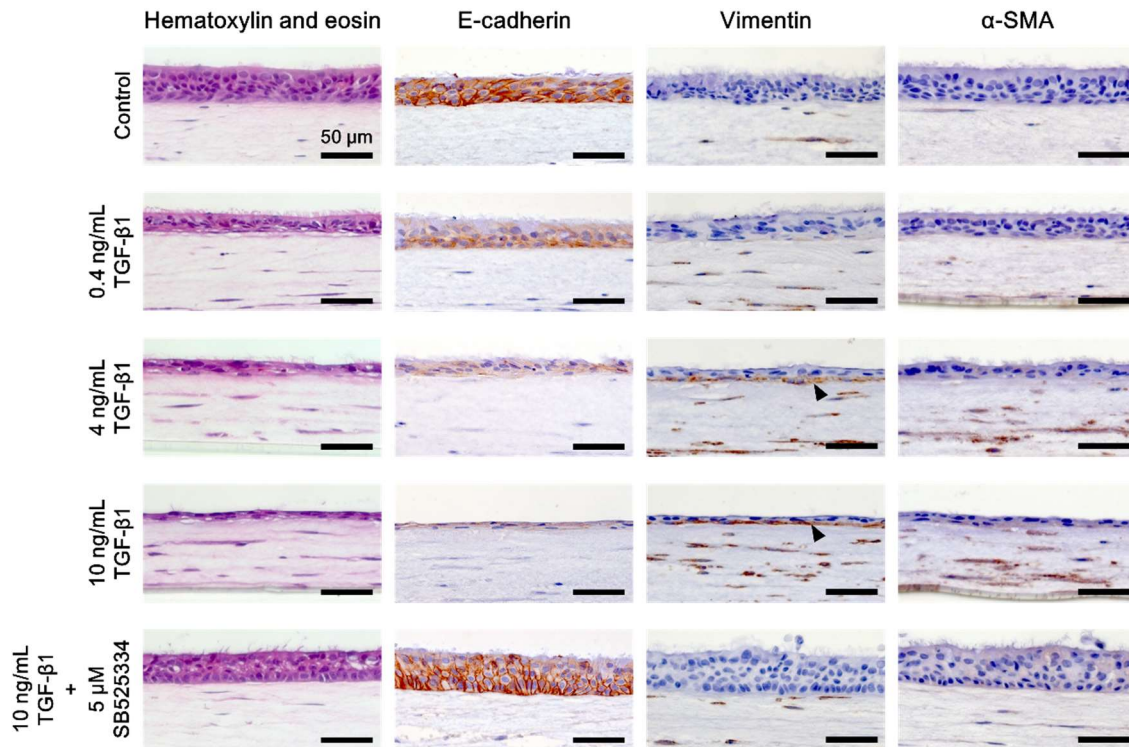


Figure 3.5 Histological analysis of the bronchial tissue model stimulated with TGF- β 1 on culture day 21.

In addition to hematoxylin and eosin staining, immunostaining was performed with E-cadherin (epithelial cell marker), vimentin (mesenchymal cell marker), and α -smooth muscle actin (α -SMA; myofibroblast marker). Arrowheads indicate vimentin-positive basal cells in the epithelial layer. TGF, transforming growth factor.

The changes detected by immunostaining were quantified by image analysis. A significant decrease in E-cadherin expression (Figure 3.6a) and a significant increase in vimentin expression (Figure 3.6b) in the epithelial layer were detected after TGF- β 1 treatment. In the mesenchymal layer, significant increases in vimentin and α -SMA expression were observed after TGF- β 1 treatment (Figure 3.6c and d).

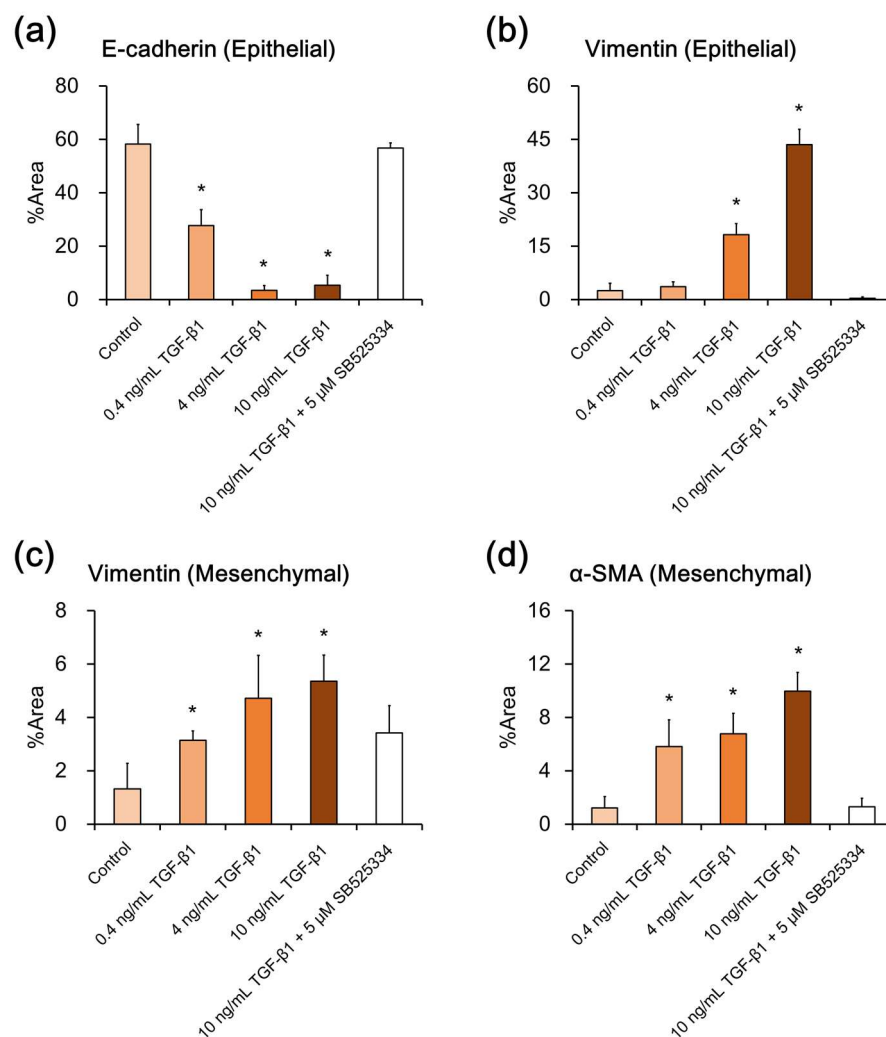


Figure 3.6 Quantitative analysis of the immunostaining results.

The percentages of E-cadherin-positive (a) and vimentin-positive (b) areas in the epithelial layer. The percentages of vimentin-positive (c) and α -smooth muscle actin (α -SMA)-positive (d) areas in the mesenchymal layer. The results indicate means and standard deviations for three tissue samples. * $p < 0.05$ in Dunnett's test against the control. TGF, transforming growth factor.

3.3.4 Effect of TGF-β1 on expression of MMPs

The histological data indicated that TGF-β1 promoted remodeling of bronchial tissue *in vitro*. In the pathogenesis of airway remodeling, altered ECM homeostasis (i.e., the balance of ECM production and degradation) is an important process. Therefore, the activities of ECM degrading enzymes MMP-2 and MMP-9 in the basolateral culture

medium were analyzed by gelatin zymography on ALI culture day 21. Pro-MMP-9, pro-MMP-2, and active MMP-2 were detected (Figure 3.7a). Enzymatic activity of pro-MMP-9 secreted from the 3D bronchial tissue model was not affected following stimulation with TGF- β 1 (Figure 3.7b). However, treatment with 5 μ M SB525334 suppressed secretion of pro-MMP-9 from the 3D bronchial tissue model (Figure 3.7b). Secretions of pro-MMP-2 and active MMP-2 were increased following stimulation with TGF- β 1 in a concentration-dependent manner (Figure 3.7c and d). By the addition of 5 μ M SB525334, the increased secretions of pro-MMP-2 and active MMP-2 were blocked (Figure 3.7c and d).

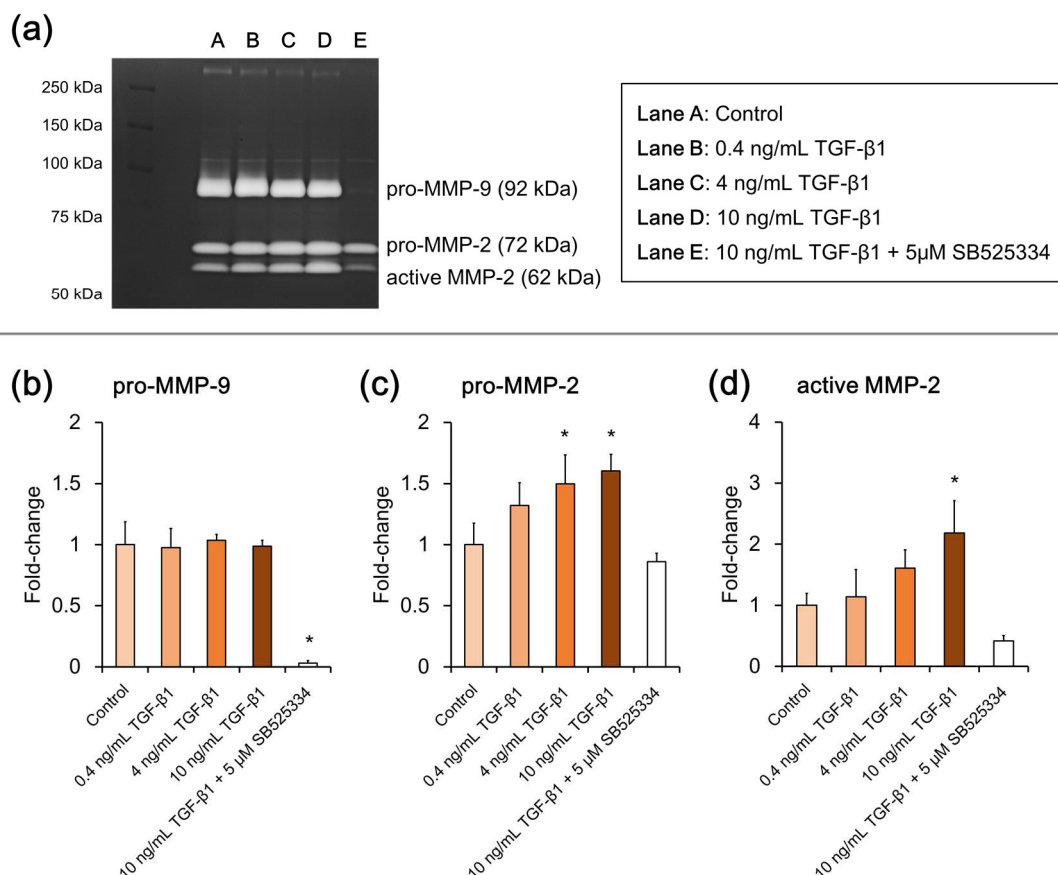


Figure 3.7 Analysis of MMPs secreted from the bronchial tissue model on culture day 21.

(a) Gelatin zymography image. The fold change of band density relative to the control for (b) pro-matrix metalloproteinase (MMP)-9, (c) pro-MMP-2, and (d) active MMP-2. The results indicate means and standard deviations of three tissue samples. * $p < 0.05$ in Dunnett's test against the control. TGF, transforming growth factor.

3.3.5 Effect of TGF- β 1 on expression of TIMPs

In addition to analysis of the expression levels of MMPs, the expression levels of their natural inhibitor TIMPs were analyzed on ALI culture day 21. The level of TIMP-1 (inhibitor for MMP-9) showed significant increase following stimulation with 4 or 10 ng/mL TGF- β 1 (Figure 3.8a). The increased secretion of TIMP-1 with 10 ng/mL TGF- β 1 stimulation was suppressed to the level of the control by addition of 5 μ M SB525334 (Figure 3.8a). The level of TIMP-2 (inhibitor for MMP-2) showed a similar trend to that of TIMP-1, and significantly increased following stimulation with TGF- β 1 (Figure 3.8b).

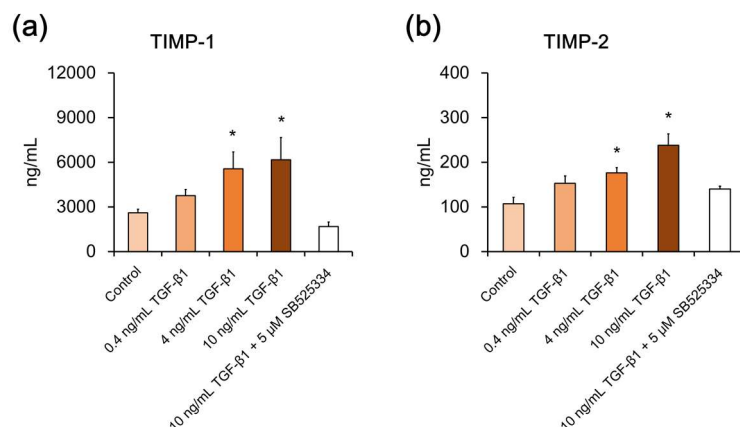


Figure 3.8 Analysis of TIMPs secreted from the bronchial tissue model on culture day 21.

Concentration of tissue inhibitor of metalloproteinase (TIMP)-1 (a) and TIMP-2 (b) in the medium were analyzed. The results indicate means and standard deviations of three tissue samples. * $p < 0.05$ in Dunnett's test against the control. TGF, transforming growth factor.

3.3.6 Effect of TGF-β1 on ECM-related genes

To further understand ECM homeostasis in the TGF-β1 stimulated 3D bronchial tissue model, expression of ECM-related genes was analyzed on ALI culture day 21. The expression levels of 84 genes were analyzed, and 33 genes showed significant increases following stimulation with TGF-β1 (Figure 3.9). These genes were categorized as follows: TGF-β and integrins, adhesion molecules, TIMPs and MMPs, collagens, and ECM glycoproteins and proteoglycans. Expression levels of these genes were concentration-dependently upregulated by TGF-β1 stimulation, and these increases were suppressed by adding 5 μM SB525334 (Figure 3.9). The top five upregulated genes in the bronchial tissue model following treatment with 10 ng/mL TGF-β1 were *FNI* (29.32-fold change), *TNC* (10.53-fold change), *VCAN* (7.75-fold change), *MMP9* (7.38-fold change), and *COL1A1* (6.80-fold change).

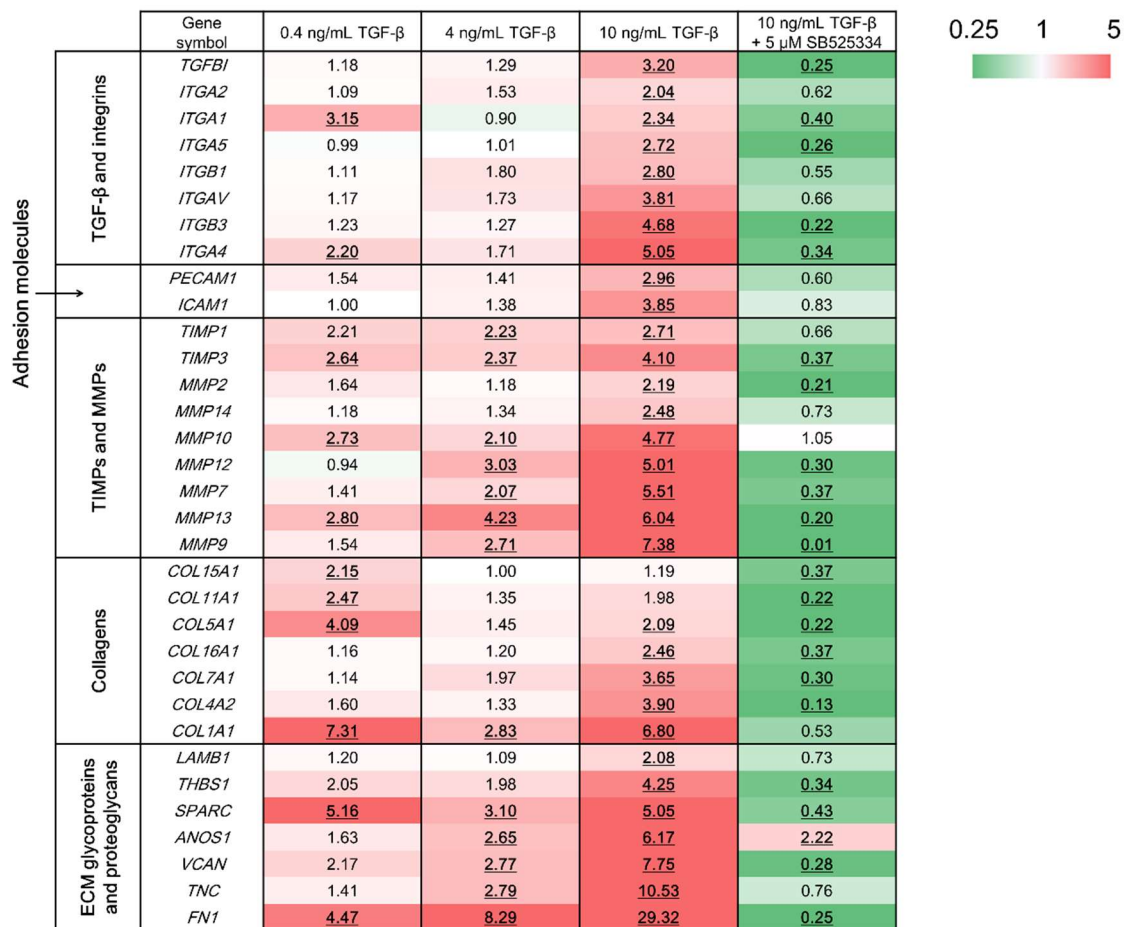


Figure 3.9 Significantly increased expression of extracellular matrix-related genes in the 3D bronchial tissue model following TGF-β1 stimulation on culture day 21.

All data are expressed as means of three tissue samples. Results where the fold change was more than 2 or less than 0.5 and significantly different compared with the control ($p < 0.05$, Student's t -test) are underlined. ECM, extracellular matrix; MMP, matrix metalloproteinase; TGF, transforming growth factor; TIMP, tissue inhibitor of metalloproteinase.

3.3.7 Effect of TGF-β1 on the ECM protein expression pattern

As expressions of *FN1* and *TNC* were dramatically upregulated (Figure 3.9), the proteins encoded by these genes were analyzed in their expression patterns in the 3D bronchial tissue model by immunostaining. Although fibronectin expression was mainly across the mesenchymal layer (Figure 3.10), the existence of fibronectin-positive basal cells was confirmed in the epithelium following TGF-β1 stimulation (Figure 3.10, arrowheads).

Same as in the fibronectin, tenascin-C was expressed across the mesenchymal layer, and stained denser following TGF- β 1 stimulation. Heavy staining of tenascin-C was detected in the basement membrane zone of the bronchial tissue model (Figure 3.10, arrows). Expression of both fibronectin and tenascin-C decreased when TGF- β signaling was suppressed by 5 μ M SB525334.

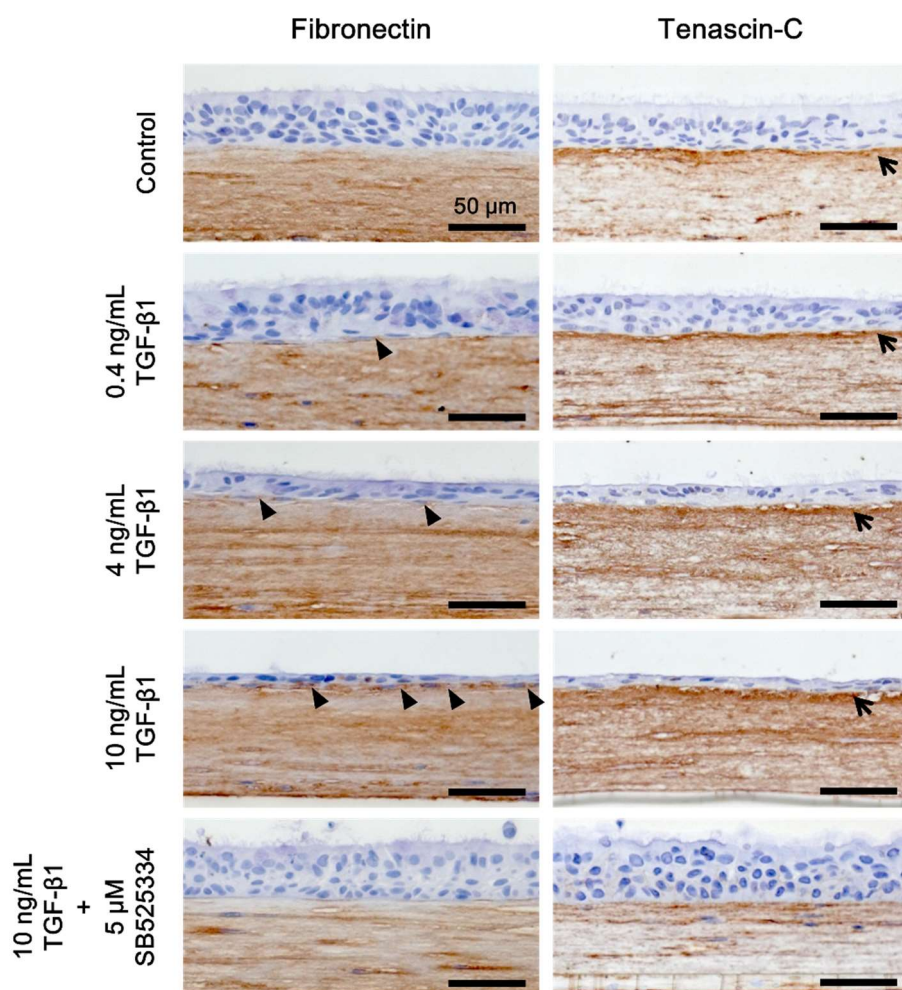


Figure 3.10 Histological analysis of extracellular matrix proteins on culture day 21.

Tissues were stained with fibronectin and tenascin-C. For the fibronectin results, arrowheads indicate fibronectin-positive basal cells following transforming growth factor (TGF)- β 1 stimulation. For the tenascin-C results, arrows indicate strong expression of tenascin-C in the sub-epithelial basement membrane following TGF- β 1 stimulation.

3.3.8 Effect of TGF- β 1 on a fibroblast mono-culture

To highlight the importance of the co-culture of HBECs and fibroblasts in the bronchial tissue model, several experiments were performed with a fibroblast mono-culture model (Figure 3.11a). The mono-culture model of collagen embedded fibroblast was stimulated with 10 ng/mL of TGF- β 1, and expression levels of MMPs (Figure 3.11b, c, and d), TIMPs (Figure 3.11e and f), and ECM-related genes (Figure 3.12) were analyzed. Unlike the results in the co-cultured bronchial tissue model, secretion of pro-MMP-9 was very low in the fibroblast mono-culture model, even after the stimulation with TGF- β 1 (Figure 3.11b). Although secretion of pro-MMP-2 increased following stimulation with TGF- β 1 (Figure 3.11c), the levels of active MMP-2 did not increase in the fibroblast mono-culture model with TGF- β 1 stimulation (Figure 3.11d). Secretion of TIMP-1 and TIMP-2 increased in the fibroblast mono-culture model stimulated with TGF- β 1 in the same manner as in the co-cultured bronchial tissue model (Figure 3.11e and f). The expression profiles of 33 genes, which showed significant changes in the co-cultured bronchial tissue model (Figure 3.9), were analyzed in the fibroblast mono-culture model following TGF- β 1 stimulation. The results indicated that stimulation with 10 ng/mL TGF- β 1 upregulated only 9 out of the 33 genes in the fibroblast mono-culture model (Figure 3.12).

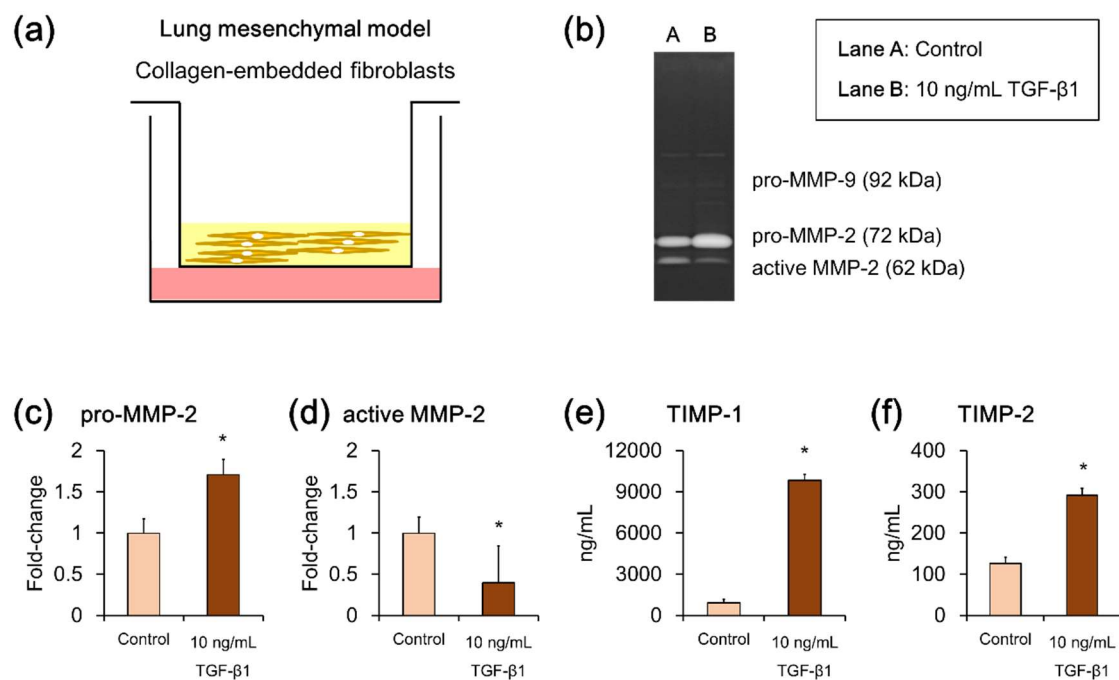


Figure 3.11 Expression of MMPs and TIMPs in the lung mesenchymal model (fibroblast mono-culture model) following TGF- β 1 stimulation on culture day 21.

(a) Illustration of the lung mesenchymal model. (b) Gelatin zymography image. The fold change of the band density relative to the control for (c) pro-matrix metalloproteinase (MMP)-2 and (d) active MMP-2. The concentrations of tissue inhibitor of metalloproteinase (TIMP)-1 (a) and TIMP-2 (b) in the medium were also analyzed. The results indicate means and standard deviations of three tissue samples. * $p < 0.05$ in Student's t -test against the control. TGF, transforming growth factor.

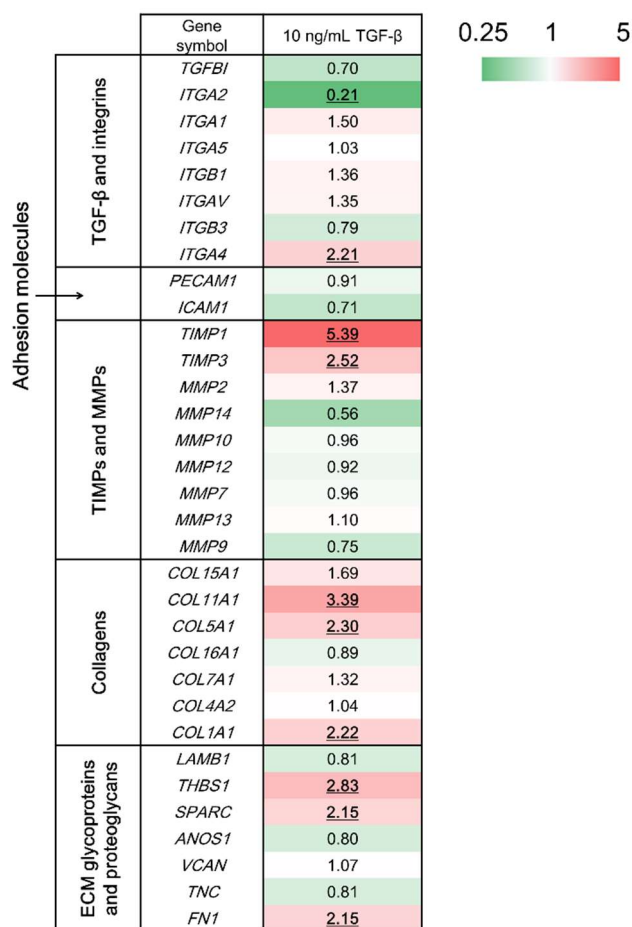


Figure 3.12 Expression of extracellular matrix-related genes in the 3D lung mesenchymal model following TGF-β1 stimulation on culture day 21.

All data are expressed as means of three tissue samples. Results where the fold change was more than 2 or less than 0.5 and significantly different compared with the control ($p < 0.05$, Student's t -test) are underlined. ECM, extracellular matrix; MMP, matrix metalloproteinase; TGF, transforming growth factor; TIMP, tissue inhibitor of metalloproteinase.

3.4 Discussion

Recent advancements in bioengineering have enabled generation of lung organoids made of matrigels and biocompatible alginate beads^{28, 29}. The co-culture of multiple types of cells (e.g., epithelial, mesenchymal, and endothelial cells) is one of the novelties of these organoid models. The 3D bronchial tissue model developed in this chapter is a co-culture model prepared using an ALI culture of HBECs on fibroblasts in a collagen gel matrix.

This 3D bronchial tissue model contains ciliated cells, goblet cells, and basal cells, as observed in actual human bronchial tissue (Figure 3.3). The novelty of this tissue model is the potential to recapitulate cell–cell and cell–ECM interactions, which is possible when epithelial cells are directly co-cultured with a mesenchymal layer. This was not recapitulated in the transmembrane co-culture model (MucilAir-HF) in the previous studies (Table 1.1). Various studies suggest that the ECM composition affects cell signaling, cell proliferation, apoptosis and EMT in the epithelial cells through adhesion through integrins³⁰⁻³². Therefore, the developed co-culture model can replicate the tissue response *in vivo* to the agent being tested. To confirm if this model could develop the lung disease phenotype, the model was subjected to TGF- β 1 stimulation, which is involved in the pathogenesis of various lung diseases.

The collagen gel contraction assay is an established assay, and various previous studies have shown that gel contractility in the fibroblast culture in the matrix was enhanced by TGF- β signaling⁷⁻⁹. As in these previous studies, collagen gel contraction was detected in the 3D bronchial tissue model and the contraction at each time point was enhanced by TGF- β 1 stimulation (Figure 3.4). This gel contraction was suppressed by inhibiting activin receptor-like kinase (ALK) 5-mediated Smad2/3 phosphorylation with the TGF- β type I receptor blocker SB525334^{33, 34}. This suggests that the TGF- β 1/ALK5 pathway is important for collagen gel contraction in this experiment, and is supported by a previous study showing that TGF- β 1 signaling mediated by Smad3 is necessary for collagen gel contraction³⁵.

To investigate the mechanisms underlying the gel contraction, histological analysis was performed on the 3D bronchial tissue model following TGF- β 1 stimulation. Induction of the EMT is one of the most prominent effects of TGF- β in various tissues^{36, 37}. The decrease in E-cadherin (epithelial marker) expression and increase in vimentin (mesenchymal marker) expression observed in the epithelial layer (Figures 3.5, 3.6a, and 3.6b) are typical of the EMT following stimulation with TGF- β ^{38, 39}. In addition, increases in vimentin-positive fibroblasts and α -SMA-positive myofibroblasts were confirmed in the mesenchymal layer (Figures 3.5, 3.6c, and 3.6d). These results indicate that TGF- β 1 promotes fibroblast proliferation in the mesenchymal layer and that they differentiate into

contractile myofibroblasts. These changes in fibroblasts are critical process in collagen gel contraction^{9, 40}. Thus, an increase in the number of contractile myofibroblasts in the mesenchymal layer of the 3D bronchial tissue model may have promoted the observed gel contraction.

Apart from accumulation of myofibroblasts, an increased deposition of ECM proteins is an important step in the airway remodeling induced by TGF- β 1⁴¹, and both MMPs and TIMPs are the main regulators of the ECM turnover. MMPs digest ECM components and TIMPs are their natural inhibitors⁴²⁻⁴⁴. Thus, the MMP/TIMP balance is an important determinant in various tissues in controlling the overall proteolytic activity⁴⁵⁻⁴⁷. Therefore, the expression levels of MMP-9 and MMP-2 (Figure 3.7) and of TIMP-1 and TIMP-2 (Figure 3.8) were measured in the 3D bronchial tissue model on culture day 21. TGF- β 1 stimulation upregulated secretion of pro-MMP-2 and active MMP-2 (Figure 3.7c and d). TGF- β 1 stimulation did not change the levels of pro-MMP-9 secretion (Figure 3.7b). However, when TGF- β signaling was blocked with SB525334, TGF- β signaling was shown to be involved in pro-MMP-9 secretion. As both MMPs and TIMPs were upregulated (Figures 3.7 and 3.8), the MMP/TIMP balance might not be affected in the 3D bronchial tissue model even with TGF- β 1 stimulation. In a study using a mono-culture model of collagen embedded fibroblasts, secretions of pro-MMP-9 and active MMP-2 were not promoted with TGF- β 1 stimulation (Figure 3.11b and d), whereas TIMP-1 and TIMP-2 were (Figure 3.11e and f). These findings suggest that epithelial cells are necessary for secretion of pro-MMP-9 and active MMP-2 in the bronchial tissue model, and that the proteolytic activities of these MMPs are controlled by TIMPs secreted from the mesenchymal fibroblasts. This supports the importance of the epithelial-mesenchymal interaction in controlling the ECM homeostasis.

For further characterization of the TGF- β 1 effects on ECM deposition in the 3D bronchial tissue model, changes in the expression of the genes related to ECM homeostasis were analyzed. Thirty-three genes that were significantly upregulated in the 3D bronchial tissue model (Figure 3.9) could be regulated by the TGF- β 1/ALK5 pathway because these increases were suppressed by SB525334. Transmembrane receptor integrins are reported to contribute to EMTU homeostasis and play various roles in tissue

remodeling^{19, 48}. Upregulation of integrin families affects tissue remodeling through mechanisms such as activation of TGF- β and induction of myofibroblasts⁴⁹. Consistent with the findings for TIMPs and MMPs, gene expression of *MMP2*, *MMP9*, and *TIMP1* was regulated by TGF- β 1 signaling. In addition, increased expression was confirmed in various *MMPs*, which reportedly play important roles in airway tissue remodeling⁵⁰. The increased expression was also observed in genes encoding various collagens, ECM glycoproteins, and ECM proteoglycans, which could be substrates for MMPs. Promotion of ECM production was suggested by the increased expression levels of these genes. The lower expression levels of these genes in the fibroblast mono-culture model following TGF- β 1 stimulation (Figure 3.12) indicate that co-culture conditions are necessary for induction of these genes. This indicates HBECs plays some important roles in the pathogenesis of airway remodeling induced by TGF- β 1.

The expression of *FNI* and *TNC* increased dramatically following stimulation with 10 ng/mL TGF- β 1 in the 3D bronchial tissue model (Figure 3.9). The expression pattern of fibronectin and tenascin-C (proteins encoded by *FNI* and *TNC*) in the lungs is reportedly related to inflammatory lung diseases such as asthma and COPD^{51, 52}. These proteins were shown to be expressed across the mesenchymal layer by histological analysis (Figure 3.10). However, TGF- β 1 promoted expression of fibronectin in basal cells of the 3D bronchial tissue model (Figure 3.10, arrowheads). In addition to expression of vimentin, expression of fibronectin in basal cells of the bronchial epithelium is considered one aspect of EMT⁵³. In the case of tenascin-C, strong expression was observed in the basement membrane of the bronchial tissue model (Figure 3.10, arrows), in a pattern consistent with *in vivo* expression⁵⁴. The expression of both tenascin-C in the sub-epithelial region and fibronectin in basal cells decreased when TGF- β 1 signaling was blocked with SB525334. This indicates involvement of the TGF- β 1/ALK5 pathway in ECM deposition in bronchial tissues. When bronchial epithelial cells are directly co-cultured on collagen-embedded fibroblasts, sub-epithelial region is reproduced in *in vitro* model. Because fibrotic changes in this region known as sub-epithelial fibrosis are important process in the pathogenesis of asthma and COPD^{55, 56}, the 3D bronchial tissue model, which reproduces the EMTU *in vitro*, could be useful for elucidating the

mechanisms how sub-epithelial changes are induced by interactions between bronchial epithelial cells and mesenchymal cells.

3.5 Conclusions

The co-culture model of 3D bronchial tissue developed in this chapter enables direct interactions between bronchial epithelial cells, fibroblasts, and their ECM components. The developed model successfully reproduces multiple events observed in fibrosis following stimulation with TGF- β 1, including EMT in the epithelial layer, accumulation of myofibroblasts in the mesenchymal layer, and ECM deposition in the mesenchymal layer (Figure 3.13). Therefore, this model could develop airway remodeling, which is an important phenotype observed in inflammatory lung diseases. This 3D bronchial tissue model could be a useful tool for detection of disease-relevant changes associated with exposure to whole CS.

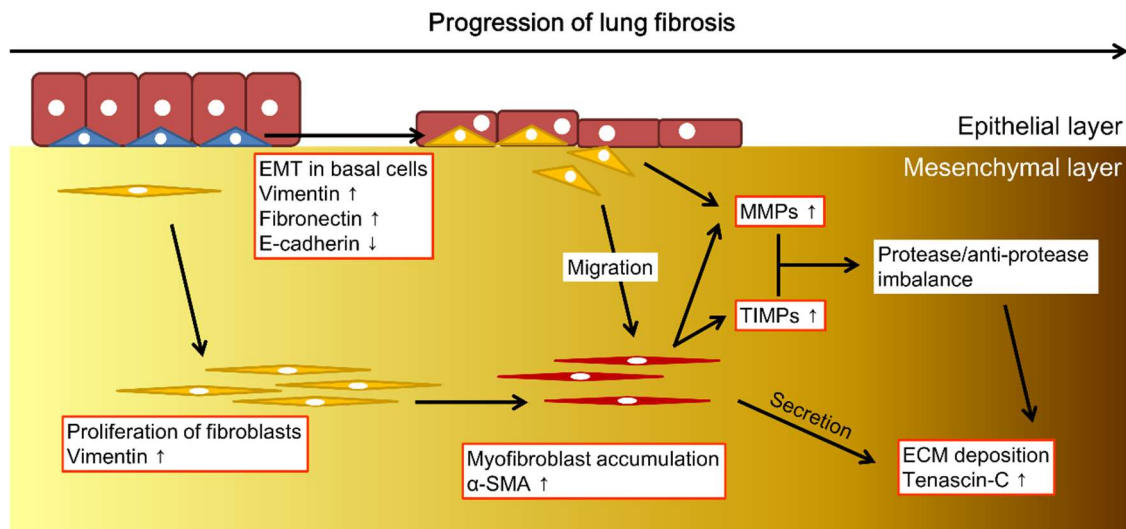


Figure 3.13 Schematic illustration of fibrotic changes in the epithelial mesenchymal trophic unit. The events observed in the 3D bronchial tissue model following transforming growth factor- β 1 stimulation in this study are in red rectangles. ECM, extracellular matrix; EMT, epithelial mesenchymal transition; MMP, matrix metalloproteinase; SMA, smooth muscle actin; TIMP, tissue inhibitor of metalloproteinase.

3.6 References

1. Whitcutt, M.J., Adler, K.B. & Wu, R. A biphasic chamber system for maintaining polarity of differentiation of cultured respiratory tract epithelial cells. *In Vitro Cell Dev Biol* **24**, 420-428 (1988).
2. Baxter, A. *et al.* Targeted omics analyses, and metabolic enzyme activity assays demonstrate maintenance of key mucociliary characteristics in long term cultures of reconstituted human airway epithelia. *Toxicol In Vitro* **29**, 864-875 (2015).
3. Boei, J. *et al.* Xenobiotic metabolism in differentiated human bronchial epithelial cells. *Arch Toxicol* **91**, 2093-2105 (2017).
4. Hill, D.B. & Button, B. Establishment of respiratory air-liquid interface cultures and their use in studying mucin production, secretion, and function. *Methods Mol Biol* **842**, 245-258 (2012).
5. Kesimer, M. *et al.* Tracheobronchial air-liquid interface cell culture: a model for innate mucosal defense of the upper airways? *Am J Physiol Lung Cell Mol Physiol* **296**, L92-L100 (2009).
6. Tarran, R., Grubb, B.R., Gatzky, J.T., Davis, C.W. & Boucher, R.C. The relative roles of passive surface forces and active ion transport in the modulation of airway surface liquid volume and composition. *J Gen Physiol* **118**, 223-236 (2001).

7. Montesano, R. & Orci, L. Transforming growth factor beta stimulates collagen-matrix contraction by fibroblasts: implications for wound healing. *Proc Natl Acad Sci U S A* **85**, 4894-4897 (1988).
8. Finesmith, T.H., Broadley, K.N. & Davidson, J.M. Fibroblasts from wounds of different stages of repair vary in their ability to contract a collagen gel in response to growth factors. *J Cell Physiol* **144**, 99-107 (1990).
9. Kurosaka, H., Kurosaka, D., Kato, K., Mashima, Y. & Tanaka, Y. Transforming growth factor-beta 1 promotes contraction of collagen gel by bovine corneal fibroblasts through differentiation of myofibroblasts. *Invest Ophthalmol Vis Sci* **39**, 699-704 (1998).
10. Carroll, N., Elliot, J., Morton, A. & James, A. The structure of large and small airways in nonfatal and fatal asthma. *Am Rev Respir Dis* **147**, 405-410 (1993).
11. Kuhn, C. & McDonald, J.A. The roles of the myofibroblast in idiopathic pulmonary fibrosis. Ultrastructural and immunohistochemical features of sites of active extracellular matrix synthesis. *Am J Pathol* **138**, 1257-1265 (1991).
12. Jeffery, P.K. Remodeling in asthma and chronic obstructive lung disease. *Am J Respir Crit Care Med* **164**, S28-38 (2001).
13. Berube, K., Prytherch, Z., Job, C. & Hughes, T. Human primary bronchial lung cell constructs: the new respiratory models. *Toxicology* **278**, 311-318 (2010).
14. Kolb, M., Margetts, P.J., Anthony, D.C., Pitossi, F. & Gauldie, J. Transient expression of IL-1beta induces acute lung injury and chronic repair leading to pulmonary fibrosis. *J Clin Invest* **107**, 1529-1536 (2001).
15. Temelkovski, J., Hogan, S.P., Shepherd, D.P., Foster, P.S. & Kumar, R.K. An improved murine model of asthma: selective airway inflammation, epithelial lesions and increased methacholine responsiveness following chronic exposure to aerosolised allergen. *Thorax* **53**, 849-856 (1998).
16. Doherty, T. & Broide, D. Cytokines and growth factors in airway remodeling in asthma. *Curr Opin Immunol* **19**, 676-680 (2007).
17. Evans, M.J., Van Winkle, L.S., Fanucchi, M.V. & Plopper, C.G. The attenuated fibroblast sheath of the respiratory tract epithelial-mesenchymal trophic unit. *Am J Respir Cell Mol Biol* **21**, 655-657 (1999).
18. Holgate, S.T. *et al.* Epithelial-mesenchymal interactions in the pathogenesis of asthma. *J Allergy Clin Immunol* **105**, 193-204 (2000).
19. Araya, J., Cambier, S., Morris, A., Finkbeiner, W. & Nishimura, S.L. Integrin-mediated transforming growth factor-beta activation regulates homeostasis of the pulmonary epithelial-mesenchymal trophic unit. *Am J Pathol* **169**, 405-415 (2006).
20. de Boer, W.I., Alagappan, V.K. & Sharma, H.S. Molecular mechanisms in chronic obstructive pulmonary disease: potential targets for therapy. *Cell Biochem Biophys* **47**, 131-148 (2007).

21. Davies, D.E. The role of the epithelium in airway remodeling in asthma. *Proc Am Thorac Soc* **6**, 678-682 (2009).
22. Ruifrok, A.C. & Johnston, D.A. Quantification of histochemical staining by color deconvolution. *Anal Quant Cytol Histol* **23**, 291-299 (2001).
23. Levardon, H., Yonker, L.M., Hurley, B.P. & Mou, H. Expansion of Airway Basal Cells and Generation of Polarized Epithelium. *Bio Protoc* **8** (2018).
24. Yonker, L.M. *et al.* Development of a Primary Human Co-Culture Model of Inflamed Airway Mucosa. *Sci Rep* **7**, 8182 (2017).
25. Gras, D., Chanez, P., Vachier, I., Petit, A. & Bourdin, A. Bronchial epithelium as a target for innovative treatments in asthma. *Pharmacol Ther* **140**, 290-305 (2013).
26. Chen, T. *et al.* Epithelial-mesenchymal transition involved in pulmonary fibrosis induced by multi-walled carbon nanotubes via TGF-beta/Smad signaling pathway. *Toxicol Lett* **226**, 150-162 (2014).
27. Lv, Z.D. *et al.* Transforming growth factor-beta 1 enhances the invasiveness of breast cancer cells by inducing a Smad2-dependent epithelial-to-mesenchymal transition. *Oncol Rep* **29**, 219-225 (2013).
28. Tan, Q., Choi, K.M., Sicard, D. & Tschumperlin, D.J. Human airway organoid engineering as a step toward lung regeneration and disease modeling. *Biomaterials* **113**, 118-132 (2017).
29. Wilkinson, D.C. *et al.* Development of a Three-Dimensional Bioengineering Technology to Generate Lung Tissue for Personalized Disease Modeling. *Stem Cells Transl Med* **6**, 622-633 (2017).
30. Aoshiba, K., Rennard, S.I. & Spurzem, J.R. Cell-matrix and cell-cell interactions modulate apoptosis of bronchial epithelial cells. *Am J Physiol* **272**, L28-37 (1997).
31. Han, S.W. & Roman, J. Fibronectin induces cell proliferation and inhibits apoptosis in human bronchial epithelial cells: pro-oncogenic effects mediated by PI3-kinase and NF-kappa B. *Oncogene* **25**, 4341-4349 (2006).
32. Mamuya, F.A. & Duncan, M.K. α V integrins and TGF-beta-induced EMT: a circle of regulation. *J Cell Mol Med* **16**, 445-455 (2012).
33. Higashiyama, H. *et al.* Inhibition of activin receptor-like kinase 5 attenuates bleomycin-induced pulmonary fibrosis. *Exp Mol Pathol* **83**, 39-46 (2007).
34. Thomas, M. *et al.* Activin-like kinase 5 (ALK5) mediates abnormal proliferation of vascular smooth muscle cells from patients with familial pulmonary arterial hypertension and is involved in the progression of experimental pulmonary arterial hypertension induced by monocrotaline. *Am J Pathol* **174**, 380-389 (2009).
35. Kobayashi, T. *et al.* Smad3 mediates TGF-beta1-induced collagen gel contraction by human lung fibroblasts. *Biochem Biophys Res Commun* **339**, 290-295 (2006).

36. Zavadil, J. & Bottinger, E.P. TGF-beta and epithelial-to-mesenchymal transitions. *Oncogene* **24**, 5764-5774 (2005).
37. Katsuno, Y., Lamouille, S. & Derynck, R. TGF-beta signaling and epithelial-mesenchymal transition in cancer progression. *Curr Opin Oncol* **25**, 76-84 (2013).
38. Hackett, T.L. *et al.* Induction of epithelial-mesenchymal transition in primary airway epithelial cells from patients with asthma by transforming growth factor-beta1. *Am J Respir Crit Care Med* **180**, 122-133 (2009).
39. Kalluri, R. & Weinberg, R.A. The basics of epithelial-mesenchymal transition. *The Journal of clinical investigation* **119**, 1420 (2009).
40. Desmouliere, A., Chaponnier, C. & Gabbiani, G. Tissue repair, contraction, and the myofibroblast. *Wound Repair Regen* **13**, 7-12 (2005).
41. Halwani, R., Al-Muhsen, S., Al-Jahdali, H. & Hamid, Q. Role of transforming growth factor-beta in airway remodeling in asthma. *Am J Respir Cell Mol Biol* **44**, 127-133 (2011).
42. Lagente, V. *et al.* Role of matrix metalloproteinases in the development of airway inflammation and remodeling. *Braz J Med Biol Res* **38**, 1521-1530 (2005).
43. Visse, R. & Nagase, H. Matrix metalloproteinases and tissue inhibitors of metalloproteinases: structure, function, and biochemistry. *Circ Res* **92**, 827-839 (2003).
44. Nagase, H. & Woessner, J.F., Jr. Matrix metalloproteinases. *J Biol Chem* **274**, 21491-21494 (1999).
45. Mercer, P.F. *et al.* MMP-9, TIMP-1 and inflammatory cells in sputum from COPD patients during exacerbation. *Respir Res* **6**, 151 (2005).
46. Perez, P. *et al.* Increased acinar damage of salivary glands of patients with Sjogren's syndrome is paralleled by simultaneous imbalance of matrix metalloproteinase 3/tissue inhibitor of metalloproteinases 1 and matrix metalloproteinase 9/tissue inhibitor of metalloproteinases 1 ratios. *Arthritis Rheum* **52**, 2751-2760 (2005).
47. Watanabe, N. & Ikeda, U. Matrix metalloproteinases and atherosclerosis. *Curr Atheroscler Rep* **6**, 112-120 (2004).
48. Cox, D., Brennan, M. & Moran, N. Integrins as therapeutic targets: lessons and opportunities. *Nat Rev Drug Discov* **9**, 804-820 (2010).
49. Margadant, C. & Sonnenberg, A. Integrin-TGF-beta crosstalk in fibrosis, cancer and wound healing. *EMBO Rep* **11**, 97-105 (2010).
50. Pardo, A., Cabrera, S., Maldonado, M. & Selman, M. Role of matrix metalloproteinases in the pathogenesis of idiopathic pulmonary fibrosis. *Respir Res* **17**, 23 (2016).
51. Annoni, R. *et al.* Extracellular matrix composition in COPD. *Eur Respir J* **40**, 1362-1373 (2012).
52. Estany, S. *et al.* Lung fibrotic tenascin-C upregulation is associated with other extracellular matrix proteins and induced by TGFbeta1. *BMC Pulm Med* **14**, 120 (2014).

- 53. Gohy, S.T. *et al.* Imprinting of the COPD airway epithelium for dedifferentiation and mesenchymal transition. *Eur Respir J* **45**, 1258-1272 (2015).
- 54. Laitinen, A. *et al.* Tenascin is increased in airway basement membrane of asthmatics and decreased by an inhaled steroid. *Am J Respir Crit Care Med* **156**, 951-958 (1997).
- 55. Homer, R.J. & Elias, J.A. Airway remodeling in asthma: therapeutic implications of mechanisms. *Physiology (Bethesda)* **20**, 28-35 (2005).
- 56. Roche, W.R., Beasley, R., Williams, J.H. & Holgate, S.T. Subepithelial fibrosis in the bronchi of asthmatics. *Lancet* **1**, 520-524 (1989).

Chapter 4.

**Establishment of whole CS exposure conditions reproducing
actual human airway tissue doses**

4.1 Introduction

4.1.1 Objectives

The 3D bronchial tissue model described in the previous chapter developed a disease phenotype under appropriate stimulation. The use of this human-relevant tissue model with the whole CS exposure system will enable determination of the toxicological effects of CS on the development of smoking-related lung disease. However, when performing whole CS exposure, not only human relevance to the tissue model, but also human relevance to the exposed CS dose will be important to recapitulate the actual human tissue response *in vitro*. Therefore, in the experiments presented in this chapter, characterization of the newly developed whole CS exposure module was performed before applying it to whole CS exposure of the 3D bronchial tissue model. The objective of the characterization was to establish whole CS exposure conditions reproducing the actual human airway tissue dose.

4.1.2 Study approaches

A whole CS exposure module named the RFS module has been developed by Cultex Technologies GmbH for application to CS and aerosolized particle exposure experiments with ALI cultured cells (Figure 4.1) ^{1,2}. This module is characterized by a radial feed of the test aerosol from one sampling point to the cells (Figure 4.1c). This results in homogeneous deposition of the aerosolized particles on the cells, which has been confirmed by computational fluid dynamics and experiments with model particles ^{3,4}. As demonstrated in Chapter 2, dosimetry data (i.e., the cell CS exposure dose) are important for determining dose-dependent biological effects in whole CS exposure experiments. Moreover, when using toxicological data obtained in whole CS exposure experiments for risk assessments, knowledge of the *in vitro* dose and comparison with an *in vivo* dose are necessary ⁵. In other words, a 3D bronchial tissue model should be exposed to whole CS at a dose similar to the actual *in vivo* bronchial tissue dose. Therefore, in this chapter, one *in vitro* dosimetry study was performed with this module and another with human volunteers.

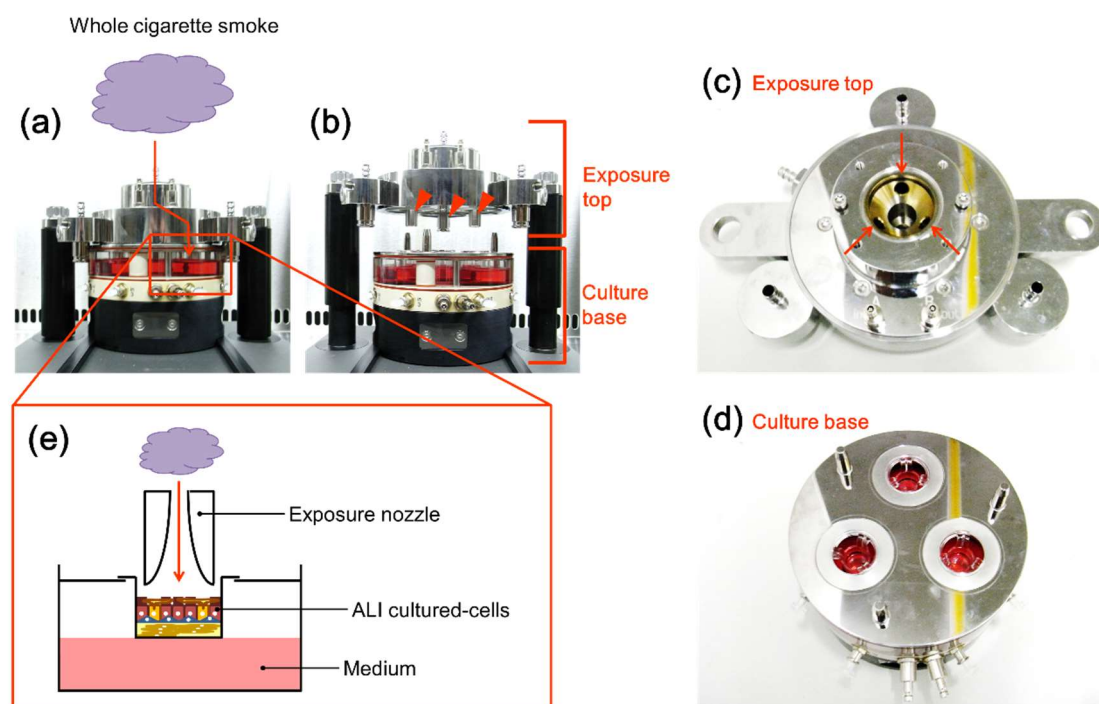


Figure 4.1 Images of the Cultex RFS module.

(a) The Cultex RFS module is closed for whole cigarette smoke exposure. (b) The Cultex RFS module is open for sampling. Arrowheads indicate exposure nozzles. (c) Exposure top. Arrows indicate holes that lead to the radially arranged exposure nozzles. (d) Culture base. Three culture inserts can be placed on the culture base. (e) Inside the exposure module. Air–liquid interface (ALI) cultured cells are exposed to whole cigarette smoke delivered from the exposure nozzle at a constant flow rate. The cells are supplied to the medium and warmed with a water jacket during the exposure.

For the dosimetry study, solanesol and acetaldehyde were selected as representative chemicals to simulate the PP and GVP of whole CS, respectively. Solanesol is frequently used as a PP marker of CS because of its abundance and non-volatility^{6,7}. Acetaldehyde is reportedly present in the GVP of CS^{8,9}. Whole CS exposure was performed with a cell culture insert containing a trapping solution for solanesol and acetaldehyde (Figure 4.2). Reference cigarettes (3R4F) were smoked in accordance with the ISO standard or intensive regime. The smoke was diluted with air (0.5–8.0 L/min) in a tunnel and delivered to the cell culture insert containing the trapping solution (Figure 4.2). Then, the mass of solanesol and acetaldehyde deposited on the cell culture insert were calculated from the concentrations of these chemicals in the trapping solution. From this *in vitro*

dosimetry test, relationships between the dilution flow rate and PP/GVP chemical deposition were estimated. In a previous report on whole CS exposure experiments, the quantity of whole CS supplied to the exposure module was calculated according to a formula¹⁰⁻¹². However, not all of the CS supplied to the exposure module will be deposited onto the cell culture. Thus, it will be better to use the mass of CS chemicals actually deposited on the surfaces of the cells for discussing dose-dependent biological reactions. Several previous studies have revealed that use of a target tissue dose rather than less specific dosimetry information, such as the exposure concentration, can improve the correlation with the dose response for inhaled gases and particles^{13, 14}.

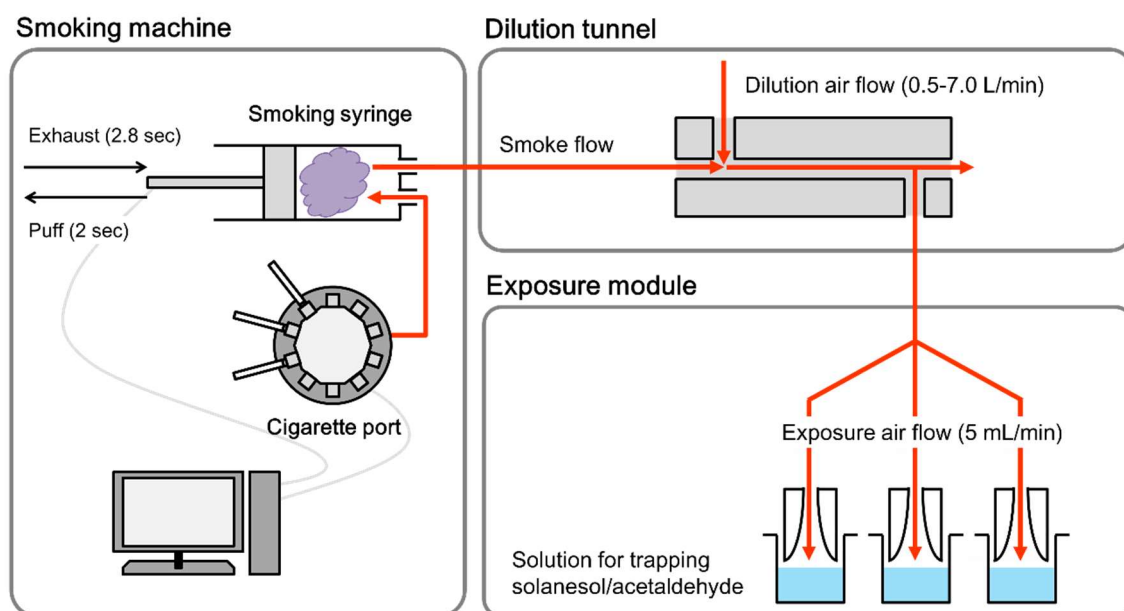


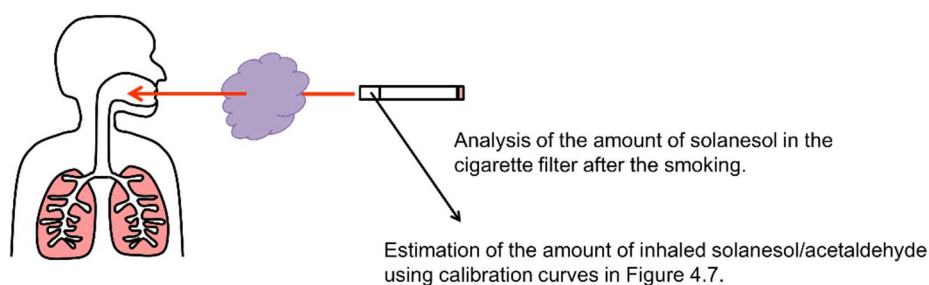
Figure 4.2 Illustration of the whole cigarette smoke exposure system with the Cultex RFS module.

Test cigarettes are inserted in the cigarette holder on a cigarette port and smoked by a computer controlled syringe. In this research, the volume of puff taken by the syringe was 35 mL in the ISO standard regime and 55 mL in the ISO intensive regime. Then, generated cigarette smoke was introduced into the dilution system with a 2.8-s puff exhaust time. The cigarette smoke was mixed with air for dilution in the dilution system and introduced into the exposure module with air at a constant flow rate of 5 mL/min.

To clarify whether the *in vitro* dosimetry data were consistent with the *in vivo* data, the deposition of solanesol and acetaldehyde in the respiratory system of a smoker was

estimated in a human retention study. As previously reported, the amounts of inhaled CS chemicals can be estimated because they show good correlations with the amount of solanesol retained in the cigarette filter after smoking (Figure 4.3a) ^{15, 16}. In addition, the amounts of exhaled CS chemicals can be determined by direct sampling (Figure 4.3b). By comparing the amounts of inhaled CS chemicals and exhaled CS chemicals, the *in vivo* deposition percentages can be calculated. Moreover, the differences in the deposition percentages among different inhalation patterns (i.e., mouth hold, shallow inhalation, and normal inhalation) can be used to estimate the regional deposition of each representative chemical in the subject (Figure 4.4).

(a) Inhalation



(b) Exhalation

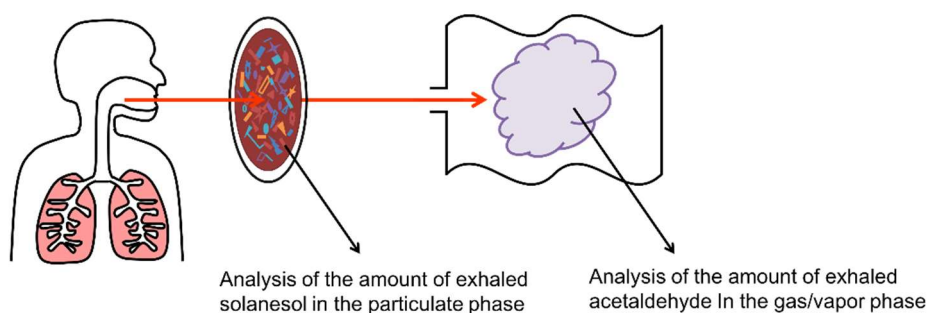


Figure 4.3 Retention study concept.

(a) Estimation of the amount of inhaled cigarette smoke. The amount of solanesol in the cigarette filter after smoking is correlated with the amounts of cigarette smoke constituents inhaled by the smoker. This relationship is used for estimation of the amounts of inhaled solanesol and acetaldehyde. (b) Estimation of the amount of exhaled cigarette smoke. Exhaled smoke is collected on a glass filter and in a sampling bag, and is then analyzed.

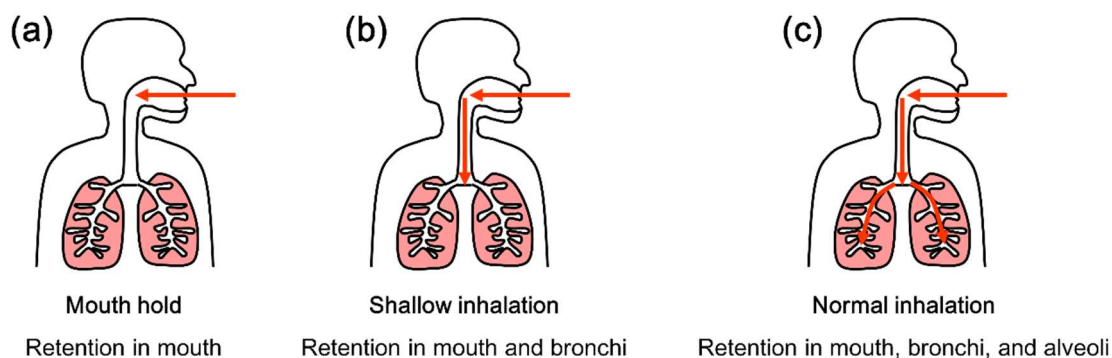


Figure 4.4 Inhalation patterns used in the retention study.

(a) Mouth hold: to measure deposition in mouth, the human subject did not inhale the smoke. (b) Shallow inhalation: to measure deposition in the mouth and bronchi, the subject inhaled the cigarette smoke and then 150 mL of air from a sampling bag before exhaling. (c) Normal inhalation: to measure deposition in the whole respiratory system (i.e., mouth, bronchi, and alveoli), the subject inhaled the cigarette smoke normally.

Two dosimetry studies were performed in this chapter: an *in vitro* dosimetry study with the whole CS exposure system and an *in vivo* dosimetry study with human volunteers (Figure 4.5). In the *in vitro* dosimetry study, CS was generated by the smoking machine. Because it is difficult to select a specific set of machine smoking parameters (e.g., puff volume, puff number, and puff interval) that reflect variations in the human smoking profile, two regulatory accepted machine smoking conditions (ISO standard and intensive smoking regimens^{17, 18}) were employed for smoke generation to cover the differences in smoking parameters of humans. Whole CS generated by the two smoking regimens was introduced into the exposure system and the introduced mass was considered as 100%. Then, whole CS introduced into the system was diluted by air flow (0.5–8.0 L/min) and the mass of tracer chemicals (solanesol and acetaldehyde) deposited on the culture surface was measured. The mass deposited on the culture surface was expressed as the percentage to introduction (%/cm²). In the *in vivo* dosimetry study, the masses of tracer chemicals inhaled and exhaled were analyzed. The mass introduced into the respiratory system (mass inhaled) was considered as 100%. The mass deposited (mass inhaled - mass exhaled) was expressed as the percentage to introduction. By comparing the data obtained from the three inhalation patterns, the mass deposited on the bronchial tissue surface was

expressed as the percentage to introduction ($\%/cm^2$). The obtained *in vitro* and *in vivo* deposition efficiencies were used to determine appropriate dilution air flow for whole CS exposure to reproduce the actual human bronchial tissue dose *in vitro*.

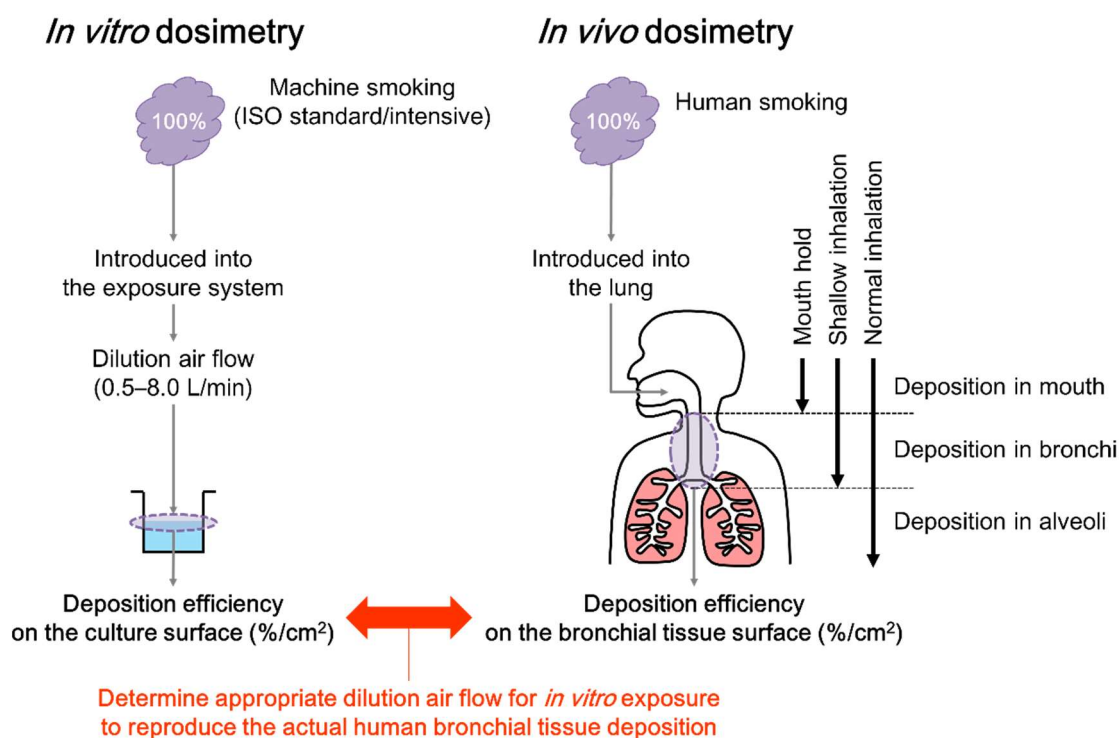


Figure 4.5 Approaches for comparison of *in vitro* and *in vivo* dosimetry data.

ISO, International Organization for Standardization.

4.2 Materials and methods

4.2.1 *In vitro* dosimetry test

4.2.1.1 Whole CS exposure

The experimental setup for the *in vitro* exposure experiments (Figure 4.2) consisted of a VC10 smoking robot (Vitrocell Systems GmbH), dilution tunnel, and Cultex RFS module (Cultex Technologies GmbH). The reference cigarettes (3R4F; University of Kentucky) were conditioned at 22 ± 2 °C and $60 \pm 5\%$ relative humidity for 48 h before use, and

then smoked in accordance with the ISO standard (35-mL puff volume, 60-s puff interval, 2-s puff duration, and no blocking of ventilation holes) or ISO intensive (55-mL puff volume, 30-s puff interval, 2-s puff duration, and 100% blocking of ventilation holes) regime. The CS that was generated by the smoking robot was released into a dilution tunnel with a 2.8-s exhaust time, and diluted with humidified clean air (> 90% relative humidity). For humidification of the dilution air, clean air was bubbled through water in an impinger maintained at 37 °C. Diluted smoke was introduced into the RFS module and directed into the exposure chamber (5 mL/min) using a vacuum pump.

4.2.1.2 Collection of chemicals in the mainstream CS

Solanesol in the whole CS was trapped using 44-mm Cambridge filter pads (Borgwaldt KC GmbH) inserted between the cigarette ports and the syringe. Solanesol was extracted from the pads and diluted with methanol. Each extract was filtered with a DISMIC-13HP filter (pore size 0.2 µm; Advantec) before HPLC analysis. Acetaldehyde in the mainstream CS was trapped by two or three 2,4-dinitrophenylhydrazine (DNPH) active gas tubes (Yotsubishi Corporation, Tokyo, Japan) connected in-line. The acetaldehyde trapped in each tube was eluted with 40 mL of a DNPH/acetonitrile/H₂O mixture containing 4.76 g of DNPH diluted to 500 mL with acetonitrile, 2.8 mL of perchloric acid, and sufficient H₂O to give a final volume of 1 L. For HPLC analysis, the eluted solvent was stabilized in 1.5 parts of a 2-amino-2-(hydroxymethyl)-1,3-propanediol (trizma base) solution containing 2 g of trizma base diluted to 200 mL with H₂O and sufficient acetonitrile to reach a final volume of 1 L. The masses of solanesol and acetaldehyde in the mainstream smoke were determined three times, and the mean and standard deviation were calculated.

4.2.1.3 Collection of CS deposited on the culture surface

To collect smoke, two cell culture inserts (Becton Dickinson) were stacked and bound. The bottom membrane of the upper insert was removed and the bottom membrane of the lower insert was sealed to create a space for the trapping solution (1.4 mL). The surface

height of the solution was adjusted to the position of the removed membrane. Solanesol was trapped by 1.4 mL of methanol and analyzed by HPLC. Acetaldehyde was trapped by 1.4 mL of H₂O and derivatized using equal parts of a DNPH/perchloric acid/acetonitrile mixture containing 9.52 g of DNPH, 5.6 mL of perchloric acid, and sufficient acetonitrile to reach a final volume of 1 L. Each trapping solution was filtered and stabilized in 1.5 parts of the trizma base solution before HPLC analysis. The experiment was repeated three times for each experimental condition, and the mean value for the three inserts in each experiment was used to calculate the mean and standard deviation for each experimental condition.

4.2.1.4 Calculation of *in vitro* dosimetry

The following equations were used to calculate the deposition efficiencies of solanesol and acetaldehyde.

$$\text{In vitro deposition efficiency (\%)} = \frac{\text{Mass deposited}}{\text{Mass introduced}} \times 100$$

The deposition efficiency per unit of surface area (%/cm²) was calculated by dividing the deposition efficiency (%) by the surface area of the insert cup (0.9 cm²). There are variations of the formula for calculating the *in vitro* deposition efficiency. However, the basic structure was common, and the amount collected (mass deposited) was divided by the input amount (mass introduced) per exposure¹⁹.

4.2.2 Human retention study for the *in vivo* dosimetry test

4.2.2.1 Study design

This study was conducted in compliance with the principles of the Declaration of Helsinki (2008). Seventeen male smokers who were employees of Japan Tobacco Inc. were provided with details of all of the study procedures before providing written informed

consent to participate. Each subject was made aware that they were free to leave the study at any time.

All cigarettes used in this study were CC1. The volunteers smoked three cigarettes using three different inhalation patterns (Figure 4.4). Each cigarette was smoked until a point approximately 3 mm from the tipping paper was reached, and the cigarette filter was removed from the remaining cigarette butt after smoking. The masses of smoke components inhaled by each subject were estimated using the mass of solanesol retained in the filter (Figure 4.3a). For the first cigarette, each subject took a puff every minute and held the smoke in their mouth for 2 s before exhaling (mouth hold). For the second cigarette, each subject took a puff every minute, held the smoke in their mouth for 2 s, and then inhaled 150 mL of air stored in a sampling bag (Omi Odor Air Service, Shiga, Japan) before exhaling (shallow inhalation). This inhalation pattern was based on those used in previous reports^{20,21}. For the third cigarette, each subject took a puff every minute, held the smoke in their mouth for 2 s, and then inhaled normally before exhaling (normal inhalation). Exhaled CS was collected using 92-mm Cambridge filter pads and sampling bags (Figure 4.3b). Solanesol was extracted from the filter pads using methanol. Each extract was diluted and filtered before HPLC analysis. CS exhaled into the sampling bag was passed through DNPH active gas tubes to collect acetaldehyde, and then eluted using 40 mL of the DNPH/acetonitrile/H₂O mixture. The eluted solvent was stabilized in 1.5 parts of the trizma base solution for HPLC analysis.

4.2.2.2 Estimation of the masses of inhaled smoke constituents

According to previous reports, there are good relationships between the mass of solanesol retained in the cigarette filter and the masses of delivered mainstream smoke constituents^{15, 16}. These relationships were used to estimate the masses of inhaled CS constituents. The commercial cigarettes used for the human retention study were smoked under six different smoking conditions (Table 4.1) using the Vitrocell VC10 smoking robot. Mainstream solanesol samples collected by 44-mm Cambridge filter pads and acetaldehyde samples collected by DNPH active gas tubes were analyzed using HPLC.

The experiment was repeated three times for each smoking condition. At the same time, the cigarette filter was removed from the remaining cigarette butt and solanesol retained in the filter was extracted into methanol and analyzed by HPLC. The relationships between the mainstream delivery mass for each constituent and the solanesol mass in the cigarette filter under different smoking conditions were analyzed using linear regression. The masses of smoke constituents inhaled by each subject were estimated using these relationships.

Table 4.1 Machine smoking conditions for the cigarettes used in the retention study.

Puff volume (mL)	Puff duration (sec)	Puff interval (sec)
30	2	30, 60
70	2	30, 60
120	2	30, 60

4.2.2.3 Calculation of regional deposition

The respiratory deposition of solanesol and acetaldehyde for each inhalation pattern was calculated as follows. This formula is used to analyze the deposition efficiency of various chemicals *in vivo* ²².

$$\begin{aligned}
 \text{In vivo deposition efficiency (\%)} &= \frac{\text{Mass deposited}}{\text{Mass introduced}} \times 100 \\
 &= \frac{\text{Mass inhaled} - \text{Mass exhaled}}{\text{Mass inhaled}} \times 100
 \end{aligned}$$

The mean deposition for the seventeen volunteers for each inhalation pattern was calculated and then used to calculate the regional deposition as shown below. Under the mouth-hold inhalation pattern, CS was considered to be deposited only in the mouth. The average volume of dead space in the upper airway where no exchange is possible between blood and breath is reportedly 150 mL ²³. Therefore, CS was assumed to be mainly deposited in the mouth and bronchi (dead space) under the shallow inhalation pattern.

With this presumption, deposition in the bronchial region was calculated as the difference between deposition under the shallow inhalation pattern and that under the mouth hold pattern. Deposition in the alveoli was also calculated as the difference between deposition under the normal inhalation pattern and that under the shallow inhalation pattern. The deposition efficiency per unit of surface area ($\%/cm^2$) of each respiratory region was calculated by dividing the deposition efficiency (%) by the surface area of each region ²⁴.

4.2.3 HPLC conditions

An Agilent 1100 series HPLC system (Agilent Technologies) was used for HPLC analysis. Solanesol analysis was performed as described in Chapter 2 (Section 2.2.7 HPLC conditions for analyzing solanesol). Acetaldehyde analysis was performed in accordance with a previously reported method ²⁵. For acetaldehyde analysis, a LiChrospher 100 RP-18e column (250 mm \times 4 mm inside diameter, 5- μ m particle size; Merck Millipore, Darmstadt, Germany) was used. The sample injection volume was 20 μ L. The HPLC separation used mobile phase flow rate of a 1.5 mL/min and a gradient to elute the analytes within 25 min. The gradient settings were as follows: 0–8 min, 70%/30% mobile phase A/B; 8–20 min, 47%/53% mobile phase A/B; and 20–27 min, 0%/100% mobile phase A/B. Mobile phase A was composed of 59% water, 30% acetonitrile, 10% tetrahydrofuran, and 1% 2-propanol. Mobile phase B was composed of 65% acetonitrile, 33% water, 1% tetrahydrofuran, and 1% 2-propanol. The detection wavelength was 365 nm.

4.2.4 Statistical analysis

Statistical analysis was performed with Welch's *t*-test and results were considered to be significant at $p < 0.05$.

4.3 Results

4.3.1 *In vitro* dosimetry test with the Cultex RFS module

4.3.2.1 Analysis of whole mainstream CS from 3R4F cigarettes

Solanesol and acetaldehyde levels in whole mainstream CS obtained from 3R4F cigarettes under the ISO standard and intensive smoking regimes were analyzed using HPLC. The masses of solanesol and acetaldehyde in whole CS under the ISO intensive smoking regime were approximately 2.9 times more than those under the ISO standard smoking regime (Table 4.2).

Table 4.2 Masses of solanesol and acetaldehyde in whole mainstream cigarette smoke from 3R4F cigarettes.

Smoking regime	Solanesol (µg/cig.)	Acetaldehyde (µg/cig.)
ISO standard	260.1 ± 11.1	555.7 ± 104.3
ISO intensive	755.7 ± 35.4	1619.2 ± 143.2

Mean and standard deviation of three independent experiments.

4.3.2.2 Analysis of smoke deposited on culture surfaces

The surface of the trapping solution was exposed to whole CS from 3R4F cigarettes at various dilutions and then analyzed by HPLC. The deposited mass of solanesol per cigarette was divided by the area of the cell culture insert to obtain a deposited mass per unit surface area. The deposited mass of solanesol decreased with the dilution flow rate under both smoking regimes (Figure 4.6a). In line with the increased mass of solanesol in mainstream CS per cigarette under the ISO intensive smoking regime (Table 4.2), the deposited mass of solanesol under the ISO intensive smoking regime was more than two times that under the ISO standard smoking regime at the same dilution (Figure 4.6a). Similar findings were observed for acetaldehyde (Figure 4.6b).

For further analysis, the deposited mass was expressed as a percentage of the generated mass in the whole CS. There were no significant differences between the deposition efficiencies of the constituents under the ISO intensive and standard regimes at the same dilution flow rate (Figure 4.7a and b).

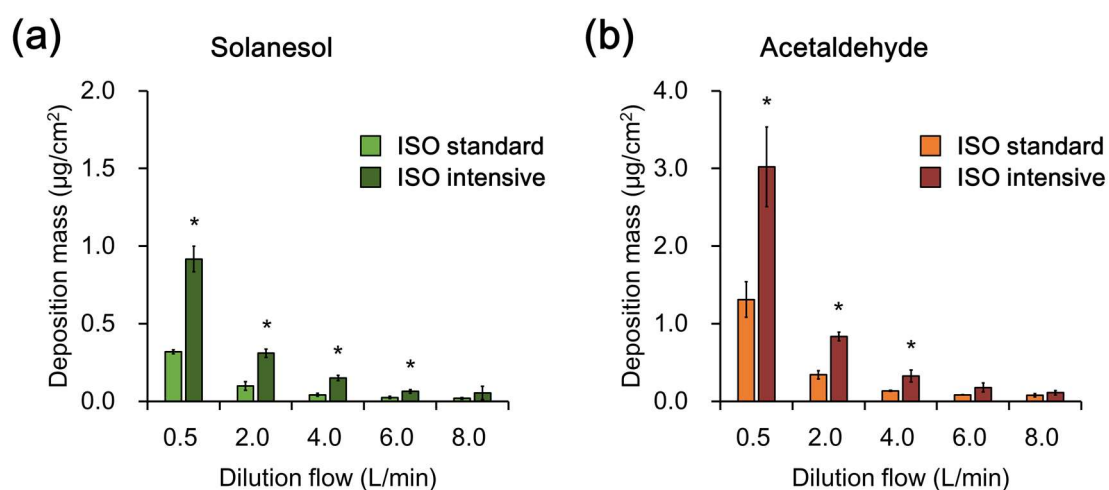


Figure 4.6 *In vitro* dosimetry results.

(a) Deposited mass of solanesol per unit surface area of the cell culture insert for one cigarette smoked under the ISO standard and intensive smoking regimes. (b) Deposited mass of acetaldehyde per unit surface area of the cell culture insert for one cigarette smoked under the ISO standard and intensive smoking regimes. * $p < 0.05$ (Welch's t -test).

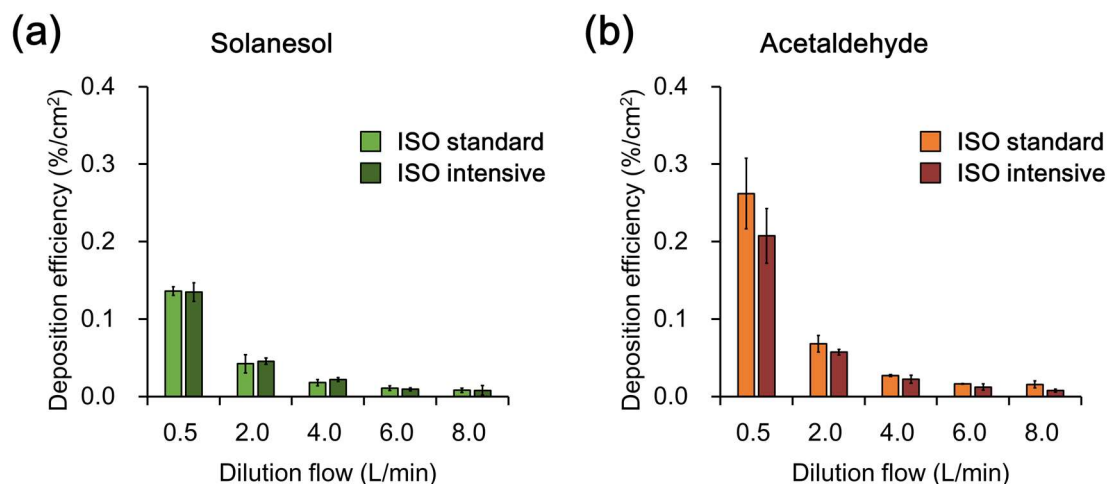


Figure 4.7 *In vitro* dosimetry results.

(a) The percentage of deposited solanesol to generated solanesol per unit surface area of the cell culture insert under the ISO standard and intensive smoking regimes. (b) The percentage of deposited acetaldehyde to generated acetaldehyde per unit surface area of the cell culture insert for one cigarette smoked under the ISO standard and intensive smoking regimes. The lack of a significant difference between the deposition efficiencies of the ISO standard and intensive regimes was confirmed with Welch's t -test ($p > 0.05$) at each dilution flow rate.

4.3.2 Human retention study for the *in vivo* dosimetry test

4.3.2.1 Establishment of an equation to estimate the mass of inhaled smoke

Commercially available CC1s were used for the solanesol and acetaldehyde retention study. The relationships between the mainstream delivery mass and the mass of solanesol retained in the cigarette filter for the two constituents are presented in Figure 4.8. Both constituents showed good correlations and the coefficients of determination (R^2) were approximately 0.9. The masses of solanesol in the filters of cigarette butts collected from the human study were analyzed to estimate the mass of smoke inhaled by each subject using the obtained formula.

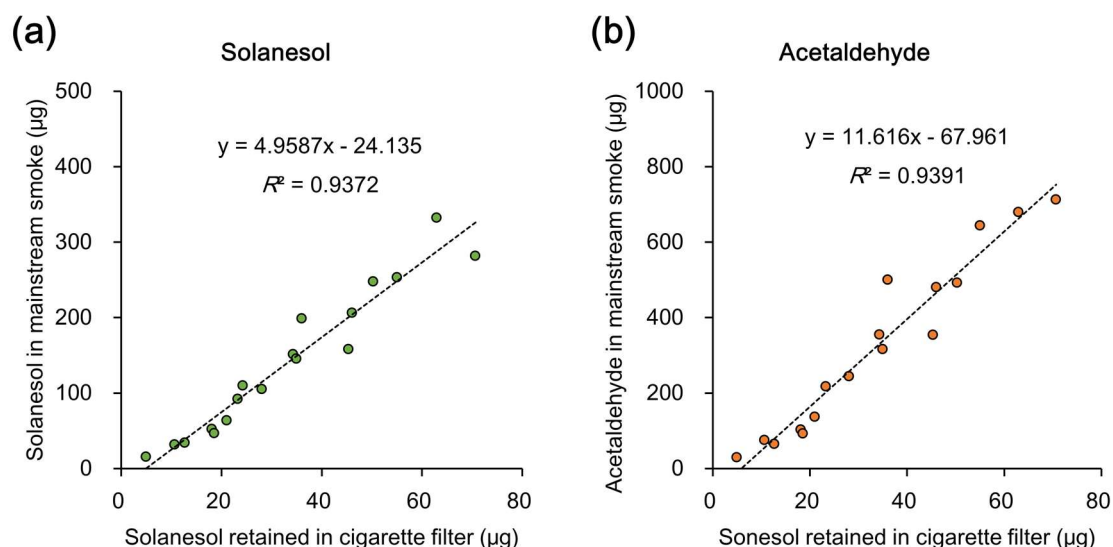


Figure 4.8 Regression lines between the masses of solanesol and acetaldehyde in the mainstream cigarette smoke used in the retention study and the mass of solanesol in the cigarette filter.

4.3.2.2 Retention study

Subjects smoked cigarettes under three different inhalation patterns (mouth hold, shallow inhalation, and normal inhalation) (Figure 4.4), and exhaled CS samples were collected on 92-mm Cambridge filter pads and in sampling bags for analysis (Figure 4.3b). The difference between the inhaled CS mass estimated from the mass of solanesol retained in the cigarette filter (Figure 4.3a) and the exhaled CS mass (Figure 4.3b) was used to calculate the deposition percentages of CS constituents for each inhalation pattern (Figure 4.9). Deposition of solanesol and acetaldehyde increased with the inhalation depth, and the deposition of acetaldehyde was higher than that of solanesol under each inhalation pattern. The deposition in each area (i.e., mouth, bronchi, and alveoli) was calculated by comparing the deposition for each inhalation pattern (Table 4.3). The deposition of solanesol was comparable among the respiratory areas (range 17.3%–22.6%), whereas that of acetaldehyde was higher in the upper respiratory tract than that in the lower respiratory tract (range 9.3%–44.4%). The deposition per unit area (Table 4.3) was calculated using the surface area of each respiratory region²⁴. Deposition of both solanesol and acetaldehyde per unit area was higher in the upper respiratory tract than in the lower respiratory tract (Table 4.3).

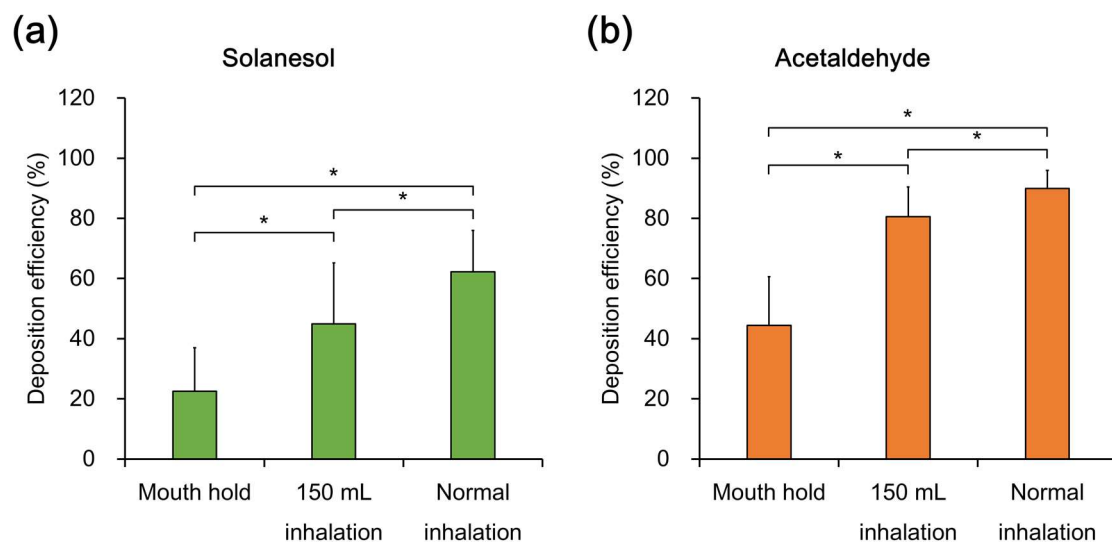


Figure 4.9 Respiratory deposition efficiencies of solanesol and acetaldehyde under three inhalation patterns.

The results represent means and standard deviations of results from 17 volunteers. *Significant difference between the inhalation patterns (Bonferroni-corrected $p < 0.05$, Welch's t -test).

Table 4.3 Deposition efficiency per unit surface area in each region of the respiratory tract.

Region	Area (cm ²)	Solanesol		Acetaldehyde		Acetaldehyde/Solanesol balance
		(%)	(%/cm ²)	(%)	(%/cm ²)	
Mouth	470	22.6	0.0480	44.4	0.0945	1.97
Bronchi	2690	22.4	0.00832	36.2	0.0135	1.62
Alveoli	1475000	17.3	0.0000117	9.3	0.0000063	0.54

Results are the means of those from 17 volunteers. Inhaled smoke was taken as 100%. The acetaldehyde/solanesol ratio of inhaled smoke was taken as 1.00. The surface area for each region was obtained from the literature ²⁴.

4.3.3 Comparison of *in vitro* and *in vivo* dosimetry

The results of the *in vitro* (Figure 4.7) and *in vivo* (Table 4.3) dosimetry studies were compared to establish human-relevant exposure conditions for whole CS exposure with

the RFS module. Single exponential decay regression of the *in vitro* dosimetry data provided a reasonable fit to the relationship between the deposition efficiency and the dilution flow rate (Figure 4.10). Because the 3D bronchial tissue model developed in Chapter 3 was subjected to whole CS exposure with this module, the deposition efficiencies in actual human bronchi (Table 4.3) are depicted in the graph at 0.00832%/cm² for solanesol and 0.0135%/cm² for acetaldehyde (Figure 4.10). The results indicated that with a dilution flow rate of approximately 8 L/min for exposure, actual bronchial tissue deposition efficiency would be achieved. Lines showing deposition efficiencies 10 times those in actual human bronchi are also depicted in the graph at 0.0832%/cm² for solanesol and 0.135%/cm² for acetaldehyde (Figure 4.10). The results indicated that a dilution flow rate of 1 L/min for exposure to one cigarette gave deposition of more than 10 times that in actual bronchial tissue, (i.e., similar to actual bronchial tissue deposition after smoking 10 cigarettes).

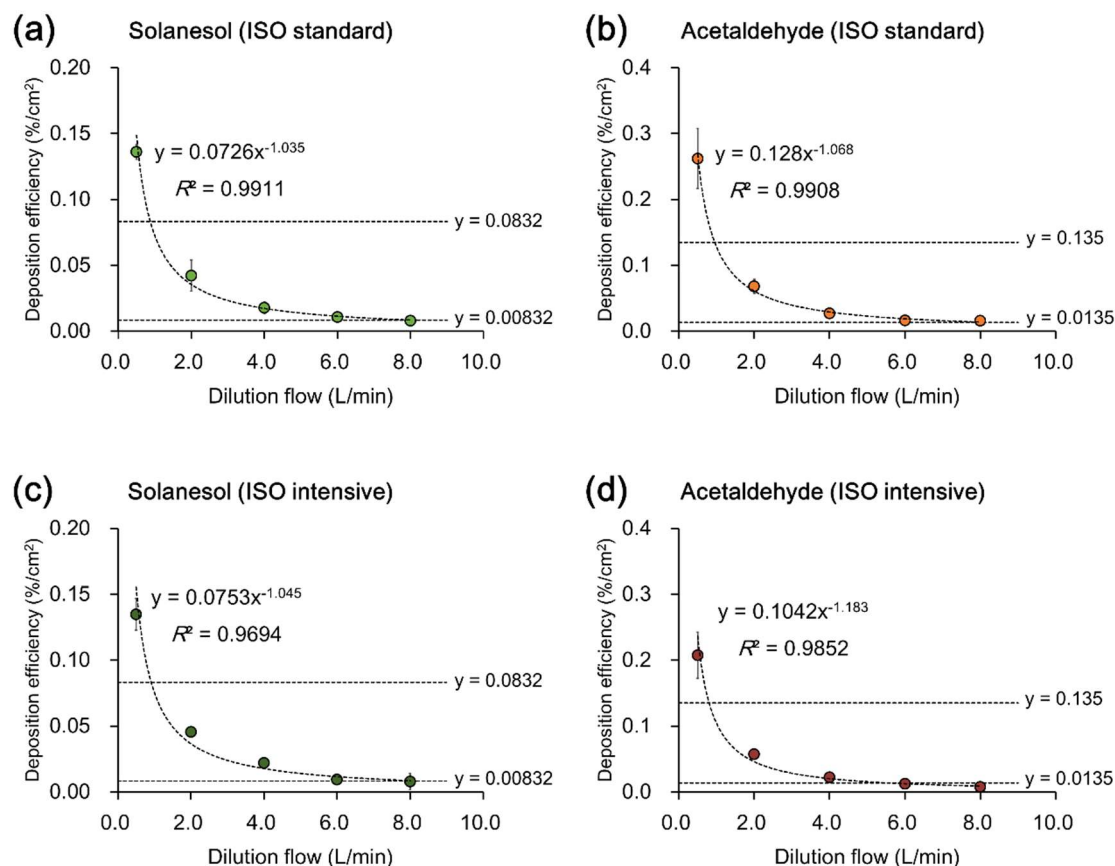


Figure 4.10 Relationship between *in vitro* and *in vivo* dosimetry data.

In vitro dosimetry data with cigarette smoke generated under the ISO standard smoking regime for (a) solanesol and (b) acetaldehyde. *In vitro* dosimetry data with cigarette smoke generated under the ISO intensive smoking regime for (c) solanesol and (d) acetaldehyde. *In vivo* dosimetry in actual bronchi is shown by the lines at 0.00832%/cm² for solanesol and 0.0135%/cm² for acetaldehyde.

4.4 Discussion

In this chapter, an *in vitro* dosimetry study was performed using the Cultex RFS module to clarify the deposition efficiency of CS. Some previous studies have conducted dosimetry tests using other exposure modules. In those studies, a quartz crystal microbalance was applied to the whole CS exposure module to measure the deposited PP mass and a gas analyzer was connected to the whole CS exposure system to measure the carbon monoxide concentration^{26, 27}. The quartz crystal microbalance was inappropriate for particles containing liquid because the physiological properties of the particles and re-

evaporation of liquid in the particles affected the values measured by the microbalance²⁸,²⁹. Therefore, a different approach was used to measure the deposited CS particles on the culture surface. In addition to CS particles, GVP chemicals on the culture surface were measured. Data from the carbon monoxide analyzer provided the carbon monoxide concentration to which the cells were exposed. However, the amount of carbon monoxide deposited on the cell culture surface was not provided. Therefore, the tissue dose used in the whole CS exposure system was measured to understand the biological data and compare it with human tissue doses.

In this chapter, dosimetry studies were conducted by measuring the mass of representative chemicals in the PP and the GVP that were deposited on the culture surface. The advantage of this method is that it enables estimation of the masses of the constituents that are actually deposited on cells cultured at an ALI condition. According to the results of the *in vitro* dosimetry study with the RFS module, there was little difference between the deposition efficiency of each constituent at the same dilution under the ISO standard and intensive smoking regimes (Figure 4.7). The mainstream masses of solanesol and acetaldehyde under the ISO intensive smoking regime were approximately 2.9 times more than those under the ISO standard regime (Table 4.2), which might indicate that the total masses of constituents in the mainstream CS have little effect on their deposition efficiencies. The *in vitro* dosimetry data also indicated that the deposition efficiency of acetaldehyde tended to be higher than that of solanesol under the same dilution flow rate. For example, with a dilution flow rate of 0.5 L/min, the deposition efficiency of acetaldehyde was approximately 0.2%/cm² (Figure 4.7a) and that of solanesol was approximately 0.15%/cm² (Figure 4.7b). The diffusion coefficient affects chemical deposition of smoke in the exposure module, and the diffusion coefficient of acetaldehyde (1.24×10^{-1} cm²/s) is much higher than that of particles with similar diameters to CS particles (6.8×10^{-6} cm²/s)^{30, 31}. Thus, acetaldehyde can reach the culture surface more efficiently in the exposure chamber than the PP chemical solanesol.

For comparison with *in vitro* deposition data, a human retention study was performed as an *in vivo* dosimetry test. Seventeen male adult smokers each smoked CC1 under three inhalation patterns: mouth hold, shallow inhalation, and normal inhalation. Deposition of

solanesol and acetaldehyde increased as the inhalation depth increased (Figure 4.9). Under the normal inhalation pattern, the deposition efficiencies of solanesol (approximately 60%), and acetaldehyde (approximately 90%) were consistent with previous findings^{15, 20, 21, 25}. Regional deposition was calculated by comparing the results under the three different inhalation patterns. Because alveoli have large surface areas, the deposition efficiencies of solanesol and acetaldehyde per unit area were markedly lower in alveoli than in the mouth or bronchi (Table 4.3). The ratio of deposited acetaldehyde to deposited solanesol ranged from 0.54 to 1.97. Because acetaldehyde was well deposited in the mouth (Table 4.3), the ratio was higher in the mouth than in the bronchi or alveoli. This acetaldehyde behavior in the upper respiratory tract is consistent with a recent simulation data³⁰. The estimation of regional deposition efficiency was based on the hypothesis that deposition was restricted in the mouth and bronchi under the shallow inhalation pattern. However, this hypothesis did not account for variation between individuals, and corrections were not applied for this. In addition, CS is not equally deposited over the entire surface of the respiratory tract, and there must be deposition hot spots where better deposition of inhaled CS occurs^{32, 33}. Thus, the estimation of regional deposition efficiency presented in this chapter has some limitations. However, the regional deposition data will be helpful when discussing the results of direct smoke-exposure experiments from the point of view of actual tissue doses because *in vitro* oral, bronchi, and alveolar models have already been developed and applied to whole CS exposure experiments³⁴⁻³⁷.

By comparing *in vitro* and *in vivo* dosimetry data, whole CS exposure conditions that can reproduce the dose delivered to actual human bronchial epithelium were investigated. Actual bronchial tissue deposition efficiency was achieved using a dilution flow rate of 8.0 L/min for exposure (Figure 4.10). However, smokers consume many cigarettes in a day. Ng et al. reported that mean cigarette consumption ranged from 10 to 40 cigarettes per day in most countries and the global average was approximately 20 cigarettes per day³⁸. Therefore, whole CS exposure should be performed with 20 cigarettes for reproduction of the daily tissue dose when using a dilution flow rate of 8.0 L/min. By contrast, when using a dilution flow rate of 1.0 L/min, the deposition efficiency will be 10 times that in the actual tissue (Figure 4.10). This would allow for whole CS exposure using only two

cigarettes to reproduce the total daily tissue dose of the average smoker (i.e., 20 cigarettes per day).

Although the approach employed in this study worked well to compare *in vitro* and *in vivo* deposition data, we did not consider post-deposition events. For example, CS particles deposited on the lung surface are removed by mucociliary clearance and the remaining particles are absorbed through the lung, distributed to various tissues, metabolized by the liver, and excreted by the kidney ³⁹. Because these events are important for toxicological effects of inhaled CS, these post-deposition events should ideally be considered in an *in vivo* dosimetry study. Several studies are ongoing to develop physiologically based pharmacokinetics (PBPK) modeling of inhaled aerosol to analyze ADME (absorption, distribution, metabolism, and excretion) profiles in the human body ^{40, 41}. However, it is still challenging because the complexity in the physicochemical properties of CS and the morphology of the human airway prevent establishment of appropriate modeling ⁴². In addition to understanding *in vivo* dosimetry data including post-deposition events, reproduction of these events in the *in vitro* 3D bronchial tissue model is also important. Several studies have indicated that absorption is well reproduced in 3D bronchial epithelial models ⁴³⁻⁴⁵. However, because the 3D bronchial tissue model used in this study was cultured in the closed system (i.e., wells of the culture plates) without perfusion of the medium, the events following absorption (i.e., distribution, metabolism, and excretion) were not reproduced. Moreover, mucociliary clearance did not remove CS particles outside of the cell culture inserts. Considering these limitations, development of appropriate PBPK modeling of inhaled CS and improvement of the 3D bronchial tissue model are necessary for deeper comparisons of *in vivo* and *in vitro* dosimetry data of CS, including post-deposition events.

4.5 Conclusions

In the experiments presented in this chapter, the deposition efficiencies of solanesol and acetaldehyde per unit surface area in the Cultex RFS module were comparable to the deposition efficiency per unit surface area in the bronchi. It is particularly noteworthy that with a dilution flow rate of 1 L/min, exposure to whole CS from two cigarettes can

approximate the global average of the total daily tissue dose in actual human bronchial epithelium. These results show that the Cultex RFS module is a reliable whole CS exposure module for simulating *in vivo* CS exposure in terms of PP and GVP exposure doses. Therefore, combination of the Cultex RFS module with the 3D bronchial tissue model developed in Chapter 3 will be useful for understanding the toxicological effects of CS on the human respiratory system.

4.6 References

1. Aufderheide, M., Scheffler, S., Mohle, N., Halter, B. & Hochrainer, D. Analytical in vitro approach for studying cyto- and genotoxic effects of particulate airborne material. *Anal Bioanal Chem* **401**, 3213-3220 (2011).
2. Steinritz, D. *et al.* Use of the Cultex(R) Radial Flow System as an in vitro exposure method to assess acute pulmonary toxicity of fine dusts and nanoparticles with special focus on the intra- and inter-laboratory reproducibility. *Chem Biol Interact* **206**, 479-490 (2013).
3. Aufderheide, M., Halter, B., Mohle, N. & Hochrainer, D. The CULTEX RFS: a comprehensive technical approach for the in vitro exposure of airway epithelial cells to the particulate matter at the air-liquid interface. *Biomed Res Int* **2013**, 734137 (2013).
4. Aufderheide, M., Heller, W.D., Krischenowski, O., Mohle, N. & Hochrainer, D. Improvement of the CULTEX((R)) exposure technology by radial distribution of the test aerosol. *Exp Toxicol Pathol* **69**, 359-365 (2017).
5. Paur, H.-R. *et al.* In-vitro cell exposure studies for the assessment of nanoparticle toxicity in the lung—A dialog between aerosol science and biology. *Journal of Aerosol Science* **42**, 668-692 (2011).
6. Benowitz, N.L. Biomarkers of environmental tobacco smoke exposure. *Environ Health Perspect* **107 Suppl 2**, 349-355 (1999).
7. Tang, H. *et al.* Solanesol: a tracer for environmental tobacco smoke particles. *Environmental Science & Technology* **24**, 848-852 (1990).
8. Adam, T., McAughey, J., McGrath, C., Mockler, C. & Zimmermann, R. Simultaneous on-line size and chemical analysis of gas phase and particulate phase of cigarette mainstream smoke. *Anal Bioanal Chem* **394**, 1193-1203 (2009).
9. Baker, R.R. The generation of formaldehyde in cigarettes--Overview and recent experiments. *Food Chem Toxicol* **44**, 1799-1822 (2006).

10. Nara, H., Fukano, Y., Nishino, T. & Aufderheide, M. Detection of the cytotoxicity of water-insoluble fraction of cigarette smoke by direct exposure to cultured cells at an air-liquid interface. *Exp Toxicol Pathol* **65**, 683-688 (2013).
11. Okuwa, K. *et al.* In vitro micronucleus assay for cigarette smoke using a whole smoke exposure system: a comparison of smoking regimens. *Exp Toxicol Pathol* **62**, 433-440 (2010).
12. Weber, S., Hebestreit, M., Wilms, T., Conroy, L.L. & Rodrigo, G. Comet assay and air-liquid interface exposure system: a new combination to evaluate genotoxic effects of cigarette whole smoke in human lung cell lines. *Toxicol In Vitro* **27**, 1987-1991 (2013).
13. Brown, J.S., Wilson, W.E. & Grant, L.D. Dosimetric comparisons of particle deposition and retention in rats and humans. *Inhal Toxicol* **17**, 355-385 (2005).
14. Schroeter, J.D. *et al.* Incorporation of tissue reaction kinetics in a computational fluid dynamics model for nasal extraction of inhaled hydrogen sulfide in rats. *Toxicol Sci* **90**, 198-207 (2006).
15. Feng, S. *et al.* A new method for estimating the retention of selected smoke constituents in the respiratory tract of smokers during cigarette smoking. *Inhal Toxicol* **19**, 169-179 (2007).
16. Watson, C., McCraw, J., Polzin, G., Ashley, D. & Barr, D. Development of a method to assess cigarette smoke intake. *Environ Sci Technol* **38**, 248-253 (2004).
17. International Organization for Standardization ISO 3308: Routine Analytical Cigarette Smoking Machine — Definitions and Standard Conditions. (2012).
18. International Organization for Standardization ISO 20778: Routine Analytical Cigarette Smoking Machine — Definitions and Standard Conditions with an Intense Smoking Regime. (2018).
19. Secondo, L.E., Liu, N.J. & Lewinski, N.A. Methodological considerations when conducting in vitro, air-liquid interface exposures to engineered nanoparticle aerosols. *Crit Rev Toxicol* **47**, 225-262 (2017).
20. Armitage, A., Dixon, M., Frost, B., Mariner, D. & Sinclair, N. The Effect of Inhalation Volume and Breath-Hold Duration on the Retention of Nicotine and Solanesol in the Human Respiratory Tract and on Subsequent Plasma Nicotine Concentrations During Cigarette Smoking. **21**, 240 (2004).
21. Armitage, A.K., Dixon, M., Frost, B.E., Mariner, D.C. & Sinclair, N.M. The effect of tobacco blend additives on the retention of nicotine and solanesol in the human respiratory tract and on subsequent plasma nicotine concentrations during cigarette smoking. *Chem Res Toxicol* **17**, 537-544 (2004).
22. Baker, R.R. & Dixon, M. The retention of tobacco smoke constituents in the human respiratory tract. *Inhal Toxicol* **18**, 255-294 (2006).
23. West, J.B. *Respiratory physiology: the essentials*. (Lippincott Williams & Wilkins, 2012).

24. International Commission on Radiological Protection *Human Respiratory Tract Model for Radiological Protection: A Report of a Task Group of the International Commission on Radiological Protection*, Vol. 66. (ICRP Publication, 1994).
25. Moldoveanu, S., Coleman, W. & Wilkins, J. Determination of Carbonyl Compounds in Exhaled Cigarette Smoke. **22**, 346 (2007).
26. Thorne, D. *et al.* Characterisation of a Vitrocell(R) VC 10 in vitro smoke exposure system using dose tools and biological analysis. *Chem Cent J* **7**, 146 (2013).
27. Adamson, J., Hughes, S., Azzopardi, D., McAughey, J. & Gaca, M.D. Real-time assessment of cigarette smoke particle deposition in vitro. *Chem Cent J* **6**, 98 (2012).
28. Adamson, J., Thorne, D., McAughey, J., Dillon, D. & Meredith, C. Quantification of cigarette smoke particle deposition in vitro using a triplicate quartz crystal microbalance exposure chamber. *Biomed Res Int* **2013**, 685074 (2013).
29. Steiner, S. *et al.* Characterization of the Vitrocell(R) 24/48 aerosol exposure system for its use in exposures to liquid aerosols. *Toxicol In Vitro* **42**, 263-272 (2017).
30. Zhang, Z., Kleinstreuer, C. & Feng, Y. Vapor deposition during cigarette smoke inhalation in a subject-specific human airway model. *Journal of Aerosol Science* **53**, 40-60 (2012).
31. Rostami, A.A. Computational modeling of aerosol deposition in respiratory tract: a review. *Inhal Toxicol* **21**, 262-290 (2009).
32. Martonen, T.B. & Musante, C.J. Importance of cloud motion on cigarette smoke deposition in lung airways. *Inhal Toxicol* **12 Suppl 4**, 261-280 (2000).
33. Zhang, Z., Kleinstreuer, C. & Hyun, S. Size-change and deposition of conventional and composite cigarette smoke particles during inhalation in a subject-specific airway model. *Journal of Aerosol Science* **46**, 34-52 (2012).
34. Fukano, Y., Yoshimura, H. & Yoshida, T. Heme oxygenase-1 gene expression in human alveolar epithelial cells (A549) following exposure to whole cigarette smoke on a direct in vitro exposure system. *Exp Toxicol Pathol* **57**, 411-418 (2006).
35. Mathis, C. *et al.* Human bronchial epithelial cells exposed in vitro to cigarette smoke at the air-liquid interface resemble bronchial epithelium from human smokers. *Am J Physiol Lung Cell Mol Physiol* **304**, L489-503 (2013).
36. Maunders, H., Patwardhan, S., Phillips, J., Clack, A. & Richter, A. Human bronchial epithelial cell transcriptome: gene expression changes following acute exposure to whole cigarette smoke in vitro. *Am J Physiol Lung Cell Mol Physiol* **292**, L1248-1256 (2007).
37. Schlage, W.K. *et al.* In vitro systems toxicology approach to investigate the effects of repeated cigarette smoke exposure on human buccal and gingival organotypic epithelial tissue cultures. *Toxicol Mech Methods* **24**, 470-487 (2014).

38. Ng, M. *et al.* Smoking prevalence and cigarette consumption in 187 countries, 1980-2012. *Jama* **311**, 183-192 (2014).
39. Forbes, B. *et al.* In Vitro Testing for Orally Inhaled Products: Developments in Science-Based Regulatory Approaches. *Aaps j* **17**, 837-852 (2015).
40. Borghardt, J.M., Kloft, C. & Sharma, A. Inhaled Therapy in Respiratory Disease: The Complex Interplay of Pulmonary Kinetic Processes. *Can Respir J* **2018**, 2732017 (2018).
41. Borghardt, J.M., Weber, B., Staab, A. & Kloft, C. Pharmacometric Models for Characterizing the Pharmacokinetics of Orally Inhaled Drugs. *Aaps j* **17**, 853-870 (2015).
42. Kolli, A.R. *et al.* Bridging inhaled aerosol dosimetry to physiologically based pharmacokinetic modeling for toxicological assessment: nicotine delivery systems and beyond. *Crit Rev Toxicol* **49**, 725-741 (2019).
43. Forbes, B., Shah, A., Martin, G.P. & Lansley, A.B. The human bronchial epithelial cell line 16HBE14o- as a model system of the airways for studying drug transport. *Int J Pharm* **257**, 161-167 (2003).
44. Manford, F. *et al.* Drug permeability in 16HBE14o- airway cell layers correlates with absorption from the isolated perfused rat lung. *Eur J Pharm Sci* **26**, 414-420 (2005).
45. Mathia, N.R. *et al.* Permeability characteristics of calu-3 human bronchial epithelial cells: in vitro-in vivo correlation to predict lung absorption in rats. *J Drug Target* **10**, 31-40 (2002).

Chapter 5.

Repeated whole CS exposure of the 3D bronchial tissue model

5.1 Introduction

5.1.1 Objectives

A human-relevant 3D bronchial tissue model was developed in Chapter 3. The human-relevant whole CS exposure condition that reproduced the actual airway tissue dose of a smoker was also established in Chapter 4. The objective of this chapter was to investigate whether the combination of whole CS exposure and the 3D bronchial tissue model can detect tissue/organ-level toxicological effects of CS. For this purpose, 3D bronchial tissues were exposed to whole CS repeatedly to reproduce the actual exposure pattern in smokers.

5.1.2 Study approaches

In this chapter, whole CS exposure was performed on the 3D bronchial tissue model developed in Chapter 3. This model has fibroblasts embedded in a collagen matrix layer directly below ALI-cultured HBECs. Whole CS exposure was performed with a dilution flow rate of 1 L/min, which gave an *in vitro* deposition efficiency of CS that was 10 times more than that in actual human bronchial tissue, as described in Chapter 4. Therefore, the quantity of CS delivered to the cells by whole CS exposure with two cigarettes will be comparable to that delivered to the bronchial tissue in an actual smoker who smokes 20 cigarettes per day, which is global daily average ¹.

In addition to reproduction of the actual daily tissue dose, reproduction of the exposure patterns of actual smokers is important to reproduce the actual airway tissue response with the combination of the whole CS exposure system and 3D bronchial tissue model. Because the *in vivo* effects of CS exposure appear after chronic lifetime exposure, exposure repetition is important when investigating the toxicological effects of CS using the bronchial tissue model. Therefore, in this chapter, whole CS exposure was performed every other day for 2 weeks. Following the 2 weeks of repeated whole CS exposure, the differentiation status of the 3D bronchial tissue model was investigated by histological and gene expression analyses because attenuation of the differentiation process of 3D

bronchial tissue can be related to development of COPD phenotypes ². In addition, activation of inflammatory networks and secretion of inflammatory mediators are reportedly important in early development of COPD ³. Therefore, the effects of whole CS exposure on the inflammatory process of the 3D bronchial tissue model were also investigated using gene and protein expression analyses.

5.2 Materials and methods

5.2.1 Whole CS exposure of the 3D bronchial tissue model

The 3D bronchial tissue model was prepared as described in Chapter 3 (Section 3.2.1 Construction of a 3D culture model of human bronchial tissue). Whole CS exposure of the 3D bronchial tissue model was conducted on ALI culture day 7 for a single exposure experiment (Figure 5.1) and ALI culture days 7, 9, 11, 13, 15, 17, and 19 for a repeated exposure experiment (Figure 5.2). Whole CS from 3R4F cigarettes (University of Kentucky) generated with the ISO standard regime (35-mL puff volume, 60-s puff interval, 2-s puff duration, and no blocking of ventilation holes) was diluted with air at a flow rate of 1 L/min and used for exposure of the 3D bronchial tissue model. The whole CS exposure was performed using the procedure described in Chapter 4 (Section 4.2.1.1 Whole CS exposure) and took approximately 10 min. The volume of diluted air delivered to the tissue model during 10 min of exposure was 10 L (1 L/min × 10 min). The volume of smoke delivered to the tissue during 10 min of exposure was 0.35 L/cig (35 mL/puff × 1 puffs/min/cig × 10 min). Therefore, the smoke concentration delivered to the tissue was calculated as follows using the calculator provided by the Vitrocell Systems GmbH.

$$\text{Smoke concentration (\%)} = \frac{0.35 \text{ (L/cig.)} \times \text{no. of cig.}}{10 \text{ (L)} + 0.35 \text{ (L/cig.)} \times \text{No. of cig.}} \times 100$$

The smoke exposure concentrations produced from one, two, four, six and eight cigarettes were 3.4%, 6.5%, 12.3%, 17.4%, and 21.9% (vol/vol).

In Chapters 2 and 4, whole CS exposure was performed with CS generated with both the ISO standard and intensive regimes. However, whole CS exposure of the 3D bronchial

tissue model was performed with only the ISO standard regime in this chapter because a previous study showed that the ISO standard regime was sufficient for detecting toxicological effects with a 3D bronchial epithelial model ⁴.

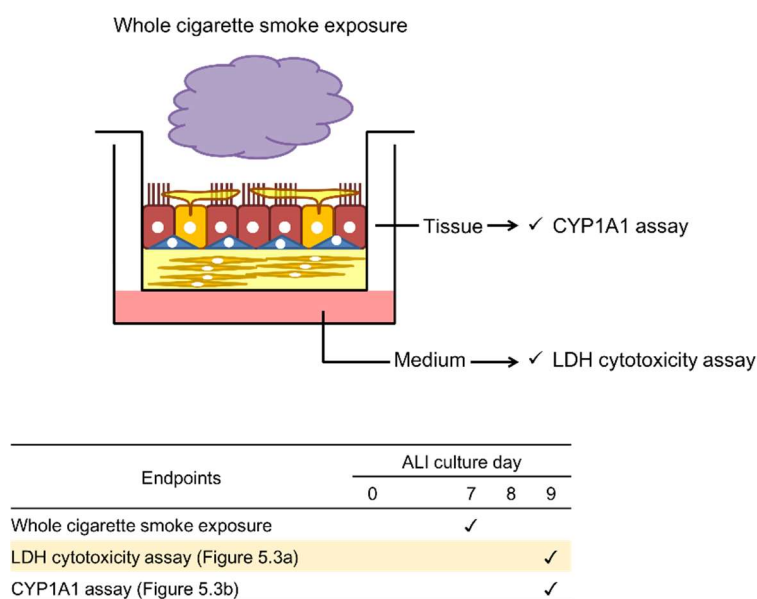
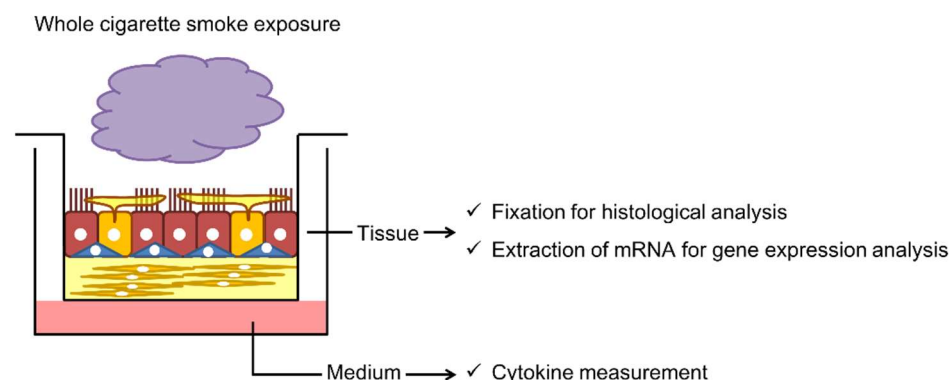


Figure 5.1 Single exposure experiment.

After 7 days of air–liquid interface (ALI) culture, whole cigarette smoke exposure was performed once. Two days after the exposure, the lactate dehydrogenase (LDH) assay was performed to detect the activity of LDH that had leaked into the medium, and this was used as an indicator of cytotoxicity. The tissues were subjected to the cytochrome P450 (CYP) 1A1 assay to detect metabolic activity of the CYP1A1 enzyme following whole cigarette smoke exposure.



Endpoints	ALI culture day																
	0	7	8	9	10	11	12	13	14	15	16	17	18	19	20	21	
Whole cigarette smoke exposure		✓		✓		✓		✓		✓		✓		✓			
Histological analysis (Figure 5.4)																✓	
Gene expression analysis (Figure 5.6 and 5.7)																✓	
Cytokine measurement (Figure 5.8 and 5.9)		✓						✓				✓				✓	

Figure 5.2 Repeated exposure experiment.

After 7 days of air–liquid interface (ALI) culture, whole cigarette smoke exposure was performed every other day from day 7 to day 19. Histological analysis and gene expression analysis were performed with tissue samples collected on ALI day 21. Cytokine measurements were performed with medium samples collected on ALI days 9, 13, 17, and 21.

5.2.2 Interleukin-13 stimulation

As a positive control for goblet cell hyperplasia, 5 ng/mL interleukin (IL)-13 (FUJIFILM Wako Pure Chemical Corporation) was added to the ALI culture medium ⁵. IL-13 stimulation was carried out from ALI culture day 0 to day 21.

5.2.3 Cytochrome P450 and lactate dehydrogenase cytotoxicity assay

The cytochrome P450 (CYP) assay was performed with the P450-Glo CYP1A1 Assay (Promega, Fitchburg, WI, USA) in a single exposure experiment on ALI culture day 9 (Figure 5.1). Luciferin-CEE solution (100 μ M) was prepared following the

manufacturer's protocol, and 250 μ L of luciferin-CEE solution was applied to the apical surface of the bronchial tissue after removal of the basolateral medium from the bottom well. Bronchial tissues were incubated with luciferin-CEE solution in an incubator at 37 °C under a 5% CO₂ atmosphere for 3 h. The luminescence was measured using a GloMax-Multi Detection System (Promega). The basolateral medium removed for the CYP assay was used for lactate dehydrogenase (LDH) analysis using the CytoTox-One Homogeneous Membrane Integrity Assay (Promega) in accordance with the manufacturer's protocol. The fluorescence was measured using the GloMax-Multi Detection System.

5.2.4 Histological analysis of the tissues

Following repeated whole CS exposure, the 3D bronchial tissue models were subjected to histological analysis (Figure 5.2) using the protocol described in Chapter 3 (Section 3.2.3 Histological analysis of the tissues). The sections were subjected to immunostaining with anti-acetylated α -tubulin (ab24610; Abcam) and anti-mucin 5AC antibody (ab3649; Abcam), following heat-mediated antigen retrieval in 10 mM sodium citrate buffer (pH 6.0) at 95 °C for 30 min.

5.2.5 RNA extraction, reverse transcription, and quantitative PCR

Following repeated whole CS exposure, the gene expression profiles of the 3D bronchial tissue models were analyzed (Figure 5.2). RNA extraction and complementary DNA synthesis were performed as described in Chapter 3 (Section 3.2.6 PCR array analysis for ECM-related genes). The TaqMan Gene Expression Assays (Applied Biosystems, Waltham, MA, USA) used were *FOXJ1* (Hs00230964), *MUC5AC* (Hs00873651), *MUC5B* (Hs00861595), *SCGB1A1* (Hs00171092), and *TP63* (Hs00978340). Quantitative PCR data were analyzed using the $\Delta\Delta$ CT method, and the CT value of each target gene was normalized to the expression levels of *GAPDH*. The nuclear factor-kappa B (NF κ B) Signaling Pathway PCR Array (PAHS-025; SABiosciences) was also used for gene

expression analysis following the manufacturer's protocol. This array allows for measurements of the expression of 84 genes related to the NF κ B signaling pathway. PCR array data calculations were performed using RT² Profiler PCR Array Data Analysis software (version 3.5; SABiosciences).

5.2.6 Analysis of secreted cytokines

Samples of the medium collected during repeated whole CS exposure experiments were analyzed with the Procarta Cytokine Assay (Affymetrix, Santa Clara, CA, USA) using a Bio-Plex system (Bio-Rad). Medium samples were collected on ALI culture days 9, 13, 17, and 21 (Figure 5.2). The secretions were analyzed for IL-8, GRO- α , IL-1 β , granulocyte macrophage-colony stimulating factor (GM-CSF), granulocyte-colony stimulating factor (G-CSF), and macrophage-colony stimulating factor (M-CSF). For analysis of IL-8 and GRO- α , each medium sample was diluted at a 1:2,000 ratio with ALI culture medium.

5.2.7 Statistical analysis

Each exposure experiment was conducted with triplicate inserts, and the results are presented as the means and standard deviations. Significant differences between whole CS-exposed samples and control samples were evaluated by Dunnett's test with log-transformed data. The test results were considered to be significant at $p < 0.05$.

5.3 Results

5.3.1 Effects of a single exposure to whole CS

The toxicological effects of a single whole CS exposure on 3D bronchial tissue were examined before conducting repeated whole CS exposure (Figure 5.1). Whole CS exposure of the 3D bronchial tissue was conducted on ALI culture day 7 and the

basolateral medium was collected on culture day 9 for cytotoxicity analysis, using the enzymatic activity of LDH that had leaked into the basolateral medium (Figure 5.3a). The increase in the enzymatic activity of LDH was not detected after exposure to CS from six or fewer cigarettes, but an increase in the enzymatic activity of LDH was observed after exposure to CS from eight cigarettes (Figure 5.3a). The enzymatic activity of CYP1A1 was also measured on culture day 9 (Figure 5.3b). A significant increase in CYP1A1 activity was detected in all exposure conditions, and the highest activity was detected for the four-cigarette exposure (Figure 5.3b). Because of the cytotoxic effects of whole CS with exposure to more cigarettes, CYP1A1 activity was lower for the six- and eight-cigarette exposures than in the other experiments.

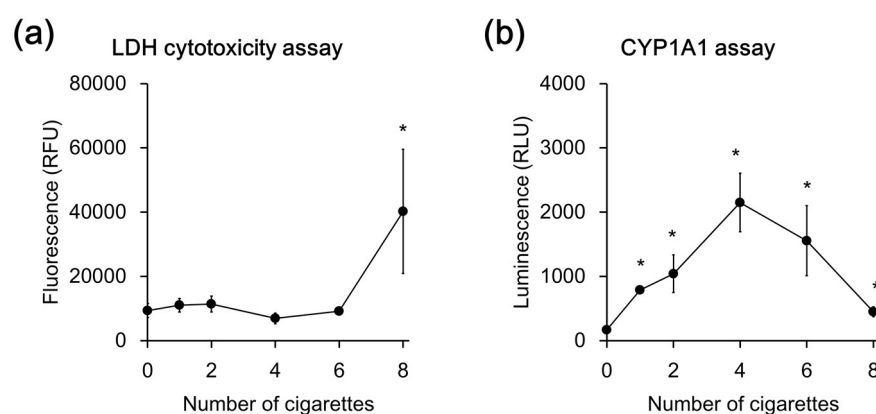


Figure 5.3 Results of single exposure experiments.

(a) The lactate dehydrogenase (LDH) assay results. (b) The cytochrome P450 (CYP) 1A1 assay results. The results represent the means and standard deviations of three tissue samples. *Significantly different from the results under the control condition ($p < 0.05$, Dunnett's test with log-transformed data).

5.3.2 Tissue histology following repeated exposure to whole CS

For the repeated exposure experiment, the 3D bronchial tissue model was exposed to whole CS every other day from ALI culture day 7 to day 19 (Figure 5.2). On the basis of the single exposure experiment results, non-cytotoxic exposure was performed with one, two, and four cigarettes. The exposure smoke doses produced by one, two, and four

cigarettes are comparable to the actual bronchial tissue doses observed in smokers who consume 10, 20, and 40 cigarettes per day, respectively. The smoke exposure concentrations produced from one, two, and four cigarettes were 3.4%, 6.5%, and 12.3% (vol/vol). Histological analysis with hematoxylin and eosin staining revealed well-differentiated columnar epithelium in air-exposed control tissue, and the presence of ciliated cells was confirmed by immunostaining with anti-acetylated α -tubulin antibody (Figure 5.4). Goblet cells and the mucus layer secreted onto the apical surface of the tissue were positively stained with anti-mucin 5AC antibody in the air-exposed control tissue (Figure 5.4). After repeated whole CS exposure, dose-dependent decreases in the epithelium thickness and number of ciliated cells were observed (Figure 5.4). Goblet cells were increased in the center of the epithelium after repeated whole CS exposure (Figure 5.4, arrowheads), while they were on the apical surface of the epithelium in the air-exposed control. When stimulated with IL-13, which is frequently used for induction of goblet cell hyperplasia, an increase in the number of large goblet cells and a decrease in the number of ciliated cells were observed (Figure 5.5).

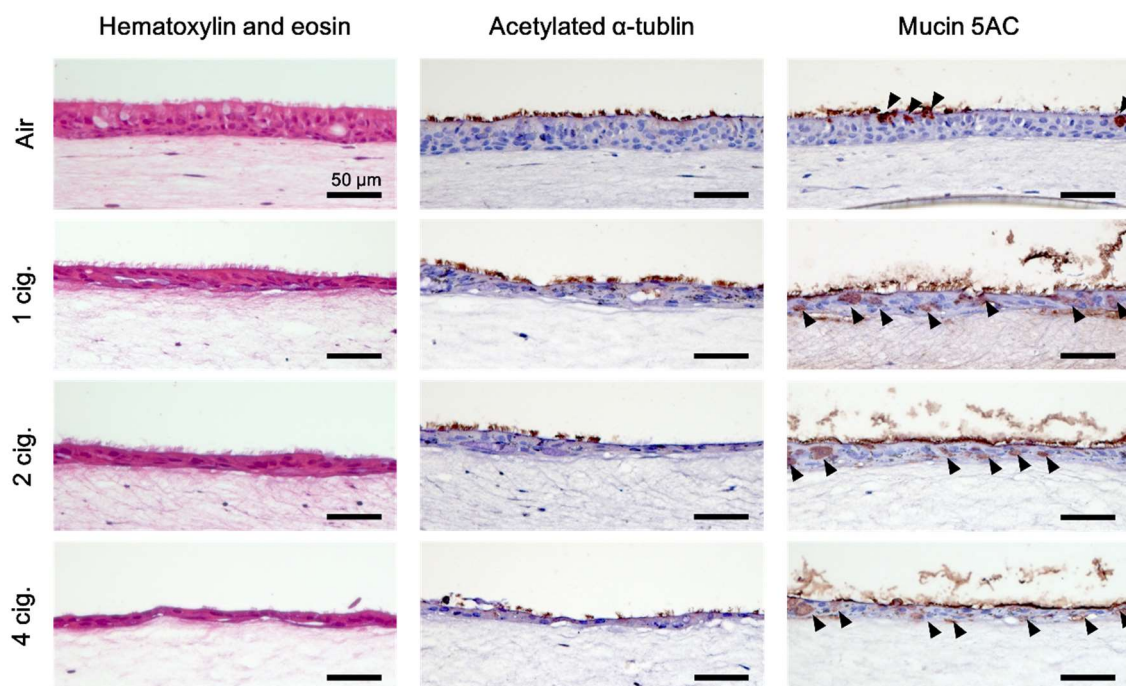


Figure 5.4 Histological analysis of the 3D bronchial tissue model following repeated whole cigarette smoke exposure.

Hematoxylin and eosin staining, immunostaining with acetylated α -tubulin (marker for ciliated cells), and immunostaining with mucin 5AC (marker for goblet cells) were performed. Arrowheads indicate mucin 5AC-positive goblet cells.

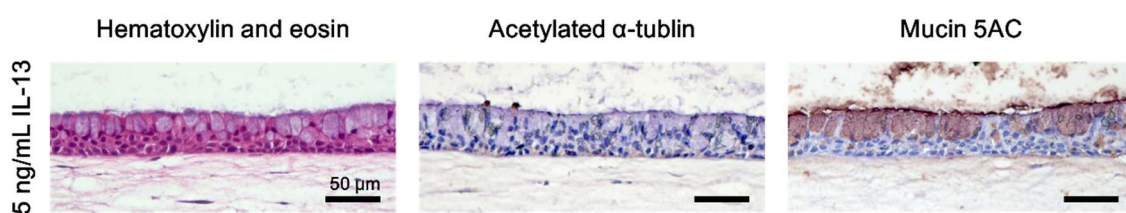


Figure 5.5 Histological analysis of the 3D bronchial tissue model following IL-13 stimulation.

Hematoxylin and eosin staining, immunostaining with acetylated α -tubulin (marker for ciliated cells), and immunostaining with mucin 5AC (marker for goblet cells) were performed. IL, interleukin.

5.3.3 Gene expression of differentiation markers and growth factors following repeated exposure to whole CS

The differentiation profile of the 3D bronchial tissue model on day 21 was also analyzed by quantitative PCR. Several differentiation markers (*FOXJ1* for ciliated cells, *MUC5AC* and *MUC5B* for goblet cells, *SCGB1A1* for Club cells, and *TP63* for basal cells) were selected, and their expression levels were measured (Figure 5.6). These markers were used to confirm mucociliary differentiation of the bronchial epithelium *in vitro*^{6,7}. Dose-dependent decreases were observed in the expression levels of *FOXJ1*, *MUC5B*, and *SCGB1A1*. Significant decreases were observed in the expression levels of *FOXJ1* after the four-cigarette exposure (Figure 5.6a), *MUC5B* after the two- and four-cigarette exposures (Figure 5.6c), and *SCGB1A1* after the four-cigarette exposure (Figure 5.6d). A significant increase in *MUC5AC* expression was observed after exposure to CS from two cigarettes (Figure 5.6b). There was no significant change in the expression levels of *TP63* after repeated whole CS exposure (Figure 5.6e).

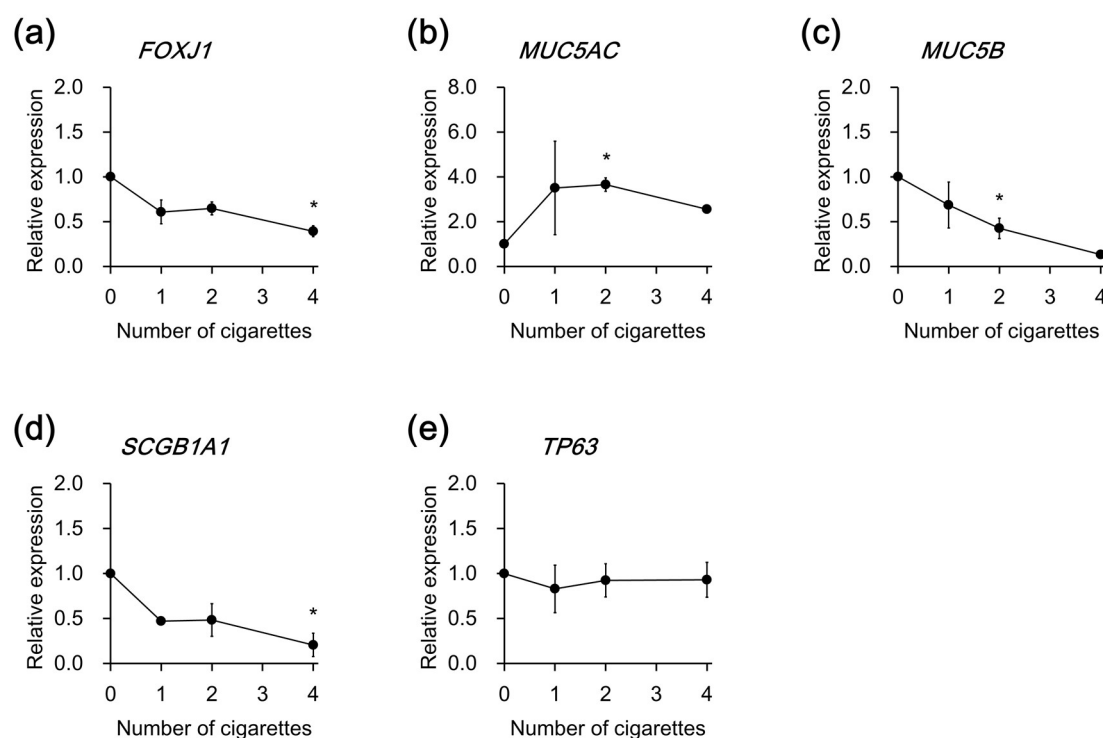


Figure 5.6 Effects of repeated whole cigarette smoke exposure on differentiation markers.

Expression levels of differentiation marker genes were analyzed on culture day 21. (a) Ciliated cell gene *FOXJ1*, (b) goblet cell genes *MUC5AC* and (c) *MUC5B*, (d) Club cell gene *SCGB1A1*, and (e) basal cell gene *TP63* were analyzed. The results represent means and standard deviations of three tissue samples. *Significantly different from the results under the control condition ($p < 0.05$, Dunnett's test with log-transformed data).

5.3.4 Gene expression of NFκB-signaling components following repeated exposure to whole CS

To determine the repeated whole CS exposure effects on the inflammatory response, a NFκB PCR array was used. Expression levels of genes coding NFκB-signaling components were measured on culture day 21 (Figure 5.7). *IL1B* was only one gene significantly increased its expression more than twice the levels of control after the one-cigarette exposure. Significant perturbation of other genes to more than twice the levels of control depended on the CS exposure dose. The increased expressions of inflammatory mediators (*IL1B* and *IL8*) and chemokines (*GROb*, *GROg*, and *MIP3A*), which are known

downstream components of NF κ B pathway, were detected on day 21 after the four-cigarette exposure (Figure 5.7). The expression level of the anti-inflammatory mediator, *IL10*, was increased on day 21 after exposure to two cigarettes (Figure 5.7).

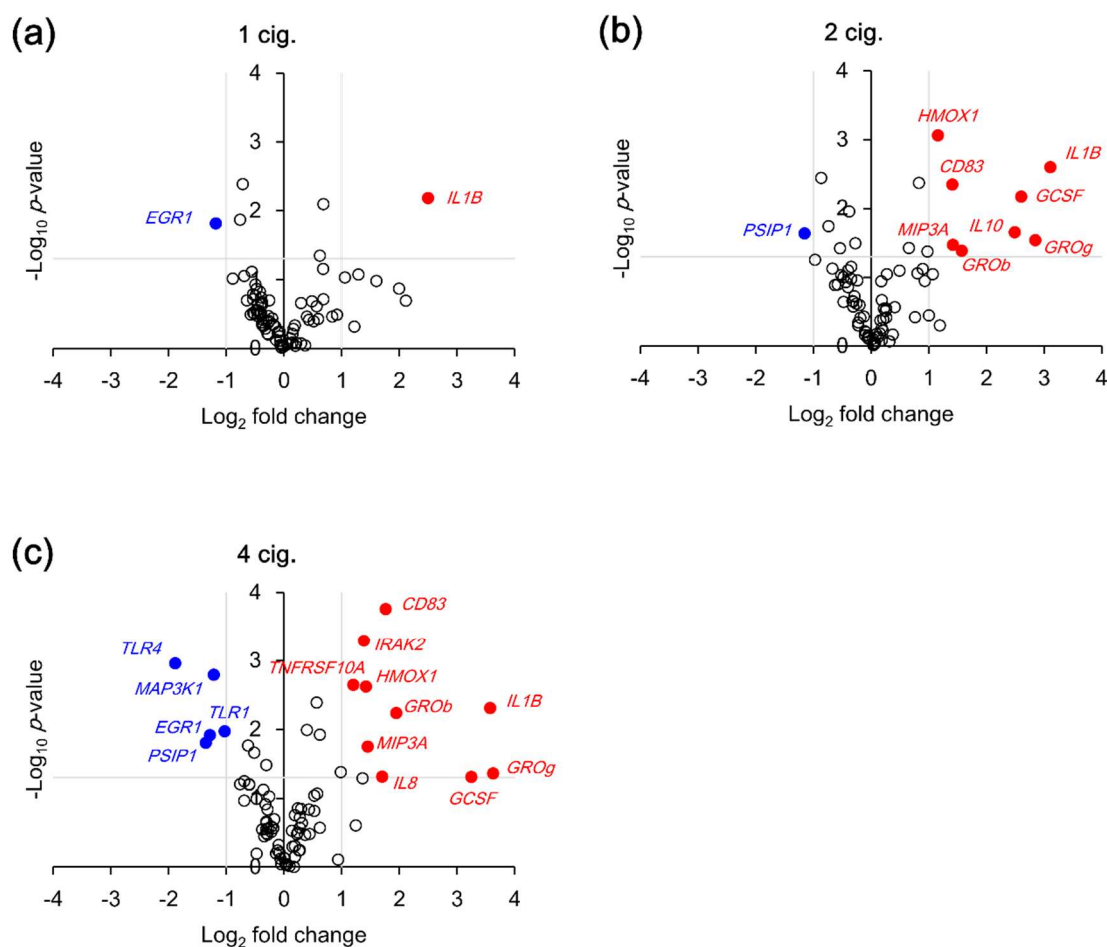


Figure 5.7 Effects of repeated whole cigarette smoke exposure on transcription of NF κ B pathway components.

Expression levels of 84 genes related to the nuclear factor-kappa B (NF κ B) pathway were analyzed on culture day 21 using a PCR array. Red dots indicate genes with significant increases (>two-fold increase and $p < 0.05$ (t -test)). Blue dots indicate genes with significant decreases (> two-fold decrease and $p < 0.05$ (t -test)).

5.3.5 Cytokine secretion into the basolateral medium during repeated exposure to whole CS

Because the results confirmed dose-dependent activation of NF κ B signaling pathway components, the effect of repeated exposure on the inflammatory response was analyzed at the protein level. Six mediators were selected (IL-8, GRO- α , IL-1 β , G-CSF, GM-CSF, and M-CSF) and their concentrations in the basolateral medium of the 3D bronchial tissue model were analyzed in samples collected on days 9, 13, 17, and 21. Dose-dependent increases in IL-8, GRO- α , and IL-1 β secretion occurred on days 13, 17, and 21 (Figure 5.8). The secretion levels of these proteins were highest on day 21. The secretion of GM-CSF showed a similar trend (Figure 5.9a). By contrast, G-CSF did not show a dose-dependent increase on culture day 21 and M-CSF did not show a clear dose-dependent change on any of the culture days (Figure 5.9b and c).

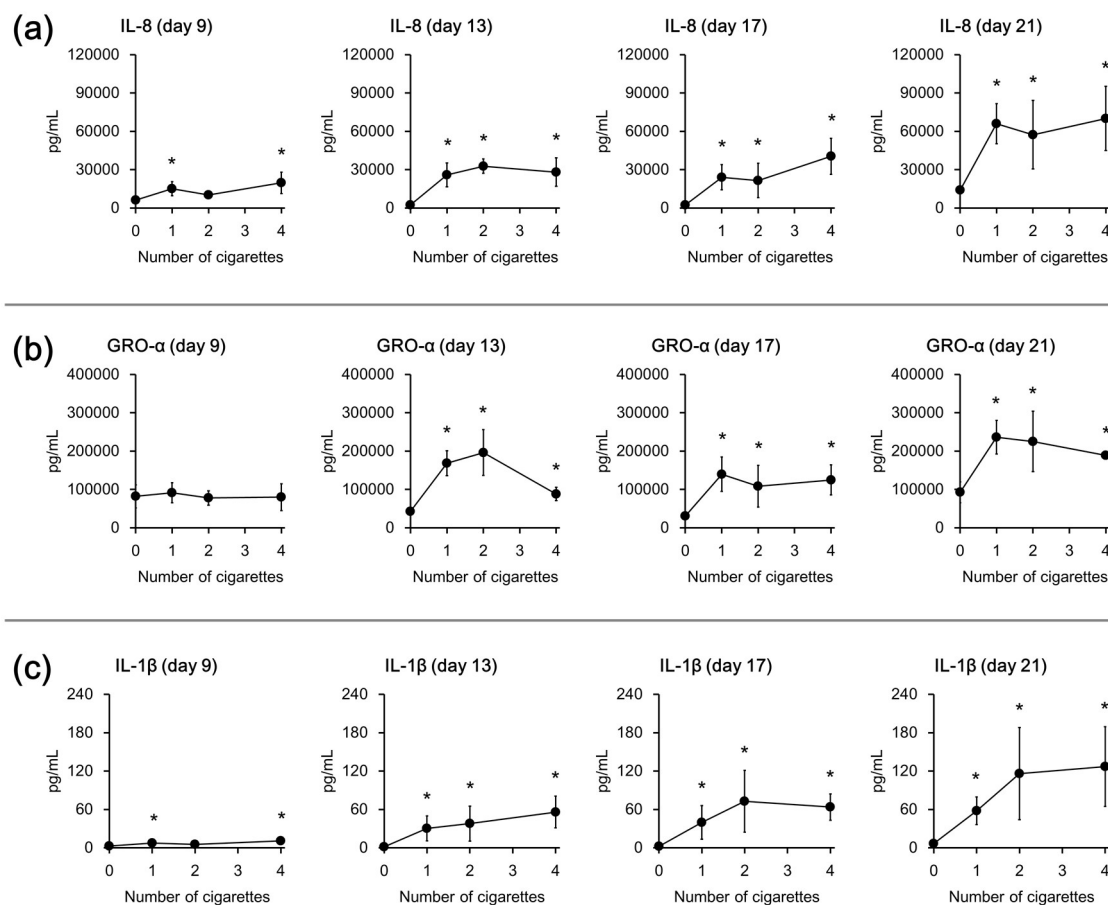


Figure 5.8 Effects of repeated whole cigarette smoke exposure on cytokine secretion.

Secreted (a) interleukin (IL)-8, (b) GRO-α, and (c) IL-1β in the basolateral medium were analyzed in the air-liquid interface culture on days 9, 13, 17, and 21. *Significantly different from the results under the control condition ($p < 0.05$, Dunnett's test with log-transformed data).

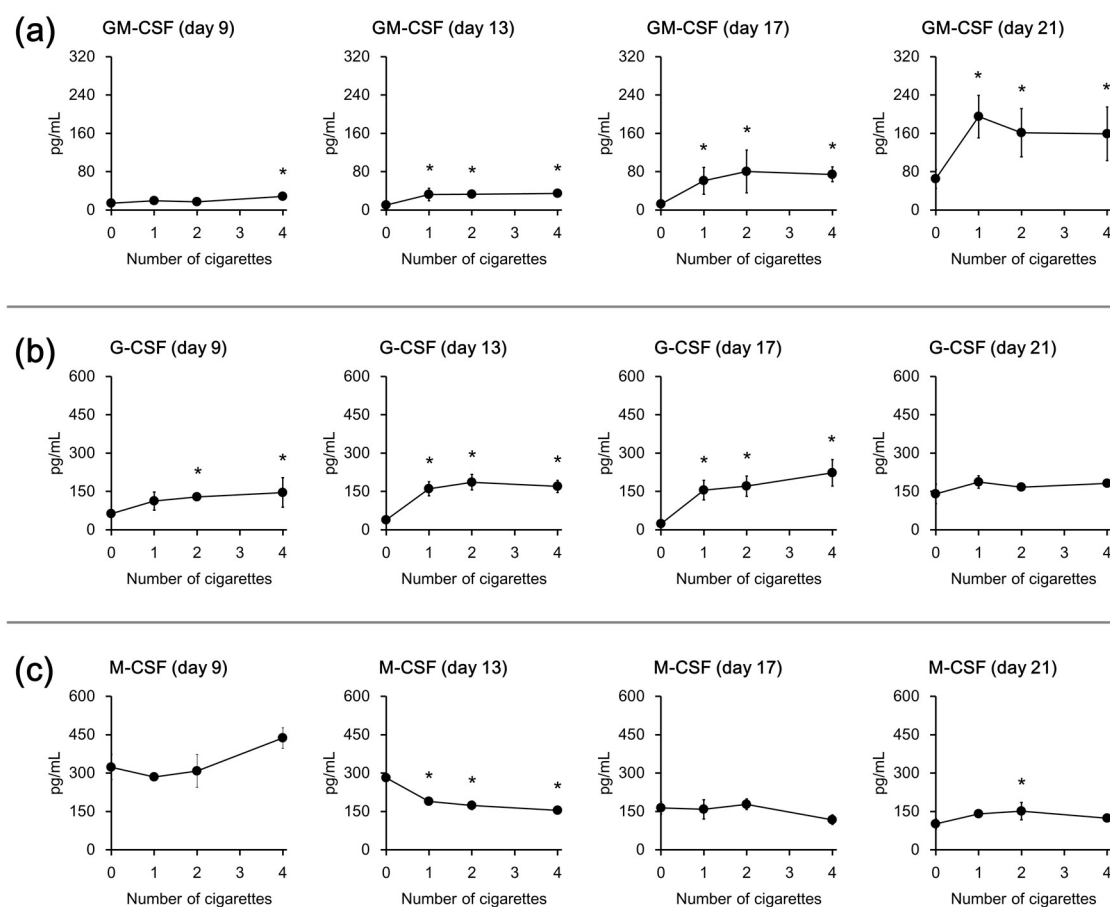


Figure 5.9 Effects of repeated whole cigarette smoke exposure on cytokine secretion.

Secreted (a) granulocyte macrophage-colony stimulating factor (GM-CSF), (b) granulocyte-colony stimulating factor (G-CSF), and (c) macrophage-colony stimulating factor (M-CSF) in the basolateral medium were analyzed in the air-liquid interface culture on days 9, 13, 17, and 21. *Significantly different from the results under the control condition ($p < 0.05$, Dunnett's test with log-transformed data).

The cytokine secretion results are expressed as fold-changes on the heatmap. IL-8 showed the highest fold increase of 16.6 after exposure to four cigarettes on culture day 17 (Figure 5.10c). IL-1 β showed the highest secretion level (a 41.6-fold increase) after exposure to four cigarettes on culture day 13 (Figure 5.10c). All other inflammatory cytokines, except M-CSF, showed the highest secretion levels on days 13 or 17 (Figure 5.10).

(a)					
	day 9	day 13	day17	day 21	
IL-8	<u>2.5</u>	<u>10.5</u>	<u>9.9</u>	<u>4.7</u>	
GRO- α	1.1	<u>4.0</u>	<u>4.6</u>	<u>2.5</u>	
IL-1 β	<u>2.7</u>	<u>22.7</u>	<u>17.1</u>	<u>9.0</u>	
GM-CSF	1.4	<u>3.1</u>	<u>4.9</u>	<u>3.0</u>	
G-CSF	1.8	<u>4.2</u>	<u>6.5</u>	1.3	
M-CSF	0.9	<u>0.7</u>	1.0	1.4	

(b)					
	day 9	day 13	day17	day 21	
IL-8	1.7	<u>13.3</u>	<u>8.8</u>	<u>4.1</u>	
GRO- α	0.9	<u>4.6</u>	<u>3.5</u>	<u>2.4</u>	
IL-1 β	1.9	<u>28.1</u>	<u>31.6</u>	<u>18.0</u>	
GM-CSF	1.2	<u>3.2</u>	<u>6.5</u>	<u>2.5</u>	
G-CSF	<u>2.0</u>	<u>4.9</u>	<u>7.1</u>	1.2	
M-CSF	1.0	<u>0.6</u>	1.1	<u>1.5</u>	

(c)					
	day 9	day 13	day17	day 21	
IL-8	<u>3.2</u>	<u>11.4</u>	<u>16.6</u>	<u>5.0</u>	
GRO- α	1.0	<u>2.1</u>	<u>4.1</u>	<u>2.0</u>	
IL-1 β	<u>4.0</u>	<u>41.6</u>	<u>27.6</u>	<u>19.7</u>	
GM-CSF	<u>2.0</u>	<u>3.4</u>	<u>6.0</u>	<u>2.4</u>	
G-CSF	<u>2.3</u>	<u>4.5</u>	<u>9.3</u>	1.3	
M-CSF	1.4	<u>0.5</u>	<u>0.7</u>	1.2	

Figure 5.10 Effects of repeated whole CS exposure on cytokine secretion.

The results in Figures 5.9 and 5.10 are summarized in a heatmap showing the fold changes to the air-exposure control condition after (a) one cigarette, (b) two cigarettes, and (c) four cigarettes on days 9, 13, 17, and 21. The values that significantly differed from those under the control condition ($p < 0.05$, Dunnett's test with log-transformed data) are underlined.

5.4 Discussion

In this chapter, a 3D co-culture model of human bronchial tissue was subjected to whole CS exposure to investigate the biological effects of repeated whole CS exposure on the differentiation and inflammation of tissue. The experimental conditions used in this chapter were designed to mimic actual conditions in the human respiratory system in terms of tissue composition, exposure dose, and exposure pattern.

Before conducting a repeated whole CS exposure experiment, a single exposure experiment was conducted to find the appropriate dose (Figure 5.1). In the single exposure experiment, changes in CYP enzymes after whole CS exposure were assessed because large increases in the activity of the major phase I xenobiotic metabolizing enzyme CYP1A1 after CS exposure have been reported *in vitro* and in actual human tissue⁸⁻¹⁰. The results indicated an increase in CYP1A1 activity with exposure, and the activity after a four-cigarette exposure was approximately 13 times that in the air-exposed control

(Figure 5.2b). This indicates that the 3D bronchial tissue model possesses the basic metabolic functions that participate in the biological activity of CS chemicals, such as benzo[a]pyrene ¹¹. The LDH cytotoxicity assay was also performed and the results indicated that exposure to between one and six cigarettes would not increase cytotoxicity with a single whole CS exposure (Figure 5.2a). According to those results, repeated whole CS exposure was performed with one, two, or four cigarettes. The quantities of CS delivered to the 3D bronchial tissue model when using one, two, or four cigarettes were comparable to the total daily tissue doses in the bronchi of smokers who smoked 10, 20, or 40 cigarettes per day. This is aligned with the mean consumption of cigarettes in most countries (10–40 cigarettes per day) ¹, as discussed in Chapter 4 (Section 4.4 Discussion).

First, histological analysis was performed to investigate the differentiation status of the tissue following repeated whole CS exposure (Figure 5.4). As observed in a previous report ¹², a dose-dependent decrease in epithelium thickness occurred (Figure 5.4). Because the epithelial thickness is known to rely on the proliferation of epithelial cells ¹³, this result indicates that exposure to whole CS affects epithelial cell proliferation. The whole CS exposure also affected ciliated cell differentiation. Decreases in ciliated cell marker acetylated α -tubulin (Figure 5.4) and *FOXJ1* expression (Figure 5.6a) were observed following whole CS exposure. Similar changes have been reported in several previous studies ^{2, 4, 14}. A decrease in the number of ciliated cells is one of the phenotypic changes reported in COPD patients ¹⁵. In addition to a decrease in ciliated cells, an increase in goblet cells (i.e., goblet cell hyperplasia) is another phenotypic change related to COPD ¹⁶. An increase in mucin 5AC positive-large goblets was induced with IL-13 treatment in the 3D bronchial tissue model (Figure 5.5). The histological data indicated that mucin 5AC-positive cells were present in the center of the epithelial layer after exposure (Figure 5.4, arrowheads). Club cells are known to differentiate into goblet cells after tissue damage caused by *in vivo* exposure in mice ¹⁷, and they are reportedly present in the center of the epithelial layer in ALI-cultured HBECs during the differentiation process ¹⁸. Thus, the mucin 5AC-positive cells increased in the center of the epithelium may be in the process of differentiation from Club cells to goblet cells. The increased expression of *MUC5AC* and decreased expression of *SCGB1A1* (Club cell marker gene) could support this hypothesis (Figure 5.6b and d). Therefore, it is possible that

differentiation of goblet cells is promoted by repeated whole CS exposure. Overall, the histological data indicate that repeated whole CS exposure affects cell proliferation, ciliogenesis, and goblet cell differentiation, as observed in COPD patients¹⁹⁻²¹.

CS reportedly induces acute exposure effects on inflammatory and oxidative stress responses in human lung²². To determine whether these responses are activated following repeated whole CS exposure, the NF κ B signaling pathway was looked at because it is reported to play a pivotal role in inflammatory and oxidative stress responses²³. The number of significantly perturbed genes increased in a dose-dependent manner, and significant induction of gene expression of cytokines (*IL1B*, *IL8*, and *GCSF*), chemokine ligands (*MIP3A*, *GROb*, and *GROg*), and an oxidative stress response element (*HMOX1*) were confirmed after four-cigarette exposure on culture day 21 (Figure 5.7). Because the proteins coded by these genes are reported to play key roles in inflammatory and oxidative stress responses, the 3D bronchial tissue model is considered to be suitable for analyzing these responses by repeated whole CS exposure. Toll-like receptors are reported to play important roles in the host defense against external stimuli in the airway epithelium²⁴. The observed decrease in *TLR4* expression (Figure 5.7c) was similar to that reported in a lung cell line exposed to CS and the nasal mucosa of COPD patients and smokers²⁵. Overall, the PCR array data revealed a dose-dependent induction of NF κ B pathway components.

The effects of repeated whole CS exposure on inflammatory responses were also determined on the expression levels of proteins. Multi-plex analysis of proteins in the basolateral medium showed significant increases in secretions of IL-8, GRO- α , IL-1 β , and GM-CSF on culture day 21 (Figures 5.8 and 5.9). IL-8 and GRO- α are chemokines reported to be produced from bronchial epithelium, and mediate neutrophil recruitment, which has been observed in the bronchial epithelium of asthma and COPD patients²⁶. IL-1 β is a primary mediator in inflammation, and interaction between bronchial epithelial cells and fibroblasts is reported to be important in its secretion in the human bronchial epithelium *in vivo*²⁷. Thus, the increase in IL-1 β secretion detected in the 3D bronchial tissue model can be attributed to co-culturing bronchial epithelial cells with fibroblasts. Because the basolateral medium of the 3D bronchial tissue model can be collected in a

non-invasive way, the medium collected on days 9, 13, 17, and 21 was analyzed to investigate the repeated exposure effect on secretion of the inflammatory mediators. The basolateral medium from the four-cigarette exposed tissue showed increased secretions in IL-8, GRO- α , IL-1 β , and GM-CSF time-dependently (Figures 5.8 and 5.9). There was no clear dose-dependent change in M-CSF secretion during the exposure period (Figure 5.9c). However, GM-CSF and M-CSF are reported to play competitive roles in various biological processes, and their balance is known as indicator of inflammation²⁸. Thus, the increased level of GM-CSF and stable level of M-CSF observed in this experiment may indicate that the 3D bronchial tissue model is driven to a pro-inflammatory condition during the period of repeated whole CS exposure²⁸. Because the basolateral medium was changed every other day during the repeated exposure, the concentrations of these mediators indicate the quantities secreted in the 48 h after each exposure. Therefore, the cytokine data indicate that the secretion of inflammatory mediators was augmented in the 3D bronchial tissues during repeated whole CS exposure.

In this study, inflammatory cytokine secretions for IL-8, GRO- α , IL-1 β , and GM-CSF were analyzed during repeated whole CS exposure. In recent years, the importance of both inflammatory and anti-inflammatory cytokines has been reported in the COPD pathogenesis. For example, abnormal secretion of anti-inflammatory cytokines IL-4, IL-10, and IL-13 has been reported in the plasma and sputum of COPD patients²⁹⁻³¹, and the lamina propria lymphocyte population is considered the primary source of these cytokines³². Future studies should examine how secretion of these anti-inflammatory cytokines affects the 3D bronchial tissue model during repeated whole CS exposure.

The CS exposure concentrations produced by one, two, and four cigarettes were 3.4%, 6.5%, and 12.3% (vol/vol). In this experiment, a 3D bronchial tissue model was exposed to whole CS for 10 min at these concentrations. These exposure conditions were mild relative to those of previous experiments because the CS concentration was lower and the exposure duration was shorter (Table 5.1). These exposure conditions increased the number of goblet cells and expression of the marker gene, *MUC5AC* (Figure 5.4 and 5.6). Previous studies using 3D culture models of the bronchial epithelium failed to confirm this increase (Table 5.1), thus indicating the importance of co-culturing or repeated

exposure for inducing goblet cell hyperplasia. In addition to histological analyses, several previous studies measured IL-8 secretion as an inflammatory response indicator and revealed a 2–4-fold increase in IL-8 secretion after whole CS exposure (Table 5.1). However, in this experiment, IL-8 secretion reached a maximum 16.6-fold increase after repeated whole CS exposure (Table 5.1). This indicates the importance of repeated exposure for promoting tissue inflammation, which is important in COPD development.

Table 5.1 Summary of previous studies.

	3D culture model		Exposure conditions			Histological analysis		Inflammation
	Name	Fibroblasts	Concentration	Duration	Repetition	Goblet cell	Squamous cell	IL-8
Mathis et al. (2013)	EpiAirway	without	15%	7–28 min	1 day	-	-	-
Talikka et al. (2014)	MucilAir-HF	with	16.7%	24–28 min	1 day	Slight increase	-	-
Iskandar et al. (2015)	MucilAir-HF	with	8, 15%	28 min	1 day	-	-	2.3–3.9
Haswell et al. (2017)	MucilAir	without	3.3%	60 min	1 day	No change	-	-
Iskandar et al. (2017)	MucilAir	without	8, 15%	28 min	1 day	Decrease	-	2.1–4.1
Haswell et al. (2018)	MucilAir	without	3.3%	60 min	1 day	No change	-	2.8†
Iskandar et al. (2018)	MucilAir	without	7, 13%	28 min	1 day	No change	-	3.3†
Ishikawa and Ito (2017)	Original	with	3.4–12.3%	10 min	7 days*	Increase	No change	1.7–16.6

Summary of data from previous publications^{10, 12, 33–37}. ND, not detected. *every other day in two weeks.

†value estimated from published graph.

5.5 Conclusions

In this chapter, the 3D bronchial tissue model was subjected to repeated whole CS exposure with an exposure dose comparable to the actual human daily tissue dose of the average smoker. The results indicate that perturbation of mucociliary differentiation and induction of inflammation are induced in the tissue following repeated whole CS exposure. Moreover, the observed augmentation of inflammatory mediator secretion may indicate the importance of exposure repetition for inducing chronic inflammatory changes in an *in vitro* model. Therefore, the *in vitro* test with the 3D bronchial tissue model and repeated whole CS exposure with a daily tissue dose could be a useful alternative to *in vivo* experiments to investigate the chronic effects of CS exposure.

5.6 References

1. Ng, M. *et al.* Smoking prevalence and cigarette consumption in 187 countries, 1980-2012. *Jama* **311**, 183-192 (2014).
2. Schamberger, A.C., Staab-Weijnitz, C.A., Mise-Racek, N. & Eickelberg, O. Cigarette smoke alters primary human bronchial epithelial cell differentiation at the air-liquid interface. *Sci Rep* **5**, 8163 (2015).
3. Barnes, P.J. New anti-inflammatory targets for chronic obstructive pulmonary disease. *Nat Rev Drug Discov* **12**, 543-559 (2013).
4. Aufderheide, M., Scheffler, S., Ito, S., Ishikawa, S. & Emura, M. Ciliotoxicity in human primary bronchiolar epithelial cells after repeated exposure at the air-liquid interface with native mainstream smoke of K3R4F cigarettes with and without charcoal filter. *Exp Toxicol Pathol* **67**, 407-411 (2015).
5. Yasuo, M. *et al.* Relationship between calcium-activated chloride channel 1 and MUC5AC in goblet cell hyperplasia induced by interleukin-13 in human bronchial epithelial cells. *Respiration* **73**, 347-359 (2006).
6. Levardon, H., Yonker, L.M., Hurley, B.P. & Mou, H. Expansion of Airway Basal Cells and Generation of Polarized Epithelium. *Bio Protoc* **8** (2018).
7. Yonker, L.M. *et al.* Development of a Primary Human Co-Culture Model of Inflamed Airway Mucosa. *Sci Rep* **7**, 8182 (2017).
8. Iskandar, A.R. *et al.* Systems approaches evaluating the perturbation of xenobiotic metabolism in response to cigarette smoke exposure in nasal and bronchial tissues. *Biomed Res Int* **2013**, 512086 (2013).
9. Zhang, X. *et al.* Similarities and differences between smoking-related gene expression in nasal and bronchial epithelium. *Physiol Genomics* **41**, 1-8 (2010).
10. Mathis, C. *et al.* Human bronchial epithelial cells exposed in vitro to cigarette smoke at the air-liquid interface resemble bronchial epithelium from human smokers. *Am J Physiol Lung Cell Mol Physiol* **304**, L489-503 (2013).
11. Gelboin, H.V. Benzo[alpha]pyrene metabolism, activation and carcinogenesis: role and regulation of mixed-function oxidases and related enzymes. *Physiol Rev* **60**, 1107-1166 (1980).
12. Iskandar, A.R. *et al.* Impact Assessment of Cigarette Smoke Exposure on Organotypic Bronchial Epithelial Tissue Cultures: A Comparison of Mono-Culture and Coculture Model Containing Fibroblasts. *Toxicol Sci* **147**, 207-221 (2015).
13. Costea, D.E., Loro, L.L., Dimba, E.A., Vintermyr, O.K. & Johannessen, A.C. Crucial effects of fibroblasts and keratinocyte growth factor on morphogenesis of reconstituted human oral epithelium. *J Invest Dermatol* **121**, 1479-1486 (2003).

14. Brekman, A., Walters, M.S., Tilley, A.E. & Crystal, R.G. FOXJ1 prevents cilia growth inhibition by cigarette smoke in human airway epithelium in vitro. *Am J Respir Cell Mol Biol* **51**, 688-700 (2014).
15. Shaykhiev, R. & Crystal, R.G. Early events in the pathogenesis of chronic obstructive pulmonary disease. Smoking-induced reprogramming of airway epithelial basal progenitor cells. *Ann Am Thorac Soc* **11 Suppl 5**, S252-258 (2014).
16. Mullen, J.B., Wright, J.L., Wiggs, B.R., Pare, P.D. & Hogg, J.C. Structure of central airways in current smokers and ex-smokers with and without mucus hypersecretion: relationship to lung function. *Thorax* **42**, 843-848 (1987).
17. Tsao, P.N. *et al.* Notch signaling prevents mucous metaplasia in mouse conducting airways during postnatal development. *Development* **138**, 3533-3543 (2011).
18. Emura, M., Aufderheide, M. & Mohr, U. Target cell types with stem/progenitor function to isolate for in vitro reconstruction of human bronchiolar epithelia. *Exp Toxicol Pathol* **67**, 81-88 (2015).
19. Hessel, J. *et al.* Intraflagellar transport gene expression associated with short cilia in smoking and COPD. *PLoS One* **9**, e85453 (2014).
20. Lam, H.C. *et al.* Histone deacetylase 6-mediated selective autophagy regulates COPD-associated cilia dysfunction. *J Clin Invest* **123**, 5212-5230 (2013).
21. Randell, S.H. Airway epithelial stem cells and the pathophysiology of chronic obstructive pulmonary disease. *Proc Am Thorac Soc* **3**, 718-725 (2006).
22. van der Vaart, H., Postma, D.S., Timens, W. & ten Hacken, N.H. Acute effects of cigarette smoke on inflammation and oxidative stress: a review. *Thorax* **59**, 713-721 (2004).
23. Lawrence, T. The nuclear factor NF-kappaB pathway in inflammation. *Cold Spring Harb Perspect Biol* **1**, a001651 (2009).
24. Bowie, A.G. Translational mini-review series on Toll-like receptors: recent advances in understanding the role of Toll-like receptors in anti-viral immunity. *Clin Exp Immunol* **147**, 217-226 (2007).
25. MacRedmond, R.E., Greene, C.M., Dorscheid, D.R., McElvaney, N.G. & O'Neill, S.J. Epithelial expression of TLR4 is modulated in COPD and by steroids, salmeterol and cigarette smoke. *Respir Res* **8**, 84 (2007).
26. Barnes, P.J. New molecular targets for the treatment of neutrophilic diseases. *J Allergy Clin Immunol* **119**, 1055-1062; quiz 1063-1054 (2007).
27. Araya, J. *et al.* Squamous metaplasia amplifies pathologic epithelial-mesenchymal interactions in COPD patients. *J Clin Invest* **117**, 3551-3562 (2007).
28. Hamilton, J.A. Colony-stimulating factors in inflammation and autoimmunity. *Nat Rev Immunol* **8**, 533-544 (2008).

29. Grubek-Jaworska, H. *et al.* IL-6 and IL-13 in induced sputum of COPD and asthma patients: correlation with respiratory tests. *Respiration* **84**, 101-107 (2012).
30. Huang, A.X., Lu, L.W., Liu, W.J. & Huang, M. Plasma Inflammatory Cytokine IL-4, IL-8, IL-10, and TNF-alpha Levels Correlate with Pulmonary Function in Patients with Asthma-Chronic Obstructive Pulmonary Disease (COPD) Overlap Syndrome. *Med Sci Monit* **22**, 2800-2808 (2016).
31. Takanashi, S. *et al.* Interleukin-10 level in sputum is reduced in bronchial asthma, COPD and in smokers. *Eur Respir J* **14**, 309-314 (1999).
32. Zund, G., Madara, J.L., Dzusz, A.L., Awtrey, C.S. & Colgan, S.P. Interleukin-4 and interleukin-13 differentially regulate epithelial chloride secretion. *J Biol Chem* **271**, 7460-7464 (1996).
33. Talikka, M. *et al.* The response of human nasal and bronchial organotypic tissue cultures to repeated whole cigarette smoke exposure. *Int J Toxicol* **33**, 506-517 (2014).
34. Haswell, L.E. *et al.* Reduced biological effect of e-cigarette aerosol compared to cigarette smoke evaluated in vitro using normalized nicotine dose and RNA-seq-based toxicogenomics. *Sci Rep* **7**, 888 (2017).
35. Iskandar, A.R. *et al.* A systems toxicology approach for comparative assessment: Biological impact of an aerosol from a candidate modified-risk tobacco product and cigarette smoke on human organotypic bronchial epithelial cultures. *Toxicol In Vitro* **39**, 29-51 (2017).
36. Haswell, L.E. *et al.* In vitro RNA-seq-based toxicogenomics assessment shows reduced biological effect of tobacco heating products when compared to cigarette smoke. *Sci Rep* **8**, 1145 (2018).
37. Iskandar, A.R. *et al.* Comparative biological impacts of an aerosol from carbon-heated tobacco and smoke from cigarettes on human respiratory epithelial cultures: A systems toxicology assessment. *Food Chem Toxicol* **115**, 109-126 (2018).

Chapter 6.

**Omics analysis of the 3D bronchial tissue model following
repeated whole CS exposure**

6.1 Introduction

6.1.1 Objectives

Omics technologies and their applications in toxicological investigations have been evolving. Omics data provide deep insights into the biological mechanisms affected by CS exposure ¹⁻⁴. In the previous chapter, whole CS exposure of the 3D bronchial tissue model revealed that several phenotypic changes and augmentation of inflammation were induced after 2 weeks of repeated exposure at a dose equivalent to the daily tissue dose of the average smoker. The objective of this chapter was to understand the complex mechanisms underlying these changes using omics technologies (i.e., metabolomics, transcriptomics, and proteomics).

6.1.2 Study approaches

Omics technologies such as transcriptomics, proteomics, and metabolomics are becoming important for support of regulatory toxicity studies ⁵⁻⁷. CS smoke is a complex mixture of thousands of chemicals, and it is expected that various toxicological pathways are affected in cells exposed to CS ^{8, 9}. In this case, omics technologies could be a useful tool for analysis because these technologies can capture global changes in the expression of genes, proteins, and metabolites in CS-exposed cells. Omics data can be analyzed by various tools, and these tools can predict what pathways are biologically affected in CS-exposed cells ¹⁰⁻¹². No regulatory authorities make decisions on omics data alone. However, the US Food and Drug Administration and US Environmental Protection Agency encourage voluntary submission of omics data and consider the use of data submitted for case-by-case assessments (e.g., to contribute to a weight-of-evidence determination or find out mechanism of action) ¹³.

Repeated whole CS exposure of the 3D bronchial tissue model successfully reproduced the promoted inflammatory responses similar to those in actual COPD patients. The relationship between metabolism and chronic inflammation has been pointed out in various organs ¹⁴, and CS exposure is reported to have relation to

mitochondrial dysfunction and can affect various cellular metabolic processes^{15, 16}. Consequently, the analysis in this chapter first focused on perturbation of the metabolic homeostasis in the 3D bronchial tissue model after repeated whole CS exposure. Then, global gene expression profiles were analyzed by microarray analysis and identify the cell signaling pathways that were perturbed in the 3D bronchial tissue model after repeated whole CS exposure. Obtained metabolomic and transcriptomic data were then subjected to the upstream regulator analysis to identify key molecules regulating global metabolome and transcriptome changes. Because the changes in cellular signaling pathways could affect apical secretion of several mediators from the 3D bronchial tissue model known as the airway surface liquid (ASL)^{17, 18}, proteomic analysis was performed to detect changes in the ASL protein components that could occur in the sputum of smokers.

6.2 Materials and methods

6.2.1 Whole CS exposure of the 3D bronchial tissue model

Whole CS exposure of 3D bronchial tissue model was performed under the conditions described in Chapter 5 (Section 5.2.1 Whole CS exposure of the 3D bronchial tissue model). Whole CS exposure was conducted from ALI culture day 7 to 19 on every other day, and the medium was replaced before each exposure (Figure 6.1). Forty-eight hours after the last exposure on ALI culture day 21, the ASL was sampled by rinsing the apical surface of the 3D bronchial tissue twice with 200 μ L of pre-warmed PBS. The tissue was then sampled for histology and to extract total mRNA and metabolites.

Chapter 6. Omics analysis of the 3D bronchial tissue model following repeated whole CS exposure

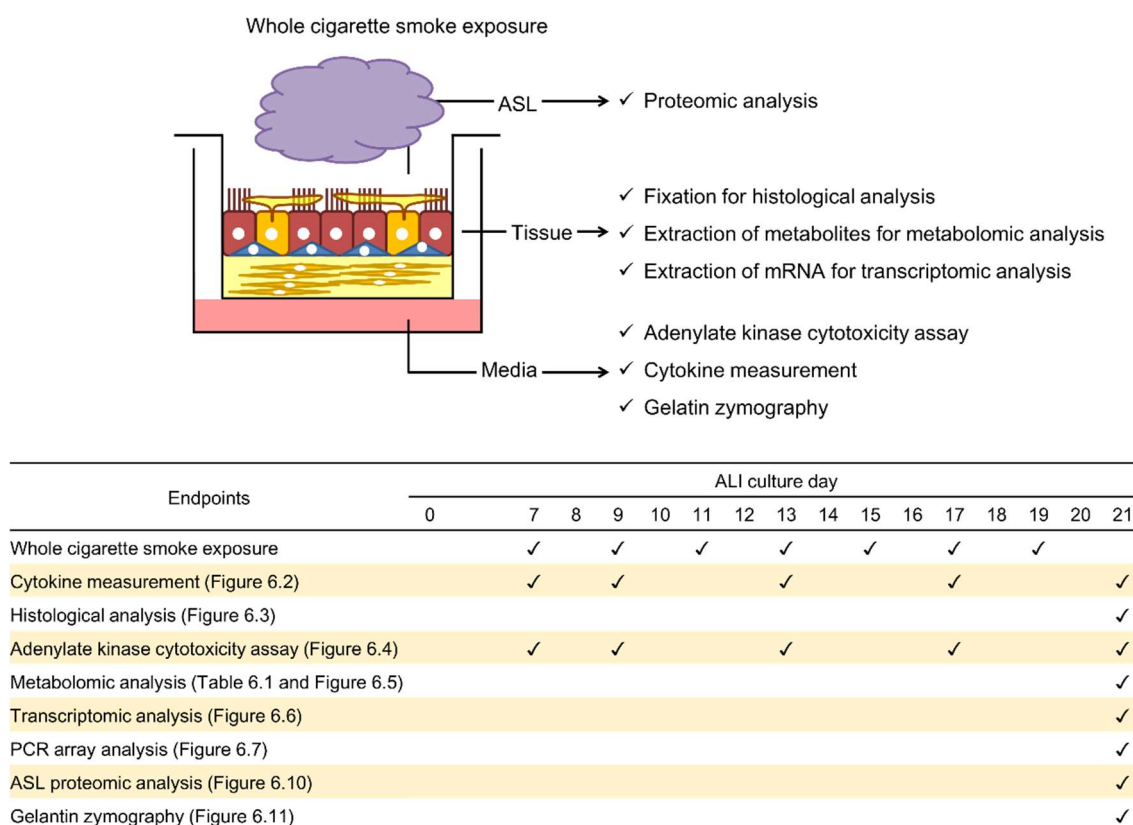


Figure 6.1 Experimental design for repeated whole cigarette smoke exposure.

The 3D bronchial tissues were exposed to whole cigarette smoke from one, two, or four cigarettes through an air–liquid interface (ALI) culture on every other day from day 7 to 19. The medium samples collected on ALI culture days 7, 9, 13, 17, and 21 were subjected to cytokine measurements for detection of inflammation and an adenylate kinase assay for detection of cytotoxicity. The medium sample collected on ALI culture day 21 was also subjected to gelatin zymography. The apical surface of the tissue was washed with PBS for collection of the airway surface liquid (ASL) for proteomic analysis on ALI culture day 21. Then, the tissue was fixed for histological analysis. The tissue samples that were not used for histological analysis were subjected to mRNA extraction for transcriptomic/PCR array analysis and extraction of metabolites for metabolomics analysis.

6.2.2 Analysis of secreted cytokines

Cytokine measurements were performed in accordance with the protocol described in Chapter 5 (Section 5.2.6 Analysis of secreted proteins). Significant differences between

whole CS-exposed samples and air-exposed controls were evaluated by Welch's *t*-test with log-transformed data. Results were considered significant if the Bonferroni-corrected *p*-value was less than 0.05.

6.2.3 Histological analysis of the tissues

Histological analysis was performed as described in Chapter 3 (Section 3.2.3 Histological analysis of the tissues).

6.2.4 Adenylate kinase cytotoxicity assay

Media from the three tissue samples used for each exposure condition were sampled on ALI culture days 7, 9, 13, 17, and 21 and analyzed using a ToxiLight (Lonza) in accordance with the manufacturer's instructions. Luminescence was measured using an Infinite 200 PRO microplate reader (Tecan, Männedorf, Switzerland). The results are presented as the means and standard deviations of the three tissue samples. Significant differences between whole CS-exposed samples and air-exposed controls were evaluated by Welch's *t*-test. Results were considered significant if the Bonferroni-corrected *p*-value was less than 0.05.

6.2.5 Global metabolome analysis

Intracellular metabolites were extracted by homogenization of the 3D bronchial tissue model with 50% acetonitrile. Metabolites were extracted from four tissue cultures for each exposure condition. Global metabolome analysis was performed with the HMT Basic Scan package (Human Metabolome Technologies, Inc., Yamagata, Japan), which targets about 900 ionic metabolites. The peaks were annotated according to the HMT metabolite database, and the areas of the annotated peaks were normalized using the

internal standard levels. Each peak area was normalized to the total sample amount (relative area), and then integrated using Mass Profiler Professional (Agilent Technologies). The expression ratio and p -value corrected using the Benjamini–Hochberg false discovery rate (FDR) ¹⁹ were computed, using the “limma” R package ²⁰ to detect differences between the CS-exposed groups and the controls that were significant at FDR-corrected $p < 0.3$. When observations were below the limit of detection, 2^{-52} was used as a proxy.

6.2.6 Targeted metabolomic analysis

To complement the HMT Basic Scan analysis, metabolites related to glycolysis, the pentose phosphate pathway (PPP), and the tricarboxylic acid (TCA) cycle were analyzed by liquid chromatography (Agilent 1200, Agilent Technologies) with electrospray tandem mass spectrometry (API4000, AB Sciex, Framingham, MA, USA) as a targeted metabolomics approach. Three out of four samples used for global metabolome analysis were used for targeted analysis. Separation of metabolites related to glycolysis and the PPP was performed with a gradient elution on a HILICpak VT-50 2D column (150 mm × 2.1 mm inside diameter; Showa Denko K.K., Tokyo, Japan). The mobile phase was a mixture of a 20% acetonitrile solution (Solvent A) and a 20% acetonitrile solution containing 250 mM ammonium formate (Solvent B). For the gradient, solvent B was held at 12% for 6 min, increased to 75% over 19 min, and held at 75% for 10 min. Equilibration was performed for 25 min. The mobile phase flow rate was set at 0.2 mL/min and the column oven temperature was set at 55 °C. The injection volume was 5 µL. Tandem mass spectrometry detection was performed in selected reaction monitoring mode, and the ion source was operated in negative ionization mode. Separation of metabolites related to the TCA cycle was performed using an isocratic elution on a CAPCELL CORE ADME column (150 mm × 2.1 mm inside diameter, Shiseido, Tokyo, Japan), using a 5 mM ammonium formate aqueous solution containing 0.1% formic acid and methanol (95:5, v/v). The flow rate was set at 0.2 mL/min, and column oven temperature was set at 40 °C. The total run time was 7 min, and the injection volume was 5 µL. Tandem mass

spectrometry detection was performed in selected reaction monitoring mode, and the ion source was operated in negative ionization mode. Targeted metabolome analysis was performed without an internal standard and the data are described in comparison with absolute areas. Each peak area was normalized to the total sample amount (relative area), and significant differences between whole CS-exposed samples and air-exposed controls were evaluated using a Student's *t*-test with Welch's correction for unequal variances. Results were considered significant if the Bonferroni-corrected *p*-value was less than 0.05.

6.2.7 Microarray analysis

Following repeated whole CS exposure, total RNA was isolated from tissue cultures as described in Chapter 3 (Section 3.2.6 PCR array analysis for ECM-related genes). Transcriptomic analysis was conducted by Takara Bio, Inc. (Shiga, Japan) according to the Affymetrix GeneChip Expression Analysis Technical Manual. Briefly, after synthesis of double-stranded complementary DNA from 250 ng of total RNA, biotinylated complementary RNA was generated using a GeneChip 3' IVT PLUS Reagent Kit, and fragmented using a GeneChip Hybridization, Wash and Stain Kit. Biotinylated fragmented complementary RNA (15 µg) was hybridized to a GeneChip HG-U133 Plus 2.0 array for 16 h at 60 rpm in a 45 °C GeneChip Hybridization Oven 645 (Affymetrix). The arrays were washed and stained on a GeneChip Fluidics Station 450 (Affymetrix), and then scanned using a GeneChip 3000 7G Scanner (Affymetrix). After scanning, expression data were obtained using Affymetrix GeneChip Command Console software and Affymetrix Expression Console Software 1.4. Transcriptomic data are available in ArrayExpress (accession number E-MTAB-6175).

6.2.8 Microarray data processing

Raw data were normalized to the 75th percentile and baseline-transformed to the mean of all samples, and then summarized with GC-Robust Multiarray Average in GeneSpring

(version 14.0; Agilent Technologies). Next, the summarized data were filtered by expression (lower cutoff: 20th percentile) and error (coefficient of variation < 50%). The filtered list was evaluated by a moderated *t*-test, and multiple-testing correction was performed on the *t*-test *p*-values using the Benjamini–Hochberg FDR to detect significant differences at FDR-corrected $p < 0.05$ between the CS-exposed groups and the controls. The filtered list was used to extract expression data for specific genes to create heatmaps of gene expression (glycolysis-, TCA cycle-, and PPP-related genes) and to conduct correlation analysis with proteomic data.

6.2.9 Ingenuity pathway analysis

Analyses of the differentially expressed genes (DEGs) and metabolites were performed using Ingenuity Pathway Analysis (IPA) software (Qiagen). Genes were considered differentially expressed if they had an absolute \log_2 fold change greater than 1.0 and a FDR-corrected *p*-value of less than 0.05. To annotate sufficient quantities of metabolites for the analysis, a loose threshold was set for metabolomic data (absolute \log_2 fold change > 0.5 and FDR-corrected $p < 0.3$) compared with the microarray analysis threshold. The data obtained from both global and targeted metabolomic analyses were used for IPA. Canonical pathway analysis and biofunction analysis with microarray data were performed to identify the most relevant pathways perturbed by repeated whole CS exposure. Upstream regulator analysis was also performed to predict the molecules involved in regulating DEGs and differentially expressed metabolites. Only endogenous upstream regulators were analyzed in this study; drugs and toxicants were disregarded. The networks were constructed with downstream targets and upstream regulators using the “Connect” option under the “Build” functionality in IPA, and then the Molecular Activity Predictor was used to predict the activities of the target molecules in the networks.

6.2.10 PCR array analysis

Following repeated whole CS exposure, total RNA was isolated from tissue cultures and used for PCR array analysis as described in Chapter 3 (Section 3.2.6 PCR array analysis for ECM-related genes). The human glucose metabolism PCR Array (PAHS-006; SABiosciences) was used to analyze the expression of 84 genes related to human glucose metabolism following the manufacturer's protocol. Statistical analysis of the PCR array data was performed using RT2 Profiler PCR Array Data Analysis version 3.5 (SABiosciences). The obtained data were assessed using the “limma” R package to detect significant differences at FDR-corrected $p < 0.05$ between CS-exposed groups and controls.

6.2.11 ASL proteomics analysis

ASL samples were centrifuged at 10,000 rpm for 5 min to eliminate cellular debris, and protein concentrations were analyzed using a Micro BCA Protein Assay Kit (Thermo Fisher Scientific, Waltham, MA, USA). To obtain the total amount of protein necessary for proteomic analysis, pooled ASL samples from four tissue cultures for each exposure condition were analyzed. Proteomic analysis was conducted by APRO Science (Tokushima, Japan) using iTRAQ technology. Normalization was performed against the total abundance values in individual samples, and abundance ratios (whole CS-exposed sample/control) were calculated. Statistical analysis of proteomics data was not performed because pooled samples from each exposure condition were used.

6.2.12 Measurement of MMP by gelatin zymography

Gelatin zymography was performed using the protocol described in Chapter 3 (Section 3.2.4 Measurement of matrix metalloproteinases by gelatin zymography). Significant differences between the whole CS-exposed samples and air-exposed controls were

evaluated by Welch's *t*-test. Results were considered significant if the Bonferroni-corrected *p*-value was less than 0.05.

6.3 Results

6.3.1 Cytokine secretion and tissue damage following repeated whole CS exposure

The 3D bronchial tissue model was exposed to whole CS repeatedly every other day for two weeks in accordance with the protocol in Chapter 5 (Section 5.2.1 Whole CS exposure of the 3D bronchial tissue model), and various endpoints were analyzed following the exposure (Figure 6.1). The observed exposure repetition-dependent changes in cytokine secretion (Figure 6.2) and thinning of the epithelial layer in histological data (Figure 6.3) were consistent with the results in Chapter 5. Consistent with the histological evaluation, dose-dependent increase in the enzymatic activity of adenylate kinase released into the basolateral culture medium was observed following repeated whole CS exposure (Figure 6.4). The promotion of inflammatory state indicates that tissues are under chronic exposure conditions after repeated whole CS exposure. Therefore, tissue samples were collected on ALI culture day 21 and subjected to omics analyses (i.e., metabolomic, transcriptomic, and proteomic analysis) for comprehensive understanding of the global impact of chronic CS exposure on the 3D bronchial tissue model.

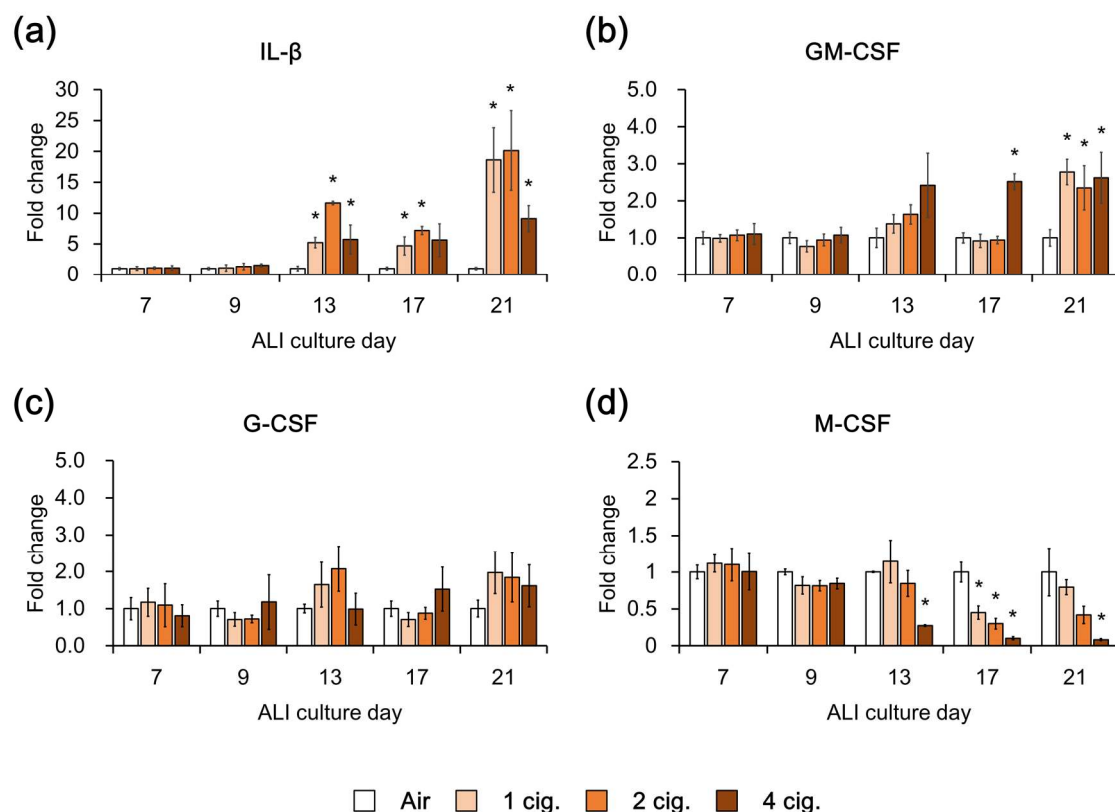


Figure 6.2 Results of cytokine measurements.

Medium samples collected on air-liquid interface (ALI) culture days 7, 9, 13, 17, and 21 were analyzed. *Significantly different from the air-exposed control (Bonferroni-corrected $p < 0.05$, Welch's t -test). GM-CSF, granulocyte macrophage-colony stimulating factor; G-CSF, granulocyte-colony stimulating factor; IL, interleukin; M-CSF, macrophage-colony stimulating factor

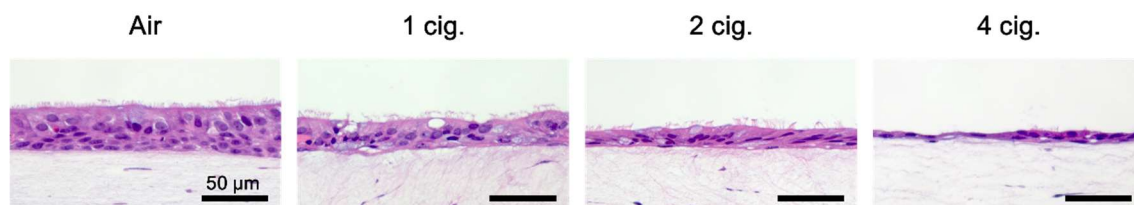


Figure 6.3 Results of histological analysis.

Tissue samples collected on air-liquid interface culture day 21 were subjected to hematoxylin and eosin staining.

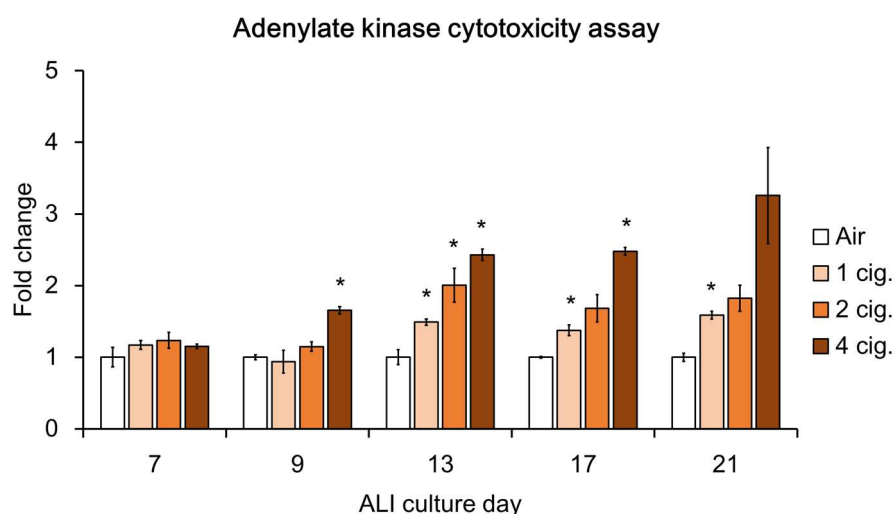


Figure 6.4 Results of the adenylate kinase cytotoxicity assay.

Medium samples collected on air–liquid interface (ALI) culture days 7, 9, 13, 17, and 21 were analyzed.

*Significantly different from the air-exposed control (Bonferroni-corrected $p < 0.05$, Welch's t -test).

6.3.2 Dose-dependent perturbation of metabolites by repeated whole CS exposure and its effect on central carbon metabolism

Global metabolomic analysis was performed with the metabolites extracted from the 3D bronchial tissue. Under each exposure condition, the metabolites showed significant differences in their abundance. In the extracted metabolites, nicotine derived from CS was detected and its levels in the tissue samples increased dose-dependently (Table 6.1). This indicated that the exposure system could deliver whole CS effectively to the 3D bronchial tissue. The metabolites showed significant increases included reduced glutathione (GSH; γ -L-Glu-L-Cys-Gly) and oxidized glutathione (GSSG) (Table 6.1). Through conversion to GSSG, GSH detoxify oxidants. Amino acids used for synthesis of GSH (i.e., Glu and Cys), also showed increases after repeated whole CS exposure. In addition, the levels of ATP and ADP indicating energy transfer in the cell, decreased dose-dependently in the 3D bronchial tissue after repeated whole CS exposure (Table 6.1).

Table 6.1 Metabolites identified by global metabolomics analysis.

	Fold change		
	1 cig.	2 cig.	4 cig.
Nicotine	0.0016*	0.0044*	0.0098*
GSH	1.80	10.32	<u>0.77</u>
GSSG	<u>2.09</u>	<u>3.27</u>	0.86
Glu	<u>1.91</u>	<u>1.94</u>	<u>1.44</u>
Cys	2.01	3.02	1.97
Gly	1.19	0.95	0.85
ADP	0.74	<u>0.49</u>	<u>0.16</u>
ATP	0.69	<u>0.45</u>	<u>0.12</u>

Mean fold changes between air-exposed controls and cigarette smoke-exposed tissues were calculated. The data represent the means of four tissue cultures. Values that are significantly different from those in the air-exposed control cultures (FDR-corrected $p < 0.3$) are underlined. *Data are expressed as relative areas because nicotine was not detected in the air-exposed control. GSH, reduced glutathione; and GSSG, oxidized glutathione.

Because a disruption in energy production was observed, the next analysis was focused on the metabolites related to central carbon metabolism, which generates ATP and reducing agents (i.e., glycolysis, the TCA cycle, and the PPP). A target metabolomics approach was selected for analysis of the metabolites related to the central carbon metabolism. The results are summarized in Figure 6.5a. Dose-dependent decreases were observed for all TCA cycle metabolites except for oxaloacetate. The levels of glycolysis metabolites also decreased following two- and four-cigarette exposures except for glucose 6-phosphate (G6P) and fructose 6-phosphate (F6P) (Figure 6.5a). These two metabolites are branch points between the PPP and glycolysis. The levels of 6-phosphogluconate (6-PG), ribose 5-phosphate (R5P), and erythrose 4-phosphate (E4P), which are involved in the PPP, increased in the one- and two-cigarette exposures (Figure 6.5a). The two-cigarette exposure results suggested the PPP for production of GSH was promoted and the TCA cycle for production of ATP was inhibited (Figure 6.5b). These results are aligned with global metabolomics data, which suggest increased levels of GSH and decreased levels of ATP following repeated whole CS exposure (Table 6.1).

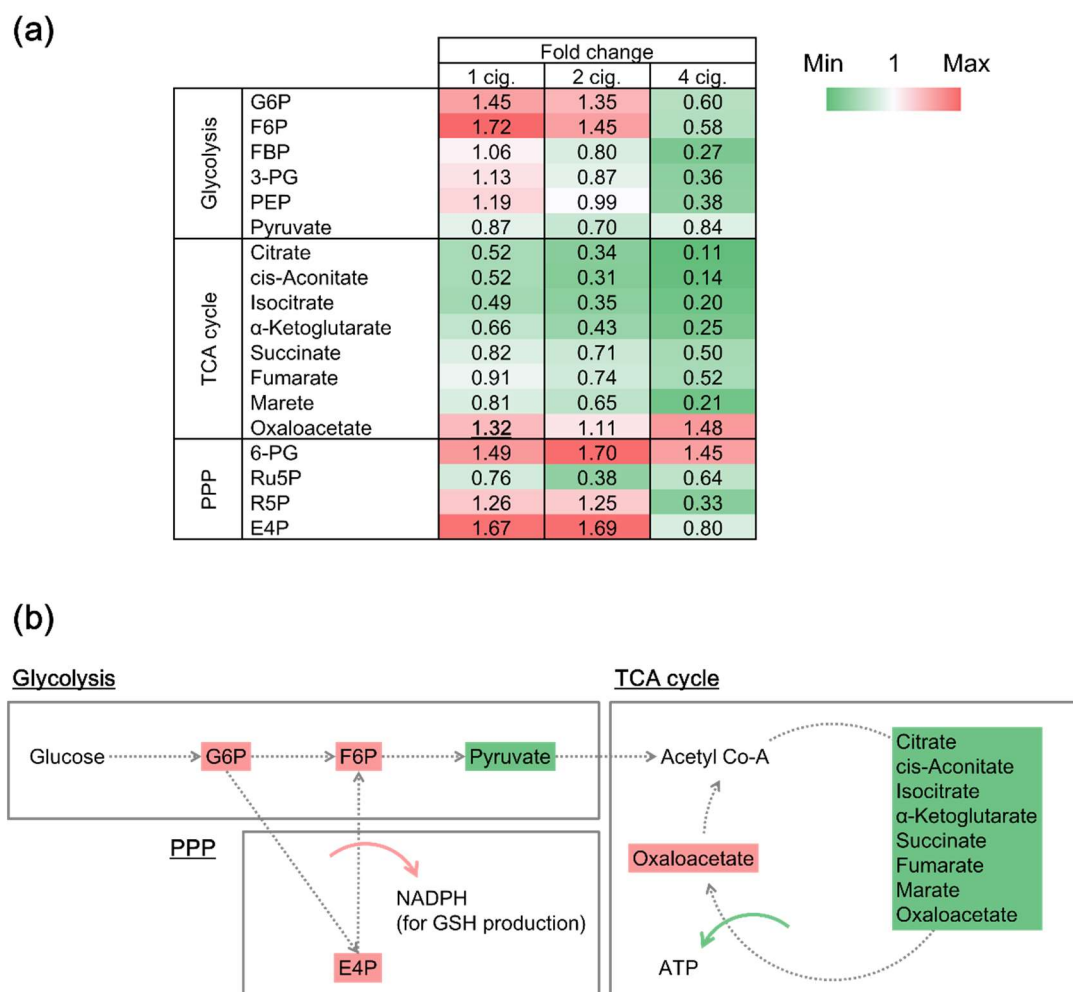


Figure 6.5 Results of targeted metabolomics for analysis of metabolites related to central carbon metabolism.

(a) The expression levels of analyzed metabolites. The results represent the means of three tissue samples. Values that are significantly different from those in the air-exposed control tissues (Bonferroni-corrected $p < 0.05$, Welch's t -test) are underlined. (b) Summary of the results of targeted metabolomics. Upregulated metabolites with two-cigarette exposure are colored in red and downregulated metabolites with two-cigarette exposure are colored in green. 3-PG, 3-phosphoglycerate; 6-PG, 6-phosphogluconate; E4P, erythrose 4-phosphate; F6P, fructose 6-phosphate; FBP, fructose 1,6-bisphosphate; G6P, glucose 6-phosphate; GSH, reduced glutathione; PEP, phosphoenolpyruvate; PPP, pentose phosphate pathway; R5P, ribose 5-phosphate; Ru5P, ribulose-5-phosphate; TCA, tricarboxylic acid.

6.3.3 Microarray analysis of central carbon metabolism perturbation

To determine the effect of repeated whole CS exposure on central carbon metabolism on a transcriptomic level, 3D bronchial tissues were subjected to microarray analysis. The expression levels of genes related to central carbon metabolism are summarized in Figure 6.6. Some genes involved in the PPP (*G6PD*, *TKT*, and *TALDO1*) showed increased expression in a dose-dependent manner after repeated whole CS exposure. By contrast, many genes related to glycolysis and the TCA cycle showed decreased expression after repeated whole CS exposure. These changes were clearer in the PCR results for mRNA extracted from another set of 3D bronchial tissues after repeated whole CS exposure, where most of the genes related to glycolysis and the TCA cycle showed decreased expression (Figure 6.7). In addition, expression of *G6PD*, *TKT*, and *TALDO1* related to the PPP showed increased expression in a dose-dependent manner after repeated whole CS exposure (Figure 6.7). These gene expression data are consistent with the metabolomic data obtained from the 3D bronchial tissues exposed to whole CS..

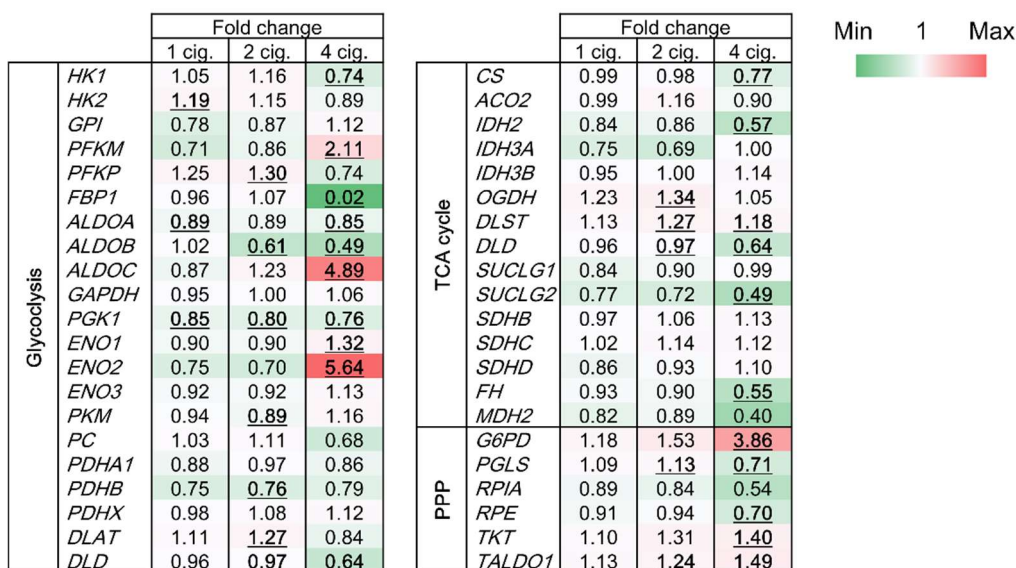


Figure 6.6 Expression levels of genes related to central carbon metabolism.

(a) The data were extracted from filtered microarray data. The results represent the means of three tissue samples. Values that are significantly different from those in the air-exposed control tissues (FDR-corrected $p < 0.05$) are underlined. PPP, pentose phosphate pathway; and TCA, tricarboxylic acid.

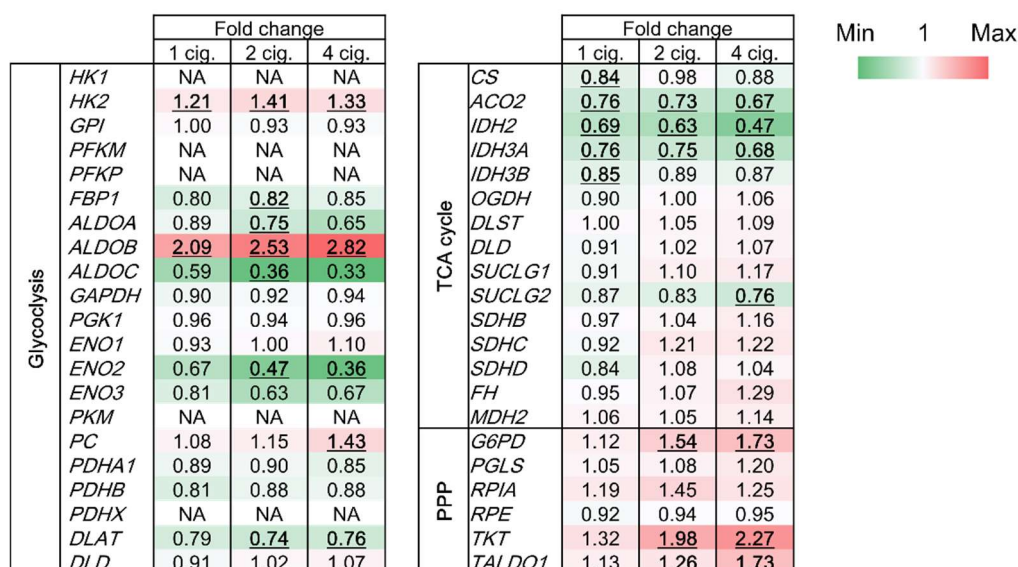


Figure 6.7 PCR analysis of expression of genes related to human glucose metabolism.

The results represent the means of three tissue samples. Values that are significantly different from those in the air-exposed control cultures ($p < 0.05$, Student's t -test) are underlined. NA, not analyzed; PPP, pentose phosphate pathway; and TCA, tricarboxylic acid.

6.3.4 Global gene expression and pathway analysis from microarray data

Transcriptomic data were used for analysis of perturbations in various biological processes other than central carbon metabolism. Venn diagrams of DEGs indicated that 216, 482, and 2,213 genes were upregulated after exposure to one, two, and four cigarettes, respectively (Figure 6.8a). Similarly, 367, 952, and 3,437 genes were downregulated after exposure to one, two, and four cigarettes, respectively (Figure 6.8b). Among the common DEGs identified by comparing exposure conditions, 70 genes were upregulated (Figure 6.8a) and 268 genes were downregulated (Figure 6.8b). These DEGs were used for canonical pathway analysis with IPA software to identify cellular signaling pathways perturbed after repeated whole CS exposure. Among several panels, “Ingenuity Toxicity List Pathways” was selected and significantly perturbed pathways included inflammatory pathways (“Inflammasome Pathway” and “NF κ B Signaling” in Figure 6.8c), an oxidative stress response pathway (“Nrf2 [nuclear factor erythroid 2-related factor 2]-mediated Oxidative Stress Response” in Figure 6.8c), and xenobiotic metabolic pathways

(“Xenobiotic Metabolism Signaling” and “Aryl Hydrocarbon Receptor [AhR] Signaling” in Figure 6.8c). In addition to pathway analysis using the DEGs that were expressed under all exposure conditions, functional analysis using the DEGs in each exposure condition was performed applying the “Disease and Biofunctions” panel. The results showed the cellular condition was different in each exposure dose. The functions related to the lungs are extracted and summarized in Figure 6.8d. After one- or two-cigarette exposures, genes involved in activation and stimulation of lung cells were significantly perturbed (Figure 6.8d). However, after four-cigarette exposure, genes involved in apoptosis and cell death of lung were significantly perturbed.

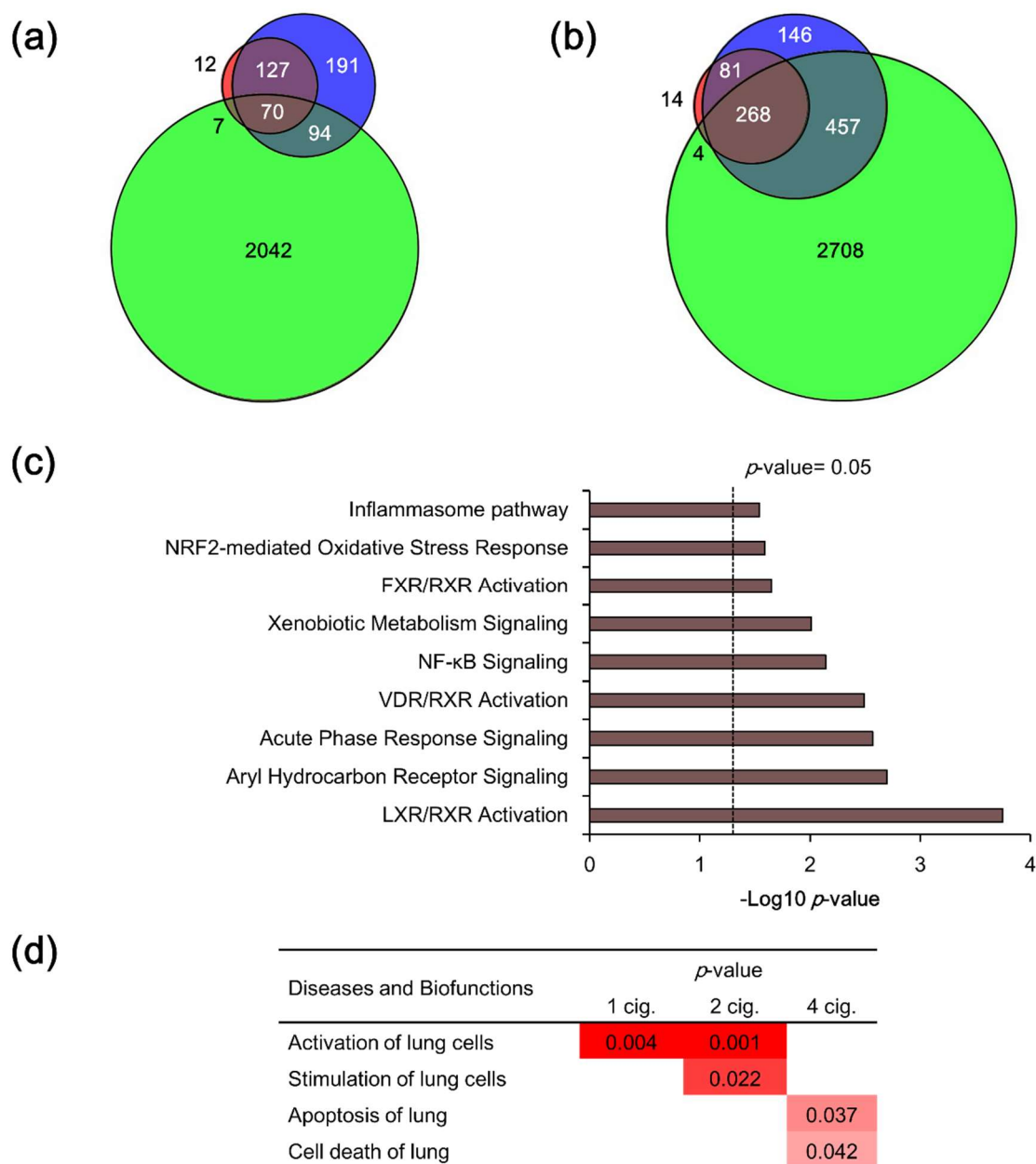


Figure 6.8 Results of microarray analysis.

(a) Venn diagrams of up- and (b) downregulated genes following exposure to one, two, and four cigarettes. (c) Canonical pathway analysis (Ingenuity Toxicity List Pathways) of differentially expressed genes ($|\log_2$ fold change| > 1.0 , FDR-corrected $p < 0.05$) and common differentially expressed genes under all exposure conditions. The pathways listed were altered significantly ($p < 0.05$). (d) Biofunction analysis (Disease and Biofunctions) of genes that were differentially ($|\log_2$ fold change| > 1.0 , FDR-corrected $p < 0.05$) expressed under each exposure condition. The listed functions related to lungs were altered significantly ($p < 0.05$). cig., cigarette.

6.3.5 Multi-omics-based estimation of epidermal growth factor receptor-related network perturbation

The metabolomic and transcriptomic data were analyzed further using IPA software to identify upstream regulators controlling the molecular changes observed in the 3D bronchial tissue. Under all exposure conditions, epidermal growth factor receptor (EGFR) was identified as an upstream regulator of the differentially expressed metabolites (Table 6.2). Moreover, epidermal growth factor was identified as an upstream regulator in the four-cigarette exposure.

Table 6.2 Predicted upstream regulators of metabolome alterations following repeated whole CS exposure.

Name	Molecule Type	<i>p</i> -value of overlap		
		1 cig.	2 cig.	4 cig.
ICMT	enzyme		1.91E-06	8.66E-09
EGFR	kinase	2.52E-03	2.31E-03	1.24E-07
UCP2	transporter			1.23E-04
HTT	transcription regulator		1.66E-04	8.84E-04
EGF	growth factor			1.97E-02
TNF	cytokine		2.51E-02	

Differentially expressed metabolites ($|\log_2 \text{fold change}| > 0.5$, FDR-corrected $p < 0.3$) following cigarette smoke exposure were used in the analysis. Significantly altered upstream regulators (p -value of overlap < 0.05).

Furthermore, in agreement with metabolomic data, EGFR was identified as a significant upstream regulator of DEGs in the two- and four-cigarette exposures. Moreover, epidermal growth factor was identified as a significant upstream regulator in the four-cigarette exposure (Table 6.3). TNF and IL1A, which are related to inflammatory responses, were identified as upstream regulators under all exposure conditions (Table 6.3).

Table 6.3 Predicted upstream regulators of transcriptome alterations following repeated whole CS exposure.

Name	Molecule Type	<i>p</i> -value of overlap		
		1 cig.	2 cig.	4 cig.
TNF	cytokine	5.35E-07	3.56E-06	1.15E-05
TGFA	growth factor			3.25E-04
EHF	transcription regulator	7.89E-03	1.93E-02	1.66E-03
EGFR	kinase		4.12E-02	6.44E-03
EGF	growth factor			6.96E-03
TLR3	transmembrane receptor			7.61E-03
CDKN1A	kinase			9.50E-03
IL1A	cytokine	1.31E-02	1.19E-02	1.73E-02
SMAD3	transcription regulator			1.80E-02
SOCS1	other			2.51E-02
IL17A	cytokine			2.59E-02
CAMP	other		2.56E-02	2.59E-02
TGFB1	growth factor			4.06E-02
HRAS	enzyme			4.08E-02
IL1B	cytokine		4.97E-02	4.29E-02
HGF	growth factor		2.61E-03	
MYC	transcription regulator		3.27E-02	
KRAS	enzyme		4.93E-02	

Differentially expressed metabolites ($|\log_2$ fold change| > 1.0, FDR-corrected $p < 0.05$) following cigarette smoke exposure were used in the analysis. Significantly altered upstream regulators (p -value of overlap < 0.05).

Because EGFR was identified as a common upstream regulator of differentially expressed metabolites and genes, the IPA “Connect” tool was used to build up a molecular network related to EGFR that included both downstream genes and metabolites. Then molecular Activity Predictor analysis was performed to predict activation of EGFR. This analysis can predict the activation of a specific molecule in a network given a starting set of neighboring molecules with known expression. The analysis with combined transcriptomic and metabolomic data predicted the activation of EGFR after repeated whole CS exposure (Figure 6.9).

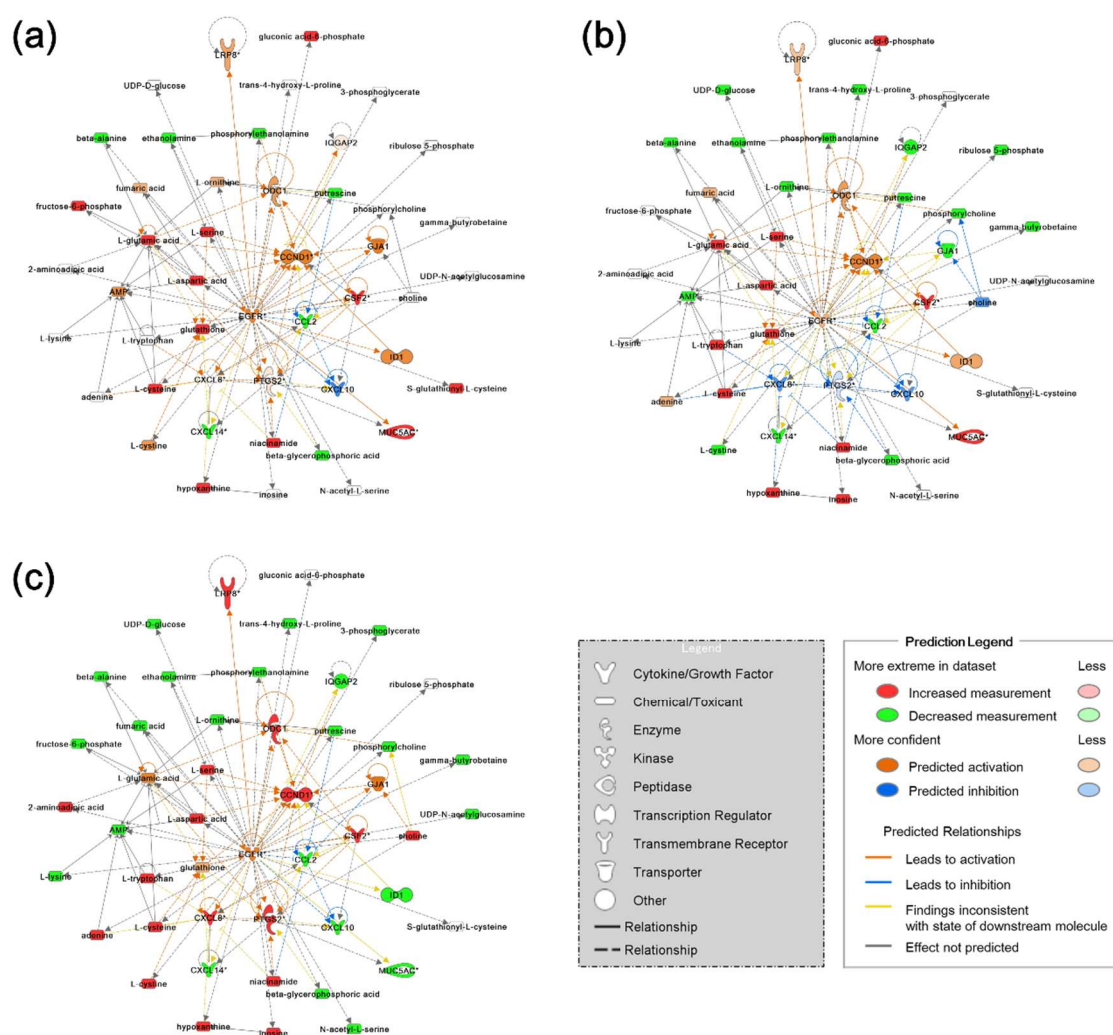


Figure 6.9 Prediction of epidermal growth factor receptor (EGFR) pathway activation from combined metabolomic and transcriptomic data.

An EGFR-related biological network was constructed using the Ingenuity database. Molecules in the network represent differentially expressed metabolites ($|\log_2 \text{ fold change}| > 0.5$, FDR-corrected $p < 0.3$) and genes ($|\log_2 \text{ fold-change}| > 1.0$, FDR-corrected $p < 0.05$) following cigarette smoke exposure. Molecular activity predictor analysis was used to predict the activity of EGFR (placed at the center of the network). Red and green indicate significant increases and decreases, respectively, of gene and metabolite expression. Molecules are colored orange and blue for predicted activation and inhibition, respectively. Color intensity qualitatively represents the magnitude of the fold change (red and green) and z-score (orange and blue). Solid and dashed lines show direct and indirect interactions, respectively.

6.3.6 Proteomic analysis of apical secretions of mucins and MMPs in CS-exposed 3D bronchial tissue cultures

As a result of perturbed biological processes, which shown by transcriptomic and metabolomic analyses, the 3D bronchial tissue may show abnormal function. Therefore, to detect functional deficiencies induced in the 3D bronchial tissue, the secretory capability of the tissue was analyzed after repeated whole CS exposure. Proteomic analysis was applied for this purpose and used to quantify the levels of ASL mucins and MMPs of the 3D bronchial tissues (Figure 6.10a). Under all exposure conditions, the levels of mucin 2 and mucin 20 were increased by repeated whole CS exposure. By contrast, the level of mucin 5B decreased dose-dependently. The levels of mucin 1, 4, 5AC, and 16 showed increase in the one- and two-cigarette exposures, and substantial decrease in the four-cigarette exposure. The levels of MMP-1 and MMP-3 in the ASL showed dose-dependent increase, whereas the levels of MMP-2 and MMP-7 in the ASL showed dose-dependent decrease. The levels of MMP-9, MMP-10, and MMP-14 showed increase in the one- and two-cigarette exposures but showed slight decrease in the four-cigarette exposure. In addition to mucins and MMPs, alpha-1 antitrypsin (AAT) was identified in the ASL components and showed dose-dependent decrease after repeated whole CS exposure. Interestingly, AAT deficiency has been linked to COPD ^{21, 22}. The correlations between the expression levels of these proteins and the corresponding mRNAs were analyzed, and the Pearson correlation coefficient (R) was 0.697 (Figure 6.10b).

The changes in the ASL levels of MMP-2 and MMP-9 observed by proteomic analysis were consistent with the result of gelatin zymography, showing enzymatic activity of pro-MMP-2, active MMP-2 and pro-MMP-9 secreted into the basolateral culture medium (Figure 6.11).

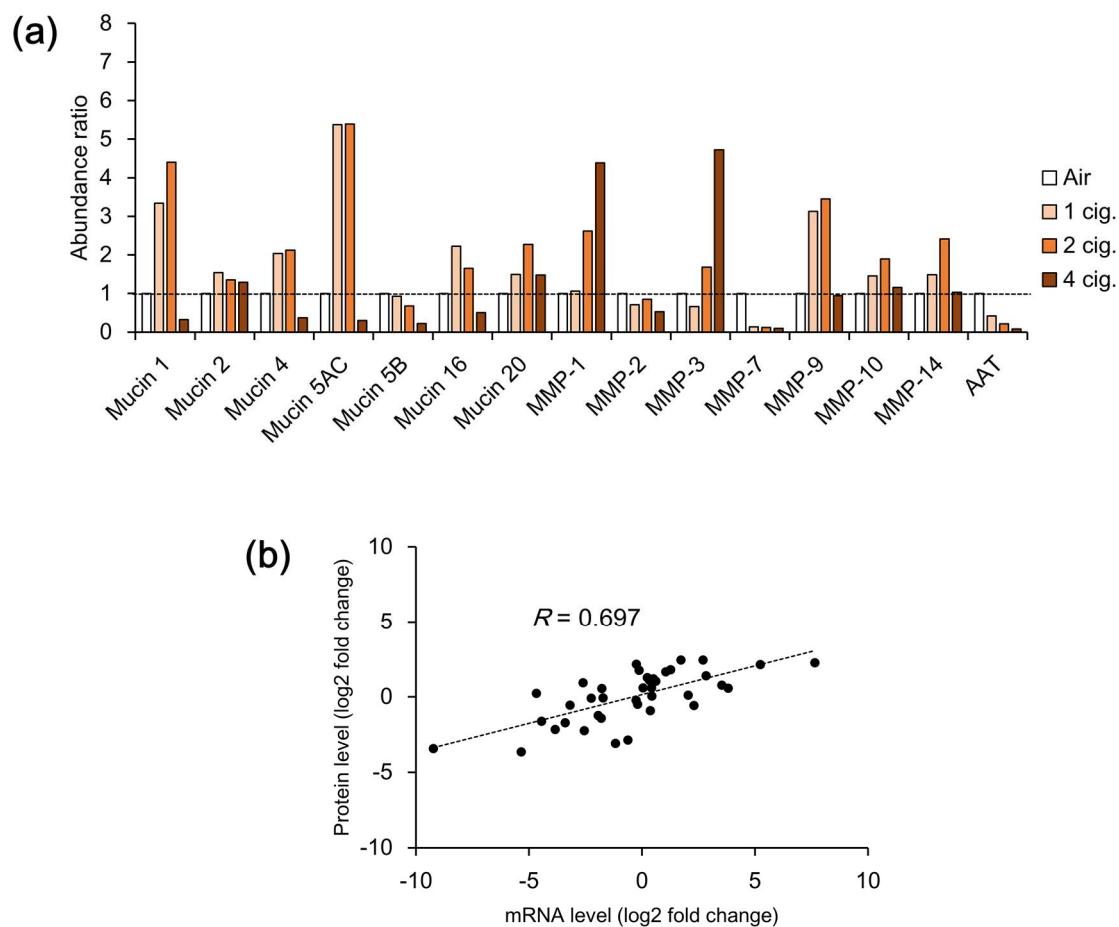


Figure 6.10 Proteomic analysis of apical surface liquid samples following repeated exposure to whole cigarette smoke.

(a) Relative expression ratios of mucins, matrix metalloproteinases (MMPs), and alpha-1 antitrypsin (AAT) in apical surface liquid samples obtained from the 3D bronchial tissue cultures exposed to whole cigarette smoke. The results represent pooled data from four tissue cultures. (b) Correlation between mRNA and the protein levels of mucins, MMPs, and AAT under all exposure conditions. Mucin, MMP, and AAT mRNA levels were extracted from filtered transcriptomic data.

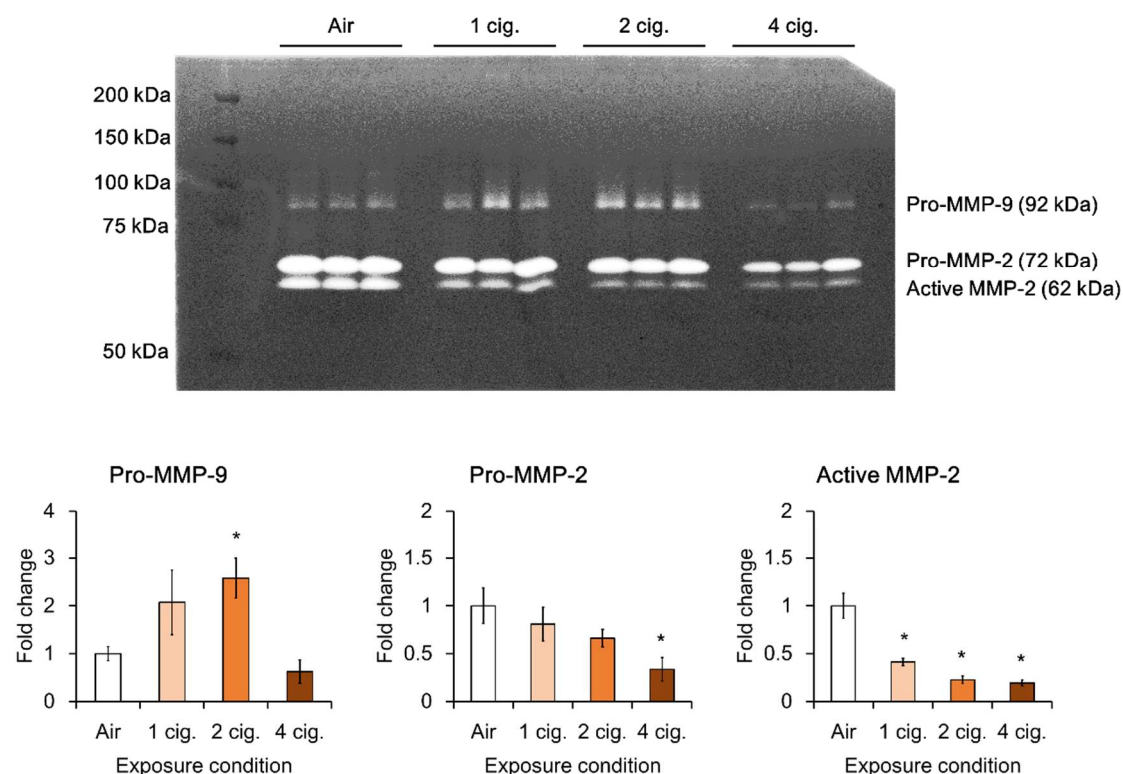


Figure 6.11 Gelatin zymography of culture medium samples collected on culture day 21.

The results represent fold changes relative to the control, and the means and standard deviation of three tissue cultures. *Significantly different from the air-exposed controls ($p < 0.05$, Student's t -test). MMP, matrix metalloproteinase.

6.4 Discussion

Omics data (i.e., transcriptomic, proteomic, and metabolomic data) and their analysis with bioinformatics enabled detection of global changes in the 3D bronchial tissue model at the molecular level. In this chapter, the 3D bronchial tissue model was subjected to multi-omics analysis to provide deeper insight into the mechanisms of CS toxicological effects.

The 3D bronchial tissue model was subjected to two weeks of repeated whole CS exposure, which reproduced an exposure dose similar to the actual human daily tissue dose, as described in Chapter 4 (Section 4.4 Discussion). As observed in the previous chapter, IL-1 β secretion increased during the exposure period, but a greater decrease in

secretion on ALI culture day 21 occurred following a four-cigarette exposure than a two-cigarette exposure (Figure 6.2a). Similar results were confirmed in other analyses, with the levels of GSH, GSSG, and several mucins and MMPs showing decrease between the two- and four-cigarette exposures (Table 6.1 and Figure 6.10a). These results indicate that continual inflammation and oxidative stress responses are induced after the repeated one- and two-cigarette exposures in the 3D bronchial tissues, but because of severe stress these responses decrease following four-cigarette exposure.

The results of the cytokine measurement indicated that the 3D bronchial tissues were in chronic inflammatory state, and therefore tissue samples collected on ALI culture day 21 were used for omics analysis to find out the biological processes significantly altered after repeated whole CS exposure. Firstly, the analysis focused on perturbations in central carbon metabolic pathways, and revealed disruption in the pathways related to energy production such as glycolysis and the TCA cycle after repeated whole CS exposure, whereas the PPP appeared to be upregulated, except for after repeated four-cigarette exposure (Figure 6.5). In addition to the analysis of metabolomic data, transcriptomic analysis showed that various genes, involved in glycolysis and the TCA cycle, were downregulated, and several genes such as *G6PD*, *TKT*, and *TALDO1* involved in the PPP were upregulated (Figure 6.6). As those genes are reported to be regulated by Nrf2²³, which was activated under oxidative stress, repeated whole CS exposure may have induced oxidative stress in the 3D bronchial tissues. Significant perturbation in the “Nrf2-mediated Oxidative Stress Response” pathway suggested from transcriptomic analysis support this hypothesis (Figure 6.8c). However, some metabolites involved in the PPP showed decrease after the repeated four-cigarette exposure, whereas some genes involved in the PPP showed dose-dependent increase (Figures 6.5a, 6.6, and 6.7). This inconsistent result can be explained by impaired protein synthesis in severely damaged tissues²⁴, and increased cytotoxicity and epithelium thinning were observed after the repeated four-cigarette exposure (Figures 6.3 and 6.4). These results suggest that repeated whole CS exposure upregulated the PPP and downregulated the TCA cycle and glycolysis, and that these homeostatic pathways are disrupted under severe stress regardless of the expression levels of corresponding genes.

An upregulation in the PPP would promote NADPH generation, which is necessary to regenerate GSH from GSSG²⁵. This suggests that the 3D bronchial tissues are under chronic oxidative stress by repeated whole CS exposure, and GSH is required continuously to eliminate oxidants. This hypothesis is supported by perturbation of amino acid metabolism, and Cys and Glu—the precursors of GSH—were upregulated (Table 6.1)²⁶. Upregulation of GSH was also observed in the 3D bronchial tissues after the repeated one- or two-cigarette exposure, but repeated four-cigarette exposure resulted in a decrease in GSH (Table 6.1), which implies that the 3D bronchial tissues could not generate the GSH because of severe damage and oxidative stress. These results indicate that the 3D bronchial tissues subjected to repeated whole CS exposure attempt to normalize the intracellular environment by reducing GSSG and producing GSH to eliminate the oxidants prior to energy production.

The next study was focused on analysis of transcriptomic data to identify significantly perturbed biological processes other than central carbon metabolism. The signaling pathways related to NFκB, AhR, and xenobiotic metabolism were identified to be significantly perturbed by canonical pathway analysis (Figure 6.8c). NFκB signaling is shown to be activated by polycyclic aromatic hydrocarbons²⁷, as is activation of the AhR signaling pathway^{28, 29}. While these signaling pathways were significantly perturbed under all exposure conditions, analysis on cellular functions revealed that apoptosis and cell death signaling were significantly perturbed after repeated four-cigarette exposure (Figure 6.8d). These results support the hypothesis that the cells were under severe damage and their cellular functions were disrupted by repeated four-cigarette exposure. The results of transcriptomic analysis revealed that the pathways affected in the 3D bronchial tissues were the pathways reported to be perturbed by CS constituents.

EGFR was identified as a common upstream regulator controlling the metabolomic and transcriptomic changes observed in the 3D bronchial tissues after repeated whole CS exposure (Tables 6.2 and 6.3). EGFR is reported to contribute to early-stage development of inflammatory lung diseases through its effects on mucus hypersecretion and increases in the number of goblet cell³⁰. Previous study reported that activation of EGFR led to decreased lung function, and this was initiated by reactive oxygen species³¹. As

perturbation of biological processes and activation of their potential regulator (EGFR) could result in decreased lung function, analysis was performed on the levels of mucins and MMPs, which are potential biomarkers of inflammatory lung diseases. The ASL levels of several mucins and MMPs were increased in the 3D bronchial tissues by exposure to one and two cigarettes (Figure 6.10). The increased levels of mucins indicated that mucus hypersecretion was caused by repeated whole CS exposure. Mucus hypersecretion is one of the hallmark symptoms of chronic bronchitis in COPD, which is considered to be derived from abnormal differentiation of bronchial epithelial cells^{32, 33}. In particular, mucin 5AC is a major mucus protein in asthma and COPD, and is reported to be regulated by the Sp1 transcription factor³⁴, concomitant with activation of the EGFR signaling pathway³⁵. Moreover, activation of the EGFR signaling promote secretion of various MMPs such as MMP-1 and MMP-9³⁶. These gelatinolytic/collagenolytic enzymes are reported to be associated with airflow obstruction in COPD through remodeling, and their relationship to smoking has been pointed out³⁷⁻³⁹. By contrast, the levels of mucin 5B showed substantial dose-dependent decrease. Previous study reported that mucin 5B is essential for airway defense such as mucociliary clearance and for maintenance of airway homeostasis, and that a deficiency in mucin 5B is reported to cause severe airway obstruction in mice⁴⁰. A dose-dependent decrease was also found in AAT (Figure 6.10), a serine protease inhibitor that can be inactivated through oxidation of its active site by oxidants such as CS⁴¹. The imbalance in AAT–neutrophil elastase leads to a breakdown of elastin and loss of elasticity in the lungs, resulting in emphysema in COPD⁴². The results of ALS proteomic analysis suggested that repeated whole CS exposure promote secretion of potential biomarkers of COPD.

6.5 Conclusions

Overall, the multi-omics analysis suggested that repeated whole CS exposure induced oxidative stress and led to disruption in central carbon metabolism and alterations in the expression profiles of genes governed by EGFR activation. Moreover, the 3D bronchial tissues secreted known biomarkers (Mucins and MMPs) of COPD^{33, 38}, suggesting that

the 3D bronchial tissue model can exhibit disease symptoms specific for COPD. The multi-omics approach is useful to understand the mechanisms of action of CS, and can also be leveraged in investigating the mechanisms of action of other toxic airborne materials.

6.6 References

1. D'Anna, C. *et al.* Cigarette smoke alters the proteomic profile of lung fibroblasts. *Mol Biosyst* **11**, 1644-1652 (2015).
2. Gonzalez-Suarez, I. *et al.* Systems biology approach for evaluating the biological impact of environmental toxicants in vitro. *Chem Res Toxicol* **27**, 367-376 (2014).
3. Titz, B. *et al.* Proteomics for systems toxicology. *Comput Struct Biotechnol J* **11**, 73-90 (2014).
4. Vulimiri, S.V., Misra, M., Hamm, J.T., Mitchell, M. & Berger, A. Effects of mainstream cigarette smoke on the global metabolome of human lung epithelial cells. *Chem Res Toxicol* **22**, 492-503 (2009).
5. Aardema, M.J. & MacGregor, J.T. Toxicology and genetic toxicology in the new era of "toxicogenomics": impact of "-omics" technologies. *Mutat Res* **499**, 13-25 (2002).
6. Robertson, D.G. Metabonomics in toxicology: a review. *Toxicol Sci* **85**, 809-822 (2005).
7. Waters, M.D. & Fostel, J.M. Toxicogenomics and systems toxicology: aims and prospects. *Nat Rev Genet* **5**, 936-948 (2004).
8. Heijne, W.H., Kienhuis, A.S., van Ommen, B., Stierum, R.H. & Groten, J.P. Systems toxicology: applications of toxicogenomics, transcriptomics, proteomics and metabolomics in toxicology. *Expert Rev Proteomics* **2**, 767-780 (2005).
9. Donaldson, K. *et al.* Combustion-derived nanoparticles: a review of their toxicology following inhalation exposure. *Part Fibre Toxicol* **2**, 10 (2005).
10. Ben-Ari Fuchs, S. *et al.* GeneAnalytics: An Integrative Gene Set Analysis Tool for Next Generation Sequencing, RNAseq and Microarray Data. *Omics* **20**, 139-151 (2016).
11. Cirillo, E., Parnell, L.D. & Evelo, C.T. A Review of Pathway-Based Analysis Tools That Visualize Genetic Variants. *Front Genet* **8**, 174 (2017).
12. Kramer, A., Green, J., Pollard, J., Jr. & Tugendreich, S. Causal analysis approaches in Ingenuity Pathway Analysis. *Bioinformatics* **30**, 523-530 (2014).
13. Corvi, R. *et al.* Meeting report: Validation of toxicogenomics-based test systems: ECVAM-ICCVAM/NICEATM considerations for regulatory use. *Environ Health Perspect* **114**, 420-429 (2006).
14. Hotamisligil, G.S. Inflammation and metabolic disorders. *Nature* **444**, 860-867 (2006).

15. Slebos, D.J. *et al.* Mitochondrial localization and function of heme oxygenase-1 in cigarette smoke-induced cell death. *Am J Respir Cell Mol Biol* **36**, 409-417 (2007).
16. van der Toorn, M. *et al.* Cigarette smoke-induced blockade of the mitochondrial respiratory chain switches lung epithelial cell apoptosis into necrosis. *Am J Physiol Lung Cell Mol Physiol* **292**, L1211-1218 (2007).
17. Candiano, G. *et al.* Proteomic analysis of the airway surface liquid: modulation by proinflammatory cytokines. *Am J Physiol Lung Cell Mol Physiol* **292**, L185-198 (2007).
18. Voynow, J.A., Gendler, S.J. & Rose, M.C. Regulation of mucin genes in chronic inflammatory airway diseases. *Am J Respir Cell Mol Biol* **34**, 661-665 (2006).
19. Benjamini, Y. & Hochberg, Y. Controlling the False Discovery Rate: A Practical and Powerful Approach to Multiple Testing *Journal of the Royal Statistical Society. Series B (Methodological)* **57**, 289-300 (1995).
20. Smyth, G.K. Linear models and empirical bayes methods for assessing differential expression in microarray experiments. *Stat Appl Genet Mol Biol* **3**, Article3 (2004).
21. Eriksson, S. Pulmonary Emphysema and Alpha1-Antitrypsin Deficiency. *Acta Med Scand* **175**, 197-205 (1964).
22. Eden, E. Asthma and COPD in alpha-1 antitrypsin deficiency. Evidence for the Dutch hypothesis. *COPD* **7**, 366-374 (2010).
23. Mitsuishi, Y. *et al.* Nrf2 redirects glucose and glutamine into anabolic pathways in metabolic reprogramming. *Cancer Cell* **22**, 66-79 (2012).
24. Shenton, D. & Grant, C.M. Protein S-thiolation targets glycolysis and protein synthesis in response to oxidative stress in the yeast *Saccharomyces cerevisiae*. *Biochem J* **374**, 513-519 (2003).
25. Stincone, A. *et al.* The return of metabolism: biochemistry and physiology of the pentose phosphate pathway. *Biol Rev Camb Philos Soc* **90**, 927-963 (2015).
26. Yang, M. & Vousden, K.H. Serine and one-carbon metabolism in cancer. *Nat Rev Cancer* **16**, 650-662 (2016).
27. Ji, K. *et al.* Benzo[a]pyrene induces oxidative stress and endothelial progenitor cell dysfunction via the activation of the NF-kappaB pathway. *Int J Mol Med* **31**, 922-930 (2013).
28. Hussain, T. *et al.* Induction of CYP1A1, CYP1A2, CYP1B1, increased oxidative stress and inflammation in the lung and liver tissues of rats exposed to incense smoke. *Mol Cell Biochem* **391**, 127-136 (2014).
29. Kasai, A. *et al.* High levels of dioxin-like potential in cigarette smoke evidenced by in vitro and in vivo biosensing. *Cancer Res* **66**, 7143-7150 (2006).
30. Burgel, P.R. & Nadel, J.A. Epidermal growth factor receptor-mediated innate immune responses and their roles in airway diseases. *Eur Respir J* **32**, 1068-1081 (2008).

31. Luettich, K. *et al.* The adverse outcome pathway for oxidative stress-mediated EGFR activation leading to decreased lung function. *Applied In Vitro Toxicology* **3**, 99-109 (2017).
32. Vignola, A.M. *et al.* Transforming growth factor-beta expression in mucosal biopsies in asthma and chronic bronchitis. *Am J Respir Crit Care Med* **156**, 591-599 (1997).
33. Kesimer, M. *et al.* Airway Mucin Concentration as a Marker of Chronic Bronchitis. *N Engl J Med* **377**, 911-922 (2017).
34. Di, Y.P., Zhao, J. & Harper, R. Cigarette smoke induces MUC5AC protein expression through the activation of Sp1. *J Biol Chem* **287**, 27948-27958 (2012).
35. Lee, Y.C. *et al.* 2,3,7,8-Tetrachlorodibenzo-p-dioxin-induced MUC5AC expression: aryl hydrocarbon receptor-independent/EGFR/ERK/p38-dependent SP1-based transcription. *Am J Respir Cell Mol Biol* **45**, 270-276 (2011).
36. Homma, T. *et al.* Involvement of Toll-like receptor 2 and epidermal growth factor receptor signaling in epithelial expression of airway remodeling factors. *Am J Respir Cell Mol Biol* **52**, 471-481 (2015).
37. Geraghty, P., Dabo, A.J. & D'Armiento, J. TLR4 protein contributes to cigarette smoke-induced matrix metalloproteinase-1 (MMP-1) expression in chronic obstructive pulmonary disease. *J Biol Chem* **286**, 30211-30218 (2011).
38. Culpitt, S.V., Rogers, D.F., Traves, S.L., Barnes, P.J. & Donnelly, L.E. Sputum matrix metalloproteinases: comparison between chronic obstructive pulmonary disease and asthma. *Respir Med* **99**, 703-710 (2005).
39. Kang, M.J. *et al.* Lung matrix metalloproteinase-9 correlates with cigarette smoking and obstruction of airflow. *J Korean Med Sci* **18**, 821-827 (2003).
40. Roy, M.G. *et al.* Muc5b is required for airway defence. *Nature* **505**, 412-416 (2014).
41. Hubbard, R.C. *et al.* Oxidants spontaneously released by alveolar macrophages of cigarette smokers can inactivate the active site of alpha 1-antitrypsin, rendering it ineffective as an inhibitor of neutrophil elastase. *J Clin Invest* **80**, 1289-1295 (1987).
42. Abboud, R.T. & Vimalanathan, S. Pathogenesis of COPD. Part I. The role of protease-antiprotease imbalance in emphysema. *Int J Tuberc Lung Dis* **12**, 361-367 (2008).

Chapter 7.

General conclusions and perspectives

7.1 Achievements of the research

The series of experiments presented in this thesis were performed to develop human-relevant *in vitro* test methods for inhalation toxicology of CS. For this purpose, a whole CS exposure system was used to improve human relevance of the exposure method, and a 3D culture model of human bronchial tissue was used to improve human relevance of the culture model used for exposure.

In the experiments described in Chapter 2, the whole CS exposure system was applied to the Ames reverse mutation assay. The mutagenic potentials of various cigarettes were successfully detected and compared using the slopes of dose–response curves of test cigarettes. The low genotoxicity observed in the HC was in line with the results obtained in the *in vivo* experiments. These experiments revealed that the toxicity of CS can be detected by the *in vitro* test system while maintaining its complex aerosol properties using the whole CS exposure system.

Because the utility of the whole CS exposure system was confirmed, the system was then used to develop test methods that could detect tissue/organ-level responses such as those observed in patients with smoking-related lung disease. For this purpose, a 3D model of human bronchial tissue was developed in Chapter 3. This model contained both HBECs and fibroblasts in the collagen matrix layer, and presented the fibrotic phenotype related to lung diseases upon stimulation with TGF- β 1.

The experiments presented in Chapter 4 were performed to establish whole CS exposure conditions for the 3D bronchial tissue model, which provided a CS exposure dose similar to the actual human tissue dose. Deposition of solanesol and acetaldehyde on the culture surface of the 3D bronchial tissue model and the surfaces of the bronchial region of smokers were investigated. A comparison of *in vitro* and *in vivo* dosimetry data was used to establish whole CS exposure conditions that enabled exposure of the 3D bronchial tissue model to the *in vivo* daily tissue dose. The established conditions were used for whole CS exposure of the 3D bronchial tissue model, as described in Chapters 5 and 6.

In Chapter 5, repeated whole CS exposure was performed for 2 weeks with the *in vivo* daily tissue dose, and the effects of whole CS exposure on differentiation and the inflammatory status of the tissue were analyzed. The 3D bronchial tissue model represented a COPD-related tissue phenotype with a decrease in cilia and attenuation of goblet cell differentiation^{1,2}. Moreover, secretion of several cytokines was increased with exposure repetition.

The results obtained in Chapter 5 indicated that the tissue was under disease-related conditions. Therefore, the tissue conditions were investigated further by omics technologies in Chapter 6. Omics technologies revealed that pathways related to inflammation, oxidative stress, and xenobiotic metabolism were perturbed in the tissues following repeated whole CS exposure. Increased mucus secretion was observed by ASL proteomic analysis, indicating that disruption of tissue function occurred after repeated whole CS exposure. The mucus hypersecretion observed in the 3D bronchial tissue model is a major phenotype of COPD patients and leads to over-production of sputum³.

In the experiments presented in this thesis, the 3D bronchial tissue model was exposed to whole CS and then various endpoints were analyzed. As reported previously, airway remodeling is a major aspect of COPD, and various changes are induced in the bronchial epithelial tissue of COPD patients following lifetime chronic exposure to CS (Figure 7.1). Interestingly, various results related to these events were obtained with the 3D bronchial tissue model following 2 weeks of repeated whole CS exposure at a human-relevant daily tissue dose (Table 7.1). Although several events (e.g., loss of junctions, EMT, altered ECM, and airway fibrosis) were not observed after whole CS exposure, these changes were clearly induced by TGF- β 1 stimulation (Table 7.1). Therefore, the 3D bronchial tissue model is appropriate to detect the effects of CS exposure on COPD development. Thus, the 3D bronchial tissue model may be an appropriate alternative to animal experimentation for inhalation toxicology of CS.

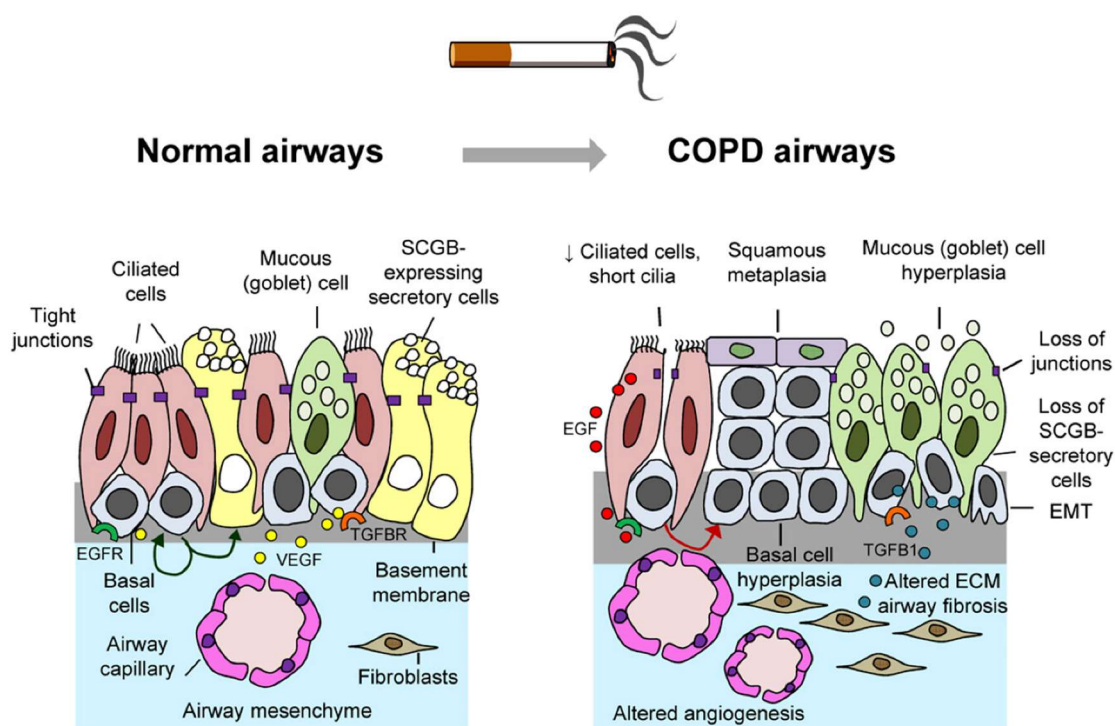


Figure 7.1 Smoking-induced airway epithelial remodeling in COPD patients.

This diagram is reproduced from the literature ⁴. COPD, chronic obstructive pulmonary disease; ECM, extracellular matrix; EGF, epidermal growth factor; EMT, epithelial mesenchymal transition; SCGB, secretoglobulin; TGF, transforming growth factor; VEGF, vascular endothelial growth factor.

Table 7.1 COPD-related changes observed in the 3D bronchial tissue model in this thesis.

Airway remodeling in COPD	The results obtained with 3D bronchial tissue model		
	Exposure	Observations	
Loss of ciliated cells, short cilia	Whole CS	Decrease of acetylated α -tubulin-positive cells	(Figure 5.4)
	Whole CS	Decreased expression of <i>FOXJ1</i>	(Figure 5.6a)
Mucous (goblet) cell hyperplasia	Whole CS	Attenuation of goblet cell differentiation	(Figure 5.4)
	Whole CS	Increased expression of <i>MUC5AC</i>	(Figure 5.6b)
	Whole CS	Increased secretion of several mucins in airway surface liquid	(Figure 6.10a)
	IL-13	Increase of mucin 5AC-positive large goblet cells	(Figure 5.5)
Loss of SCGB-secretory cells	Whole CS	Decreased expression of <i>SCGB1A1</i>	(Figure 5.6b)
EGF	Whole CS	Upstream regulator of metabolomic changes	(Table 6.2)
	Whole CS	Upstream regulator of transcriptomic changes	(Table 6.3)
Loss of junction	TGF- β	Decreased expression of E-cadherin in the epithelial layer	(Figure 3.5 and 3.6a)
EMT	TGF- β	Increased expression of vimentin in the epithelial layer	(Figure 3.5 and 3.6b)
Altered ECM airway fibrosis	TGF- β	Various changes related to ECM homeostasis	(Figure 3.13)

COPD, chronic obstructive pulmonary disease; CS, cigarette smoke; ECM, extracellular matrix; EGF, epidermal growth factor; EMT, epithelial mesenchymal transition; IL, interleukin; SCGB, secretoglobin; TGF, transforming growth factor

7.2 Limitations of the research

To detect tissue/organ-level responses that are observed in an actual smoker, the traditional *in vitro* test system was improved from the view-points of human relevance in the CS exposure and cell culture methods. Although this strategy successfully reproduced various COPD-related events (Table 7.1), the typical histological changes observed in the bronchial epithelium of COPD patients were not observed, i.e., squamous metaplasia and basal cell hyperplasia (Figure 7.1). These histological changes in airway remodeling are the main contributors to airway obstruction in COPD patients. In addition to squamous metaplasia and basal cell hyperplasia, an increase of mucus-producing goblet cells (goblet cell hyperplasia) is a major histological change in COPD. While goblet cell numbers and mucus secretion were increased after whole CS exposure in this study (Figure 6.10), the observed tissue histology (Figure 5.4) was different from the typical tissue histology observed in goblet cell hyperplasia induced by IL-13 (Figure 5.5). Thus, the *in vitro* tissue

model and exposure methods used herein were insufficient for reproducing COPD-related histological changes (e.g., squamous metaplasia, basal cell hyperplasia, and goblet cell hyperplasia). This insufficient reproduction of the COPD phenotype indicated that the *in vitro* model used in this thesis was missing some of the key mechanisms that drive COPD development. Therefore, the *in vitro* tissue model and exposure methods must be further improved to detect the COPD phenotype as described below in 7.2.1 to 7.2.3.

These activities will help clarify the key mechanisms underlying COPD development; these mechanisms remain unclear because COPD is a complex disease with a multifactorial background based on interaction between environmental and genetic factors ⁵. In addition to smoking, for example, occupational exposures (e.g., dusts, gases, and fumes) and several genetic syndromes (e.g., AAT deficiency) are implicated as causes of COPD ⁵. Moreover, genetic polymorphisms of *CYP*, *MMP*, and *NRF2* are reported to be risk factor for COPD ⁶⁻⁸. The proteins encoded by these genes play important roles in metabolic, inflammatory, and oxidative stress responses in smokers. Because oxidative stress is one of the key responses which contribute to the pathogenesis of COPD, a diet high in antioxidants (e.g., vitamin C, vitamin E, and carotenoids) could be protective for this disease ⁵. The establishment of *in vitro* COPD model will be useful to provide mechanistic evidence to support these clinical and epidemiological findings.

7.2.1 Composition of 3D cell culture

The 3D bronchial tissue model used in this thesis was developed by co-culturing epithelial cells (HBECs) and mesenchymal cells (fibroblasts). However, there are several other components in actual human bronchial tissue, including endothelial cells, smooth muscle cells, and chondrocytes (Figure 3.2). Therefore, applying other types of cells to the 3D bronchial tissue model may improve the human relevance of the model. However, the introduction of immune cells, such as neutrophils and macrophages, is the first priority because they are critically involved in the development of COPD ^{9,10}. These immune cells secrete various inflammatory mediators in response to CS, which reportedly affect

epithelial and mesenchymal cells and induce development of inflammatory lung diseases¹¹. In the present research, goblet cell hyperplasia and subepithelial fibrosis, which are major phenotypes observed in COPD patients, were clearly detected after IL-13 (Figure 5.5) and TGF- β 1 (Figure 3.13) stimulations, respectively. Because immune cells are the source of these mediators, they might play important roles in the induction of the histological changes observed in COPD.

7.2.2 Whole CS exposure dose

The whole CS exposure conditions used in this thesis were established to produce an exposure dose comparable with the actual human daily tissue dose in bronchi as described in Chapter 4. When whole CS from one to four cigarettes diluted with a 1 L/min flow rate was exposed to cells in the RFS module in approximately 10 min, the exposure dose was similar to the total daily tissue dose in the bronchial epithelium of a smoker who smokes 10–40 cigarettes (the range of cigarettes smoked per day in most countries). This exposure condition was used in Chapters 5 and 6 to investigate CS exposure effects on the 3D bronchial tissue model. However, this condition was rather intense compared with the actual human condition because smokers do not consume 10–40 cigarettes in 10 min. Therefore, to improve the conditions, whole CS exposure should be performed with a higher dilution flow rate (e.g., 8 L/min), and the 3D bronchial tissue should be exposed to whole CS in a pattern that reflects the actual exposure in smokers (e.g., spreading the 20-cigarettes exposure out to one cigarette every 30 min for 10 h). Several studies have shown the importance of low-dose chronic exposure to investigate the chronic toxicities of chemicals¹²⁻¹⁴. Therefore, multiple exposures to whole CS per day may be a useful approach to detect low-dose chronic exposure effects of CS.

7.2.3 Whole CS exposure duration

Another point that should be investigated further for the whole CS exposure condition is the exposure duration for repeated exposure. To study the chronic toxicity of CS, repeated exposure of the 3D bronchial tissue model to whole CS was performed for 2 weeks in Chapters 5 and 6. However, there is no consensus on the exposure duration that is sufficient to represent a chronic exposure effect *in vitro*. In some *in vivo* experiments, an exposure duration longer than 10% of the animals' lifespan is considered as chronic exposure¹⁵. However, this guideline cannot be applied to *in vitro* whole CS exposure experiments because it is difficult to establish the lifespan of *in vitro* tissue. In Chapters 5 and 6, repeated exposure for 2 weeks increased inflammation, perturbation of several pathways, and mucus hypersecretion in the 3D bronchial tissue culture. These events were frequently observed in COPD patients^{3, 16-18}. Thus, the chronic exposure effect was somewhat reproduced by this exposure duration. However, other disease-related phenotypes (e.g., squamous metaplasia, basal cell hyperplasia, and goblet cell hyperplasia in COPD) were not induced in the 3D bronchial tissue by this exposure duration. Therefore, longer whole CS exposure might be necessary to induce these changes in the 3D bronchial tissue culture.

7.3 Future perspectives

As described above, further improvement of human relevance of the test methods used in this thesis may be necessary to detect tissue phenotypes observed in smoking-related lung disease. For this purpose, as an example, immune cells should be incorporated into the 3D bronchial tissue model and whole CS exposure should be performed for a longer duration. Investigating the factors that contribute to inducing the COPD phenotype (e.g., cell culture composition, exposure dose, and exposure duration) will clarify the mechanisms behind the COPD pathogenesis. In this study, a co-culture model of human bronchial tissue was used as a 3D culture model (Figure 3.1c) because reproducing EMTU *in vitro* is considered important in the COPD pathogenesis. However, a mono-

culture model of HBECs and lung fibroblasts should be added to future experiments (Figure S.2 in Supplementary information). Investigating differences in the response to whole CS exposure among these three culture models will further clarify the effect of co-culturing. GVP and PP exposure should also be examined in future studies. Investigating differences in the cellular response among these three exposure methods will clarify which fraction of the whole CS contributes to COPD development¹⁹. This approach may help clarify whether a specific chemical or particle size contributes to COPD development^{20, 21}. Because CS is complex mixture of various chemicals, and human bronchial tissue is a complex mixture of various cell types, the factors contributing to COPD development *in vitro* should be investigated relative to the cell composition of the 3D culture model and the chemical composition of whole CS.

In line with these activities, the development of 3D tissue models of other human respiratory regions will be necessary. In the experiments presented in this thesis, a 3D model of human bronchial tissue was developed and subjected to whole CS exposure. However, the human lung is composed of not only a bronchial region, but also an alveolar region (Figure 1.8). Because the destruction of alveolar walls is a major phenotype related to COPD (Figure 1.4), the development of a 3D culture model of alveolar tissue and its application to the whole CS exposure system is necessary to understand CS toxicity in the whole human lung. Establishing a 3D culture model of alveolar tissue is difficult because no gold standard protocol exists for isolating alveolar epithelial cells. Moreover, primary alveolar epithelial cells have a low capacity to proliferate, and obtaining enough cells for 3D culturing is difficult. Because of these difficulties, developing a 3D culture model of human bronchial tissue was prioritized instead. However, a recent study revealed that alveolar organoid models can be developed from induced pluripotent stem cells²². The culture conditions used in these studies will help develop 3D culture models of human alveolar tissue under ALI culture conditions. Moreover, although the primary target organ for inhalation toxicity of CS is the lung, CS also has toxicity in other organs. Therefore, both the development of *in vitro* 3D bronchial and alveolar tissue models to detect local toxicity of CS in the human lung as well as *in vitro* models to detect systemic toxicity in the human body will be necessary. For this purpose, microphysiological

systems will be useful tools to connect 3D lung models with other available *in vitro* organ models to detect of CS toxicity in the whole human body.

The *in vitro* model developed to detect of inhalation toxicity of CS can also be used to detect of inhalation toxicity of other airborne materials. Because the repeated exposure effects of CS were detected in this study, the developed *in vitro* model has the potential to detect the chronic inhalation toxicities of various chemicals *in vitro*. For both inhalation toxicity testing and other toxicity testing, there is no validated *in vitro* test method to detect the chronic toxicities of target chemicals. Development of an *in vitro* chronic inhalation test would have a significant effect, because chronic *in vivo* testing is more expensive and time-consuming than acute testing. More importantly, the burden on the animals in chronic exposure testing is higher than that in acute exposure testing. Therefore, a future objective will be the application of the developed *in vitro* test methods to detect the toxicity of various airborne materials in addition to CS. The use of nanomaterials, such as carbon nanotubes, is increasing, and the chronic inhalation toxicity of these nanomaterials remains uncertain. In addition to nanomaterials, chronic inhalation toxicity of various aerosols derived from human activities (e.g., PM_{2.5} and diesel exhaust) are of great interest. Development of an appropriate *in vitro* human model for studying inhalation toxicology will provide hazard and risk information for aerosol chemicals without requiring animal testing.

7.4 References

1. Aufderheide, M., Scheffler, S., Ito, S., Ishikawa, S. & Emura, M. Ciliotoxicity in human primary bronchiolar epithelial cells after repeated exposure at the air-liquid interface with native mainstream smoke of K3R4F cigarettes with and without charcoal filter. *Exp Toxicol Pathol* **67**, 407-411 (2015).
2. Schamberger, A.C., Staab-Weijnitz, C.A., Mise-Racek, N. & Eickelberg, O. Cigarette smoke alters primary human bronchial epithelial cell differentiation at the air-liquid interface. *Sci Rep* **5**, 8163 (2015).
3. Prescott, E., Lange, P. & Vestbo, J. Chronic mucus hypersecretion in COPD and death from pulmonary infection. *Eur Respir J* **8**, 1333-1338 (1995).

4. Shaykhiev, R. & Crystal, R.G. Early events in the pathogenesis of chronic obstructive pulmonary disease. Smoking-induced reprogramming of airway epithelial basal progenitor cells. *Ann Am Thorac Soc* **11 Suppl 5**, S252-258 (2014).
5. Eisner, M.D. *et al.* An official American Thoracic Society public policy statement: Novel risk factors and the global burden of chronic obstructive pulmonary disease. *Am J Respir Crit Care Med* **182**, 693-718 (2010).
6. Cheng, S.L., Yu, C.J. & Yang, P.C. Genetic polymorphisms of cytochrome p450 and matrix metalloproteinase in chronic obstructive pulmonary disease. *Biochem Genet* **47**, 591-601 (2009).
7. Vibhuti, A. *et al.* CYP1A1, CYP1A2 and CYBA gene polymorphisms associated with oxidative stress in COPD. *Clin Chim Acta* **411**, 474-480 (2010).
8. Yamamoto, T. *et al.* Identification of polymorphisms in the promoter region of the human NRF2 gene. *Biochem Biophys Res Commun* **321**, 72-79 (2004).
9. Barnes, P.J. Alveolar macrophages as orchestrators of COPD. *Copd* **1**, 59-70 (2004).
10. O'Donnell, R., Breen, D., Wilson, S. & Djukanovic, R. Inflammatory cells in the airways in COPD. *Thorax* **61**, 448-454 (2006).
11. Holtzman, M.J. Asthma as a chronic disease of the innate and adaptive immune systems responding to viruses and allergens. *J Clin Invest* **122**, 2741-2748 (2012).
12. Kim, S.A., Lee, Y.M., Choi, J.Y., Jacobs, D.R., Jr. & Lee, D.H. Evolutionarily adapted hormesis-inducing stressors can be a practical solution to mitigate harmful effects of chronic exposure to low dose chemical mixtures. *Environ Pollut* **233**, 725-734 (2018).
13. Rizzetti, D.A. *et al.* Ameliorative effects of egg white hydrolysate on recognition memory impairments associated with chronic exposure to low mercury concentration. *Neurochem Int* **101**, 30-37 (2016).
14. Satarug, S. & Moore, M.R. Adverse health effects of chronic exposure to low-level cadmium in foodstuffs and cigarette smoke. *Environ Health Perspect* **112**, 1099-1103 (2004).
15. Arts, J.H. *et al.* Inhalation toxicity studies: OECD guidelines in relation to REACH and scientific developments. *Exp Toxicol Pathol* **60**, 125-133 (2008).
16. Fischer, B.M., Pavlisko, E. & Voynow, J.A. Pathogenic triad in COPD: oxidative stress, protease-antiprotease imbalance, and inflammation. *Int J Chron Obstruct Pulmon Dis* **6**, 413-421 (2011).
17. Hessel, J. *et al.* Intraflagellar transport gene expression associated with short cilia in smoking and COPD. *PLoS One* **9**, e85453 (2014).
18. Saetta, M. Airway inflammation in chronic obstructive pulmonary disease. *Am J Respir Crit Care Med* **160**, S17-20 (1999).
19. Adamson, J., Haswell, L.E., Phillips, G. & Gaça, M.D. In vitro models of chronic obstructive pulmonary disease (COPD). *Bronchitis* **41**, 66 (2011).

20. Mesquita, S.R. *et al.* Toxic assessment of urban atmospheric particle-bound PAHs: relevance of composition and particle size in Barcelona (Spain). *Environ Pollut* **184**, 555-562 (2014).
21. Zhou, G. *et al.* Chemical constituents of tobacco smoke induce the production of interleukin-8 in human bronchial epithelium, 16HBE cells. *Tob Induc Dis* **14**, 24 (2016).
22. Yamamoto, Y. *et al.* Long-term expansion of alveolar stem cells derived from human iPS cells in organoids. *Nat Methods* **14**, 1097-1106 (2017).

Supplementary information

Establishment of co-culture conditions for 3D bronchial tissue models

A 3D culture model of human bronchial tissue was developed using lung fibroblasts (IMR-90) and normal HBECs. The cell culture conditions for this 3D bronchial tissue model were established in several preliminary studies using various lung epithelial cell lines (H292, Calu-3, A549, LC-AI, and BEAS-2B) in addition to HBECs. H292, Calu-3, A549, and LC-AI cells were derived from lung cancer patients. BEAS-2B cells were immortalized HBECs. These cell lines were co-cultured with IMR-90 and ALI cultured with Airway Epithelial Cell Growth Medium. After 21 days of ALI culturing, hematoxylin and eosin staining was performed for histological analysis (Figure S.1). Lung cell lines derived from cancer patients showed abnormal epithelial cell growth and thick epithelium over the mesenchymal layer (H292, A549, and LC-AI; Figure S.1). Abnormally growing epithelial cells migrated into the mesenchymal layer in the LC-AI cells (arrowheads in Figure S.1). In contrast to the other cell lines derived from cancer patients, Calu-3 cells showed no abnormal epithelial growth (Figure S.1). Although BEAS-2B cells were derived from normal HBECs, the BEAS-2B cells showed abnormal epithelial growth and a metastatic phenotype similar to the cancer cell lines (Figure S.1). Thus, these lung cell lines were not suitable for developing a 3D culture model of human bronchial tissue with a well-differentiated normal bronchial epithelium.

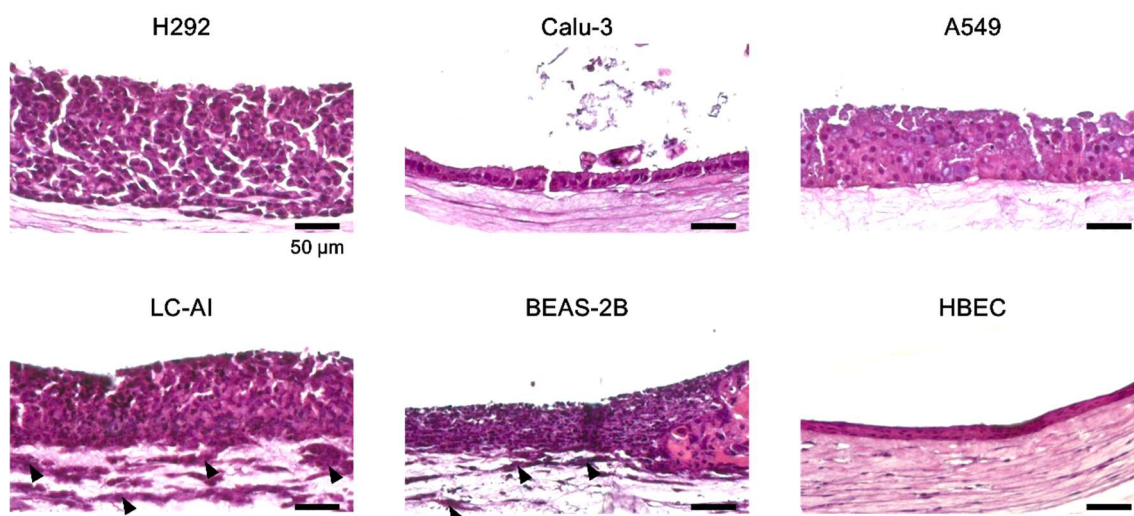


Figure S.1 Histological analysis of the bronchial tissue model developed from lung cell lines.

Arrowheads indicate epithelial cells migrating into the mesenchymal layer (metastatic phenotype).

In contrast to most of the lung cell lines, HBECs (passage number six) showed no abnormal growth (Figure S.1). However, mucociliary differentiation was unconfirmed under the culture conditions in the preliminary study (i.e., ALI culture with Airway Epithelial Cell Growth Medium). As summarized in a previous paper, the use of early passaged cells and well-characterized ALI culture medium were crucial to obtaining well-differentiated bronchial epithelium *in vitro*^{1,2}. Therefore, HBECs (passage number three) were cultivated with PneumaCult ALI medium in the present study. The developed 3D culture model of human bronchial tissue showed mucociliary differentiation (Figure 3.3). Several suppliers provide HBECs: Lonza, PromoCell, and ScienCell Research Laboratories (Carlsbad, CA, USA). In this study, HBECs were purchased from Lonza because Lonza confirmed mucociliary differentiation capacity of their HBECs under ALI culture conditions prior to distribution.

Establishment of a mono-culture model of 3D bronchial epithelium

To emphasize the effects of co-culturing HBECs with fibroblasts, mono-culture models of HBECs and fibroblasts were tried to be prepared (Figure S.2). The fibroblast mono-culture model was established by excluding HBEC seeding from the co-culture model

protocol (Section 3.2.1). This fibroblast mono-culture model was used in the experiments described in this chapter (Figures 3.11 and 3.12). The HBEC mono-culture model was prepared by excluding the collagen-embedded fibroblast layer from the co-culture model protocol (Section 3.2.1). However, after 21 days of ALI culturing, no mucociliary differentiation was observed in the HBEC mono-culture model (data not shown). In this experiment, a collagen type I-coated cell culture insert with a 1.0- μm pore size was used. These culture conditions must be further optimized to establish the HBEC mono-culture model because a previous report indicated that a collagen type IV-coated cell culture insert with a 0.4- μm pore size was suitable for inducing mucociliary differentiation of the HBEC mono-culture model ^{1,2}. Introducing established mono-culture model of HBEC in the experimental design will be the next step because investigating differences in the response to external stimulation among three culture models will clarify the effect of co-culture in more detail (Figure S.2).

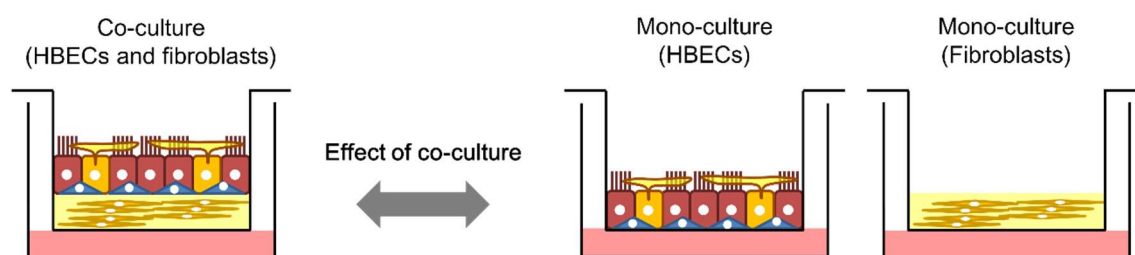


Figure S.2 Study design for investigating co-culture effects.

HBECs, human bronchial epithelial cells.

References

1. Fulcher, M.L., Gabriel, S., Burns, K.A., Yankaskas, J.R. & Randell, S.H. Well-differentiated human airway epithelial cell cultures. *Methods Mol Med* **107**, 183-206 (2005).
2. Karp, P.H. *et al.* An in vitro model of differentiated human airway epithelia. Methods for establishing primary cultures. *Methods Mol Biol* **188**, 115-137 (2002).

List of Figures

Figure 1.1 Phase composition of whole mainstream cigarette smoke.	3
Figure 1.2 Approximate composition of whole mainstream cigarette smoke.....	4
Figure 1.3 Smoking machines used for generation of whole mainstream cigarette smoke.	5
Figure 1.4 Symptoms and phenotypic changes observed in COPD patients.	6
Figure 1.5 An aerosol exposure system for <i>in vivo</i> inhalation experiments with rodents.	8
Figure 1.6 Schematic view of the preparation of a cigarette smoke extract.	9
Figure 1.7 Standard <i>in vitro</i> test methods used with cigarette smoke extracts.	10
Figure 1.8 Illustration of the human respiratory system and the 3D culture model of human bronchial epithelium.	12
Figure 1.9 Whole cigarette smoke exposure modules from Cultex Technology GmbH and Vitrocell Systems GmbH.	14
Figure 1.10 Conceptual framework of the thesis.	18
Figure 1.11 Workflow for Chapters 1–7.	19
Figure 2.1 A schematic view of the Ames reverse mutation assay.	28
Figure 2.2 Illustration of the Vitrocell whole cigarette smoke exposure system for the Ames test. ...	30
Figure 2.3 Vitrocell whole cigarette smoke exposure module for the Ames test.	30
Figure 2.4 Illustration of the heated cigarette used in this experiment.	32
Figure 2.5 Mean number of revertants induced by whole cigarette smoke exposure produced by three different cigarettes with the ISO standard smoking regime.	37
Figure 2.6 Mean number of revertants induced by exposure to whole cigarette smoke produced by four different cigarettes with the ISO intensive smoking regime.	39

List of Figures

Figure 2.7 Mean number of revertants induced by exposure to the GVP fractions produced by four different cigarettes with the ISO intensive smoking regime.	40
Figure 2.8 Relationship between the numbers of revertants induced by whole cigarette smoke and the TPM equivalents that were delivered to the cells.	44
Figure 2.9 Specific mutagenic activity of each test cigarette.	46
Figure 3.1 Illustration of human 3D lung models.	55
Figure 3.2 Model showing the importance of the epithelial–mesenchymal trophic unit following exposure-induced damage.	56
Figure 3.3 Histological analysis of the differentiation status of the bronchial tissue model.	62
Figure 3.4 Quantitative analysis of collagen gel contraction in the bronchial tissue model stimulated with TGF- β 1.	63
Figure 3.5 Histological analysis of the bronchial tissue model stimulated with TGF- β 1 on culture day 21.	65
Figure 3.6 Quantitative analysis of the immunostaining results.	66
Figure 3.7 Analysis of MMPs secreted from the bronchial tissue model on culture day 21.	68
Figure 3.8 Analysis of TIMPs secreted from the bronchial tissue model on culture day 21.	69
Figure 3.9 Significantly increased expression of extracellular matrix-related genes in the 3D bronchial tissue model following TGF- β 1 stimulation on culture day 21.	70
Figure 3.10 Histological analysis of extracellular matrix proteins on culture day 21.	71
Figure 3.11 Expression of MMPs and TIMPs in the lung mesenchymal model (fibroblast mono-culture model) following TGF- β 1 stimulation on culture day 21.	73
Figure 3.12 Expression of extracellular matrix-related genes in the 3D lung mesenchymal model following TGF- β 1 stimulation on culture day 21.	74
Figure 3.13 Schematic illustration of fibrotic changes in the epithelial mesenchymal trophic unit. ..	79

List of Figures

Figure 4.1 Images of the Cultex RFS module.	87
Figure 4.2 Illustration of the whole cigarette smoke exposure system with the Cultex RFS module.	88
Figure 4.3 Retention study concept.	89
Figure 4.4 Inhalation patterns used in the retention study.	90
Figure 4.5 Approaches for comparison of <i>in vitro</i> and <i>in vivo</i> dosimetry data.	91
Figure 4.6 <i>In vitro</i> dosimetry results.	98
Figure 4.7 <i>In vitro</i> dosimetry results.	99
Figure 4.8 Regression lines between the masses of solanesol and acetaldehyde in the mainstream cigarette smoke used in the retention study and the mass of solanesol in the cigarette filter. ...	100
Figure 4.9 Respiratory deposition efficiencies of solanesol and acetaldehyde under three inhalation patterns.	101
Figure 4.10 Relationship between <i>in vitro</i> and <i>in vivo</i> dosimetry data.	103
Figure 5.1 Single exposure experiment.	114
Figure 5.2 Repeated exposure experiment.	115
Figure 5.3 Results of single exposure experiments.	118
Figure 5.4 Histological analysis of the 3D bronchial tissue model following repeated whole cigarette smoke exposure.	120
Figure 5.5 Histological analysis of the 3D bronchial tissue model following IL-13 stimulation.	120
Figure 5.6 Effects of repeated whole cigarette smoke exposure on differentiation markers.	122
Figure 5.7 Effects of repeated whole cigarette smoke exposure on transcription of NFκB pathway components.	123
Figure 5.8 Effects of repeated whole cigarette smoke exposure on cytokine secretion.	125
Figure 5.9 Effects of repeated whole cigarette smoke exposure on cytokine secretion.	126
Figure 5.10 Effects of repeated whole CS exposure on cytokine secretion.	127

List of Figures

Figure 6.1 Experimental design for repeated whole cigarette smoke exposure.....	138
Figure 6.2 Results of cytokine measurements.	145
Figure 6.3 Results of histological analysis.	145
Figure 6.4 Results of the adenylate kinase cytotoxicity assay.	146
Figure 6.5 Results of targeted metabolomics for analysis of metabolites related to central carbon metabolism.	148
Figure 6.6 Expression levels of genes related to central carbon metabolism.	149
Figure 6.7 PCR analysis of expression of genes related to human glucose metabolism.	150
Figure 6.8 Results of microarray analysis.	152
Figure 6.9 Prediction of epidermal growth factor receptor (EGFR) pathway activation from combined metabolomic and transcriptomic data.	155
Figure 6.10 Proteomic analysis of apical surface liquid samples following repeated exposure to whole cigarette smoke.	157
Figure 6.11 Gelatin zymography of culture medium samples collected on culture day 21.	158
Figure 7.1 Smoking-induced airway epithelial remodeling in COPD patients.	168
Figure S.1 Histological analysis of the bronchial tissue model developed from lung cell lines.	178
Figure S.2 Study design for investigating co-culture effects.	179

List of Tables

Table 1.1 Studies of whole CS exposure using 3D culture models of human bronchial epithelium ..	15
Table 2.1 Experimental conditions for the whole cigarette smoke exposure Ames test	31
Table 2.2 Yields of TPM and solanesol from whole smoke produced by the tested cigarettes	41
Table 2.3 Summary of dosimetry for smoke exposure on the cell surface under the ISO standard smoking regime	42
Table 2.4 Summary of dosimetry for smoke exposure on the cell surface under the ISO intensive smoking regime	42
Table 2.5 Linear regression analysis of dose-dependent curves generated using the Ames and dosimetry data.	45
Table 3.1 Antibodies used for imunohistochemical staining.	59
Table 4.1 Machine smoking conditions for the cigarettes used in the retention study.....	95
Table 4.2 Masses of solanesol and acetaldehyde in whole mainstream cigarette smoke from 3R4F cigarettes.....	97
Table 4.3 Deposition efficiency per unit surface area in each region of the respiratory tract.....	101
Table 5.1 Summary of previous studies.....	131
Table 6.1 Metabolites identified by global metabolomics analysis.	147
Table 6.2 Predicted upstream regulators of metabolome alterations following repeated whole CS exposure.....	153
Table 6.3 Predicted upstream regulators of transcriptome alterations following repeated whole CS exposure.....	154
Table 7.1 COPD-related changes observed in the 3D bronchial tissue model in this thesis.....	169

Publications and conference presentations

Publications containing the work presented in this thesis

1. **Ishikawa, Shinkichi**, Takuya Suzuki and Yasufumi Nagata. "Analysis of cigarette smoke deposition within an in vitro exposure system for simulating exposure in the human respiratory tract." Contributions to Tobacco Research 27.1 (2016): 20–29.
2. **Ishikawa, Shinkichi**, Yuki Kanemaru, Hidenori Nara, Kazuo Erami, Yasufumi Nagata. "Assessing the mutagenic activities of smoke from different cigarettes in direct exposure experiments using the modified Ames Salmonella assay." Mutation Research/Genetic Toxicology and Environmental Mutagenesis 803 (2016): 13–21.
3. **Ishikawa, Shinkichi**, Shigeaki Ito. "Repeated whole cigarette smoke exposure alters cell differentiation and augments secretion of inflammatory mediators in air-liquid interface three-dimensional co-culture model of human bronchial tissue." Toxicology in Vitro 38 (2017): 170–178.
4. **Ishikawa, Shinkichi**, Kanae Ishimori, Shigeaki Ito. "A 3D epithelial-mesenchymal co-culture model of human bronchial tissue recapitulates multiple features of airway tissue remodeling by TGF- β 1 treatment." Respiratory Research 18 (2017): 195.
5. **Ishikawa, Shinkichi**, Kazushi Matsumura, Nobumasa Kitamura, Yuichiro Takanami, Shigeaki Ito. "Multi-omic analysis: Repeated exposure of a three-dimensional bronchial epithelial culture to cigarette smoke." Toxicology in Vitro 54 (2019): 251-262.

Other publications

1. **Ishikawa, Shinkichi** and Kazuo Ito. "Plasticity and regulatory mechanisms of Hox gene expression in mouse neural crest cells." Cell and tissue research 337.3 (2009): 381-391.
2. Aufderheide, Michaela, Stefanie Scheffler, Shigeaki Ito, **Shinkichi Ishikawa** and Makito Emura. "Ciliotoxicity in human primary bronchiolar epithelial cells after repeated exposure at the air-liquid interface with native mainstream smoke of K3R4F cigarettes with and without charcoal filter." Experimental and Toxicologic Pathology 67.7 (2015): 407-411.

3. Aufderheide, Michaela, Shigeaki Ito, **Shinkichi Ishikawa** and Makito Emura. "Metaplastic phenotype in human primary bronchiolar epithelial cells after repeated exposure to native mainstream smoke at the air-liquid interface." *Experimental and Toxicologic Pathology* 69 (2017): 307-315.
4. **Ishikawa, Shinkichi**, Kazushi Matsumura, Nobumasa Kitamura, Kanae Ishimori, Yuichiro Takanami, Shigeaki Ito. "Application of a direct aerosol exposure system for the assessment of biological effects of cigarette smoke and novel tobacco product vapor on human bronchial epithelial cultures." *Regulatory Toxicology and Pharmacology* 96 (2018): 85-93.
5. Munakata, Satoru, Kanae Ishimori, Nobumasa Kitamura, **Shinkichi Ishikawa**, Yuichiro Takanami, Shigeaki Ito. "Oxidative stress responses in human bronchial epithelial cells exposed to cigarette smoke and vapor from tobacco- and nicotine-containing products." *Regulatory Toxicology and Pharmacology* 99 (2018): 122-128.
6. Ito, Shigeaki, Kanae Ishimori, **Shinkichi Ishikawa**. "Effects of repeated cigarette smoke extract exposure over one month on human bronchial epithelial organotypic culture." *Toxicology Reports* 5 (2018): 864-870.
7. Sekine, Takashi, Tadashi Hirata, **Shinkichi Ishikawa**, Shigeaki Ito, Kanae Ishimori, Kazushi Matsumura, Katsuhiko Muraki. "Regulation of NRF2, AP-1, and NF- κ B by cigarette smoke exposure in three-dimensional human bronchial epithelial cells." *Journal of Applied Toxicology* (2019): 1-9.

Oral presentations

1. **Ishikawa, Shinkichi**, Kazushi Matsumura, Nobumasa Kitamura, Yuichiro Takanami, Shigeaki Ito. "In vitro repeated exposure study using a three-dimensional cell culture model of human bronchial tissue for assessment of aerosol chemicals" Japanese Society for Alternative to Animal Experiments 30th Annual Meeting 2017.
2. **Ishikawa, Shinkichi**, Shigeaki Ito. "The development of in vitro test methods to assess biological effects of aerosols generated by tobacco products" Japanese Society for Alternative to Animal Experiments 31st Annual Meeting 2018.

Poster presentations

1. **Ishikawa, Shinkichi** and Kazuo Ito. "Regulatory mechanisms for the expression of Hox genes in mouse neural crest cells." Japanese Society of Developmental Biologists 41st Annual Meeting 2008
2. Nara, Hidenori, Kazuo Erami, **Shinkichi Ishikawa** and Yasufumi Nagata. "Report on biological research using a heated cigarette: Part 3 -in vitro toxicological study by the direct exposure method-." CORESTA congress 2012
3. **Ishikawa, Shinkichi**, Takuya Suzuki and Yasufumi Nagata. "Comparison of in vitro and in vivo exposed chemical levels following cigarette smoke exposure." CORESTA congress 2014.
4. **Ishikawa, Shinkichi** and Shigeaki Ito. "In vitro exposure study using a 3D cell culture model of human bronchial tissue for the assessment of aerosol chemicals." Japanese Society for Alternative to Animal Experiments 29th Annual Meeting 2016.
5. Munakata, Satoru, Ishimori Kanae, Yuichiro Takanami, **Shinkichi Ishikawa**, Shigeaki Ito. "Comparative effects of cigarette smoke and novel tobacco product vapor on in vitro cellular responses in human bronchial epithelial cells." Society of Toxicology 56th Annual Meeting 2017.
6. Ito, Shigeaki, **Shinkichi Ishikawa**, Kazushi Matsumura, Nobumasa Kitamura and Yuichiro Takanami. "Integration of transcriptomics and metabolomics reveals the perturbation in the central carbon metabolism by repeated whole smoke exposure to air-liquid Interface three-dimensional co-culture model of human bronchial tissue." Society of Toxicology 56th Annual Meeting 2017.
7. Matsumura, Kazushi, **Shinkichi Ishikawa** and Shigeaki Ito. "Simple scoring method for predicting oxidative stress and inflammation status in 3D organotypic cultures of human bronchial cells exposed to cigarette smoke." ISMB/ECCB 2017.
8. **Ishikawa, Shinkichi**, Kazushi Matsumura, Kanae Ishimori, Nobumasa Kitamura, Satoru Munakata, Yuichiro Takanami and Shigeaki Ito. "Comparison of whole-aerosol exposure of human bronchial tissues to cigarette smoke and nicotine-containing vapor." European Societies of Toxicology 53rd Congress 2017.
9. Matsumura, Kazushi, **Shinkichi Ishikawa** and Shigeaki Ito. "Alteration of transcriptomics profiles in organotypic culture of bronchial tissues indirectly exposed to cigarette smoke and novel tobacco product vapor" European Societies of Toxicology 53rd Congress 2017.

10. Mario, Aragon, Stefan Frentzel, Julia Hoeng, Shigeaki Ito, **Shinkichi Ishikawa**, Jessica Budde, Anna Maione, Patrick Hayden, Linsey Haswell, David Azzopardi, Brian Keyser, Wanda Fields, Holger Behrsing. “Human in-vitro models for respiratory toxicology: evaluation of goblet cell hyperplasia, mucus production, and ciliary beating assays.” Society of Toxicology 57th Annual Meeting 2018.
11. **Ishikawa, Shinkichi**, Kazushi Matsumura, Nobumasa Kitamura, Kanae Ishimori, Yuichiro Takanami, Shigeaki Ito. “Biological effects of cigarette smoke and novel tobacco product vapor on human organotypic bronchial epithelial cultures analyzed using an in vitro aerosol exposure system.” Society of Toxicology 57th Annual Meeting 2018.
12. Gilbert, Brent, Erin Hill, Aragon Mario, Stefan Frentel, Julia Hoeng, Shigeaki Ito, **Shinkichi Ishikawa**, Jessica Budde, Anna Maione, Patrick Hayden, Wanda Fields, Brian Keyser, Linsey Haswell, David Azzopardi, Holger Behrsing. “Human in-vitro models for respiratory toxicology: evaluation of goblet cell hyperplasia, mucus production, and ciliary beating assays.” Lung in vitro event for innovative & predictive models (LIVe) 2018.
13. Ishimori, Kanae, Nobumasa Kitamura, **Shinkichi Ishikawa**, Yuichiro Takanami, Shigeaki Ito. “Oxidative stress response and DNA damage in human bronchial epithelial cells exposed to cigarette smoke and novel tobacco product vapor.” The 45th Annual Meeting of the Japanese Society of Toxicology 2018.
14. **Ishikawa, Shinkichi**, Kazushi Matsumura, Nobumasa Kitamura, Kanae Ishimori, Yuichiro Takanami, Shigeaki Ito. “Transcriptome analysis of human organotypic bronchial epithelial cultures directly exposed to whole cigarette smoke.” The 45th Annual Meeting of the Japanese Society of Toxicology 2018.
15. Ito, Shigeaki, Kanae Ishimori, **Shinkichi Ishikawa**. “One-month repeated cigarette smoke exposure of human organotypic bronchial epithelial cell culture.” European Societies of Toxicology 54th Congress 2018.
16. Matsumura, Kazushi, **Shinkichi Ishikawa**, Nobumasa Kitamura, Yuichiro Takanami, Shigeaki Ito. “Integrative omics analysis for assessment the biological effect of repeated whole cigarette smoke exposure on a 3D bronchial tissue culture.” The 19th International Conference on Systems Biology 2018.

Acknowledgements

First, I would like to thank Prof. Dr. Yasuyuki SAKAI for providing the great opportunity to complete a doctoral degree with this research thesis. I would also like to thank Prof. Dr. Kouhei TSUMOTO, Prof. Dr. Madoka TAKAI, Prof. Dr. Shinsuke SANDO, and Assoc. Prof. Dr. Eiko KOIKE for kindly acting as committee members for my thesis.

Over the last decade, I have worked with many people at Japan Tobacco Inc. All of them have kindly helped me to conduct the experiments described in this thesis, and I would like to express my gratitude to all of them. Specifically, I would like to thank: Dr. Tomoki NISHINO for support with conducting the experiments, Dr. Yuki KANEMARU for teaching me the Ames reverse mutation assay, Dr. Tatsuhiko KASAOKA for teaching me the techniques for the 3D bronchial tissue culture, Dr. Yasufumi NAGATA and Mr. Takuya SUZUKI for support with the human retention study, Dr. Yasuo FUKANO for support with the whole CS exposure experiments, Dr. Shigeaki ITO for organizing the multi-omics study, Dr. Yuichiro TAKANAMI and Dr. Nobumasa KITAMURA for metabolomics analysis, Dr. Kazushi MATSUMURA for omics analysis, and Ms. Kanae ISHIMORI for assistance with various experiments.

Finally, I would like to express my special thanks to my wife Eriko for her continuous support during my completion of this work. I also express thanks to my beloved children Yukako and Haruhisa for always cheering me up.

